102.8

DOE/RW-0160

Chapter 7

Nuclear Waste Policy Act
(Section 113)

WASTE PACKAGE

G

Consultation Draft

Site Characterization Plan

Yucca Mountain Site, Nevada Research and Development Area, Nevada

Volume III

PART A

January 1988

U.S. Department of Energy
Office of Civilian Radioactive Waste Management
Washington, DC 20585

B5, 928

102.8

DOE/RW-0160

Chapter 7

Nuclear Waste Policy Act
(Section 113)

WASTE PACKAGE

Consultation Draft

Site Characterization Plan

Yucca Mountain Site, Nevada Research and Development Area, Nevada

Volume III

January 1988

U.S. Department of Energy
Office of Civilian Radioactive Waste Management
Washington, DC 20585

B5,928

Chapter 7

WASTE PACKAGE

INTRODUCTION

This chapter describes waste package components, emplacement environment, design, and status of research and development that support the Nevada Nuclear Waste Storage Investigation (NNWSI) Project. The site characterization plan (SCP) discussion of waste package components is contained entirely within this chapter and Chapter 8. The discussion of emplacement environment in this chapter is limited to considerations of the environment that influence, or which may influence, if perturbed, the waste packages and their performance (particularly hydrogeology, geochemistry, and borehole stability). The discussion considers the near-field environment based on environment described in previous chapters (especially Chapters 2, 3, 4, and portions of 6) but does not address overall site environment as do those chapters. The basis for conceptual waste package design as well as a description of the design is included in this chapter. The complete design will be reported in the advanced conceptual design (ACD) report and is not duplicated in the SCP. The site characterization data that will provide the waste package environment design envelope information to advanced conceptual designs is covered under Issue 1.10 in Section 8.3.4.2. Discussion of studies related to ACD is covered in Section 8.3.4.3. The focus of the design discussions in the SCP is on those aspects of the design that depend on site characterization information. The relationship between this chapter and other design-related documents is shown in Figure 7-1.

Chapter 7 gives the status of the NNWSI Project's knowledge and discusses the extent to which current information is sufficient to demonstrate that objectives will be satisfied. Section 8.3 discusses how the additional information needed to resolve issues will be obtained and how each issue will be resolved so that it can be demonstrated that the performance objective will be met.

WASTE PACKAGE COMPONENTS

For the purposes of this chapter, the waste package is divided into two functional components: waste form and container. In addition, constructed features of the geologic repository immediately adjacent to the container and the near-field host rock environment are discussed.

The waste forms of concern are of two generic types: spent nuclear fuel resulting from the operation of commercial power reactors and high-level waste resulting from fuel reprocessing associated with commercial and defense activities. In addition, the nonfuel components associated with commercial spent fuel are expected to be packaged and emplaced in a geologic repository.

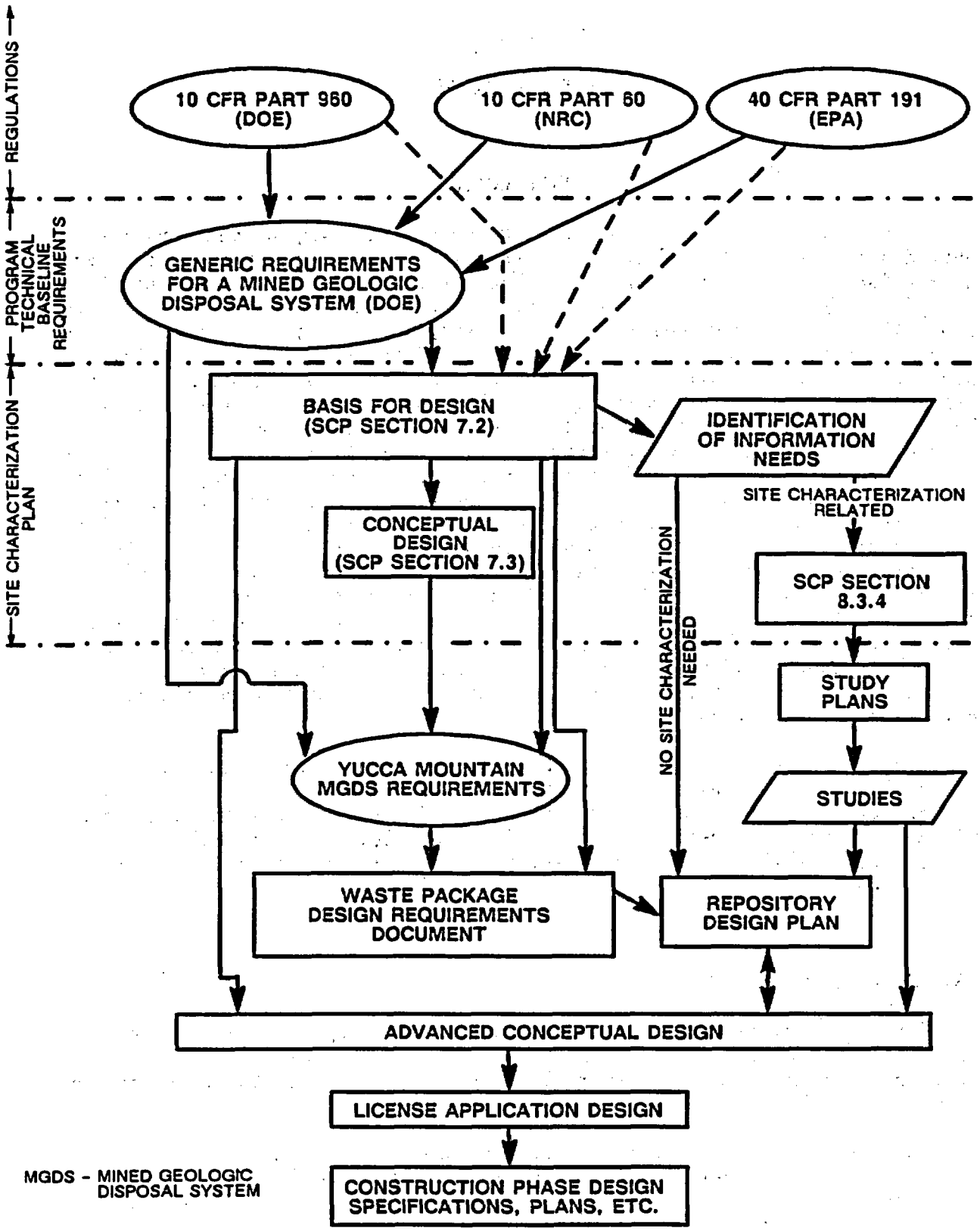

Figure 7-1. Flow chart indicating relationship of design-related documents for the waste package.

The waste package container is the component specifically designed as an engineered barrier to provide containment of the waste form during the period when the radiation and thermal conditions are dominant or are changing rapidly.

Other constructed features include the openings in the host rock, currently planned to be mechanically bored cylindrical holes, into which the waste packages are emplaced and other features such as borehole liners and any mechanical appurtenances needed to facilitate emplacement or possible retrieval of the packages.

REQUIREMENTS

The requirements for performance of the waste packages are either defined in detail or implied by three regulations (40 CFR Part 191, 10 CFR Part 60, and 10 CFR Part 960) and by a document that responds to all three regulations entitled "Generic Requirements for a Mined Geologic Disposal System" (GR) (DOE, 1984). Environmental Protection Agency (EPA) regulations (40 CFR Part 191) do not place requirements directly on the waste package. The U.S. Department of Energy (DOE) 10 CFR Part 960 contains general specifications for the waste package, deferring to 10 CFR Part 60 for details. Specific requirements for the waste package as defined in 10 CFR Part 60 and in the GR fall into two broad categories, preclosure and postclosure. Not all the requirements are appropriate for discussion in the SCP because the regulations include items that are independent of site characteristics. The specific portions of the regulations that are appropriate for discussion here are shown in Table 7-1.

Preclosure criteria or requirements are associated with the operational phases of the repository system, such as providing for waste package material compatibility, identification, waste form criteria, and handling (including emplacement and retrieval). These considerations are essentially covered in 10 CFR 60.135(b) and (c) and, except for portions of the handling, are not related to site characterization activities as defined by the Nuclear Waste Policy Act (NWPA, 1983). Therefore, these aspects will be addressed in reports on future design phases (advanced conceptual design and license application design reports) rather than the SCP. Aspects of handling require only limited site characterization information as inputs to package design and are essentially related to conduct of repository operations as described in Section 6.2.

The postclosure requirements are directed toward the long-term performance of the package components in providing containment and isolation functions. Long-term performance includes considerations of interaction between the waste package and its environment. The specific requirements are contained in 10 CFR 60.113 and 60.135(a). The requirements in 10 CFR 60.113 assign the containment function to the waste package and the controlled release of radionuclides function to the engineered barrier system, of which the waste package is a major component. The requirements in 10 CFR 60.135(a) address the waste package and its components. Therefore, this chapter will focus on the postclosure considerations of the waste package with design and other preclosure considerations summarized but not developed in detail. The

Table 7-1. Regulations that address site-specific requirements for the waste package

Regulation	Applicable sections	
	Preclosure	Postclosure
10 CFR Part 60 (NRC)[a]	60.135(b), (c)	60.113 60.135(a)
10 CFR Part 960 (DOE)[b]	960.5-1(2), (3) and Appendix II	960.5-1 Appendix I
40 CFR Part 191 (EPA)[c]	No direct requirements	Addresses overall performance, does not specify waste package directly
Generic Requirements for a Mined Geologic Disposal System (DOE)	1.3.1 1.3.2	2.2.1

[a]NRC = Nuclear Regulatory Commission.
[b]DOE = U.S. Department of Energy.
[c]EPA = Environmental Protection Agency.

detailed discussion of these nonsite-specific considerations will be contained in the advanced conceptual design (ACD).

HISTORY OF ACTIVITIES

Before 1982, waste package research and development activities were not specifically assigned to the NNWSI Project but were conducted on a generic basis by the National Waste Terminal Storage Program. The emphasis of the NNWSI Project was on identifying a suitable repository horizon in the saturated zone of Yucca Mountain, and the waste package activity was directed toward defining the applicable environment and developing design concepts appropriate to that environment. In late 1982, the emphasis of the NNWSI Project shifted to the consideration of the unsaturated zone as a potential repository setting and, specifically, to the investigation of the Topopah Spring Member of the Paintbrush Tuff as the reference repository horizon. This change was made to take advantage of the separation from the zone of saturation where the ground water provides a more direct pathway to the biosphere and also to take advantage of the expected more beneficial environment for metal barriers and for waste forms.

This represented a substantial change in the environment in which a waste package would have to exist. A different set of physical and chemical phenomena, which are useful for meeting the containment and isolation requirements, exist in the unsaturated zone. Thus the change presented an entirely new regime for testing and evaluating package components. Consequently, the specification of the environment in which the package would function was revised, and the direction of the research, development, and testing plans for evaluating the performance of package component materials was modified.

Activities that have been conducted by the NNWSI Project since 1982 regarding the waste package have centered around those necessary to support a license application for construction of a repository. The activities are grouped into four major categories: (1) waste package environment; (2) waste form and materials testing; (3) design, analysis, fabrication, and prototype testing; and (4) performance assessment. Each of these groups of activities is discussed in detail in subsequent sections of this chapter. A general description of these activities follows.

Waste package environment activities involve characterization of the variability of properties of Topopah Spring tuff in the repository area. Included are studies of (1) hydrothermal reactions between the tuff and ground water and (2) rates and mechanisms of dehydration and rehydration of rock adjacent to the boreholes.

Waste form and materials testing activities involve measurement of radionuclide release rates from spent fuel and from borosilicate glass to provide input for modeling of long-term radionuclide release rates from the waste package; determination of whether a packing material must be incorporated in the waste package design; selection of candidate metals for fabrication of containers; characterization of the corrosion rates of these metals under expected conditions; and characterization of the effect that other materials associated with the repository might have on the long-term performance of the waste form and container materials.

Design, fabrication, and prototype testing activities involve development and testing of waste package designs that are compatible with repository design.

The performance assessment activity involves the development and validation of models for use in making long-term predictions of package performance for comparison with U.S. Nuclear Regulatory Commission (NRC) performance objectives. Associated with this activity, though not an integral part of it, is the development of advanced computer codes for modeling geochemical processes in the repository environment.

UNCERTAINTIES IN WASTE PACKAGE DEVELOPMENT

Several sources of uncertainty exist in the development and analysis of performance waste packages. Some of these will be reduced significantly as a result of the investigations and tests described in Chapter 8; others are inherent in the inhomogeneous characteristics of the waste forms and the

geohydrologic setting of the repository and will, therefore, remain to be considered using statistical techniques in the analyses of projected performance.

Among the types of uncertainties that exist in the waste package development and analysis activities are

1. Variability in the geohydrologic system and uncertainty in understanding the response of the system to repository thermal loads. Significant uncertainties are associated with the present information on the characteristics of the natural system, primarily due to the limitations imposed by surface-based investigations. These data will be supplemented by extensive laboratory and in situ testing in the future that is expected to substantially improve the knowledge of the nature and response of the natural system. Residual uncertainties will result from the limitations of the laboratory and in situ testing program in both areal extent and duration.

2. Identification of the mechanisms and prediction of the rates of degradation of the metallic components of the packages, especially the metal containers. The major sources of these uncertainties are the lack of a final selection of container material and the influence of the processes that will be used to form and close the containers on their long-term performance. The selection of a material and determination of the fabrication processes will allow assessment of these uncertainties by relatively short duration tests, but residual uncertainties will exist due to the lack of relevant experience with the materials over the time periods of interest in this application. These service lifetimes are far longer than any other engineered structures, and therefore beyond the limits of engineering experience.

3. Variation of the physical and chemical characteristics of the waste forms. These uncertainties can be reduced by a systematic examination of the existing and proposed wastes, but there is a substantial residual uncertainty resulting from the fact that a large fraction of the wastes to be disposed of do not exist now, and will not exist prior to the application for a license for the disposal system.

4. Limitations on the ability to model accurately the physical and chemical processes operating on and in the waste packages. The development of fully coupled models that include all the synergistic interactions that can affect the performance of a combined engineered and natural system is beyond the existing capability of the scientific community. Therefore, simplifications of these interactions will be necessary to allow the evaluation of the known uncertainties in the system. These simplifications will themselves introduce a level of uncertainty to the analyses of the predicted performance.

The present status of the evaluation of the types of uncertainty known to be associated with the various aspects of the waste packages are discussed within the appropriate sections of this chapter and summarized in Section 7.5.5.

CHAPTER ORGANIZATION

The reference waste package emplacement environment is briefly described in Section 7.1, which is intended to orient the reader to those features of the unsaturated zone that are significant in the design and performance of waste packages.

Section 7.2 specifies the design basis for the waste packages and includes the applicable regulatory requirements, as well as design assumptions that have been adopted on an interim basis for the purpose of conceptual design. These design bases will be modified in the waste package design requirements document which will be issued after the SCP.

The initial conceptual waste package designs for the reference case (including conceptual design drawings, general material specifications, and configurations) are described in Section 7.3. These design concepts were developed during 1983 and 1984. A follow-on ACD phase will be discussed in an ACD report. Alternative waste package designs, including those of copper-based alloy containers, are also discussed in Section 7.3 but not at the same level of detail, since the reference case was based on 1984 activities. Evaluations (laboratory and analyses) have continued since that time on copper-based containers. Copper and copper-based alloy containers are being considered for future work as described in Section 8.3.4.

Section 7.4 discusses the status of waste package research and development activities that have been under direct NNWSI Project auspices since late 1982. Section 7.4 is divided into five subsections, each of which addresses a component of the research and development activity.

Section 7.4.1 describes the status of investigations of the waste package environment, including thermal effects and chemical interactions in the region adjacent to emplaced waste packages and the stability of boreholes.

Section 7.4.2 discusses tests on various candidate metal container materials, with primary emphasis on the investigation of degradation modes of austenitic stainless steels. This section also briefly discusses projected container lifetimes and likely failure modes. Recently initiated testing of copper alloys is also discussed.

Section 7.4.3 describes the waste form testing activities that have been conducted on both spent fuel and high-level waste in borosilicate glass. The activities include waste form dissolution tests as well as investigations of spent fuel oxidation and cladding corrosion. This section includes a brief discussion of release models for use in developing waste package source terms.

Section 7.4.4 describes the status of development of geochemical models that will be used in the assessment of the waste package performance.

Section 7.4.5 describes the functions of waste package performance assessment and the work on the development of a waste package system model to be used to show compliance with the waste package performance objectives and assessments.

This chapter concludes with Section 7.5 which summarizes the significant results of the activities described in the preceding sections. References are given to appropriate subsections of Chapter 8 where the performance allocation, issue resolution strategy, and detailed plans are presented for acquisition of additional required information to demonstrate satisfying performance objectives.

7.1 EMPLACEMENT ENVIRONMENT

Characterization of the emplacement environment is required to meet performance assessment goals and to provide information necessary to carry out materials and design tests. This information also provides input to development of source term models.

The NNWSI Project has selected the Topopah Spring Member of the Paintbrush Tuff as the reference repository horizon for a potential repository for high-level nuclear waste sited at Yucca Mountain. The investigations that led to the choice are discussed in the unit evaluation report (Johnstone et al., 1984). The reference horizon is the welded, devitrified section c Topopah Spring tuff that lies above the basal vitrophyre of the unit. The repository would be approximately 350 m below the ground surface and 200 to 400 m above the static water table (Sinnock et al., 1984; Ortiz et al., 1985). The stratigraphy of the site is described in Section 1.2, and the structural features of the site are discussed in Section 1.3. Hydrologic characteristics of the site are summarized in Chapter 3. Data related to these characteristics have been used by Montazer and Wilson (1984) to develop a conceptual hydrologic model of flow in the unsaturated zone at Yucca Mountain.

The choice of the unsaturated zone as the location for the reference repository horizon marks a departure from the conventional environment that has been considered for repository siting. There are many characteristics of the unsaturated zone that make it particularly attractive for a high-level waste repository site. Winograd (1981) and Roseboom (1983) have discussed waste disposal in areas where thick unsaturated sequences of rock are present. The unsaturated setting simplifies the design of waste packages and provides limits on the conditions to which the waste packages will be subjected. Some of the anticipated conditions of the setting relevant to waste package design and performance are the following:

1. The waste containers would not be submerged in a continuum of water. Anticipated conditions in the unsaturated zone suggest the containers will experience high humidity during the period of substantially complete containment (Section 7.4.1). Intermittent contact with limited amounts of liquid water for some packages is possible under some conditions.

2. The pressure exerted on the containers by the environment would be approximately one atmosphere. There would be no hydrostatic pressure because of the location above the water table. The packages would not bear lithostatic load because the host rock is not

expected to creep under the postemplacement thermal regime (Section 2.5). The load-bearing requirements for the waste packages are limited to pressures caused by sloughing of rock from emplacement boreholes.

3. The environment to which the waste packages would be exposed would be a mixture of water vapor and air, with a total pressure of about one atmosphere during the period of time when the temperature is above the local unconfined boiling point of water, approximately 96°C. Only slight variation (<1.0°C) in the boiling temperature can be expected for unconfined, unbound, non-capillary pore water even if the concentration of dissolved salts is greatly increased (Section 7.4.1.2).

4. Aqueous corrosion of waste packages by liquid water and its dissolved constituents would only commence after the temperature of the container drops to the point where a liquid film could form on the container surface. For packages containing spent fuel, liquid water may not contact the container until hundreds of yr have passed (Section 7.4.1).

5. The vadose water and atmosphere of the repository would be mildly oxidizing due to the exchange of repository air with the external environment and due to radiolysis effects (Section 7.4.1.4). The degree of oxidation has yet to be established. This condition could be used advantageously in waste package design if the metal container chosen were of the type that forms a protective oxidized surface on the metal.

6. Water available for corrosion and waste form dissolution would be limited to very small amounts. The net infiltration of water at Yucca Mountain was estimated by Montazer and Wilson (1984) to be between 0.5 and 4.5 mm/yr. However, only a small portion of the net infiltration would be expected to pass through the repository horizon. An upper estimate of 0.2 mm/yr of downward flux was given by Montazer et al. (1986) for the matrix of the Topopah Spring welded unit. The estimated range of downward flux is 0.1 micrometer per yr to 0.2 mm/yr (Montazer et al., 1986). To allow for uncertainties in this estimate, 1 mm/yr will be adopted as a working value for the purposes of waste package design and testing which is the conservative estimate of transmission through the Topopah Spring unit.

7. Thermal perturbation of the near-field environment by the waste package will dehydrate the near-field host rock and will prevent liquid water from contacting the waste packages for hundreds of yr (SCP Section 7.4.1.2; Glassley, 1986). This thermal effect will diminish the potential for liquid water to corrode the waste container for several hundred yr after emplacement and will eliminate the possibility of dissolution and transport of waste during the required period of substantially complete containment.

8. Radiation effects will be limited to those resulting from interaction of gamma and neutron radiation with the moist air and rock

although neutron doses will be negligible compared to gamma doses (Van Konynenburg, 1984, 1986). The radiolysis products will depend on the temperature of the environment, which will be a function of time. By the time temperatures are low enough for liquid water to contact the waste packages, the radiation level will be diminished by about three orders of magnitude, resulting in a similar decrease in the abundance of radiolysis products in the water-air-rock system.

The host rock at the reference repository horizon is a welded, devitrified, ash-flow tuff. The mineralogy and petrology of the rock have been investigated in detail using samples obtained from drill holes sited around the edge of the exploratory block at Yucca Mountain. Detailed reports giving quantitative estimates of mineral compositions and proportions for major and trace phases have been published by Bish et al. (1981), Vaniman et al. (1984), and Warren et al. (1984). A summary of the data is presented in Section 4.1.1. The major phases in the rock are a fine-grained assemblage of alkali feldspar, quartz, and cristobalite; minor phases include phenocrysts of plagioclase, alkali feldspar, iron-titanium oxides, quartz, and biotite, and variable amounts of montmorillonite clay. Trace phases include allanite, apatite, zircon, and occasional fluorite. Vein and fracture fillings consist of various assemblages of the minerals mordenite, calcite, quartz, feldspar, cristobalite, heulandite, clinoptilolite, and smectite (Carlos, 1985).

The chemistry of water in the saturated zone beneath Yucca Mountain has been investigated by Benson et al. (1983) and Ogard and Kerrisk (1984). The water samples showed a very limited range in chemical composition for aquifers in the tuff units. The results of water chemistry investigations are summarized in Section 4.1.2.

The composition of water from these investigations is very similar to that of vadose water in tuffs from Rainier Mesa (White et al., 1980; Henne, 1982). This similarity suggests that vadose water and ground water in the silicic tuffs of the area have similar compositions. Water from well J-13, a high flow rate well east of Yucca Mountain, has been selected as the reference water for experimental studies because its producing horizon is the Topopah Spring Member of the Paintbrush Tuff and because its composition is very similar to that of previously analyzed vadose water and ground water. The uniform composition of waters in this area suggests that the composition of vadose water at Yucca Mountain is similar to water from well J-13.

Samples of vadose water will be obtained during the sinking of the exploratory shaft. Should the water composition in the vadose zone differ markedly from that in the saturated zone, some or all the previously completed testing may have to be repeated. Present indications, based on the absence of readily soluble components in drill core samples, are that the water chemistry in the vadose zone should be similar to that in the saturated zone (Oversby, 1985; SCP Section 7.4.1.3).

The composition of the pore fluid phase may be altered as a result of evaporation, fluid-migration, and condensation processes resulting from heating of the repository host rock. It is expected that two-phase flow will be initiated in regions adjacent to the dry-out zone. During this process, evaporation of water may lead to deposition of dissolved salts that may be

redissolved during periods of rehydration when the repository cools. The magnitude of this process and the parameters controlling it are the subjects of current investigations.

The ambient hydrologic conditions at Yucca Mountain are discussed in Chapter 3. Montazer and Wilson (1984) used the available data to construct a model for the flow paths and fluxes to be expected in the repository region, and provided the following summary of characteristics of the rock. The Topopah Spring welded unit has a fracture density of 8 to 40 fractures per cubic meter, a mean matrix porosity of 14 ± 5.5 percent, and a mean saturation level of 65 ± 19 percent. The water content of 29 drill core samples averages 5.5 percent by weight. The geometric mean of measurements of saturated matrix hydraulic conductivity is 3×10^{-6} m/d, and the effective hydraulic conductivity of the matrix has been estimated to be 1.6×10^{-7} m/d (Montazer and Wilson, 1984).

The model for flow in the unsaturated zone provides estimates of water fluxes through the various units at Yucca Mountain. Because of the potential for lateral flow within some units and at unit boundaries and of the effects of capillary barriers present in the natural setting, the flux through any given unit may be less than the net downward infiltration rate for the mountain as a whole. Indeed, it is possible for some units to have a net upward flux caused by vapor transport of water even though the system as a whole has a net downward flux (Montazer and Wilson, 1984). Geothermal data from the air-drilled drillhole USW UZ-1 indicate an upward flux of 1 to 2 mm/yr in the Topopah Spring welded unit although calculations of flux through the welded unit using effective permeability and hydraulic gradient in Darcy's equation give an estimate of flux of 0.003 to 0.2 mm/yr downward (Weeks and Wilson, 1984). Calculations based on the in situ potential gradient measured in drillhole USW UZ-1 and the effective permeabilities measured using drill core from the adjacent drillhole gave estimates of downward flux ranging from 1×10^{-7} mm/yr to 2×10^{-4} mm/yr (Montazer and Wilson, 1984).

The thermal and mechanical properties of the rocks at Yucca Mountain are summarized in Chapter 2. These properties are used to determine the maximum heat loadings that could be put into each waste package without violating the thermal constraints established for the waste forms. The rock mechanical properties are also used in the analysis of the stability of borehole openings (Section 7.4.1.1).

Emplacement of waste packages into the host rock would cause changes in the environment due to thermal effects and rock-water interaction. Research and development work to establish the nature of the changes is described in Section 7.4.1, waste package environment. Some changes to the environment would also occur because of construction methods and materials used during the construction and operational phases of the repository. Some types of inorganic materials, such as portland cements and grouts, can cause a large change in the pH of water interacting with them. This can have a deleterious effect on the leaching of glass waste forms (Section 7.4.3.2). Other types of grouting materials are to be preferred if they maintain a near neutral pH for the local water chemistry and are structurally sound. Deleterious effects may also occur from other sources (such as anions). These other

sources will be considered in waste form testing as discussed in Section 8.3.5.10. Organic materials should be avoided in the immediate vicinity of waste packages because they and their radiolysis products could provide ligands for subsequent radionuclide transport. Where the use of organic materials is unavoidable, the effects caused by their use will need to be carefully evaluated and controlled, as discussed in Section 8.3.1.3.4.

7.2 DESIGN BASIS

In this section, the waste package design requirements derived directly and indirectly from regulatory requirements and the relationships of these requirements to waste package functions are discussed. Section 7.2.1 contains the waste package design requirements, performance criteria, and constraints that have been adopted for the development of the conceptual designs described in Section 7.3. Section 7.2.2 provides a reference to the baseline characteristics and receipt rates for the waste forms. Section 7.2.3 summarizes the allocation of performance for the waste package components.

The anticipated emplacement environment is described in Sections 7.1 and 7.4.1, both for the preemplacement and postemplacement periods in terms of chemical composition of the host rock and vadose water, flux and flow regimes of water, temperature, and rock stability. The postclosure radiation levels are described in Section 7.3, and the effect of these levels on the environment is discussed in Section 7.4.1.

7.2.1 DESIGN REQUIREMENTS

The design requirements for the waste package established in this section are derived from several sources. The primary source is the baseline "Generic Requirements for a Mined Geologic Disposal System" (GR) (DOE, 1984). The NNWSI Project-level document, Yucca Mountain Mined Geologic Disposal System Requirements, exists only as a draft and is not available as a baseline source of requirements at this time. Therefore, the functional requirements, performance criteria, and constraints specified in Sections 7.2.1.1 and 7.2.1.2 are cited from the GR.

Other sources of design requirements that have been included in the basis for the conceptual designs are 10 CFR Part 60, 10 CFR Part 960, and the NNWSI Project requirements established to ensure that component performance is not compromised. These design requirements are identified in Section 7.2.1.3.

The nomenclature used in the requirements, though perhaps confusing to the reader, is not intended to draw any distinction between a waste emplacement package and a waste package. These terms are used in the GR to differentiate between preclosure and postclosure system elements, but are assigned to the same physical object once it is completely assembled. The NNWSI Project waste emplacement package or waste package consists of the waste form and the disposal containers (including any required internal stabilizing structure).

7.2.1.1 Generic preclosure requirements

The preclosure waste emplacement package functional requirements are specified as follows in DOE (1984):

"1. To contain waste during unloading, handling, storage, further packaging at the repository surface facilities, emplacement, and retrieval, if necessary (10 CFR 60.135(b)(3)).

"2. To limit the potential for criticality within waste emplacement packages.

"3. To provide a means of unique identification."

The corresponding performance criteria for these requirements are specified as follows (DOE, 1984):

1. Handling--"A. The waste emplacement package must remain intact as a unit, which contains the waste and provides for safe handling of the waste, at least to the end of the period of retrievability.

   "B. The waste emplacement package must be capable of sustaining normal handling and packaging operational loads without loss of containment, and design bases accidents either without loss of containment or with a limited release of radionuclides as required in 10 CFR 20 or 10 CFR 100 [sic] when applicable."

   (In addition, pending revisions of the Generic Requirements document include an additional criterion that the waste emplacement package shall be designed and fabricated to allow retrieval of the waste by the methods planned from the emplacement configuration used in the repository.)

2. Criticality control--"The internal waste distribution in waste emplacement packages shall be such that nuclear criticality shall not be possible unless at least two unlikely, independent, and concurrent or sequential changes have occurred in the conditions essential to nuclear criticality safety. The calculated effective multiplication factor (k_{eff}) must be sufficiently below unity to show at least a 5 percent margin after allowance for the bias in the method of calculation and the uncertainty in the experiments used to validate the method of calculation."

3. Unique identification--"Provide a label or other means of identification for each waste emplacement package. The identification shall not impair the integrity of the waste emplacement package and shall be applied in such a way that the information shall be legible at least to the end of the period of retrievability. Each waste emplacement package identification shall be consistent with the waste emplacement package's permanent written records (10 CFR 60.135(b)(4))."

In addition, the following constraints apply to the waste emplacement package and are to be accommodated in the design (DOE, 1984):

1. Explosive, pyrophoric, and chemically reactive materials--"The waste emplacement package shall not consist of [sic] (contain) explosive or pyrophoric materials or chemically reactive materials in an amount that could compromise the ability of the underground facility to contribute to waste isolation or the ability of the geologic repository to satisfy the performance objectives (10 CFR 60.135(b)(1))."

2. Free liquids--"The waste emplacement package shall not contain free liquids in an amount that could compromise the ability of the waste packages to achieve the performance objectives relating to containment of high-level waste (because of chemical interaction or formation of pressurized vapor) or result in spillage and spread of contamination in the event of waste package perforation during the period through permanent closure (10 CFR 60 135(b)(2))."

In addition to the requirements and criteria cited for the waste emplacement package, specific requirements and criteria are established for the waste form and container as individual components of the waste package. These are specified as follows (DOE, 1984):

1. Waste Form.

   Functional requirement--"1. Control release if containment is lost during handling."

   Performance criteria--"1. The encapsulating or stabilizing matrix associated with spent fuel or used with reprocessed waste shall be designed to limit the availability and generation of particulates in case of an accident occurring during preclosure (10 CFR 60.135(c)(1) and (2))."

2. Container.

   Functional requirement--"1. The container shall be capable of being handled and shipped as needed."

   Performance criteria--"1. The container shall have lifting studs, the mechanical integrity to sustain routine handling and shipping, and a readily identifiable label giving contents."

7.2.1.2 Generic postclosure requirements

The waste package postclosure functional requirements are specified as follows (DOE, 1984):

"1. To contain the radionuclides for a specified period of time.

"2. To contribute to controlling the release of radionuclides after the containment period."

The corresponding performance criteria for these requirements are specified as follows (DOE, 1984):

1. Radionuclide containment--"The waste package system shall be designed, assuming anticipated processes and events, so that containment of radioactive waste will be substantially complete for a period not less than 300 yr after permanent closure of the geologic repository.* Specific numeric criteria for 'substantially complete' and the time period for containment depend on site-specific characteristics (10 CFR 60.113(a)(1)(ii)(A) and 60.113(b))."

   (In addition, pending revisions to the Generic Requirements document include an additional criterion for radionuclide release control-The waste package subsystem shall be designed, assuming anticipated processes and events, so that the release rate of any radionuclide from all of the waste packages** following the containment period shall not exceed one part in 100,000 per yr of the curie inventory of that radionuclide calculated to be present at 1000 yr following permanent closure; provided that this requirement does not apply to any radionuclide which is released at a rate less than 0.1 percent of the calculated total release rate limit. The calculated total release rate limit shall be taken to be one part in 100,000 per yr of the curie inventory of radioactive waste, originally emplaced in the underground facility, that remains after 1,000 yr of radioactive decay.)

7.2.1.3 Other design requirements

7.2.1.3.1 Waste package interactions with the emplacement environment

Packages for high-level waste shall be designed so that the in situ chemical, physical, and nuclear properties of the waste package and its interactions with the emplacement environment do not compromise the function of the waste packages or the performance of the underground facility or the geologic setting (10 CFR 60.135(a)(1)).

All the waste package designs involve materials and design configurations that interact with the near-field environment. The in situ chemical,

---

* This criterion, as stated in the GR, is incomplete because it does not include the upper limit of 1,000 yr that may be imposed by the NRC as the minimum time of required substantially complete containment.

** The engineered barrier system performance objective of 10 CFR 60.113 is applied to the waste package as a goal for design purposes and a boundary for performance assessment in the GR.

physical, and nuclear properties are being quantified and evaluated for their effects on the long-term performance of the waste package and the repository. The research and development accomplished to date are described in Section 7.4; future plans for work associated with quantification and evaluation of these interactions are outlined in Sections 8.3.4, 8.3.5.9, and 8.3.5.10.

7.2.1.3.2 Technical feasibility

A waste package design requirement derives from the preclosure siting guidelines (10 CFR 960.5-1(a)(3)). This guideline requires that the repository (and therefore the waste packages produced and emplaced therein) shall be demonstrated to be technically feasible on the basis of reasonably available technology and that the associated costs be reasonable. The specific criteria that follow from these requirements are

1. Processes specified for the fabrication, assembly, closure, and inspection of waste packages shall be based on reasonably available technology. These processes need not be reduced to commercial practice in all applicable details but shall not require significant extensions of the technology.

2. Waste package designs shall not impose requirements on the repository packaging, handling, and emplacement facilities, equipment, or operations that are beyond reasonably available technology.

3. In evaluation of design concepts, materials, and process alternatives, consideration shall be given to cost effectiveness. This consideration shall be secondary to realization of designs that will be technically conservative and meet the regulatory performance objectives.

7.2.1.3.3 Waste form temperature limitation criteria

Maximum temperature of the waste forms must be maintained below limits established for them. These limits are 500°C for West Valley (WV) and Defense High-Level Waste (DHLW) glass and 350°C for spent fuel cladding. These values are considered conservative for the following reasons. For spent fuel, the spent fuel storage program report (Einziger, 1988) indicates a 380°C temperature limit for the cladding. A more conservative value of 350°C has been selected to account for uncertainties in source characteristics as well as heat transfer calculations. For the glass waste forms, the NNWSI Project has the responsibility to maintain the peak temperature below the transition temperature. The NNWSI Project has established a 500°C temperature limitation for this reason.

These limitations have been established by the NNWSI Project to reduce the potential for degradation of the waste forms. The limit for high-level waste glass has been determined to prevent devitrification, which might degrade the properties that are important in limiting radionuclide release.

The limit for spent fuel has been determined to limit degradation of the fuel cladding, which could compromise its integrity (O'Neal et al., 1984).

7.2.1.3.4 Inert cover gas in spent fuel packages

An inert gas is to be introduced to replace ambient air in the void volume of all spent fuel waste packages. This requirement is imposed to reduce the potential for oxidation of the fuel that may be exposed to the internal container atmosphere by defects in the cladding. Tests reported by the spent fuel storage program (Johnson and Gilbert, 1984) indicate that extended storage at fuel temperatures up to 380°C in an inert gas does not degrade the fuel or the cladding.

7.2.2 WASTE FORMS

The reference waste forms to be received, packaged, and disposed of in the repository are described in Appendix B, Section B.1 of the Generic Requirements for a Mined Geologic Repository (GR) (DOE, 1984). This appendix describes characteristics such as waste types and forms, repository capacity, receipt rates, spent-fuel age and burnup distribution, physical dimensions, and output characteristics such as decay heat and radiation. The relevant parts of this information are included in the tables in Section 7.3.1, along with additional descriptions of the important variations in the waste forms and the effects that these variations have on the reference designs.

7.2.3 WASTE PACKAGE COMPONENT PERFORMANCE ALLOCATION

For the purpose of allocating performance, the waste packages consist of two components: waste forms (including any structures, canisters, or other means of encapsulation or stabilization) and containers that surround an individual waste form). In addition, since assembled and emplaced waste packages are the "product" of the repository subsystem, some aspects of the preclosure performance must be allocated to the repository facilities, equipment, and operational procedures.

7.2.3.1 Preclosure performance

The preclosure performance of the waste packages in response to the design requirements is allocated as discussed below. The impact of this preclosure requirement allocation on waste package design must be evaluated to ensure that the postclosure performance is not compromised.

Waste package handling. The container is designed to be handled with repository equipment and to provide containment of the waste forms under normal handling loads during transportation (at the repository), emplacement, and retrieval. Under accident loads, the waste package as an entity will

assist in the containment of radionuclides but is not designed to provide complete containment under all conditions. The repository facilities and equipment will be designed to provide the containment capability under these conditions.

Criticality control. The waste form geometry and internal container environment combined provide the control, including the required 5 percent margin, under normal conditions once the waste package is assembled (O'Neal et al., 1984). Before final assembly, the waste forms are subcritical unless aggregated and moderated to produce a critical arrangement. The repository facilities and equipment will be designed to preclude this arrangement.

Identification. Each container will provide a means of identification on the end with the lifting fixture. This identifier will be designed to be legible until repository closure and will be traceable through the repository record system to determine the identity of the contained waste forms. Traceability of the waste form identities before waste package assembly will be maintained by the repository operational procedures.

Reactive materials and free liquids. The waste forms, as described, will meet the constraints with the possible exceptions of water present inside failed fuel cladding and pyrophoric fine particulates of some nonfuel hardware components. Additional information on these possible exceptions will need to be obtained from the spent fuel owners as part of the documentation of fuel characteristics.

Waste form release control (Preclosure). For spent fuel, the requirements for acceptance are defined in the Standard Contract for Disposal of Spent Nuclear Fuel and/or High Level Radioactive Wastes (10 CFR Part 961). These contracts between the DOE and the spent fuel owners do not contain any requirement for spent fuel design or condition other than categorization into one of several classes and furnishing documentation to identify and describe the fuel. For the reprocessed wastes from DOE defense program sources, the waste form requirements are the subject of waste acceptance preliminary specifications that have been developed by the DOE Office of Civilian Radioactive Waste Management (OCRWM). Similar requirements are being developed for reprocessed wastes from commercial sources. The intent of this release control requirement will be included in the specifications for both West Valley commercial wastes and defense wastes from the Savannah River Plant. The waste acceptance process has not been initiated for other reprocessed wastes.

Container handling and shipping. The intent of the specific requirement and performance criterion defined for the waste package container and repository handling equipment will be incorporated into the design to be compatible and allow for all anticipated loads. The container will provide for a unique identifier that will provide traceability of the package contents through the repository records system.

Reasonably available technologies. The container will be designed so that it can be fabricated, assembled, closed, and inspected using reasonably available and cost-effective processes. Additional discussion of this topic is in Section 7.3.1.4.

Waste form temperature limitations. The waste package as an entity will be designed to control the internal temperatures to less than the limits under anticipated postemplacement conditions. The repository packaging, storage, and transfer facilities and equipment will provide sufficient heat dissipation to maintain the waste forms below the limits between receipt and emplacement. In addition, because the peak waste form temperatures following emplacement will occur during the preclosure period (typically within 5 to 10 yr after emplacement) the repository emplacement geometry will be designed to ensure that the temperature limits are observed.

7.2.3.2 Postclosure performance

The allocation of postclosure performance to components of the waste package and the engineered barrier system was not completed at the time that the conceptual designs described in this chapter were developed. Therefore, no quantitative allocation is presented here.

The postclosure performance of the waste package is intimately related to the anticipated near-field environmental conditions, because they are perturbed by the engineered features of the repository and the imposed thermal and radiation effects resulting from the waste emplacement. The status of the understanding of the environment is contained in Sections 7.1 and 7.4.1. The response of the package components to the environment will determine the postclosure performance. The research on response of the package components to the environment is described in Sections 7.4.2 and 7.4.3, and the approach to be used in assessing the package performance is discussed in Sections 7.4.4 and 7.4.5.

The strategy to be used in meeting the postclosure performance requirements and the design goals for future waste package and engineered barrier system design activities are discussed in Sections 8.3.4.2, 8.3.5.9, and 8.3.5.10.

7.3 DESIGN DESCRIPTIONS

In this section, the NNWSI Project waste package reference and alternate conceptual designs are described. These design concepts have evolved over time as the characteristics of the waste forms to be received and disposed at the repository have become better defined; the anticipated geologic, hydrologic, and geochemical properties of the repository have been characterized by laboratory and surface-based field investigations; and the conceptual design of the repository has been developed.

Section 7.3.1 discusses the reference designs, including waste forms, container materials, package designs, and fabrication processes. The alternative designs are described in Section 7.3.2. Finally, Section 7.3.3 briefly discusses other waste emplacement hole components that have potential impact on waste package performance.

The reference waste package emplacement environment is described in Section 7.1. The repository conceptual design is summarized in Chapter 6 and further described in the Site Characterization Plan-Conceptual Design Report (SCP-CDR) (SNL, 1987).

7.3.1 REFERENCE DESIGNS

Conceptual designs have been developed for spent fuel and high-level waste packages that represent general configurations and design concepts (O'Neal et al., 1984). Subsequent to that report, several modifications, primarily to internal geometries and stabilizing structures for various spent fuel loading configurations, have been evaluated.

The characteristics of the reference waste forms are described in Section 7.3.1.1 and the metal container materials in Section 7.3.1.2. Section 7.3.1.3 describes the reference waste packages, including their dimensions, internal configurations to accommodate the various waste forms, and their associated thermal decay heat and radiation characteristics. The processes that may be used for fabricating and assembling the waste package containers and the criteria for process selection based on performance are discussed in Section 7.3.1.4.

7.3.1.1 Reference waste form descriptions

Waste forms to be received and packaged for disposal will include both unreprocessed spent fuel from commercial power reactors and canisters of solidified high-level wastes from commercial and defense fuel reprocessing operations. The commercial high-level waste will be received from the West Valley Demonstration Project in New York (WVHLW). High-level wastes from the defense program activities at Savannah River, Hanford, and Idaho may be disposed of in the repository. Characteristics of the waste from the Defense Waste Processing Facility (DWPF) at the Savannah River Plant have been established; definitive information is not yet available for defense wastes from the Hanford and Idaho sites (DOE, 1984).

7.3.1.1.1 Spent fuel

For the purposes of this document, spent fuel is the enriched uranium oxide, the transuranic nuclides, and the fission and activation products resulting from operation of commercial light water power reactors (LWR) and the zirconium alloy or stainless steel cladding, which also contains activation products. Spent fuel may be received at the repository either as intact assemblies or canisters of fuel rods that have been consolidated at the reactors or other facilities. Intact assemblies include many other metallic components, such as end fittings, flow channels, guide tubes, springs, and spacer grids. These nonfuel hardware components will also be packaged for repository disposal. A summary of the quantities of spent fuel expected to

be received at the repository is given in Section 6.1.1. After the repository startup phase, a receipt rate of 3,000 metric tons of uranium (MTU) per yr is anticipated. Table 7-2 gives a tabulation of the anticipated burnup distribution and age at repository receipt of spent fuel as a function of time from 1998 to 2020.

Standard spent fuel is defined in 10 CFR Part 961, the Standard Contract for Disposal of Spent Nuclear Fuel and/or High-Level Radioactive Wastes, as spent fuel with a minimum age of 5 yr after discharge from the reactor. The Standard Contract specifies that the DOE will accept fuel for disposal on an oldest-first basis. During the early yrs of the repository receiving and emplacement period, the average spent fuel age will be greater than 10 yr. This average age will steadily decline and will be down to the 5-yr minimum during the last several yr of operation. The waste package and repository designs must be capable of receiving and disposing standard spent fuel on a routine basis. Fuel cooled less than 5 yr will remain in the transportation and storage system. Table 7-3 presents typical characteristics of 5- and 10-yr old spent fuel to be received at the repository (DOE, 1984).

The burnup of LWR fuel is expressed as the fission (thermal) energy released per unit of initial uranium weight loaded into a reactor core. A commonly used unit is megawatt-d per metric ton uranium (MWd/MTU). The build-up of fission products in the fuel is proportional to the energy generated in the reactor. These fission products and the actinides formed by neutron capture reactions are the principal sources of radioactivity in spent fuel. Thus the spent fuel burnup, together with the fuel age, determines the radionuclide inventory. Radioactive decay of this inventory produces the thermal energy that must be dissipated in the repository.

Fuel in pressurized water reactor (PWR) and boiling water reactor (BWR) assemblies is presently enriched to about 3.2 and 2.6 weight percent fissile U-235, respectively, and is irradiated to achieve burnups of 33,000 and 27,500 MWd/MTU, respectively (DOE, 1984). As nuclear power plants have matured, the average burnup of spent fuel assemblies has increased toward this value. The evolving economics of the nuclear power industry has produced an incentive to increase enrichments to allow higher burnups. A recent survey of fuel vendors (DOE, 1984) indicated that approximately two-thirds of the present United States nuclear power plants have made commitments toward the purchase of fuels with higher enrichments to allow longer fuel residence times in reactor cores, which will result in higher burnups.

As the repository operation draws down the backlog of spent fuel at reactors, the average burnup of the annual receipts will tend to increase, since the lowest burnup fuel is also generally the oldest in storage (DOE, 1984). Thus, the overall average of spent fuel burnup received for disposal is expected to show a generally increasing trend over the life of the repository, and individual assemblies with burnups substantially exceeding the average may be anticipated. For an industry-predicted average PWR fuel burnup of 35,000 MWd/MTU in 2020, a number of cases in excess of the average would occur. If a PWR plant were to discharge a batch of fuel with an average burnup of 42,000 MWd/MTU, a small number of assemblies would be expected to be as high as 60,000 MWd/MTU (DOE, 1984).

Table 7-2. Spent fuel burnups and ages at emplacement normalized to Energy Information Agency (EIA), 1983 midcase projections[a]

Discharge year	Burnup (MWD[b]/MTU) vs. year is MTUs: 0-5000 BWR	0-5000 PWR	5000-10000 BWR	5000-10000 PWR	10000-15000 BWR	10000-15000 PWR	15000-20000 BWR	15000-20000 PWR	20000-25000 BWR	20000-25000 PWR	25000-30000 BWR	25000-30000 PWR	30000-35000 BWR	30000-35000 PWR	35000-40000 BWR	35000-40000 PWR	40000-45000 BWR	40000-45000 PWR	45000-50000 BWR	45000-50000 PWR	50000-55000 BWR	50000-55000 PWR	Age (yr) at emplacement	Receipt yr	Total BWR	Total PWR	Total	MTU	Cumulative MTU
1961																							37	(1998)				4*	4
1962																							36	(1998)				6*	10
1963																							35	(1998)				10*	20
1964																							34	(1998)				11*	31
1965																							33	(1998)				11*	42
1966																							32	(1998)				11*	53
1967																							31	(1998)				11*	64
1968																							30	(1998)				11*	75
1969					1		7				8												29	(1998)	8	8		16	91
1970								41		8													28	(1998)		49		49	140
1971			14		6	5					40												27	(1998)	20	45		65	205
1972	142		13		31	8	4	45			8		22										26	('98-'99)	189	84		273	478
1973	8		18		36		40	24			40												26	(1999)	101	64		165	643
1974	60		6	7	122	77	31	40	4	14	74												25	('99-'00)	223	212		435	1078
1976			1	9	46	186	156	12	32	71	41		20										25	('00-'01)	224	339		563	1641
1976			49		108	17	148	147		84	91		37										25	('01-'02)	306	376		682	2323
1977			52		34		174	132	102	126	134		86		18								25	(2002)	362	496		858	3181
1978				2	35	51	118	78	208	45	28	402	73		62								24	('02-'03)	438	713		1151	4332
1979					20	26	92	124	161	55	176	279	230		32								24	(2003)	451	755		1206	5538
1980	15				3	9	46		262	56	110	304	228		29								23	(2002)	526	623		1149	6687
1981						26	73		256		162	304	428		16								22	('03-'04)	491	774		1265	7952
1982					15		41	80	30	88	300	161	361		13								22	(2004)	386	704		1090	9042
1983							36	48	42	48	292	296	220	16	51								21	('04-'05)	384	644		1068	10108
1984	14		9		13	52	3	41	49	16	262	118	412	14	94		3						21	(2005)	384	736		1100	11200
1985			55		52	21	15	70	25	11	248	205	380		193		24						20	(2006)	396	904		1300	12500
1986	14		62		57	46	60	127	7	52	382	107	245		266		28						19	(2006)	629	871		1500	14000
1987	20		23		34	50	102	48	127	27	256	123	378	13	340		22						18	(2006)	583	1017		1600	15600
1988			23		90	2	120	80	84	18	514	186	406	44	417		107						18	(2006)	904	1296		2200	17800
1989			44		24	27	41	27	150	64	398	185	518	501	435		96				1		17	(2006)	785	1315		2100	19900
1990			30		15		66	27	31	18	480	93	218	542	460		119						17	(2007)	841	1259		2100	22000
1991			3				47		29	46	808	104	226	629	618		190						16	(2007)	1113	1587		2700	24700
1992					3		3		152	1	470	100	272	771	598		139		1				16	(2008)	900	1600		2500	27200
1993							44	60	27	7	740	63	230	594	703		122		1				15	(2009)	1050	1550		2600	29800
1994									64	7	640	63	256	860	553		157						15	(2009)	960	1640		2600	32400
1995									50		699	73	225	825	592		135		1				14	(2009)	974	1626		2600	35000
1996									70	8	790	32	393	815	731		160		1				14	(2010)	1253	1747		3000	38000
1997									64	7	572	38	355	871	717		175		1				13	(2010)	991	1809		2800	40800
1998									56		806	71	173	848	586		169		1				13	(2011)	1125	1675		2800	43600
1999				21					86	30	638	31	370	849	728		155		1				13	(2011)	1085	1815		2900	46500
2000	1						6		31		758	41	366	1022	597		158						12	(2012)	1182	1818		3000	49500
2001						11			117	10	743	87	300	882	841		208		1				11	(2012)	1160	2040		3200	52700
2002									71	8	916	33	403	853	746		169		1				11	(2013)	1360	1810		3200	55900
2003									33		657	48	506	1167	867		219		1				10	(2013)	1198	2302		3500	59400
2004			36			27	45		109	37	844	81	281	1029	711		199		1				10	(2014)	1315	2085		3400	62800
2005									38		1120	42	516	1040	966		178		1				9	(2014)	1673	2227		3900	66700
2006		4	32	50		14	48	40	34	60	611	50	529	1127	863		228		1				9	(2015)	1254	2446		3700	70400
2007	14	17	87	56		66	93	91	114	118	1009	121	285	982	752		194		1				9	(2016)	1602	2398		4000	74400
2008	20	5	177	49	49	128	204	28	119	68	715	157	427	820	787		186		1				8	(2016)	1711	2189		3900	78300
2009		12	124	83				122	41	271	788	2	428	1120	773		236						8	(2017)	1381	2619		4000	82300
2010		18		61	37	67	144	73	80	142	910	45	273	1132	575		142		1				8	(2018)	1444	2256		3700	86000
2011				42		61		103	58	106	1236	2	481	1381	867		142		2				7	(2018)	1775	2725		4500	90500
2012		12	34	18	34	48		131	83	79	810	22	600	1216	754		167		2				7	(2019)	1551	2449		4000	94500
2013	42		160			50	160		196	83	1065	2	417	1318	787		178		2				6	(2020)	2070	2430		4500	99000
2014	34	9		43	188	90		1	244	136	1122	31	560	1100	804		110		2				6	(2020)	2157	2343		4500	103500
2015		3		83	272			63	333	166	868	83	632	1606	838		143						6	(2021)	2135	2965		5100	108600
2016			265	122	81	75	321		156	161	1225	75	277	1627	662		203						5	(2021)	2325	2975		5300	113900
2017	26			62	137			98	218		1140		404	1375	958		82						5	(2022)	1925	2575		4500	118400
2018									107		1214		547	2271	847		214						5	(2023)	1868	3332		5200	120600
2019			109		109		111		210		1501		198	1945	838		188						5-6	(24-25)	2328	2872		5300	128800
2020		27	111			129	164		113	128	1204		364	1613	1053		93						6-7	(25-27)	1956	3044		5000	133900

[a] Source is DOE (1984).

[b] MWD = megawatt-days; MTU = metric tons of uranium; BWR = boiling water reactor; PWR = pressurized water reactor.

Table 7-3. Characteristics of spent-fuel assemblies[a]

Characteristic	Pressurized water reactor	Boiling water reactor
MECHANICAL CHARACTERISTICS		
Overall length (in.)	149-186	84-179
Width (square assemblies) (in.)	8.1-8.5	4.3-6.5
Fuel rods per assembly	100-264	48-81
Fuel rod diameter (in.)	0.360-0.440	0.483-0.570
Fuel rod length (in.)	91.5-171	80.5-165
Rod pitch (in.)	0.496-0.580	0.640-0.842
MTU[b] per assembly	0.11-0.52	0.19-0.20
Assembly weight (lb)	1280-1450	600
TYPICAL CHARACTERISTICS AS RECEIVED		
FIVE-YEAR FUEL[c]		
Burnup (average conditions) MWd/MTU	33,000	27,500
Actinides and daughters (Ci/MTU)	104,000	93,000
Fission products (Ci/MTU)	453,000	365,000
Decay heat (W/MTU)	1,800	1,400
Photon release (photons/s/MTU)	1.3×10^{16}	1.0×10^{16}
Photon energy release (Mev/s/MTU)	4.8×10^{15}	3.6×10^{15}
Burnup (high condition) MWd/MTU	50,000	
Actinides and daughters	155,000	
Fission products (Ci/MTU)	640,000	
Decay heat (W/MTU)	2,800	
Photon release (photons/s/MTU)	1.9×10^{16}	
Photon energy release (Mev/s/MTU)	7.3×10^{15}	
TEN-YEAR FUEL[d]		
Burnup (average conditions) MWd/MTU	33,000	27,500
Actinides and daughters (Ci/MTU)	83,000	75,000
Fission products (Ci/MTU)	302,000	249,000
Decay heat (W/MTU)	1,100	900

Table 7-3. Characteristics of spent-fuel assemblies[a] (continued)

Characteristic	Pressurized water reactor	Boiling water reactor
Photon release (photons/s-MTU)	7.7×10^{15}	6.2×10^{15}
Photon energy release (Mev/s/MTU)	2.6×10^{15}	2.0×10^{15}
Burnup (high condition) MWd/MTU	50,000	
Actinides and daughters	124,000	
Fission products (Ci/MTU)	442,000	
Decay heat (W/MTU)	1,800	
Photon release (photons/s/MTU)	1.1×10^{16}	
Photon energy release (Mev/s/MTU)	3.8×10^{15}	

[a]Modified from DOE (1984).
[b]Metric tons of uranium.
[c]Spent fuel out of reactor for five years.
[d]Spent fuel out of reactor for ten years.

Spent fuel may be received at the repository in at least three forms. The majority will be in the form of intact assemblies that contain undamaged fuel rods. Some of these fuel rods may have minor cladding breach defects, but would not be structurally damaged to the extent that the fuel is not safely contained. The second form is fuel that has been preconsolidated by being disassembled at the reactors or other facilities, with the rods packaged in canisters whose dimensions approximate those of an intact assembly. The reference consolidation factor is 2:1 (i.e., a canister contains the fuel rods from two fuel assemblies). No reference form for the configuration of nonfuel hardware resulting from these preconsolidation operations has been established. Hence, no provisions have been made for this material in the conceptual designs for either the waste package or repository surface facilities. The third form in which spent fuel is expected to be received is "failed fuel" that has been structurally damaged to the extent that the fuel assemblies must be placed in a canister to contain the particulate fuel materials during handling and shipment from the reactor. No reference dimensions have been established for this category, but it is assumed that the canisters will be only slightly larger than the assemblies they contain.

The reference form for disposal of spent fuel is fuel rods that are removed from intact assemblies and consolidated at the repository. The option of disposing of intact spent fuel assemblies as they are received is retained in the reference design because it may not be possible to consolidate assemblies that are received at the repository in a damaged or failed condition. In addition, current planning envisages loading fuel with very

high burnup and short cooling times into containers as intact assemblies in quantities dictated by the waste form temperature limitations.

There is a wide variety of PWR and BWR fuel rod and fuel assembly dimensions. Limits are shown in Table 7-3 (DOE, 1984).

7.3.1.1.2 High-level wastes

High-level radioactive wastes from the West Valley Demonstration Project (WV) and the Defense Waste Processing Facility (DWPF) will be received in solidified form. The radionuclides will be immobilized in a borosilicate glass matrix contained in 304L stainless steel pour canisters. The 61-cm-diameter, 3.0-m-long pour canisters are nominally 1-cm-thick 304L stainless steel and essentially identical for both WV and DWPF (DOE, 1984). because of concerns that the thermal cycles associated with the glass-pouring operation will result in the pour canisters being highly stressed (Baxter, 1983), the pour canisters will not be used as the primary barrier to meet the containment performance objective.

7.3.1.2 Reference container materials

The reference waste package container material for the current conceptual design is AISI 304L stainless steel. The reference alloy system is 300 series austenitic stainless steel and alloy 825, a high nickel, iron-based austenitic alloy. Potential candidate metals initially considered for the reference material included the following alloy groups: austenitic stainless steels, ferritic stainless steels, duplex stainless steels, high-nickel alloys, titanium alloys, zirconium alloys, copper-nickel alloys, low-carbon steels, and cast irons (Russell et al., 1983). Section 7.4.2 has additional details on the candidate alloy selection. The chemical compositions of three alloys in the reference alloy system are given in Table 7-4; a comparative listing for several physical properties of these materials is presented in Table 7-5 (ASTM, 1982).

7.3.1.3 Reference waste package designs

The reference waste packages are designed as thin-walled right circular cylinders with end closures and a lifting fixture on one end. The metal containers are 66 cm diameter with a nominal wall thickness of 1 cm. The diameter was determined on the basis of the geometry of the waste forms and their thermal limitations. The wall thickness is based on structural and handling considerations as well as material degradation rates (Section 7.4.2). The length will vary from about 3.1 to 4.7 m, depending on the waste form dimensions. The total package weights will range from 2.7 to 6.4 metric tons, depending on the quantities and types of wastes in the package.

Table 7-4. Alloy compositions for candidate container materials in reference alloy systems[a]

Common alloy designation	UNS[b] designation	Chemical composition (wt % percent)[c]							
		Carbon	Manganese	Phosphorous	Sulfur	Silicon	Chromium	Nickel	Other element
304L	S30403	0.030	2.00	0.045	0.030	1.00	18.00-20.00	8.00-12.00	N: 0.10 max
316L	S31603	0.030	2.00	0.045	0.030	1.00	16.00-18.00	10.00-14.00	Mo: 2.00-3.00 N: 0.10 max
825	N08825	0.05	1.0	Not specified	0.03	0.5	19.5-23.5	38.0-46.0	Mo: 2.5-3.5 Ti: 0.6-1.2 Cu: 1.5-3.0 Al: 0.2 max

[a]Information adapted from ASTM specifications A-167, B424 (ASTM, 1982).
[b]UNS designation from Unified Numbering System for Metals and Alloys (SAE, 1977).
[c]The values given are maximums except where ranges are given.

Table 7-5. Representative mechanical properties for candidate container materials in reference alloy systems[a,b]

Alloy designation	Tensile strength MPa	Tensile strength psi	Yield strength MPa	Yield strength psi	Elongation percent	Reduction of area percent
304L (annealed)	483	70,000	170	25,000	40	40
316L (annealed)	483	70,000	170	25,000	40	40
825 (annealed)	586	85,000	241	35,000	30	ND[c]

[a]Information adapted from American Society for Testing and Materials specifications A-167, B-424 (ASTM, 1982).

[b]Minimum values are given.

[c]ND--no data specified.

For spent fuel containers, an internal structure will provide mechanical stability and facilitate loading operations. For repository-consolidated rods, preconsolidated rod canisters, or intact assemblies, the internal structure will consist of an array of internal modules fabricated from 304L stainless steel sheet metal 3 to 6 mm thick.

Figure 7-2 depicts the reference designs for a spent fuel disposal container that includes the internal configurations to accept both consolidated pressurized-water reactor (PWR) and boiling-water reactor (BWR) fuel rods and intact assemblies.

The reference waste packages include an internal structure that is configured to accommodate the rods from 6 PWR (configuration 1) or 18 BWR (configuration 2) assemblies. The configurations place the fuel rods in sectors around the perimeter of the container, with the central hexagonal space reserved for placement of compacted nonfuel hardware resulting from consolidation operations at the repository. With effective compaction, this space will accommodate the hardware from all the assemblies whose fuel rods are in the package. There is no requirement that the hardware from the same assemblies as the fuel rods be placed in a common container. This internal configuration (configuration 3) will accept six square canisters of BWR fuel rods that have been preconsolidated (2:1) before receipt, or six intact BWR assemblies. A variation of the internal structure (configuration 4) will accept three canisters of preconsolidated PWR fuel rods, or three intact PWR assemblies. The container can be fabricated to a length to accommodate fuel rods or assemblies of varying lengths, or the container length may be modified to a few standard lengths to match the fuel dimensions.

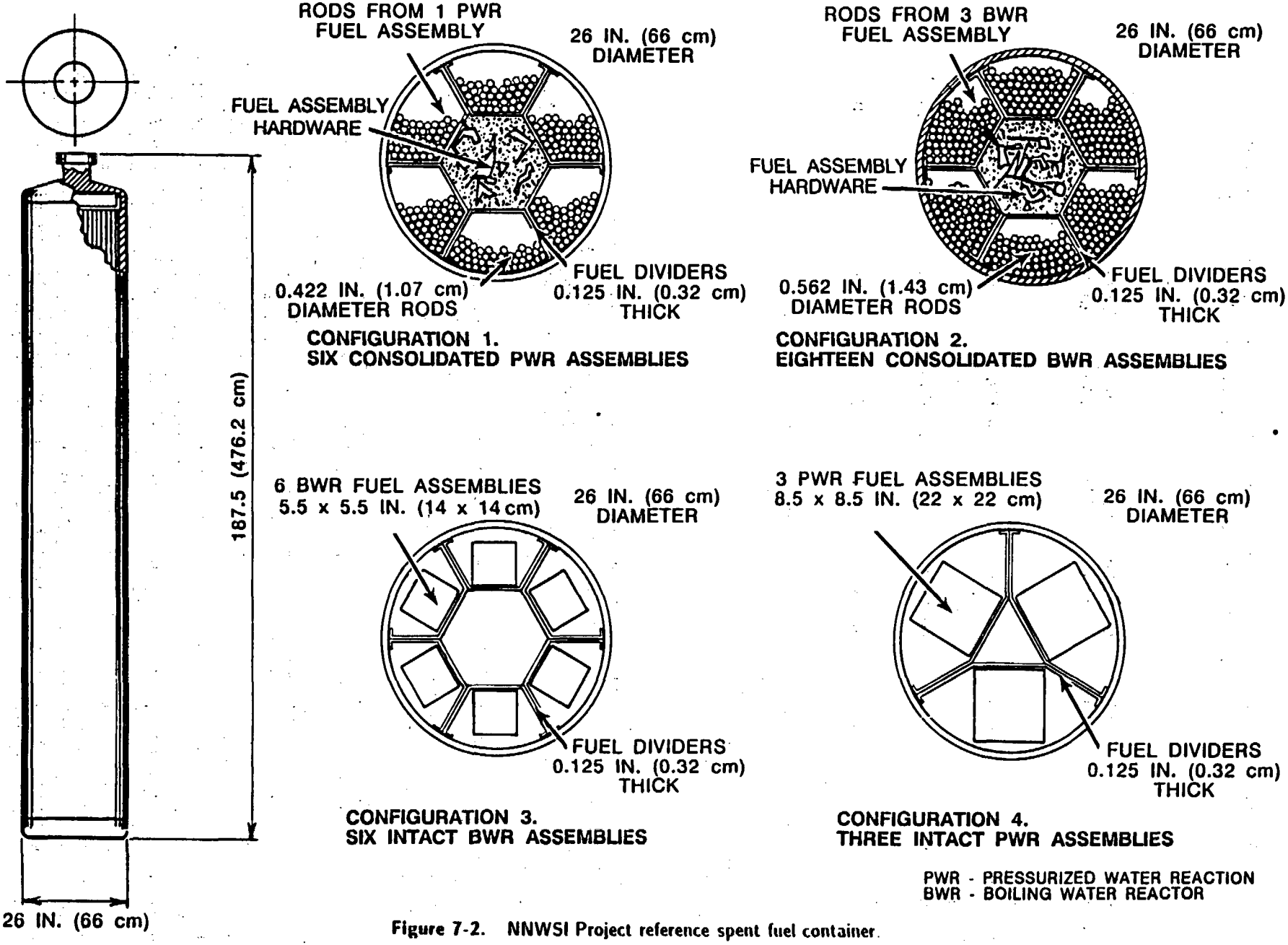

Figure 7-2. NNWSI Project reference spent fuel container.

All waste packages containing spent fuel will be filled with an inert cover gas before final closure. The design concept is to use argon as the cover gas. A small amount of helium may be included if it would be useful in closure integrity inspection.

Spent fuel packages containing nominal burnup, 10-yr-aged PWR or BWR consolidated fuel will have a thermal decay power of about 3.3 kW, based on the reference configuration (Figure 7-2) and the decay heat values from Table 7-3. Initial repository receipts of low burnup fuel aged about 27 yr would result in packages in the reference configuration with power levels of about 1.0 to 1.2 kW. Five yr minimum age high burnup BWR fuel would result in a power level of about 4.5 kW per package. This package design cannot be fully loaded with high (50,000 megawatt-d per metric ton uranium (MWd/MTU) burnup PWR fuel because this would result in a package power level of about 7.9 kW. The heat dissipation characteristics of this package configuration limits it to a maximum thermal power of approximately 5 kW per container. This limit results from the waste form temperature limitation criteria, discussed in Section 7.2.1.3. Thus in the later yrs of repository operation when high burnup, short-cooled PWR fuel will be received, the configuration that accepts intact PWR assemblies would be used. It would have a maximum package power level of about 4.0 kW. As indicated earlier, power per package will vary depending on age, burnup, and quantity of fuel in the package. The gamma dose rate at the outer surface of the package is expected to be approximately 5×10^4 rads/h for the nominal burnup 10-yr-aged fuel. This dose rate will scale approximately linearly with the thermal power output of the package. The neutron dose rate is expected to be about 1×10^4 neutrons/cm^2/s.

The reference waste package design for West Valley (WV) and Defense Waste Processing Facility (DWPF) high-level waste (HLW) is shown in Figure 7-3. This design includes a disposal container very similar to the reference spent fuel container. The 61-cm-diameter WV/DWPF pour canister filled with the glass waste form is installed in a 66-cm-diameter container that is fitted with minimal stabilizers to provide mechanical restraint during handling operations. There is no requirement for the HLW packages to contain an inert cover gas. The reference HLW package design will have a thermal power level in the range of 200 to 470 W, depending on the source and age of the reprocessing wastes in the glass matrix. The gamma radiation dose rate at the outer surface of the package will be about 5.5×10^3 rads/h. The neutron dose rate will be very low.

7.3.1.4 Container fabrication and assembly processes

A number of processes are available for fabricating the component parts of the waste package containers. These range from very conventional and widely used to recently developed, advanced metal-forming processes. An example of the former would be forming the cylindrical body by rolling flat plate and welding the longitudinal seam. The end closures could be cut from flat plate and conventionally welded to the body. More advanced processes include integral forming of the body and end closure by double extrusion, centrifugal casting, or various combinations of forging, drawing, spinning, etc. The top closure, including the lifting fixture and unique identifier,

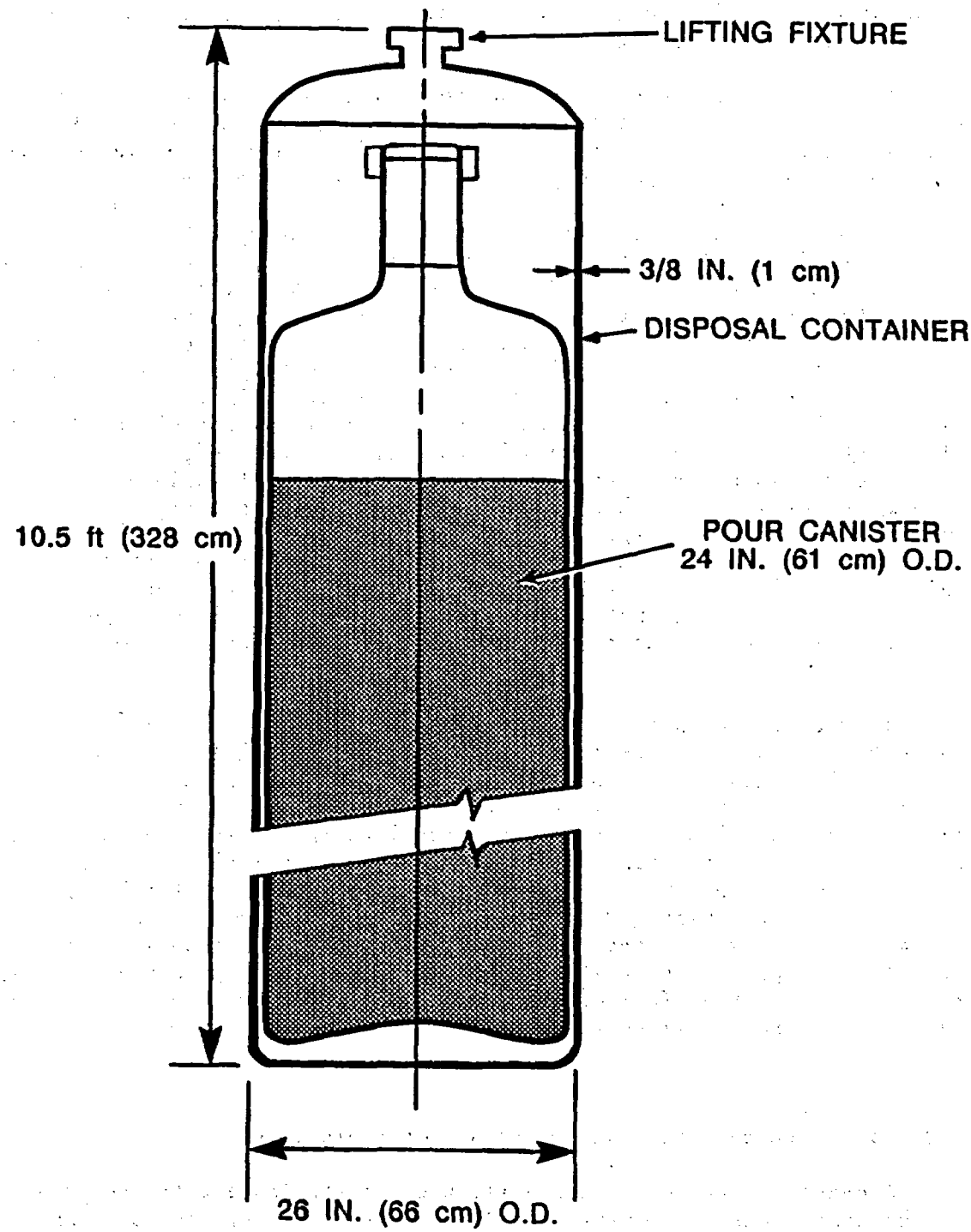

Figure 7-3. NNWSI reference West Valley and defense high-level waste package.

can be fabricated in separate pieces and joined or integrally formed by machining, forging, or casting processes. Following the forming and joining operations, the container components can be machined and/or heat treated as appropriate. Any of the conventional inspection and nondestructive evaluation (NDE) techniques can be used to verify the quality of the components. These fabrications will be produced and inspected at commercial facilities to comply with approved specifications. Finished components will be supplied to the repository for loading the waste forms and for final assembly and inspection.

The final assembly and closure of the container after loading with the waste form requires a metal-joining process. A number of potential processes are available; these range from seal-welded threaded joints to a wide variety of conventional welding processes such as gas metal arc to advanced autogenous techniques such as laser or friction welding. This closure will be made in shielded repository surface facilities. The process must be amenable to remote operation with very high reliability and low maintenance. The completed joint must also be capable of inspection by NDE techniques. The NDE technique must also be amenable to remote operation in a highly radioactive environment with high reliability and must minimize false-positive indications that would result in unnecessary rework.

Fabrication and closure processes have not been selected. The selections will depend on the details of the design as it evolves during the advanced conceptual and license application design phases. The primary criteria for process selections will be based on optimization of the long-term performance of the containers in the repository environment. This will require evaluation of the processes for ability to produce assemblies with high structural integrity, homogeneous metallurgical microstructures, and minimum residual stresses. Other criteria will include consideration of demonstrated reliability, amenability to inspection and flaw detection, flexibility to accept design modifications, vendor availability, production capacity, and cost effectiveness. Plans for evaluation, selection, and development of fabrication, closure, and inspection processes are described in Section 8.3.4.4.

Waste package assembly processes are obviously dependent on the type and geometric configuration of the waste form being packaged. Loading procedures for repository consolidated spent fuel will entail insertion of the spent fuel rods, either vertically or horizontally, into a container with a preassembled internal structure. For canistered preconsolidated spent fuel, or intact spent fuel assemblies, the individual canisters or assemblies will be inserted into the disposal container. After the inert cover gas is introduced, the final closure will be made. The WV/DWPF waste canisters will be loaded into the containers and the final container closure and inspection will be completed. Provision will be made for disassembly and transfer of the contents of completed containers that fail final inspection. Containers suspected of being damaged in handling at the repository after final inspection is completed would be reinspected and, if appropriate, disassembled, and the contents would be transferred to new containers. Additional descriptions of the packaging processes and flow sequences in the repository are found in Section 6.2.3.

7.3.2 ALTERNATIVE DESIGNS

Prior to selection of the reference alloy system for the waste package container material, a number of potential candidate metals were initially considered (Russell et al., 1983). At the time the reference conceptual designs were developed, two alternative designs were also studied. One was a conceptual design using the reference container material for a spent fuel package that supports an alternative disposal strategy for intact fuel assemblies. The other was a conceptual design that changed the container material, based on a feasibility assessment (Acton and McCright, 1986), to a different alloy system, namely a copper-based alloy. Sections 7.3.2.1 and 7.3.2.2 describe the status of these two alternative designs. Waste package design concepts, developed during the ACD phase, will be evaluated as part of the design process described in Section 8.3.4.3.

7.3.2.1 Intact spent fuel package alternative design

At the direction of DOE, the NNWSI Project has evaluated the technical and cost implications of changing the reference strategy for disposal of spent fuel from one using disassembly and consolidation of all possible fuel assemblies to one where all spent fuel received at the repository as intact assemblies is packaged as received without consolidation (O'Brien, 1986).

As an adjunct of this study, an alternative waste package design concept was developed. The approach adopted for this design concept was to retain the basic concepts of the reference design (i.e., a thin-walled cylindrical container with an internal structure to provide support for the contents). Modifications to the external diameter and internal geometry were examined to improve the packing efficiency of nominally square cross-sectional fuel assemblies in a circular cross-sectional container. A further constraint on the design is the mix of PWR and BWR fuel assemblies to be received. This mix averages approximately 40 percent PWR and 60 percent BWR assemblies.

Ideally, the waste package configuration would maintain that mix. The geometry of the situation, however, is best satisfied by the arrangement shown in Figure 7-4 as configuration 1, which places three PWR and four BWR fuel assemblies in an array. This so-called hybrid package concept leads to a surplus of BWR assemblies. Another internal arrangement, within the same 71-cm external diameter, is shown in Figure 7-4 as configuration 2. This places 10 BWR assemblies in the container and provides a means of disposing of the excess BWR assemblies. Only about 7 percent of the total number of packages would need to be of this all-BWR configuration to accommodate the excess number of assemblies.

For nominal burnup, 10-yr aged fuel, these packages would have power levels of 2.3 and 1.6 kW, respectively, for the hybrid and all-BWR configurations. These power levels would vary from about 1.0 to 4.0 kW over the reference ages and burnups projected for spent fuel receipts.

Further development of this package concept will depend on the program guidance resulting from the OCRWM consolidation strategy study in progress.

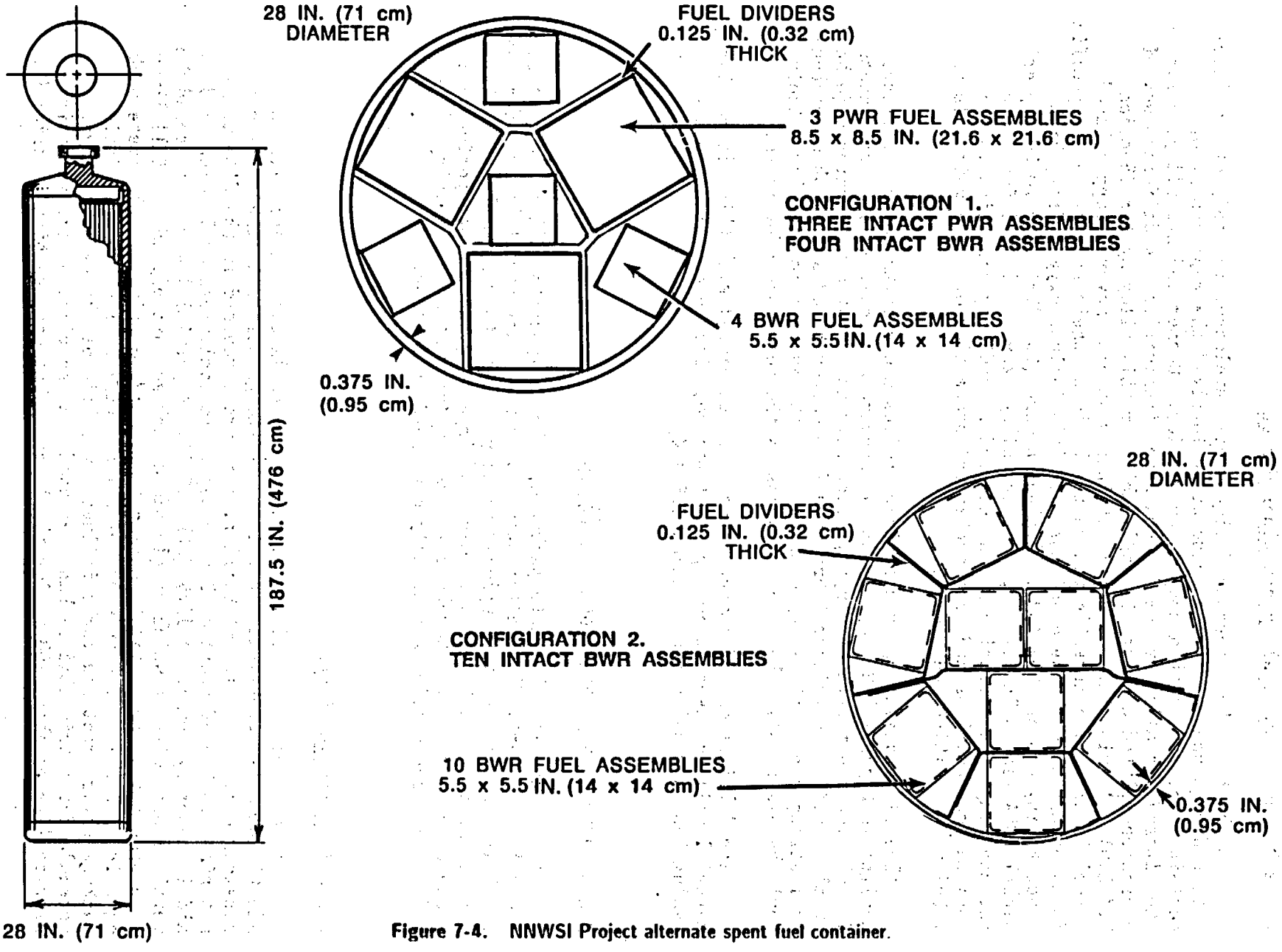

Figure 7-4. NNWSI Project alternate spent fuel container.

7.3.2.2 Copper-based alloy container design

At the time the reference designs were developed, the only other alternative design under active consideration involved the replacement of the container material with a copper-based alloy. Copper and its alloys serve as the alternative alloy system for container fabrication. A different set of corrosion-related concerns is applicable for this alloy system (Section 7.4.2.9). As with the austenitic stainless steels, several copper-based materials are being investigated on the basis of their resistance to specific forms of corrosion. The candidate materials include oxygen-free, high-conductivity copper (CDA 102), aluminum bronze (CDA 613), and 70-30 copper-nickel (CDA 715). The two copper-based alloys were selected for their expected improved corrosion resistance under oxidizing conditions. The chemical compositions and some mechanical properties of these materials are tabulated in Tables 7-6 and 7-7.

The alternative copper container designs are similar to the reference designs in Figures 7-2 and 7-3 but may require a thicker wall to compensate for the lower strength of copper, especially at elevated temperatures (O'Neal et al., 1984). Containers fabricated from copper-based alloys whose mechanical strength properties approach those of the austenitic stainless steels would be essentially the same thickness as the reference containers.

The fabrication and closure processes associated with this alternative material will be assessed as a part of the container production process, evaluation, and selection (Section 8.3.4.4).

7.3.3 OTHER EMPLACEMENT HOLE COMPONENTS

In addition to the waste packages, other components will be present in the reference vertical or alternative horizontal emplacement holes. Because of their proximity to the emplaced waste packages, they have the potential for altering the package environment and impacting the package performance. These other components, borehole liners, emplacement hole shielding plugs, and emplacement dollies are briefly described as follows.

7.3.3.1 Borehole liners

The waste packages will be placed in the emplacement holes with no additional metal containment barriers. Although borehole liners are not considered as a containment barrier, they are discussed in the Site Characterization Plan-Conceptual Design Report to facilitate emplacement and to aid in ensuring retrievability (SNL, 1987). A partial liner is proposed for vertical boreholes in which single waste packages are placed. A full liner is proposed for horizontal boreholes that would contain multiple waste packages in each hole. The presence of a liner will modify the near-field package environment and could influence the life of the waste package. A schedule for retrievability has been used that requires a nominal design service life of about 100 yr for the liners. The construction material for

Table 7-6. Alloy compositions for candidate container materials in the alternative alloy systems[a]

Alloy designation	UNS designation[b]	Chemical composition (wt %)							
		Cu	Fe	Pb	Sn	Al	Mn	Ni	Zn
CDA 102 (Oxygen-free Copper)	C10200	99.95 (minimum)	--[c]	--	--	--	--	--	--
CDA 613 (Aluminum Bronze)	C61300	92.7 (nominal)	3.5 (maximum)	--	0.2-0.5	6.0-8.0	0.5 (maximum)	0.5	--
CDA 715 (70-30 Copper-nickel)	C71500	69.5 (nominal)	0.4-0.7	0.5 (maximum)	--	--	1.0 (maximum)	29.0-33.0	1.0 (maximum)

[a]Compiled from CDA Standards Handbook Data Sheets (CDA, 1986), Copper Development Association, Greenwich, CT.
[b]UNS designation from Unified Numbering System for Metals and Alloys (ASTM, 1982).
[c]-- = Not specified.

Table 7-7. Representative mechanical properties for candidate container materials in alternative alloy systems

Common alloy designation and condition	Yield strength[a] (ksi)	Tensile strength (ksi)	Elongation (percent)
CDA 102			
Hot rolled	10	34	45
Hard	45	50	4
CDA 613			
Soft Annealed	40	80	40
Hard	58	85	35
CDA 715			
Hot rolled	20	55	45
Half hard	70	75	15

[a]0.5 percent extension under load. Compiled from CDA Standards Handbook Data Sheets (CDA, 1986).

the borehole liners will be selected to avoid adverse long-term package performance implications. The liner will probably consist of welded sections having a wall thickness of approximately 0.6 to 1.0 cm based on the expected maximum load imposed by any rock that sloughs from the borehole walls or based upon loads imposed during liner installation.

7.3.3.2 Emplacement hole shielding plugs

Regardless of the emplacement orientation, each emplacement hole will be equipped with a solid plug to prevent radiation streaming from the waste packages into the emplacement drift. The required service life of these plugs and any mating collar hardware is until permanent repository closure. A nominal design lifetime of about 100 yr is therefore appropriate. As with the liners, the construction material of the plugs must not adversely impact the long-term package performance. This is particularly important in the reference vertical emplacement orientation where corrosion products or other plug constituents could fall onto the waste packages under gravity. There will be similar constraints in material selection for the support plate planned for use in the bottom of vertical boreholes.

7.3.3.3 Emplacement dollies

For the horizontal borehole emplacement orientation, a dolly or sled type fixture will be used to permit emplacement of the waste packages without mechanically abrading, gouging, or otherwise degrading the container surface. This fixture will be designed to support the package approximately centered in the liner. This fixture is planned to provide annular air gap around the container and will help avoid contacting the waste package with liquid water should condensation occur on the interior surface of the liner. This fixture will require careful attention to design details and materials of construction to avoid adversely impacting the long-term performance of the package components.

7.4 WASTE PACKAGE RESEARCH AND DEVELOPMENT STATUS

Waste package research and development was conducted as a generic program until 1982. The studies emphasized salt emplacement media, with some work directed toward basalt. No materials performance data directly applicable to tuff as a repository host rock were obtained during the generic phase of the program. In October 1982, the materials testing work was transferred to the site-specific projects. The NNWSI Project waste package development task was then structured to provide data describing the effects of waste emplacement in tuff on the properties of the emplacement environment and on the performance of waste package components in that altered environment. The development of detailed physical and chemical models, which are needed to extrapolate measured performance of materials to the time scales relevant to waste disposal, is considered an integral part of the materials testing work under Issues 1.4 (Section 8.3.5.9), 1.5 (Section 8.3.5.10), and 1.10 (Section 8.3.4.2). The system model to be used to assess performance of the waste package will use the results from the detailed models developed under materials testing tasks, which is a need identified in Issues 1.4 and 1.5.

The status of research and development work needed to describe the post-emplacement history of the waste package environment is discussed in Section 7.4.1. The work on metal barriers is covered in Section 7.4.2. The results of waste form testing using spent fuel and borosilicate glass is summarized in Section 7.4.3. Section 7.4.4 discusses the development of a geochemical modeling code to be used in conjunction with the system model. The final section, Section 7.4.5, briefly describes the performance assessment model of the waste package system.

7.4.1 WASTE PACKAGE ENVIRONMENT MODIFICATION DUE TO EMPLACEMENT

Construction of a repository and emplacement of heat and radiation generating waste in the repository would cause changes in the physical and chemical characteristics of the environment. Design of the waste package and prediction of the performance of the package and its components can only be accomplished if there is a thorough understanding of change with time of the environment as affected by the repository construction and waste emplacement.

Definition of the waste package environment involves detailed description of the preemplacement (ambient) conditions at the proposed repository horizon and determination of the changes that will take place after the waste packages are emplaced. The effects that can be expected from development of the repository and emplacement of the waste packages are (1) physical changes in the rock unit due to mining activities; (2) changes in the physical and chemical properties of the rock and vadose water due to the waste-related radiation field; (3) heat-induced mechanical effects; (4) modification of moisture conditions due to mining ventilation; and (5) modification of the ambient rock-water system and hydrodynamic regime due to the thermal load generated by the waste packages. Research that defines the waste package environment addresses Information Need 1.10.4.

The radiation field from the waste forms will consist of alpha, beta, neutron, and gamma radiation. Alpha and beta radiation will be contained within the waste package because of the short penetration range of these particles. Neutron and gamma radiation will penetrate through the container and interact with the environment in the immediate vicinity of the waste package. Neutrons can cause damage to material by displacing atoms as a result of atomic collisions. The damage from atomic displacements in the host rock minerals would be very small at the flux levels present in the waste forms and would not significantly affect the properties of the material (Grasse et al., 1982; Van Konynenburg, 1984). The neutrons would not significantly affect the water chemistry because the flux would be small (Wilcox and Van Konynenburg, 1981). Gamma radiation interacts with matter by ionization mechanisms. The effects of gamma interaction with tuff largely will be transient and are not expected to cause significant changes in the rock or mineral properties (Durham et al., 1985). Gamma radiation can cause changes in water and vapor chemistry due to the production of radiolytic species. The research conducted in this area is described in Section 7.4.1.4.

The thermal load imposed by the waste packages on the near-field environment will be a function of the waste form and the loading density. The actual thermal output for the spent fuel will depend on burnup history, the time out of reactor, and whether consolidated fuel rods or intact fuel assemblies are stored in the container. Thermal output of the glass waste forms will depend on the age and composition of the waste and its concentration in the glass. The resulting rise in temperature of the environment would alter the local hydrologic system and would cause the pore water contained in rock in the vicinity of waste packages to vaporize. After dehydration, rehydration of the near-field environment will occur as the waste package temperature drops. Performance of the container and the waste forms is closely tied to the amount of water in the system and to the flow mechanisms operating in the vicinity of the waste packages. The rates and mechanisms of dehydration and rehydration of Topopah Spring tuff are being investigated in laboratory experiments using intact and fractured rock samples. This work is discussed in Section 7.4.1.5. Numerical modeling associated with near-field fluid flow is discussed in Section 7.4.1.6.

The elevated temperature in the host rock would also encourage rock-water interactions to occur and would thus affect the chemistry of any water in the system. To assess the potential for changes in water chemistry, a series of tests have been conducted at temperatures from 90 to 250°C using a

variety of Topopah Spring tuff samples and a representative ground water. This work is described in Section 7.4.1.7. Geochemical modeling of the rock-water reactions is presented in Section 7.4.1.8.

7.4.1.1 Stability of borehole openings

Stability of emplacement borehole openings is of concern (1) during construction, (2) after emplacement but before closure when the option to retrieve the waste package must be maintained (Section 6.4.8), and (3) for the 1,000-yr period after closure when substantially complete containment must be achieved. The anticipated loads resulting from borehole instability are needed as design input to the packages and borehole liners. The stability of the emplacement borehole during postclosure is being examined as part of the definition of the waste package environment (Section 8.3.4.2). Preclosure retrievability-related analyses are discussed in Section 6.4.8 and in Section 8.3.2.5.

Emplacement hole thermomechanical analysis is conceptually much the same for either vertical or horizontal emplacement options. Loading of packages could result from either failure of intact rock (matrix) or by movement of rocks along preexisting discontinuity planes. Loading resulting from movement along discontinuities is more likely than from failure of intact rock since discontinuities are preexisting planes of weakness within the rock mass. Discontinuity planes in the rock mass intersect to form discrete rock blocks, some of which can move by sliding, falling, or toppling. Sliding and falling involve translational movement of a block into the emplacement hole, while toppling involves rotational block movement. Rotational motion requires more room for block movement than translational motion and, therefore, may not be as likely to occur in the limited confines of an emplacement hole.

An analysis of intact rock behavior based on engineering mechanics principles will be used to estimate or bound the loading condition. Analysis of deformation involving rock mass discontinuities may require three-dimensional methods because of the geometry of the problem. This analysis includes identification of block geometries that could potentially move and evaluation of their potential motion. The necessary techniques have been developed and tested (Yow, 1985) and will be applied to the Yucca Mountain site when definition of the fracture characteristics is available. The application of these techniques to borehole stability is discussed in Section 8.3.4.2; similar techniques will also be applied in designing other underground openings of the repository as discussed in Section 8.3.4.2. Analysis of thermomechanical response during the postemplacement period will consider stress changes from heating, cooling, and possibly long-term creep. A plan for how the analyses will be performed is discussed in Section 8.3.4.2.

The primary effect of temperature changes on the near-field rock will be a change in rock volume due to isobaric thermal expansion. Except for quartz and cristobalite, the isobaric thermal expansion of most silicate minerals, on average, is 3×10^{-5}/K (Helgeson et al., 1978). The maximum temperature attained by the near-field environment, based on the modeling

studies discussed in Section 7.4.1.2, results in a total volume change of about 1 percent using the average thermal expansion value.

Cristobalite, which is present in the near-field rock, undergoes a structural transition from tetragonal (alpha-cristobalite) to cubic (beta-cristobalite) symmetry. This phase transition results in a volume increase of about 5 percent (Helgeson et al., 1978). The temperature at which this phase transition occurs has been measured for naturally occurring cristobalite at Yucca Mountain (Wolfsberg and Vaniman, 1984) and has been found to be 225 ±25°C. Within the experimental uncertainty, this temperature is in agreement with that obtained by other laboratories.

The alpha-to-beta cristobalite transition temperature falls within the temperature range expected for the very near-field waste package environment during the period immediately following emplacement. The effect of the associated volume change on the waste package environment has yet to be established. There is additional discussion of this subject in Chapter 2. Research addressing this issue is discussed in Section 8.3.1.4.

7.4.1.2 Anticipated thermal history

Waste package conceptual designs suggest that spent fuel waste packages generate a thermal output of between 1.3 and 3.3 kW per container, but processed high-level waste in the form of borosilicate glass may have an output of less than 0.5 kW per container (O'Neal et al., 1984; Baxter, 1983). Packages that contain spent fuel with higher burnup or younger age than that assumed in the conceptual design studies may have higher thermal output.

Figure 7-5 shows a typical modeled thermal history of a vertically emplaced spent fuel waste package and its immediate surroundings. For an unventilated emplacement drift, the rock at the borehole wall would reach a maximum temperature of 230°C at 9 yr after package emplacement. The rock temperature 1 m from the borehole wall would peak at 190°C about 10 to 20 yr after emplacement. The values of the thermal maxima and the time at which they are attained are sensitive functions of the container power output, the mode of heat transfer, the thermal properties of the near-field rock, and the specific configuration of the boreholes and emplacement drifts. The thermal maximum will be followed by an extended period of cooling that will last for hundreds of years (O'Neal et al., 1984; St. John, 1985). Other related heat transfer analyses are summarized in Section 6.4.8.

At the elevation of the repository horizon, the unconfined boiling point of pure water is approximately 96°C. The pore water in the repository rock is likely to be a dilute solution. Although concentration of the solute species may occur during dehydration and rehydration, elevation of the boiling point is slight (less than 1°C) (DePoorter, 1986; Montan, 1986), even for solutions that are as much as 100 times more concentrated than the reference ground water (well J-13; Section 7.4.1.3). Such solutions exceed the maximum concentration expected for solutions in the waste package environment (Morales, 1985).

Vaporization of unconfined and unbound pore fluid can therefore be assumed to be complete at approximately 97°C. This phenomenon will result in the development of a dehydration zone around the waste package, the width and duration of which will depend on the migration behavior of the boiling point isotherm. The model presented in Figure 7-5 suggests that during the period of substantially complete containment, which will last at least 300 yr, rock within 1 m of the spent fuel waste packages will be at temperatures in excess of the boiling point and will therefore be in the dehydration zone.

Modeling of the effect of thermal perturbation on local hydrologic transport has suggested that heat transfer through liquid-vapor cycling in convective cells (heat pipe effect) may occur in a closed system (Preuss et al., 1984). Experimental studies (Section 7.4.1.5) and numerical analyses (Section 7.4.1.6) are being conducted to determine the extent to which such behavior will occur in a natural system and the effect of this behavior on near-field water chemistry.

The scenario for thermal evolution of the near-field waste package environment is derived from computer codes for which some uncertainties remain. The scenario assumes that the waste package being modeled resides in the interior of a repository. Waste package environments along the perimeter of a repository will have a thermal history different from that depicted in Figure 7-5. The nature of the thermal history along the perimeter of the repository has yet to be defined. The codes assume no nonlinear effects in the near field and do not consider the effect of pore water vaporization. The histories presented in Figure 7-5 must therefore be considered approximations of the actual thermal field that will be attained in the waste package environment for a central portion of the repository. The greatest uncertainties pertain to the environment immediately adjacent to the borehole wall where nonlinear effects are expected to be most pronounced (St. John, 1985). Beyond a few meters from the borehole wall, the computed results are expected to closely represent the actual thermal history for the set of specified conditions.

Additional near-field thermal calculations, using techniques that improve the modeling of nonlinear effects will be undertaken in the future and are described in Section 8.3.4.2.

7.4.1.3 Reference water for experimental studies

The composition of pore fluid in the repository site will be established when the exploratory shaft test program recovers rock from the repository horizon. Evidence suggests that tests conducted prior to completion of the exploratory shaft can closely approximate repository pore fluid chemistry by use of water recovered from well J-13, which is located to the east of Yucca Mountain. The characteristics of water from well J-13 are discussed in Section 4.1.2. The elevation at well J-13 is lower than at Yucca Mountain, and the Topopah Spring tuff lies below the water table there, forming the major producing horizon for the well. The chemistry of well J-13 water is similar to that found in drillholes drilled to sample water from below the water table at Yucca Mountain (Table 7-8; Ogard and Kerrisk, 1984). Water from well J-13 is also similar to unsaturated zone water obtained from tuffs

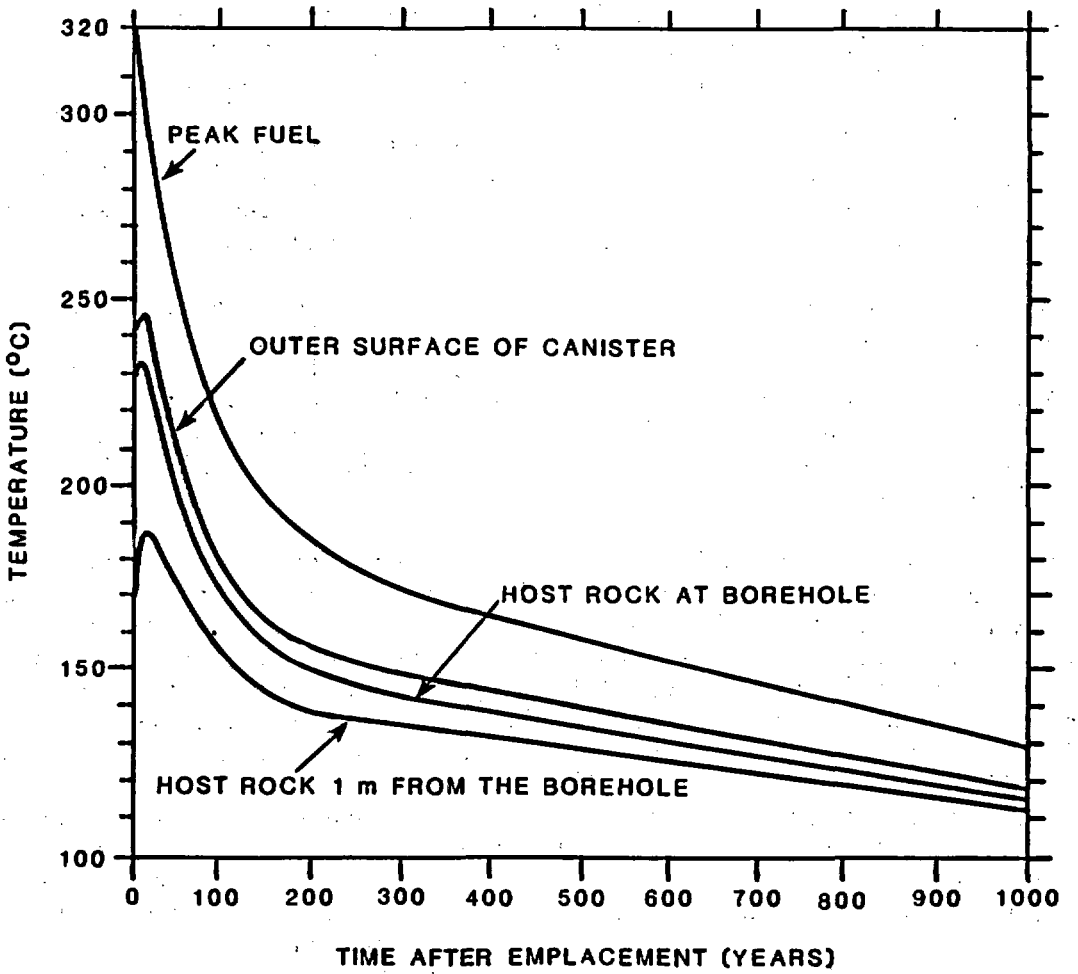

INITIAL CONDITIONS

WASTE FORM	SPENT FUEL
LOCAL POWER DENSITY	57.0 kW/acre
AREAL POWER DENSITY	48.4
AVERAGE 10-YR POWER	3.3 kW
CONTAINER DIAMETER	0.7 m
DISTANCE BETWEEN CONTAINERS	5 m
DISTANCE BETWEEN DRIFTS	47 m

Figure 7-5. Example of temperature histories of thermal waste package components and host rock for a vertically emplaced spent fuel container (O'Neal et al., 1984).

Table 7-8. Compositions[a] of various unsaturated-zone water from Rainier Mesa compared with well J-13 water[b]

Constituent	Source of data: White et al. (1980) Interstitial	White et al. (1980) fracture	Henne (1982) Tunnel water	Ogard and Kerrisk (1984) (well J-13)
Na	1.73	1.53	2.30	1.96
K	0.18	0.12	0.11	0.14
Ca	0.27	0.21	0.08	0.29
Mg	0.10	0.06	0.01	0.07
HCO_3	1.14	1.61	2.25	2.34[c]
SO_4	0.43	0.15	0.10	0.19
Cl^-	0.75	0.24	0.18	0.18
SiO_2	0.97	0.88	0.73	1.07
pH	7.8	7.5	7.0	6.9

[a] Values are averages of reported data.
[b] All species compositions are in moles/L.
[c] Measured alkalinity.

at Rainier Mesa, which is north of Yucca Mountain (White et al., 1980; Henne, 1982). Thus, the water chemistry for well J-13 water is expected to be close to that of the vadose water in the Topopah Spring tuff in the unsaturated zone. Until samples of water from the unsaturated zone are available, the water from well J-13 has been adopted as a reference ground water for the NNWSI Project experimental work. When the composition of pore fluid in the repository horizon is established, the need to complete additional experimental work will be evaluated.

7.4.1.4 Radiation field effects

The types of ionizing radiation that interact with the rock-water-vapor system will be neutron and gamma radiation; alpha and beta radiation will not penetrate the intact waste container (Van Konynenburg, 1984). The absorbed dose from gamma radiation will dominate over that from neutron radiation by more than four orders of magnitude (Van Konynenburg, 1984). The total radiation field will be less than 1×10^5 rads/h (Wilcox and Van Konynenburg, 1981). The dominant gamma radiation effects in the waste package environment will result from interaction of gamma radiation with water, steam, and air since gamma radiation at the expected doses results in negligible damage to

silicate rock (Durham et al., 1985). Less than 3 percent of the total thermal energy released by the waste package will be deposited in the host rock by gamma radiation (Van Konynenburg, 1984). Over 99 percent of the gamma radiation energy will be deposited within 1 m of the borehole wall (Van Konynenburg, 1984).

The significant radiolysis products in the waste package environment will vary with time as the thermal conditions evolve. The thermal history of rock adjacent to the waste packages will be complex (Figure 7-5, Section 7.4.1.2). Vaporization of the pore water will occur in rock immediately adjacent to the waste packages where the temperature exceeds 96°C. The width of the dehydration zone will depend on the magnitude of the thermal load imposed by the waste package on the host rock. While the rock temperature exceeds 96°C and the dehydration zone extends more than about 1 m into the rock surrounding the waste package, radiolysis products will be restricted to those resulting from interaction of gamma radiation with moist air.

Radiolysis products expected in the moist air system, although known to be temperature dependent, are not well established (Van Konynenburg, 1986). Theoretical and experimental analysis of the moist air system (Jones, 1959; Tokunaga and Suzuki, 1984) and of the tuff-water-steam system (Van Konynenburg, 1986) and consideration of the thermodynamic properties of radiolytic products (Forsythe and Giaque, 1942; Beattie, 1967) suggest that, at temperatures below 120°C, the most abundant products with relatively long lifetimes are HNO_3, N_2O, and a small amount of O_3. Between approximately 120 and 135°C, NO_2, N_2O_4, N_2O, and O_2 are expected to be the dominant chemical products; above approximately 135°C, the dominant product species would be NO, NO_2, N_2O, and O_2. How these compounds would interact with rock in the waste package environment and with the waste package will be established in activities described in Section 8.3.4.2.

When liquid water and air in contact with each other are irradiated, the identities and amounts of radiolysis products depend on the identities and concentrations of solutes in the water, the radiation dose, the oxidation-reduction conditions, the pH, and the air-water ratio. In well J-13 water that has equilibrated with tuff, solute concentrations on the order of 1×10^{-3} to 9×10^{-2} M are obtained, and the dominant species is sodium bicarbonate, buffering the pH near neutral. These concentrations are sufficient to cause the solutes to dominate the reactions with radiation-produced free radicals in the water, leading to increases in hydrogen and oxygen partial pressures due to decomposition of water at high (10^5 rads/h) radiation levels (Van Konynenburg, 1986). In addition, fixation of nitrogen from the air due to irradiation causes nitrite and nitrate ions to be added to the solution. The nitrite-nitrate ratio apparently depends on the oxidation-reduction conditions and on the abundance of materials that can catalyze the breakdown of hydrogen peroxide (e.g., iron(3+) and manganese oxide). Addition of hydrogen ions to the solution also occurs, but the pH is not strongly affected provided the total dose and the air-water ratio are such that the bicarbonate buffering capacity is not exceeded. If the solution is in contact with the rock, additional buffering is provided by the feldspars (Garrels and Howard, 1957).

The chemical effects of the radiolysis products on the initially dehydrated waste package environment host rock will be limited to oxidation

of mineral phases containing elements of variable valence states. The principal reactions will involve biotites, amphiboles, and oxides, which individually occupy less than 0.1 volume percent of the rock. The reaction products are expected to be various oxide phases, but little information is currently available on experimental studies relevant to this system. At any given temperature, the degree of oxidation will depend on the reaction kinetics and the concentration of the oxidizing species, neither of which can be quantified at this time (Section 8.3.4.2).

By the time rehydration of the host rock occurs within 1 m of the waste package, the gamma radiation flux will have decayed to levels three orders of magnitude below initial emplacement values (Baxter, 1983; Oversby, 1984b). Concentrations of radiolysis products will, therefore, also be diminished considerably. Further work is planned that will more thoroughly characterize the geochemical consequences of the radiolysis products for the host rock mineralogy and pore fluid chemistry (Section 8.3.4.2).

7.4.1.5 Thermal effects on water flow in the vicinity of waste packages

The present level of understanding of the ambient hydrologic system at Yucca Mountain has been discussed by Montazer and Wilson (1984) and Ortiz et al. (1985). These papers document that the potential repository horizon is located within a nonlithophysal unsaturated zone that is several hundred meters above the water table.

Water transport within this rock occurs by a combination of vapor transport, water migration through the matrix, and fracture flow (Montazer and Wilson, 1984). The relative importance of each flow mechanism is a function of the bulk saturation, the volume of water transported through the rock, the temperature gradients in the rock, the fracture characteristics, and the permeability of the matrix. It has been established that the fracture density within this lower nonlithophysal zone varies between 8 and 40 fractures per cubic meter (Scott et al., 1983), with a mean matrix porosity of 14 percent (56 samples, with a standard deviation of 5.5) and a mean saturation of 65 percent (44 samples, with a standard deviation of 19) (Montazer and Wilson, 1984).

The net flux of water through the repository is probably 1.0 to 2.0 mm per yr upward, although a downward flux of 1.0×10^{-7} to 0.5 mm/yr may occur as a result of matrix flow (Montazer and Wilson, 1984; Montazer et al., 1986). The current matric potential of the Topopah Spring tuff is approximately -112 kPa which results in negligible fracture flow (Wang and Narasimhan, 1985). For all fractures other than minor fractures, fracture saturation will not exceed 0.01 unless the matrix is fully saturated and the matric potential is in the range of -1 to -0.01 kPa which is two to four orders of magnitude greater than at present (Wang and Narasimhan, 1985). Precise statements regarding when fracture flow would become dominant cannot be made until more information is available about fracture roughness and other fracture characteristics (Section 8.3.4.2).

The emplacement of waste packages in the rock would produce a large thermal perturbation. This, in turn, would cause water to vaporize and

migrate in the near field and would result in an altered hydrologic regime. There is very little information, experimental or theoretical, on thermally driven flow in partially saturated rocks. Because water is the main corrosive agent for the metal container and the main agent for the transport of radionuclides, experimental and numerical modeling studies have been initiated to characterize fluid flow and the geochemistry of water-rock interactions in the Topopah Spring tuff.

The fluid flow experiments (Lin and Daily, 1984; Daily et al., 1986) were designed to investigate the mechanism of dehydration and rehydration under a variety of thermal conditions in initially saturated intact and fractured rock. These experiments were primarily conducted to investigate and develop experimental techniques. Experiments in unsaturated tuff are under development (Section 8.3.4.2). The results described in the following paragraphs are from fully saturated samples.

Studies were conducted in two stages. The initial stage involved reconnaissance experiments in which the use of electrical resistivity measurements and P-wave velocity measurements were evaluated as means of mapping fluid distribution in the rock during dehydration-rehydration cycles at various temperatures (Lin and Daily, 1984). These experiments allowed initial characterization of the hydrologic properties of the tuff during dehydration and rehydration. The second stage of the study involved development and use of computed impedance tomography (CIT) to obtain detailed images of fluid distribution in the tuff during dehydration-rehydration cycles (Daily et al., 1986). In both stages, steam and water permeability was determined for fractured and unfractured (intact) samples of tuff.

In the initial stage of this study, three samples of tuff were used in the experiments. Two samples of Topopah Spring tuff from Fran Ridge and one sample from drillhole USW G-1 were machined to form right cylinders 9 cm long and 2 cm diameter. One of the Fran Ridge samples was intact; the remaining samples each had one longitudinal fracture.

To simulate as closely as possible the chemistry of the in situ pore fluid, well J-13 water was used as the aqueous phase in these experiments. The protocol for the initial experiments and the results of permeability measurements are summarized in Lin and Daily (1984).

The resistivity images obtained during dehydration and rehydration of the intact sample identified no preferred flow paths. In addition, the permeability of this unfractured rock was independent of temperature and thermal history. These results are consistent with those reported by Morrow et al. (1981, 1985) and suggest that the hydrologic properties of unfractured rock in the waste package environment will not be modified by the anticipated thermal perturbation.

The behavior of the fractured sample was in striking contrast to that of the intact sample. The initially high permeability decreased by a factor of about 20 after initial dehydration and by more than three orders of magnitude to values indistinguishable from that of the intact sample during successive cycles of dehydration and rehydration (Table 7-9). In addition, the initial dehydration occurred eight times faster than in the intact sample. The rate

Table 7-9. Experiment protocol and measured permeability in permeability experiments on Topopah Springs tuff[a,b]

Step No.	Experimental procedure	Measured permeability (in microdarcies) Intact sample	Measured permeability (in microdarcies) Fractured sample
1	Determine permeability at 21°C	0.34	850
2	Dehydrate[c] at 140°C	--[d]	--
3	Rehydrate with liquid water at 140°C with differential pressure of 2.5 MPa	--	--
4	Determine liquid water permeability at 140°C	0.31	34[e]
5	Dehydrate at 140°C	--	--
6	Rehydrate with steam at 140°C with differential fluid pressure of 0.2 MPa	--	--
7	Determine steam permeability at 140°C	1.99	3.9
8	Dehydrate at 140°C	--	--
9	Rehydrate with liquid water at 98°C with differential fluid pressure of 2.5 MPa	--	--
10	Determine liquid water permeability at 98°C	0.35	0.24

[a]Source: Lin and Daily (1984).
[b]The confining pressure was 5 MPa. The rehydration and permeability measurements were conducted by applying the indicated pressure to one end of the sample, resulting in the indicated differential pressure.
[c]Dehydration was accomplished by drying the sample in the pressure vessel, with both ends of the sample exposed to the atmosphere.
[d]Not applicable.
[e]The value of 34 microdarcies was measured after cooling the sample to 98°C.

at which drying occurred suggests that dehydration was controlled by fluid flow along the fracture.

Healing of the fracture by deposition of silica during fluid flow appears to be responsible for the change in permeability. Before the experiment, the fracture was open, but upon completion of the experiment, the two fragments of rock were bonded together. Scanning electron microscope images of the healed fracture surface showed multiple layers of silica deposited on the fracture walls (Lin and Daily, 1984).

To isolate the main factors contributing to fracture healing, the fractured sample from drillhole USW G-1 was subjected to a sequence of thermal cycles under conditions of constant saturation. Preparation of the sample was the same as for the earlier samples. Surface conditions of the fracture were closely similar to those of the fracture in the outcrop sample. Initial room temperature permeability was 600 to 700 microdarcies, decreasing to 350 microdarcies after a day under flowing conditions. Upon heating the sample to 96°C under saturated conditions, the permeability decreased by one order of magnitude. Changes in temperature up to 140°C and back to room temperature did not produce any further large changes in permeability. Examination of this sample after the experiment showed that fracture healing had occurred, but to a lesser extent than in the first sample.

Resistivity maps document that the rate of change of resistivity is much greater for the fractured samples than for the intact sample. This is consistent with the interpretation that dehydration occurs much more rapidly in the fractured sample. The distribution of resistivity along the fracture surface was not uniform, suggesting that fluid migration along the fracture surface does not take place at a uniform rate. This behavior contrasts with that deduced from resistivity maps of the intact sample that document uniform resistivity changes and, consequently, uniform fluid flow (Lin and Daily, 1984).

Attempts to use P-wave velocity measurements to characterize fluid flow did not provide sufficient resolution to be useful.

The initial results suggested that fluid flow in fractured rock at elevated temperatures would lead to a decrease in permeability of one or more orders of magnitude. Dehydration rates were significantly faster for fractured material compared with dehydration rates obtained for intact samples.

The second experimental stage was designed to more thoroughly characterize the fracture flow process by using computed impedance tomography (CIT) to obtain higher resolution resistivity images (Daily et al., 1986). In these experiments, 14 electrodes were attached to the circumference of a fractured sample, approximately perpendicular to the plane of the fracture. Four electrode pairs were also attached parallel to the long axis of the core samples, as in the previous experiments. The resulting resistivity maps provide a cross-sectional image of fluid distribution in the core, as well as low resolution images parallel to the long axis of the core. Permeability measurements, obtained simultaneously with the CIT images, allow correlation of permeability changes with changes in fluid distribution in the core. The experimental protocol in this second set of experiments was similar to that

used during dehydration and rehydration cycles for the first fractured core sample (Daily et al., 1986).

The results of these experiments (Daily et al., 1986) are consistent with the previous results. Rapid decrease in permeability occurred during dehydration stages (Figure 7-6), resulting in permeability changes of more than three orders of magnitude. The final permeability obtained at the end of the experiment was indistinguishable from that obtained previously on intact samples.

The CIT images suggest that the aperture of the fracture decreases during the course of the experiment. This result suggests that, as the aperture of the fracture is diminished, ventilation is restricted, resulting in a decreased rate of dehydration. These observations are consistent with the interpretation of the previous studies that healing along the fracture during dehydration and rehydration cycles is responsible for the drop in permeability observed in the experiments using fractured samples.

These initial results suggest that the hydrologic properties of intact rock may not be modified by dehydration and rehydration cycles resulting from the thermal load imposed on the waste package environment by the waste containers. Uniform fluid flow under postemplacement conditions can be expected. The hydrologic properties of fractured samples in a thermally perturbed environment may be sensitive to solution/deposition processes and to thermal gradients. Because the mechanism responsible for this behavior is unknown, and the behavior in a two-phase system has not been characterized, further work is planned to address these questions under isothermal and polythermal conditions. Completion of the planned work will allow evaluation of the implications of the fracture healing process and will contribute to resolution of Issue 1.10 (Section 8.3.4.2). Field studies in the exploratory shaft establishing the characteristics of flow in natural systems will be used to examine the applicability of these experimental studies (Section 8.3.4.2).

7.4.1.6 Numerical modeling of hydrothermal flow and transport

Numerical modeling studies of coupled multiphase heat and fluid flow in the vicinity of waste packages are being conducted in conjunction with the laboratory activities. These studies and accompanying transport calculations will aid in the prediction of the waste package hydrologic environment and will contribute to the calculation of radionuclide release source terms. The numerical simulations focus on understanding the fundamental mechanisms governing heat and fluid flow in partially saturated fractured rock. Understanding the roles that fractures and adjoining matrix blocks play as conduits to liquid and vapor phase transport is of particular importance. This interaction will influence the extent of dry out in the surrounding host rock and the rate at which rewetting can occur as the thermal output of the waste decreases. These processes impact assessment of waste package corrosion mechanisms and rates and will influence transport rates near the waste package after loss of containment. Upon completion of the exploratory shaft, field studies will provide data to aid in verifying the results of the laboratory and numerical studies.

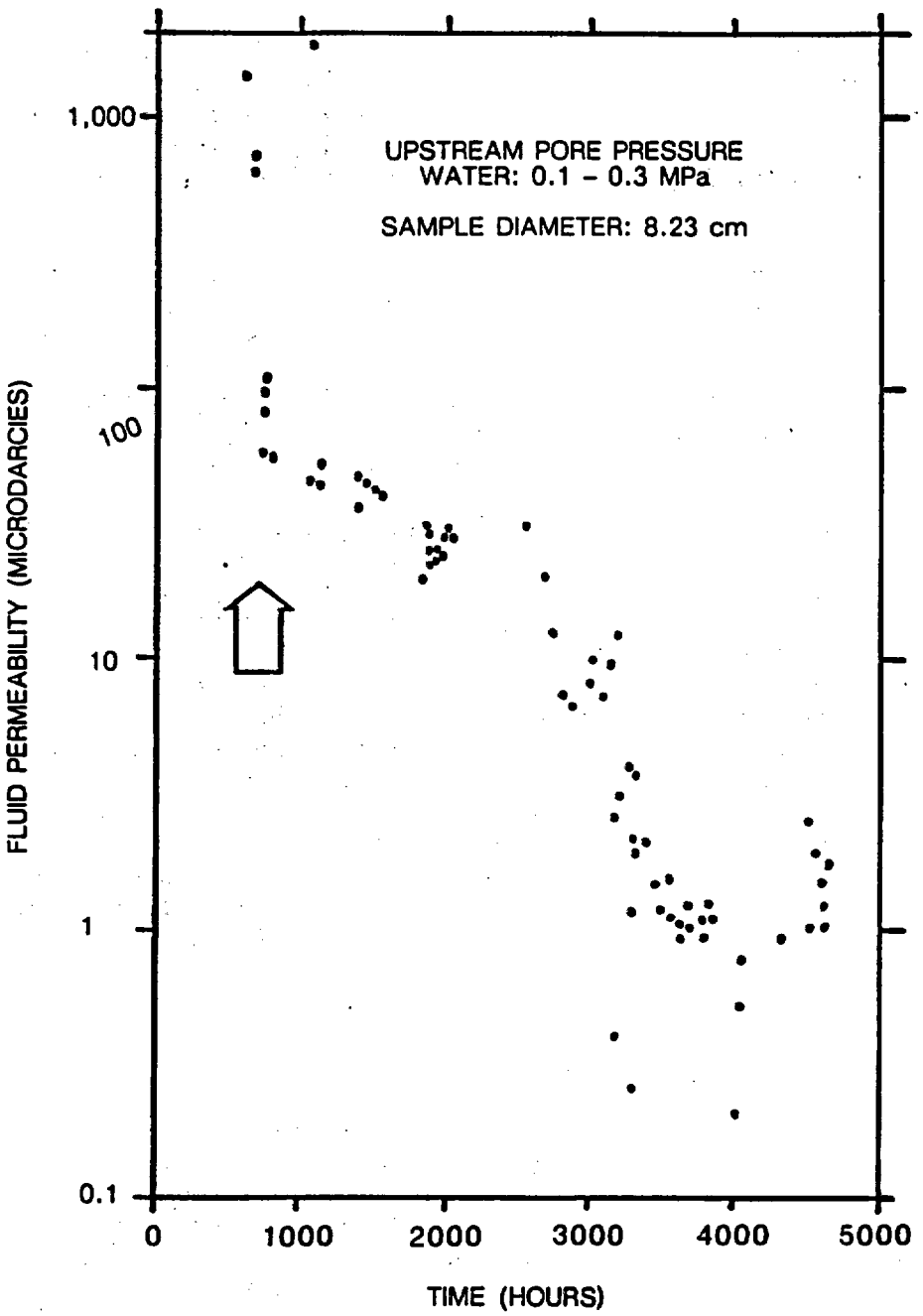

Figure 7-6. Fluid permeability versus time for fractured Topopah Spring tuff. The initial permeability was measured at room temperature. The first rapid drop in permeability, indicated by the arrow, occurred during the initial dehydration period at 90°C. The second rapid drop in permeability, at about 3,000 h, occurred during the second dehydration period. Modified from Daily et al. (1986)

The hydrologic properties and ambient conditions in the host rock at the repository horizon result in a complex conceptual model of coupled hydrothermal flow and transport with several unresolved questions. The complexity of the near-field hydrothermal problem arises from two general features. First, the host rock is partially saturated with approximately 65 percent (Montazer and Wilson, 1984) of the bulk pore volume containing water held in the porous matrix primarily by capillary suction. Because of the extremely small average pore size in the matrix, capillary suction effects are very pronounced. Second, the host rock is fractured, containing both matrix and fracture porosity and permeability. The hydrologic properties of the matrix and fracture porosity differ markedly. Experimental evidence (Lin and Daily, 1984; Daily et al., 1986) indicates that the absolute permeability in the matrix and fractures differ by at least three orders of magnitude. Based on empirical evidence and thermodynamic principles, it appears that the characteristic curves (i.e., relative permeability and capillary pressure as functions of bulk saturation) for the respective porosities differ quite markedly (Klavetter and Peters, 1986). Characteristic curves for a steam-water-air system for the full range of saturation conditions in Topopah Spring tuff will be the subject of studies during site characterization (Section 8.3.4.2).

Attempts have been made to synthesize characteristic curves for the fractures using conceptual models that use simple geometric assumptions and thermodynamic principles (Montazer and Wilson, 1984; Klavetter and Peters, 1986). Because the synthesized characteristic curves have not been validated directly by experimental means and because of the inherent geometric variability of naturally occurring fractures, the characteristic curves that are synthesized for the fracture porosity will be subject to variability and uncertainty. The sensitivity of the near-field hydrothermal response to the characteristic curves in the fractures is of interest because it is the interaction of the capillary forces and relative permeability effects on either side of the fracture-matrix interface that will determine whether liquid water is mobile in the fractures under preemplacement conditions and while the system is thermally perturbed. Consequently, any near-field hydrothermal modeling effort will need to consider the range of variability of the characteristic curves in the fractures.

Implicit in the discussion of characteristic curves is the concept of a discrete fracture model. Conceptually, it is most straightforward to model discrete fractures explicitly, using small volume elements to represent fractures adjacent to porous matrix blocks. However, at the waste package scale, limitations in the dimensioning of hydrothermal computer codes on existing mainframe computers preclude the use of discrete fracture models. For near-field hydrothermal modeling, it may be necessary to develop an equivalent continuum representation of the two porosity fracture/matrix system. An equivalent continuum model has been developed, yielding results similar to the discrete fracture model of an idealized two-dimensional near-field problem (Preuss et al., 1984). For models attempting to simulate actual repository conditions, it may be necessary to consider fracture orientation and interconnectivity in three dimensions as well as the variability of these geometric parameters in building equivalent continuum models. Studies during site characterization will attempt to resolve these issues (Sections 8.3.4.2.4 and 8.3.1.2).

The essential features of a conceptual model of the near-field hydrothermal response to the emplacement of the waste packages are described in Preuss et al. (1984). The model considers multiphase heat and fluid flow in partially saturated tuff containing both fracture and matrix porosity. Preuss et al. (1984) only consider fractures that contribute to radial flow away from the waste package. Other considerations that are also potentially important are (1) the influence of fractures oriented orthogonally to the radial direction of flow and (2) the determination of whether the waste package borehole is sealed or open to atmospheric conditions. If liquid water is immobile in the fractures, then the fractures oriented orthogonally to the radial flow direction may become capillary barriers to liquid flow in the radial direction. Emplacement of the waste packages causes temperatures to rise in both the rock matrix and fractures. Most of the vapor generated in the rock matrix flows toward the fractures, which are high conductivity conduits to the gas phase.

Gas phase flow in the radial direction may be affected by whether there is a pathway for gaseous flow from the waste package to the emplacement drift. If the waste package boreholes are ventilating to the access drifts (and are therefore maintained at approximately atmospheric pressure), then some of the vapor generated in the rock matrix will likely seek fractures that intersect the waste package borehole and flow into the borehole and toward the emplacement drift. Near-field hydrothermal calculations are required to determine how much of this vapor (1) will reach the emplacement drifts and condense along the drift walls, (2) will be pulled out through the repository ventilation system, and (3) will condense along the cooler portions of the waste package borehole wall if temperature is low enough.

Assumptions regarding gas and liquid flow geometry after waste emplacement must be evaluated during site characterization. Presently, this geometry is assumed at the waste package scale to be basically radially outward from the package centerline. The reasoning for this assumption appears in Preuss et al. (1984). Because the fractured rock mass at the repository horizon is partially saturated, an interconnected gas phase may be assumed to exist and to be at a pressure equal to the local atmospheric pressure. As the rock heats due to waste decay and the pore water begins to boil, the phase change and the relatively lower gas permeability of the matrix will induce a pressure gradient between the matrix and the fracture system where pressure gradients will move the vapor away from the waste package. Since the fractures have a very large gas-phase permeability, the total gas phase pressure in the fracture system will likely remain near atmospheric. Therefore, gas should flow from the matrix to the fracture system where pressure gradients will move the vapor away from the waste package. Even though many of the fractures within the boiling zone will not communicate with the borehole, the net gas flux in the rock mass may still be directed radially outward from the package.

The outward radial flow of vapor in the fractures will result in condensation along the cooler fracture walls. An unresolved question, which is being addressed in Section 8.3.5.10, is whether the liquid condensation along the fracture walls will attain saturations sufficient to result in liquid phase mobility within the fracture or the liquid condensation will be pulled into the rock matrix by the capillary suction gradients. The answer to this question will depend on the rate of condensation, the capillary suction

gradients, and liquid phase permeabilities within the respective matrix and fracture porosities.

The size of the dried-out region around the waste package is inversely dependent on the efficiency of the primary mechanism of heat transfer in the fractured rock mass. Where the liquid phase is mobile in the fractures, a highly efficient heat pipe system may be established within the fractures, carrying away most of the heat generated by the waste package (Preuss et al., 1984). For an immobile liquid phase in the fractures, a far less efficient vapor-liquid counterflow system may develop in which the radial inflow of liquid in the matrix is never able to balance the radial outflow of vapor in the fractures. Existence of fractures approximately perpendicular to the thermal and hydraulic gradients could further interfere with the vapor-liquid flow system. Within the growing dried-out region around the waste package, the only available mechanism of heat transfer is heat conduction, which is far less efficient than the balanced vapor-liquid counterflow heat pipe system established when the liquid phase is mobile in the fractures. Numerical modeling provides a means of examining these effects and will be applied in conjunction with laboratory and exploratory shaft field investigations during site characterization.

7.4.1.7 Rock-water interactions

The elemental and molecular constituents and the ionic species dissolved in water may have a significant effect on the corrosive action of the water and on the extent to which it may dissolve and transport radionuclides. Factors that influence the nature and concentration of dissolved constituents include the mineralogy of the rock in contact with the water, the temperature at which the contact takes place, the duration of the contact, and the ratio of rock surface area to water volume. The last two parameters are most important for interpretation of kinetically controlled dissolution and precipitation reactions. Performance assessment requires knowledge of these parameters, to establish corrosion behavior of the waste package under a variety of scenarios and to evaluate radionuclide release and transport (Sections 8.3.5.9 and 8.3.5.10).

As discussed in Chapter 3 and summarized in Section 7.1, uncertainties exist with regard to flux and flow mechanisms in the unsaturated zone. Low matrix flow rates will result in long contact times between rock and water. Flow through fractures may be slow or rapid, depending on the fracture aperture and the water flux. To cover the range of possible conditions, a number of tests have been conducted to determine the changes in water chemistry for different contact times, rock-to-water ratios, temperatures, and rock samples representative of the Topopah Spring tuff.

Rock-water interaction studies have been conducted using the following three experimental methods:

1. Solid core wafers or crushed tuff reacted in gold-bag rocking autoclaves (Dickson reaction vessels).

2. Solid core wafers or crushed tuff reacted in Teflon capsules contained in steel casings (Parr acid digestion reaction vessels).

3. Solid core wafers or crushed tuff reacted in stainless steel vessels.

Each of these methods has advantages and limitations; by combining data from all three methods, the artifacts of experimental technique can be removed from the data and a better estimate of the chemistry of the water under in situ conditions can be obtained.

The gold-bag autoclaves allow sampling of fluids without quenching the solution. The gold bag is inert and impervious, providing a nonreactive container that is gas tight. This feature is important because carbon dioxide (CO_2) is a reactant of interest in the system. The disadvantages of the gold-bag autoclaves are that the experiments are expensive to run, thereby limiting the volume of data that can reasonably be obtained; the rocking action of the system is not representative of expected repository conditions; and the sampling during reaction causes a change in fluid-to-solid ratio during the run.

Reactions in Teflon™-lined reaction vessels are inexpensive to run, and a large amount of data can be accumulated. The disadvantages of this method are that the Teflon™ capsule allows diffusion of CO_2 from the reacting mixture, thereby affecting the pH and alkalinity data (Knauss and Bieriger, 1984); the assembly must be cooled to near room temperature before opening and separating the fluid and solid phases; and the Teflon™ cannot be used in a gamma radiation field because it breaks down radiolytically and contaminates the fluid with hydrofluoric acid (HF). As will be discussed, the gas absorption effect can clearly be seen in the data, but the cooling to room temperature does not produce any detectable effects.

For tests conducted in a gamma radiation field, stainless steel vessels are used. Corrosion of the vessels is very slight under the reaction conditions, and the effects on solution chemistry are limited to minor amounts of iron, nickel, and chromium being added to the solutions.

The Topopah Spring tuff occurs in outcrop at Fran Ridge. Because many of the waste package materials interaction tests require rather large amounts of rock, the outcrop material has been characterized to determine whether it can be used in experiments and tests that require more rock than can be obtained readily from drill core (Oversby and Knauss, 1983; Oversby, 1984a). The petrologic characterization of the outcrop showed that there were no significant differences between the outcrop and samples obtained from the USW G-1 drill core (Knauss, 1984). There is a difference between the outcrop and drill core material with respect to rock-water interaction chemistry. The outcrop material contains a readily soluble component that appears to be caused by evaporation of surface runoff water from the pores, which leaves behind significant amounts of previously dissolved salts. The principal constituents of these salts are calcium, sodium, potassium, chlorine, nitrate (NO_3), sulfate (SO_4), and boron (Oversby, 1984a). The salt deposits are found only in near-surface samples and are not present in samples collected some distance from the surface (Oversby, 1985).

The choice of rock sample form is dictated by the type of data needed from the tests. If characterization of secondary phases and alteration products is required, it is necessary to use polished wafers of solid rock that are suitable for examination by surface analysis techniques after completion of the tests. If the desired information concerns the effects of rock-to-water ratio on final chemistry, then crushed rock is used because the weight added to the system can be more easily controlled.

Studies that involved characterization of secondary phases used rock wafers 2.54 cm in diameter by 0.25 cm thick that were prepared from drill core. One side of each wafer was hand-polished so that each could be examined by electron microscopy after completion of the experiment. Aliquots of the fluids from these experiments were removed periodically without interrupting the course of the reaction. These aqueous samples were analyzed for pH, dissolved carbonate species, cations, and anions. By the end of the reaction period, the fluid volume in the autoclave cell was about one-half the volume at the start of the reaction. At the end of each test, the rock wafer was removed from the autoclave, rinsed with distilled water, dried, and carbon coated for examination of phases by scanning electron microscopy (SEM) and electron microprobe analysis (EMP).

All cation analyses were conducted on acidified, filtered (0.1-micron Nucleopore™ filters) samples. Anion analyses were conducted on filtered samples. Unmodified samples were used for all pH measurements.

The results of tests conducted at 150 and 250°C in gold-bag autoclaves using rock wafers prepared from USW G-1 drill core have been published by Knauss et al. (1984). Results from gold-bag tests at 90, 150, and 250°C using crushed drillhole USW G-1 material are reported in Knauss et al. (1985). Long term studies (304 d) at 90 and 150°C are reported in Knauss et al (1987a). Parr reaction vessel data have been published for reaction temperatures of 90, 120, and 150°C (Oversby, 1984a,b). These tests used rock obtained from an outcrop of Topopah Spring tuff located at Fran Ridge. Results from reaction at 150°C in Parr reaction vessels of crushed rock from drillhole USW G-1, USW GU-3, USW G-4, and UE-25h#1 cores are contained in the report by Oversby (1985). Description of the outcrop locality and characterization data for the rock samples may be found in the report by Knauss (1984). These studies are summarized in Glassley (1986). The salient points from the summary are discussed in the remainder of this section.

The unconfined boiling point of pure water at the repository elevation would be approximately 96°C. Small pores in the rock retain water at somewhat higher temperatures due to capillary forces. Repository-scale modeling has indicated that water can be retained in pores at temperatures up to 140°C if a restriction on venting is imposed (Travis et al., 1984). Rock-water tests were conducted at 90°C to represent conditions of the near-maximum temperature expected for the main mass of water that would flow through rock and potentially contact waste packages. Tests at 150°C represent the conditions for small volumes of water retained in pores under unusual, but possible, conditions. Some tests were conducted at 250°C to investigate the nature of secondary phases formed and to assist in providing kinetics data for reaction path modeling. Because the secondary mineral assemblage at 250°C may be different from that formed at lower temperatures, these data

should be used only to guide the direction of lower temperature studies until a direct tie to lower temperature phase assemblages can be established.

The evolution of fluid composition in the rocking autoclaves for long-term and short-term experiments at 90, 150, and 250°C showed similar behavior. Figures 7-7 and 7-8 present typical examples of fluid evolution from a 150°C experiment. Silica and sodium concentrations exhibit an increase early in the experiment. During the experiment, the silica concentration approaches that expected for cristobalite saturation at the experimental conditions. Calcium, magnesium, and carbonate (not shown) exhibit an early, rapid decrease in abundance before attaining a steady-state concentration. This behavior results from the retrograde solubility of carbonate and reflects the precipitation of calcium- and magnesium-bearing carbonate early in the experiment. Potassium and aluminum tend to develop a peak concentration early in the experiments and then develop a gradual, moderate decrease in abundance before attaining a near steady-state concentration. This behavior for potassium and aluminum is believed to result from kinetically inhibited precipitation of a potassium-rich clay mineral during the course of the experiment. The concentration of anions (fluoride, chloride, NO_3, and SO_4) exhibits no significant variation for the duration of the experiment, reflecting the absence of significant sources for these anions in the rocks and the absence of precipitating phases that incorporate these constituents. The pH of the solution decreases from approximately 7.5 to 6.8 in response to the removal of carbonate from solution during carbonate precipitation.

Solid phases occurring as reaction products in the 150°C experiments were rare. A potassium-rich phase, believed to be a clay, was identified with the scanning electron microscope (SEM). This was the most abundant secondary phase observed. Also present were very small quantities of a zeolite rich in magnesium, calcium, and iron, of gibbsite, of calcite, and of a silica-rich phase believed to be cristobalite. Plagioclase feldspars, sanidine, biotite, and the fine-grained matrix in the rock wafer exhibited corroded surfaces resulting from hydrothermal reaction and dissolution. No change in the composition of the original solid phases in the rock was observed. In the 90°C experiments, only a potassium-rich clay similar to that observed in the 150°C experiments was identified. The effects of hydrothermal interaction on the primary phases in the 90°C wafer were very minor, with no observable change in the solid phase compositions. At 250°C, the zeolites dachiardite and mordenite formed in addition to previously recognized secondary phases (Knauss et al., 1987a,b).

These experiments lead to the following conclusions: (1) regardless of the temperature, the fluid in a water-saturated environment will evolve toward cristobalite and carbonate saturation; (2) secondary phases resulting from hydrothermal interaction will include sorptive clays and zeolites although the assemblage that forms is a function of temperature; and (3) the composition of the fluid phase remains benign at all temperatures, i.e., the pH is near neutral and there are low abundances of the anions chloride, fluoride, and NO_3.

Experiments to examine reaction kinetics were conducted on crushed samples of Topopah Spring tuff at the conditions just described. The fluid composition evolution in these studies was very similar to that obtained for

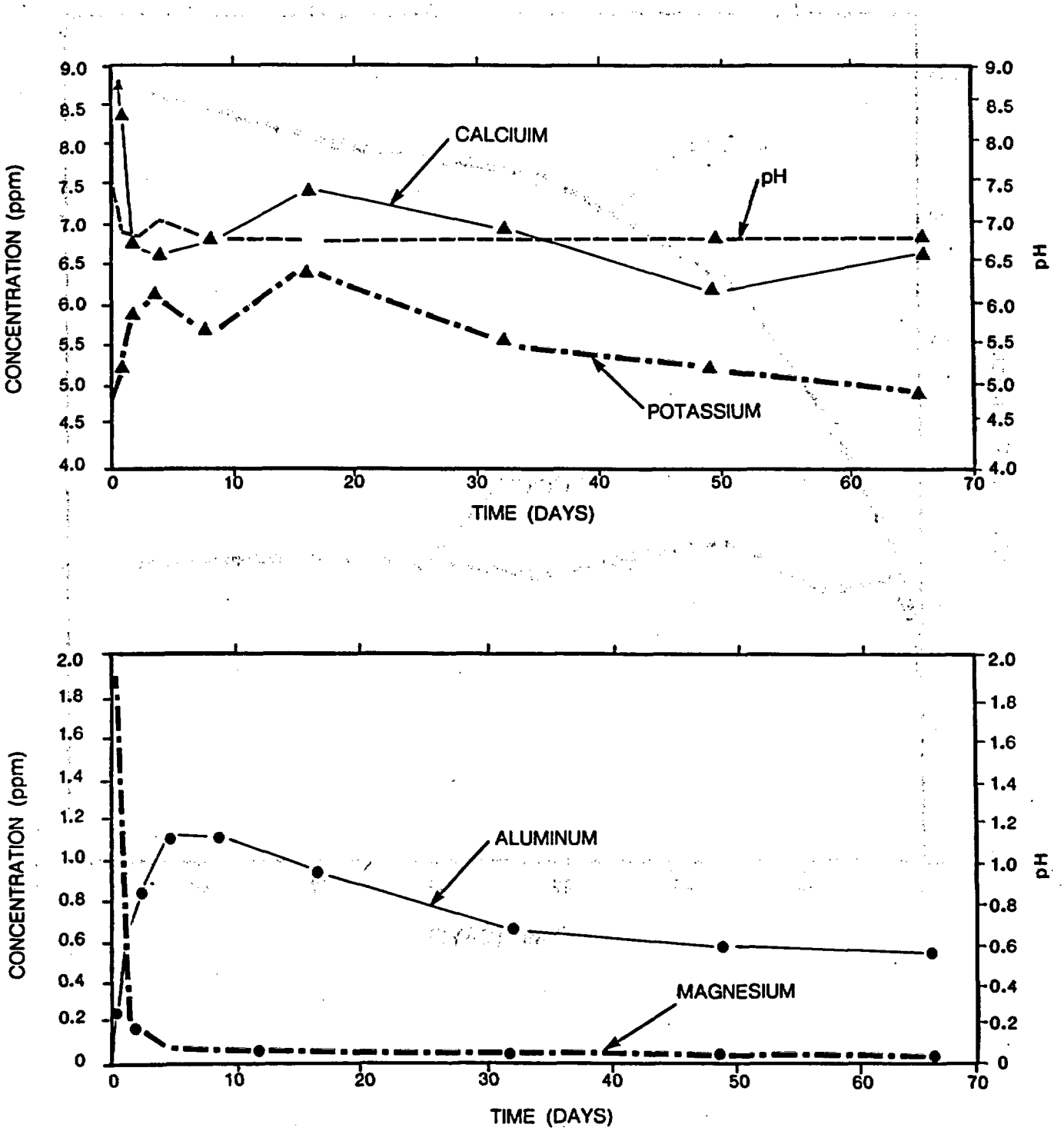

Figure 7-7. Aluminum, potassium, calcium, magnesium, and pH analyses of water from well J-13 reacted with USW G-1 core wafers at 150°C as a function of time. Modified from Knauss et al. (1987a).

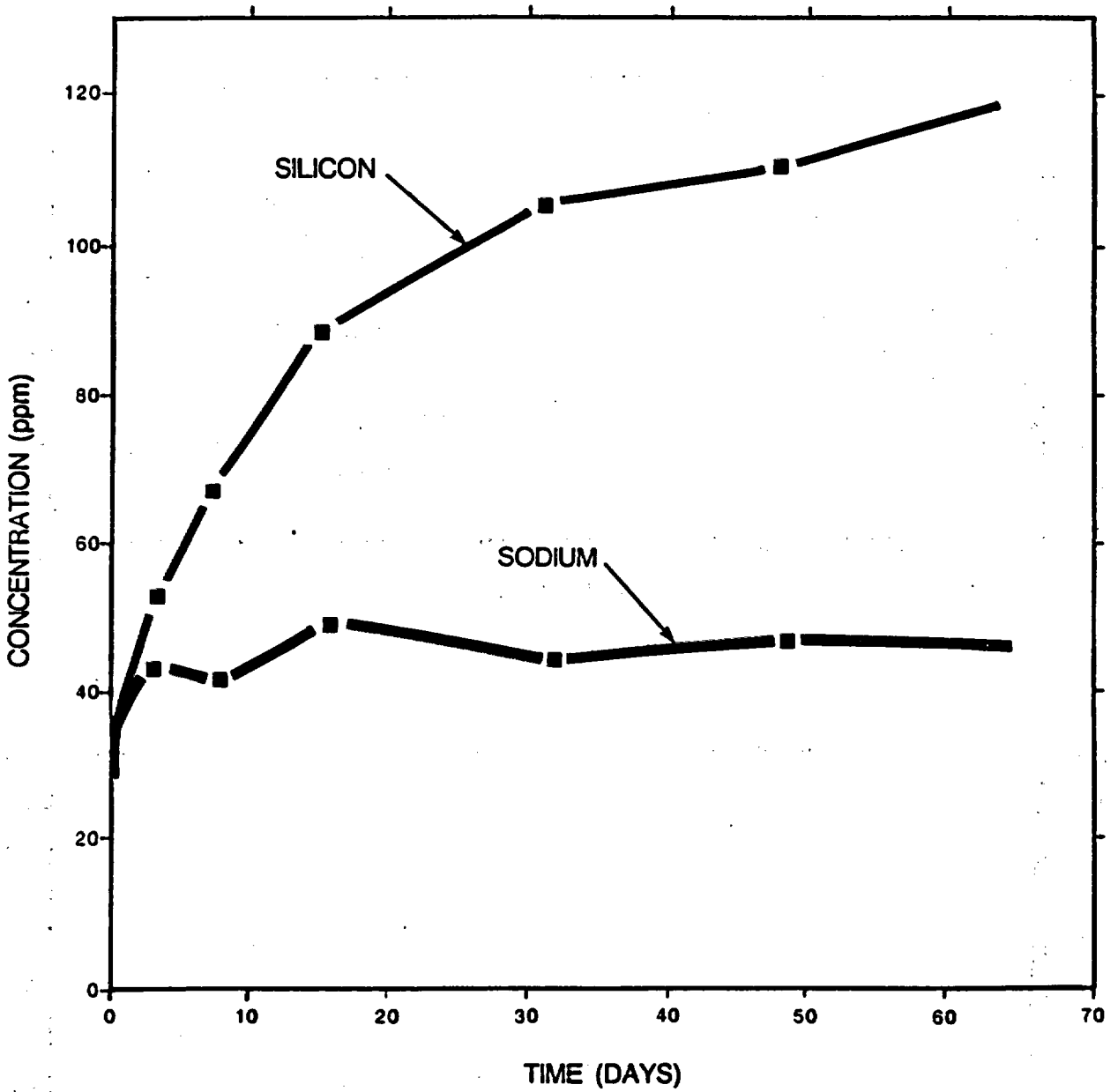

Figure 7-8. Silicon and sodium concentrations in water from well J-13 reacted with USW G-1 core wafers at 150°C as a function of time. Modified from Knauss et al. (1987a).

the solid wafer, although the rate of change for the solution was much greater during the early portion of the experiment. This result was expected since the hydrothermal reactions occurring in the experiments are expected to be kinetically controlled dissolution reactions that are dependent on the surface areas of solid in relation to fluid volume (SA:V) (Aagaard and Helgeson, 1982; Helgeson and Murphy, 1983).

Rock-water interaction tests conducted in Teflon™ capsules contained in steel casings (Parr acid digestion reaction vessels) allow comparison of the compositional evolution of fluid equilibrated with surface samples with that equilibrated with drill core obtained from much greater depth. These experiments used crushed tuff and core wafer material prepared from outcrop samples and reacted at 150°C (Knauss and Beiriger, 1984), and crushed material at 90°C (Oversby, 1984b). Tests have also been conducted using crushed outcrop material at 120°C (Oversby, 1984a). Results from the latter tests were intermediate between the 90 and 150°C results, as expected, and will not be discussed further here.

The trends of solution chemistry with time for the 150°C experiment were similar for both the outcrop material and the drillhole USW G-1 crushed rock except for pH, alkalinity, and final silicon concentration. The differences in alkalinity and pH may be due to diffusion of CO_2 out of the Teflon™ capsule, resulting in lower amounts of dissolved carbonate species and higher pH (Knauss et al., 1983). The lower silicon concentrations found by Oversby (1984a) may be the result of lower effective surface area in the crushed rock (less than 60 mesh) compared with the 100 to 200 mesh material used by Knauss et al. (1985). Results at 90°C also showed similar differences in pH, alkalinity, and silicon. In addition, the calcium from the outcrop samples was somewhat lower due to a higher solution pH, with final concentrations of about 8 ppm versus about 12 ppm for the drillhole USW G-1 samples.

Oversby (1985) has examined the water chemistry resulting from reaction of Topopah Spring tuff with well J-13 water as a function of lateral and vertical extent of the unit by using material taken from three vertical drillholes (USW G-1, USW GU-3, and USW G-4) and from the horizontal air-drilled hole at Fran Ridge. The solution chemistry after 70 d of reaction was very similar for all samples except that the silicon concentration was slightly lower for one of the Fran Ridge samples. The pH and alkalinity data show the expected differences from the gold-bag autoclave tests. Final silicon values ranged from 99 to 110 ppm (excluding the low-silicon Fran Ridge sample), somewhat lower than the autoclave results. Again, the differences may be due to the different mesh size used, which affects the surface area to volume ratio of the test material. Data for aluminum, magnesium, and sodium are very similar, but potassium and calcium concentrations were lower in the Parr reaction vessel tests compared with the values obtained in the gold-bag autoclave tests. The lower calcium concentration may be due to the higher pH, which increases carbonate relative to bicarbonate and may cause increased precipitation of calcite. The reason for the lower potassium (1 to 3 ppm versus 6 ppm) is not understood.

The drill core samples were tested for the presence of readily soluble salts by treating with water at room temperature and also by heating with well J-13 water overnight. This is the pretreatment procedure used on outcrop samples to remove evaporite salts. The resulting solutions showed no

evidence of readily soluble material. This result is particularly significant for the samples from the air-drilled hole at Fran Ridge since drilling fluid that could have removed soluble salts was not used in the portion of the hole from which the samples were obtained. This result strongly suggests that the presence of soluble salts is a surface evaporation phenomenon and that such materials are unlikely to be present at the depth of the repository horizon (Oversby, 1985).

It has yet to be established whether rock-water interactions in vitric- and vitrophyre-rich units are similar to those observed for the devitrified welded tuff. It is also necessary to complete detailed rock-water studies on rock material obtained from the exploratory shaft at the repository elevation to confirm the implications of previous studies and to satisfy Issue 1.10 (Section 8.3.4.2). This work will be done using water compositions appropriate for the vadose water system of the repository horizon, which will require completion of extraction techniques and analysis of vadose water from representative near-field material in the exploratory shaft (Sections 8.3.1.3, 8.3.1.16, and 8.3.4.2).

7.4.1.8 Modeling rock-water interaction

Results of the 150°C rock-water interaction tests were modeled using the EQ3/6 modeling code (Knauss et al., 1984). The EQ3/6 code (Wolery, 1979, 1983) uses finite difference derivatives with a Taylor series expansion to predict the equilibrium distribution of components between aqueous species as a reaction progress variable is incremented. Chemical affinities for all minerals that might occur in the system are then computed using a Newton-Raphson algorithm. If saturation of any of these minerals is attained, a mass action relationship is incorporated into the array of equations. The activities and molalities of all aqueous species and the number of moles per unit mass of water of each mineral produced or destroyed are then computed for each step in the reaction progress.

The composition of well J-13 water was used as input to the EQ3NR portion of the EQ3/6 software package to obtain a model aqueous solution for the reaction simulation. For the 150°C tests, the dissolved aluminum concentration was constrained to satisfy the mineral solubility equilibria for kaolinite to reduce the number of supersaturated phases listed by the model. The rock was represented in the EQ6 model by six minerals: sanidine, plagioclase, cristobalite, quartz, biotite, and montmorillonite. Specific surface area for each phase was calculated from the measured Brunauer-Emmett-Teller (BET) surface area of the rock wafer and the estimated abundance of each phase.

The precipitation of all silica phases less soluble than cristobalite was suppressed to allow the code to reproduce the experimentally observed silicon concentrations. Clays initially present in the hydrothermal experiments were modeled by magnesium-beidellite, a smectite clay that is a close compositional and structural analog to the montmorillonite identified in the experiments.

The EQ3/6 calculations realistically predicted that none of the initial reactants were exhausted and that a relatively minor amount of the rock dissolved during the reaction interval. The final concentrations for all major cations in solution predicted by the model were close to the observed values. As silica in the form of quartz and cristobalite dissolves, its concentration increases to a steady-state value, constrained by the input parameters to the steady-state solubility of cristobalite. The observed sharp rise in aluminum can be attributed to rapid dissolution of a small amount of magnesium-beidellite included in the model rock assemblage. The initial drop in calcium is due to formation of minor amounts of calcite, but the continued decrease in calcium is due to precipitation of a calcium-bearing smectite clay. The formation of the calcium-bearing smectite clay in the model also lowers the aluminum concentration in the model reaction path. The absence of thermodynamic data for potassium-bearing clays has prevented their incorporation in the model. The initial rise in potassium in the actual reaction solutions cannot be accounted for by the model.

The kinetic rate laws included in the current version of EQ6 provide only for dissolution reactions. Precipitation appears as an instantaneous process once saturation of a particular phase has been reached. Code development work is under way to include kinetically limited precipitation reactions in the EQ6 model.

The reaction path code used to model the experimental results uses equilibrium thermodynamics to establish the phase relationships. In the experimental system, it is possible that metastable phases precipitate during reaction progress. Such behavior would be a consequence of the tendency of natural and experimental systems initially to produce phases that have free energies between those of the reactants and those of the stable products of a discontinuous reaction (Ostwald, 1887). To account for the behavior of potassium, it will probably be necessary to include a metastable potassium-bearing phase (such as illite or smectite) to model the observations. When appropriate thermodynamic data are available for these phases, they will be incorporated in the code (Section 8.3.5.10).

Delany (1985) has continued the reaction path modeling of the 150°C autoclave tests, extending the work to the results of investigations with crushed tuff. Estimates of dissolution kinetic parameters were improved from the earlier work (Knauss et al., 1985) by using a combination of published rate constant data and additional kinetic constraints. Reported dissolution rate constants that are consistent with transition-state theory and that extend to temperatures as high as 150°C are available for potassium-feldspar (Helgeson et al., 1984) and for the silica phases (Rimstidt and Barnes, 1980). Dissolution rate constants are available to 70°C for pure albite (Knauss and Wolery, 1986) and to 25°C for phlogopite (Lin and Clemency, 1981). The dependence of the rate constants on temperature was estimated from transition state theory (Delany, 1985). The results of these most recent modeling efforts are compared in Figures 7-9 and 7-10 with the observed solution compositions.

A preliminary attempt to model the long-term behavior of a rock-water system was also completed (Delany, 1985).

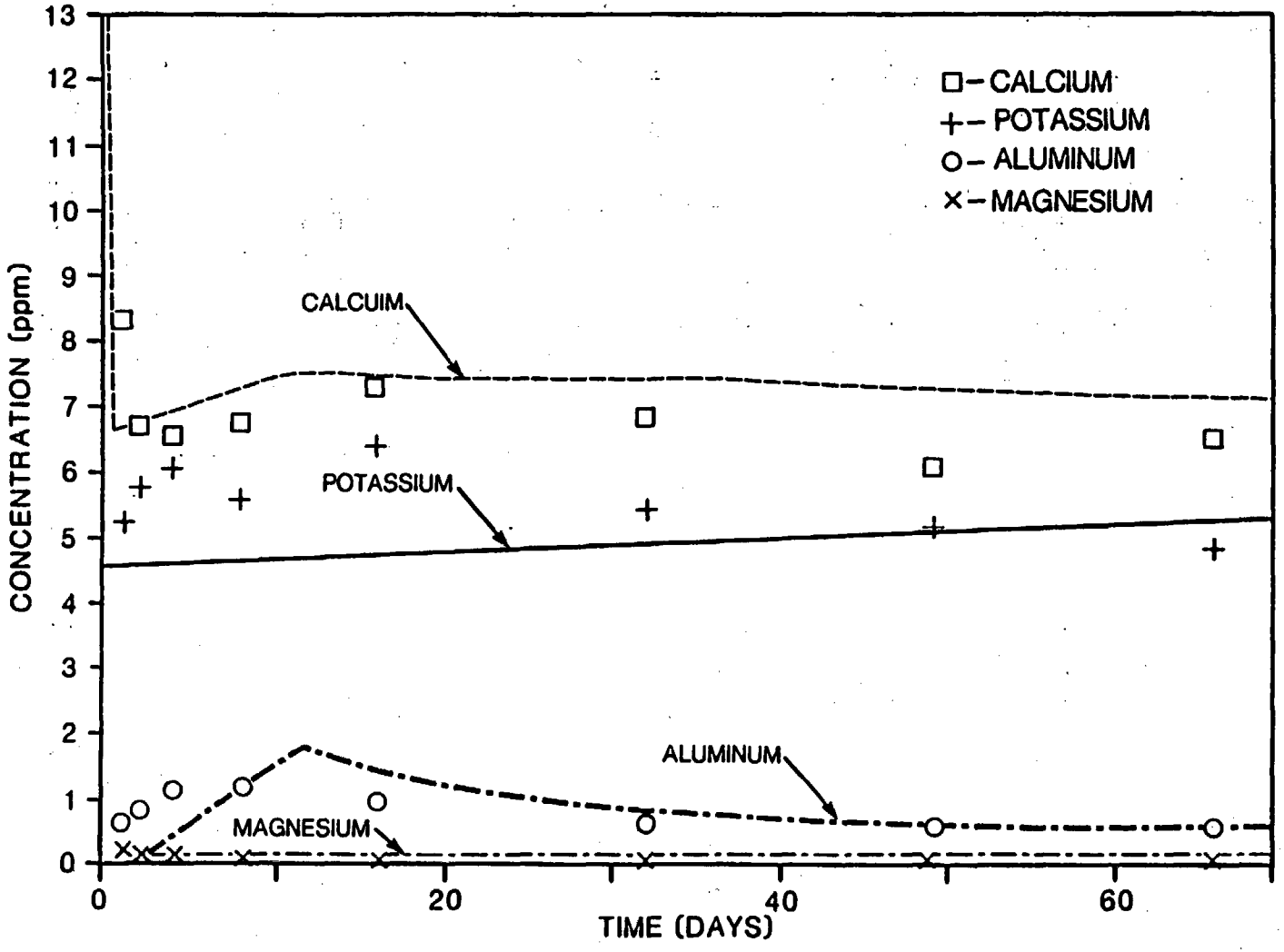

Figure 7-9. Comparison of fluid composition from EQ3/6 calculations and actual measured values for calcium, potassium, aluminum, and magnesium in water from well J-13 reacted with Topopah Spring tuff at 150°C. The lines indicate the results of the EQ3/6 calculations; the symbols represent the experimental results. Modified from Delany (1985).

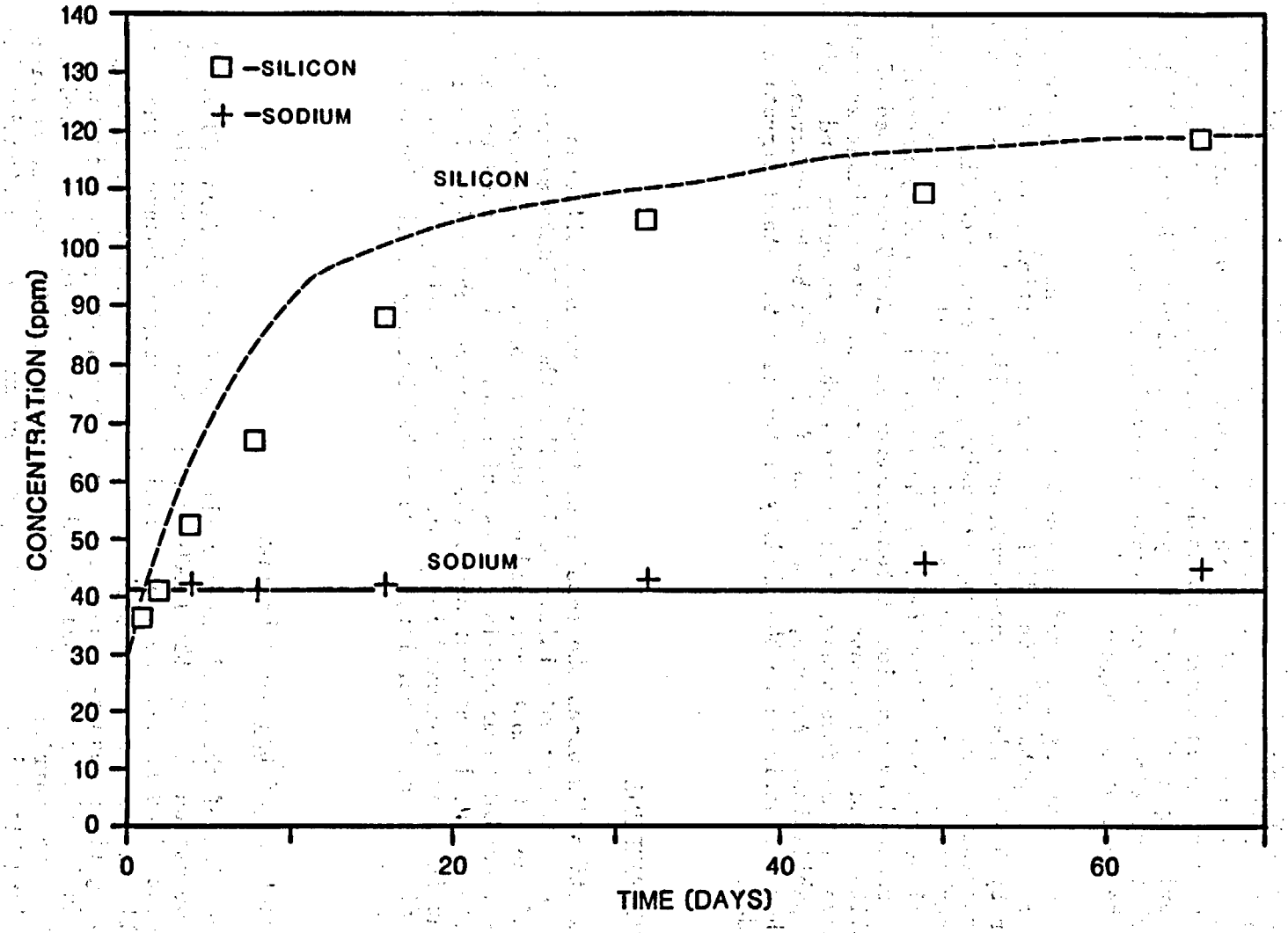

Figure 7-10. Comparison of fluid composition from EQ3/6 calculations and actual measured values for silicon and sodium in water from well J-13 reacted with Topopah Spring tuff at 150°C. The lines indicate the results of the EQ3/6 calculations; the symbols represent the experimental results. Modified from Delany (1985).

The model used a system open to the atmosphere so that carbon dioxide and oxygen were available as reactants in essentially infinite supply. The model calculation was done at 150°C using the core wafer model parameters and a reaction interval of 100 yr. EQ6 predicted that the solution composition would reach steady state at 150°C after 180 d. If adjustment is made to account for the high rock surface area-to-water volume ratios (SA:V) expected in the repository, as compared with the experiments, the dissolution that occurs during 1 yr in an experiment would be approximately comparable to that occurring during approximately 1,000 yr in the repository (Delany, 1985). The approach to steady-state concentrations should, however, be faster in the repository because of the higher SA:V.

The water chemistry measured in short-term tests and predicted through the use of reaction path modeling differed from the initial well J-13 water composition by having higher concentrations of silicon, aluminum, and sodium and lower concentrations of calcium, magnesium, potassium, and dissolved inorganic carbon species. The pH remained near neutral, and no significant source of anions has been identified in the rock. The secondary mineral assemblage produced by reaction at temperatures up to 250°C consisted of clays, zeolites, and small amounts of other minerals. The dominant secondary minerals have high surface areas, high cation exchange capacity, and positive sorption capabilities. As such, alteration of the rock by hydrothermal reaction should contribute to the ability of the site to retard migration of radionuclides.

7.4.2 METAL BARRIERS

This section discusses the results of testing several different waste-package container materials. It describes the candidate materials, the functions of the metal container, and degradation modes that can occur for the different candidate materials. This information will be used to select one candidate material that best meets the performance objectives for a waste package container, as discussed in Section 7.2. The waste package components, including the metal barrier, are described briefly in the introduction to this chapter.

7.4.2.1 Functions of the metal barrier

The function of the metal barrier will change from the first 50 yr of repository operation through the 1,000 yr containment period and the 1,000 to 10,000 yr controlled release period following repository closure. The metal barrier will function as the vessel for transporting, handling, emplacing, and retrieving (if necessary) the contents of the waste package in the repository during the operational period. During the first 1000 yr following closure, the metal barrier will be relied upon to provide complete containment for a large fraction of the waste packages and to be a substantial impediment to release of radionuclides by aqueous transport from those packages with breached containers. During the subsequent controlled release period, many containers may remain intact. Breached containers are expected to

continue to inhibit transport of liquid water into, and radionuclides out of the waste packages. The performance allocated to the metal container is disucssed further in Section 8.3.5.9.

7.4.2.2 Candidate materials for waste package containers

The NNWSI Project is evaluating six candidate materials for the waste package container. These six materials fall into two alloy families: (1) austenitic materials and (2) copper-based materials. The austenitic materials are AISI 304L, AISI 316L, and Alloy 825. Because of the high nickel content of Alloy 825 (about 40 percent) compared with the 300-series stainless steels (about 10 percent), Alloy 825 (e.g., Incoloy 825) is a transition material between iron-base and nickel-base systems. Although many of the same degradation modes that commonly affect the austenitic stainless steels can potentially affect Alloy 825, the overall difference in corrosion resistance places Alloy 825 in a separate grouping.

The candidate copper-based materials are oxygen-free copper (CDA 102), 8 percent aluminum-bronze (CDA 613), and 70-30 copper-nickel (CDA 715). The industry-standard compositions and selected mechanical properties of these candidate materials are given in Tables 7-4, 7-5, 7-6, and 7-7 in Section 7.3.

AISI 304L stainless steel (SS) was selected in 1983 as the reference material for the NNWSI Project waste package designs. A thin-walled design was chosen because of the planned location of the repository above the water table and the projected absence of significant hydrostatic or lithostatic loads. A reference material was established so that the waste package and repository design tasks could proceed in parallel with the metal barriers testing. The reference material established a benchmark to which the performance of other materials can be compared. AISI 304L SS was selected because of its excellent corrosion and oxidation resistance in steam, air, and natural waters similar in composition to well J-13 water. AISI 304L SS has adequate mechanical properties and can be fabricated and welded by a variety of processes. In addition, a substantial database exists for AISI 304L SS in a variety of engineering applications. By definition, a reference material should be a viable candidate, although it may not necessarily become the finally chosen material. The planned material selection process is described in Section 8.3.5.9.

In 1984, the NNWSI Project was requested by the Office of Geological Repositories (OGR) to evaluate copper or a copper-based alloy as a waste package container material. At the end of FY 1986, the NNWSI Project determined that copper-based materials have not been shown infeasible for containers, and further study is warranted. Some virtues of copper-based materials are (1) they have electrochemical nobility, (2) they represent simpler metallurgical systems in terms of the number of components and phases, and (3) they are potentially susceptible, under repository conditions, to degradation modes that are different from those for austenitic stainless steels. The results of studies on copper-based materials are discussed in Section 7.4.2.9.

7.4.2.3 Degradation modes of austenitic materials under repository conditions

Various forms of corrosion and oxidation attack by the environment on the metal container constitute the most likely degradation modes; the process by which the container is fabricated and closed and the strains imposed by these processes and by internal and external stresses on the container can further affect the different degradation modes. Research and development activities for metal barriers are centered around these various degradation modes with the purpose of discerning which of these degradation modes are applicable and in what time period after permanent closure of the repository each particular degradation mode may be operable.

One of the most important factors in determining which degradation modes may be operable is the anticipated postclosure environment at the Yucca Mountain repository. A summary of the anticipated conditions is given in Section 7.4.1. Summaries of important results from tests in which the candidate container materials have been subjected to different environmental conditions are presented in this section.

Some of the testing has been performed under anticipated environmental conditions; however, many tests have been performed under unanticipated conditions. The reasons for conducting tests under unanticipated conditions are (1) the particular set of environmental conditions accelerates the corrosion mode, thus making quantitative assessment of the long-term effect possible in relatively short-term laboratory tests, and (2) the set of environmental conditions, in certain instances, presents a possible worst case scenario of credible, although unlikely, conditions for comparison of the performance of different candidate materials under adverse conditions. An example of a worst-case scenario is testing in saturated vapor or moist air with a high gamma radiation field.

The austenitic materials are generally corrosion resistant because of the formation of a protective, passive film on the surface. The passive film is characteristically 50 to 100 angstroms thick; structurally, the film is an amorphous chromium-rich iron oxide when the austenitic material is in contact with aqueous environments; at higher temperatures, a more stable chromium-nickel spinel structure forms. The passive film is generally stable in mildly to moderately oxidizing environments and over a wide range of pH. The low corrosion and oxidation rates of passive austenitic materials are controlled by mass transport through the passive film; continuous dissolution and reformation of the film occurs. Breakdown of the passive film exposes the thermodynamically active substrate to the environment and is the first stage of rapid general corrosion or of initiation of localized corrosion and stress corrosion cracking. The mechanical properties of the film influence initiation of corrosion under stress and rupture of the film when the chemical environment does not favor rapid repassivation of the alloy. Projections of long-term satisfactory performance of austenitic containers depend on maintenance of the passive film. Modeling of the corrosion behavior under a variety of expected and possible (though unlikely) environmental conditions is therefore based on the chemical and mechanical stability of the passive film.

AISI 304L SS, as well as the other austenitic materials, shows excellent general corrosion resistance in aerated dry steam environments (less than the saturation steam content at the relevant temperatures and pressures) as well as in wet steam and in vadose water with a composition similar to well J-13 water. Radiolysis products, such as hydrogen peroxide and oxides of nitrogen and even dilute nitric acid, are not expected to increase the general corrosion rate by a significant factor provided that the material is not sensitized (Section 7.4.2.5). The degradation mode limiting the use of AISI 304L SS and the other austenitic materials is rarely general corrosion, but rather much more rapid penetration via localized or stress-assisted forms of corrosion. The objective of the metals testing activities is to determine to what extent these forms of corrosion would occur during the containment period, the hybrid containment-controlled release period, and the controlled release period. Corrosion modes that will receive particular attention are summarized in Sections 7.4.2.3.1 through 7.4.2.3.3.

7.4.2.3.1 Corrosion forms favored by a sensitized microstructure

A sensitized microstructure could develop during fabrication and welding of the container or possibly during the very long times (decades to centuries) in the containment period because of the elevated temperature resulting from thermal output by radioactive decay of the waste form. Such a sensitized microstructure might lead to intergranular corrosion or intergranular stress corrosion cracking if a suitable aqueous environment (liquid water intrusion or condensation of wet steam on the container surface) were to come in contact with the sensitized region. These forms of corrosion are favored by oxidizing aqueous conditions.

7.4.2.3.2 Corrosion forms favored by concentration of various chemical species in well J-13 water

Continuous evaporation during downward infiltration of water through a region where the temperature rises with depth may leave a residue of ionic salts in the rock pores. Later dissolution of these salts by new water could increase the ionic content of water now able to penetrate to the repository horizon after the boiling point isotherm has retreated to a location within the container. Another way of concentrating ionic salts is by having flow paths through fractures above the repository that admit episodic surges of water that then contact the hot container surface and evaporate, concentrating the solute species. The chloride-ion concentration is of paramount concern with regard to resistance of stainless steels to pitting, crevice, and transgranular stress corrosion cracking. The other ions present in the well J-13 water may favor or retard these kinds of corrosion attacks.

7.4.2.3.3 Corrosion and embrittlement phenomena favored by transformation products from metastable austenite

This classification includes problems that are partly related to corrosion and partly related to mechanical embrittlement. The austenite in some candidate materials (304L and 316L SS) is metastable and may transform to martensite, ferrite, or sigma phase under the influence of mechanical treatment (cold work) or thermal conditions.

Brittle phases such as sigma reduce the fracture toughness so that residual and operating stresses may initiate cracks if the transformation product is more or less continuous. Other transformation products such as martensite and possibly ferrite may be more susceptible to hydrogen pickup and embrittlement. Martensite formation is favored by high plastic deformation. These effects are most likely to occur in and around welds. Gamma radiation is the only significant radiation that the container will encounter. The rates of atomic displacement in electromagnetic (as opposed to particle) radiation are too low to cause metallurgical reactions such as austenitic transformation or carbide precipitation.

Recent investigations of potential degradation modes have revealed the occurrence of severe localized corrosion and stress corrosion cracking of stainless steel caused by microbiological organisms altering the chemical nature of the environment. Microbiologically induced corrosion has occurred under circumstances where it was quite unexpected, a recent example being cited in the paper by Stoecker and Pope (1986). An evaluation of whether the microorganism can survive in a dormant state during the hot, dry period and high accumulated gamma dose rate, and then revive at a later time is planned even though the chances of this occurring are remote. These studies are addressed in Section 8.3.5.9.

7.4.2.4 General corrosion and oxidation of austenitic materials

Low temperature oxidation will occur from the time that the waste packages are emplaced in the repository (and even before). General aqueous corrosion can occur when liquid water is present in the environment, either from intrusion of ground water to the container surface or from condensation of steam on the container surface.

Coupons of the candidate materials have been exposed to environments that approach those that may be expected in the repository during the containment period, the hybrid containment-controlled release period, and the controlled release period. Test environments have included well J-13 water, wet steam, and dry steam at various temperatures. In addition, some coupons have been exposed to irradiated well J-13 water and steam (tests conducted in a cobalt-60 gamma irradiation facility). The tests have been described by McCright et al. (1983), Juhas et al. (1984), and McCright et al. (1987). The average corrosion penetration rate is calculated from the weight loss experienced during the exposure interval, and the exposed surface is examined for the pattern of corrosion attack (uniform, localized, or edge).

7.4.2.4.1 Oxidation and general corrosion test results

Results obtained from coupons immersed in well J-13 water maintained at different temperatures show that the corrosion penetration rates were low (all substantially less than 1 micrometer per yr), with little variation during the exposure period. After more than 10,000 exposure hours in well J-13 water at different temperatures, general corrosion rates in the range 0.030 to 0.225 micrometer per yr were calculated (Glass et al., 1984; McCright et al., 1987). Data obtained at shorter exposure times have been summarized and discussed by Glass et al. (1984). Little change in the general corrosion penetration rate occurred with exposure time; for example, AISI 304L SS had time-average corrosion rates of 0.094 micrometer per yr after 3,548 h and 0.072 micrometer per yr after 10,360 h in well J-13 water at 100°C. The general corrosion rate was approximately the same for all the alloys tested; alloying differences would be expected to be distinguished only in more aggressive environments. The trend of results indicates a small decrease in the corrosion rate with increasing temperature, which may be due to the formation of a slightly thicker passive film or to the decrease in dissolved oxygen and nitrate ion concentrations at the higher temperatures.

Corrosion tests performed on candidate austenitic stainless steel coupons in wet steam (saturated at the test temperature of 100°C and at atmospheric pressure) and dry steam (unsaturated at the test temperature of 150°C and atmospheric pressure) also showed expected low general corrosion penetration rates, calculated to be comparable with those in the well J-13 water (McCright et al., 1987). However, all the specimens tested in the dry steam showed weight gains, and specimens tested in the wet steam showed weight losses. For specimens that showed weight gains, the results are expressed in terms of the corresponding amount of metal that would have been converted to oxide to create the increase (McCright et al., 1987).

Corrosion tests have been performed on AISI 304L SS coupons under irradiated environmental conditions. A 1-yr test was conducted at room temperature in partially aerated (5 ppm measured oxygen content) well J-13 water containing crushed tuff, with an average gamma dose rate of 6×10^5 rads/h (Juhas et al., 1984). An identical but nonirradiated test was conducted simultaneously for control. The nonirradiated coupons showed higher corrosion rates than comparable irradiated coupons although the amount of corrosion penetration was very small in all cases. No evidence of intergranular penetration was noted on specimens that were metallographically sectioned and examined.

7.4.2.4.2 Summary and analysis of general corrosion and oxidation testing

In summary, the general corrosion rates of the candidate stainless steels listed in Table 7-10 are quite small and, thus far, do not seem to be significantly affected by (1) alloy composition, (2) temperature (28 to 150°C), (3) exposure time (up to 11,000 h), (4) irradiation (background to more than 1×10^5 rad/h), or (5) whether the environment was wet or dry. A value of 0.2 micrometer per yr would appear to be adequate to describe conservatively the rate data so far acquired (Oversby and McCright, 1984). Extrapolation of these rates indicates that a container made of any of the

Table 7-10. General corrosion rates of candidate austenitic stainless steels in well J-13 water at different temperatures[a]

Alloy	Temp (°C)	Time (h)	Medium	Corrosion rate (μm/yr)[b] Average	Standard deviation
304L	50	11,512	Water	0.133	0.018
316L	50	11,512	Water	0.154	0.008
825	50	11,512	Water	0.211	0.013
304L	80	11,056	Water	0.085	0.001
316L	80	11,056	Water	0.109	0.005
825	80	11,056	Water	0.109	0.012
304L	100	10,360	Water	0.072	0.023
316L	100	10,360	Water	0.037	0.011
825	100	10,360	Water	0.049	0.019
304L	100	10,456	Saturated steam	0.102	(c)
316L	100	10,456	Saturated steam	0.099	(c)
825	100	10,456	Saturated steam	0.030	(c)
304L	150	3,808	Unsaturated steam	0.071	(c)
316L	150	3,808	Unsaturated steam	0.064	(c)
825	150	3,808	Unsaturated steam	0.030	(c)

[a]Source: McCright et al. (1987).
[b]Average of three replicate specimens of each alloy in each condition.
[c]Not determined.

candidate materials with a 1-cm-thick wall would not be penetrated as a result of general corrosion for well over 1,000 yr.

A model is being developed to quantify general corrosion and to allow for extrapolation of the data to long time periods (Section 8.3.5.9.3, Information Need 1.4.3).

7.4.2.5 Intergranular corrosion and intergranular stress corrosion cracking

Experience with the candidate austenitic materials has shown that they are susceptible to stress corrosion cracking. The crack propagation path (intergranular or transgranular) is often an important indication of the causative mechanism for stress corrosion and therefore serves as the basis for modeling activities for projecting container lifetimes. In some instances, both intergranular and transgranular crack paths occur but one or the other cracking pattern dominates. Cracking along intergranular paths (and intergranular attack without stress assistance) is the subject of this section.

Intergranular corrosion attack (IGA) and intergranular stress corrosion cracking (IGSCC) are most frequently associated with a sensitized microstructure as a necessary precursor to attack. A sensitized microstructure develops when chromium carbide precipitates from solid solution (austenite or gamma phase), leaving a region depleted in chromium in the vicinity of the precipitate. This precipitation occurs most frequently along grain boundaries, and it can lead to serious degradation when the precipitates and resulting chromium-depleted zones form a continuous network across the container thickness. The protective passive film on the sensitized grain boundary is not as stable as that on the bulk material because the chromium content is lower (less than 12 weight percent in the boundary compared with 18 to 20 weight percent in the bulk). When the sensitized material is exposed to oxidizing aqueous environments, the grain boundary area tends to corrode preferentially, and the attack can proceed along the continuous network of chromium-depleted zones; hence, intergranular attack occurs. In the presence of applied stress on a sensitized stainless steel, preferential intergranular attack is favored under less aggressive environmental conditions than intergranular attack without stress assistance and results in intergranular stress corrosion cracking.

There have been reported observations of IGSCC occurring in nonsensitized material. The most common occurrence is in conjunction with transgranular stress corrosion cracking (TGSCC) in chloride-containing environments where the crack propagation path has both a transgranular and an intergranular component. This has been discussed by Cowan and Gordon (1977), primarily for AISI 304 stainless steel in concentrated boiling magnesium-chloride ($MgCl_2$) solutions. The transgranular path is the dominant of the two paths in chloride-containing environments. The intergranular component appears to be favored more when the chloride concentration is low, the temperature is low, and when alloying additions are made to the base material. As discussed in Section 7.4.2.6 on TGSCC of austenitic materials, the conditions that favor development of the intergranular path over the transgranular path are the same conditions that favor an overall increase in resistance to stress corrosion cracking regardless of the propagation path.

Another environment in which both crack propagation paths can occur in nonsensitized material is in hot concentrated caustic solution (Wilson and Aspden, 1977). Polythionic acid is another reagent that occasionally causes stress corrosion cracking of nonsensitized stainless steel (Theus and Staehle, 1977). These environmental conditions appear to be extremely unlikely to develop under any scenarios envisioned for the repository.

The experience in BWR cooling water does appear to be applicable, at least as a starting point, for material testing and modeling activities. AISI 304 stainless steel is used for the recirculating piping around the reactor core and many incidents of stress corrosion cracking have occurred. All the cracking has been intergranular and all has been associated with sensitized microstructures occurring in the heat-affected zones in welded sections. The mildly oxidizing condition of both the BWR cooling water and that of ground water associated with the geological formation at the Yucca Mountain repository site suggest that the two environments are somewhat comparable.

7.4.2.5.1 Detection of sensitized microstructures

Chromium carbide precipitation is favored by exposure of austenitic stainless steels to moderately high temperatures (generally in the 500 to 800°C range) for periods ranging from minutes to many hours. The carbon content of the stainless steel is an important factor in determining susceptibility to sensitization. Time-temperature-sensitization (TTS) curves have been generated for the austenitic stainless steels; an example is shown in Figure 7-11. During post weld cooling, the heat-affected zone near the weld can cool at a rate such that it enters the "nose" of the TTS curve. Lower-carbon stainless steels such as AISI 304L with 0.03 weight percent maximum carbon have been developed to resist sensitization. For these alloys, only prolonged heating would move the material into the nose of the curve. A considerable amount of literature is available on the details of sensitization and the ways of detecting it (Clarke et al., 1978; Streicher, 1978).

Some difficulties are encountered in applying American Society for Testing and Materials (ASTM) tests to predict sensitization. More recently, tests involving electrochemical polarization of a specimen exposed to an acid thiocyanate solution have been developed. Sensitized microstructures give a polarization transient with a shape significantly different from that of nonsensitized structures, and integration of the area under the curve is quantitatively proportional to the amount of grain boundary area attacked. These electrochemical tests are called electrochemical potentiokinetic reactivation (EPR) tests (Majidi and Streicher, 1984).

Materials and processes that lead to gross sensitization would not be used in waste packages, but partial sensitization occurring along a limited number of grain boundaries or other pathways might occur. The degree of partial sensitization and the time required to achieve this condition needs to be quantified to predict the degradation mode by intergranular mechanisms. Although the EPR technique and the ASTM A 262 test methods (ASTM, 1982) use environments that are considerably more aggressive than the expected service conditions, these techniques are useful for screening materials and conditions that could lead to intergranular corrosion attack and intergranular stress corrosion cracking. Work using these techniques is planned and is discussed in Section 8.3.5.9.

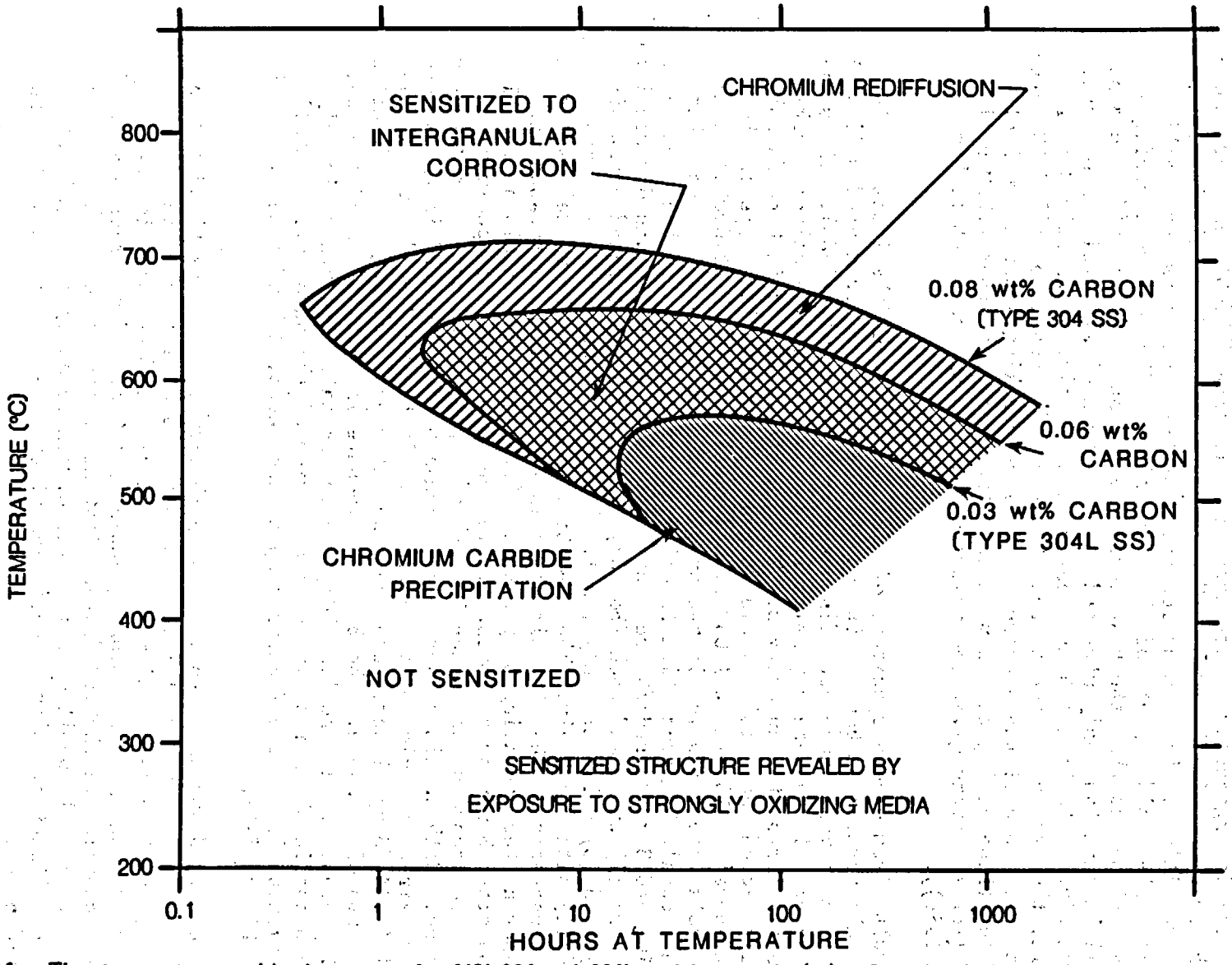

Figure 7-11. Time-temperature-sensitization curves for AISI 304 and 304L stainless steels (ss). Cross-hatched region indicates where sensitized microstructures develop as a function of heating time, heating temperature, and carbon content in the alloy. Sensitized microstructures occur when chromium carbides precipitate and deplete local areas of chromium (lower bound of hatched region); heating for longer periods of time restores original chromium content in these areas (upper bound of hatched region). Modified from Shreir (1976).

7.4.2.5.2 Tests to detect intergranular stress corrosion cracking susceptibility

Several intergranular stress corrosion cracking (IGSCC) tests are underway with specimens of AISI 304L, AISI 316L, and Alloy 825 steels in various material conditions. Four-point loaded, bent-beam specimens were machined from cold-worked welded plate of these materials. The bent-beam configuration was chosen so that the base metal, weld zone, and heat-affected zone could all be simultaneously stressed at the same nominal level. Some specimens were given intentional heat treatments to develop a sensitized microstructure; then these specimens were stressed and exposed to well J-13 water and to steam. None of the specimens exhibited cracking after 2,000 h of testing for those having no postweld heat treatment and after 4,000 h of testing (for specimens given the postweld sensitizing treatment (Juhas et al., 1984)).

Results from U-bend specimens of AISI 304 and 304L (the latter having 0.017 weight percent carbon) stainless steel exposed to irradiated well J-13 water and water vapor have been discussed by Juhas et al. (1984). The self-loading nature of the U-bend permits its use in the small available working space in the irradiated autoclaves. Maximum stress levels in U-bends substantially exceed the initial yield stress. These materials were in the solution-annealed (15 min at 1,050°C) and sensitized (24 h at 600°C) conditions. Tests were performed in two autoclaves, one at 50°C and the other at 90°C, in a cobalt-60 irradiation facility at irradiation absorbed dose rates of 6×10^5 and 3×10^5 rads/h, respectively. Each autoclave was divided into three zones: (1) water and rock (bottom), (2) rock and saturated moist air (middle), and (3) moist air only (top). The air in the test vessel was purged daily with fresh air. The operating pressure in the vessel was essentially atmospheric so that the air space in the vessel was saturated with water vapor at the operating temperature. Specimens were examined after 1 month and after 3 months of exposure. In the 50°C test, two specimen failures were recorded: one after 1 month of exposure and one after 3 months of exposure. Both specimens were sensitized AISI 304, located in the saturated moist air-only region of the autoclave. In the 90°C study, two sensitized AISI 304 SS specimens, both from the water and rock region, had failed after 1 month of exposure. The 3-month exposure inspection showed two additional failures: both were AISI 304, one in the saturated moist air only region and one in the moist air and rock region of the autoclave. Metallographic examination of the fractured specimens revealed IGSCC; an example is shown in Figure 7-12.

The observed stress corrosion susceptibility of the sensitized AISI 304 was expected. None of the AISI 304L SS specimens have cracked intergranularly, but they have exhibited transgranular stress corrosion cracking (TGSCC) in subsequent inspections (Section 7.4.2.6). The larger number of failures occurring in the irradiated moist air phase suggests that a more severe environmental condition exists there, generated by radiolysis of the environment without dilution or buffering of the species produced, than in the liquid phase.

Essentially, the slow strain rate test is a determination of the effect of the environment on degradation of mechanical properties (yield strength, tensile strength, elongation, and reduction in area). Specimens are loaded

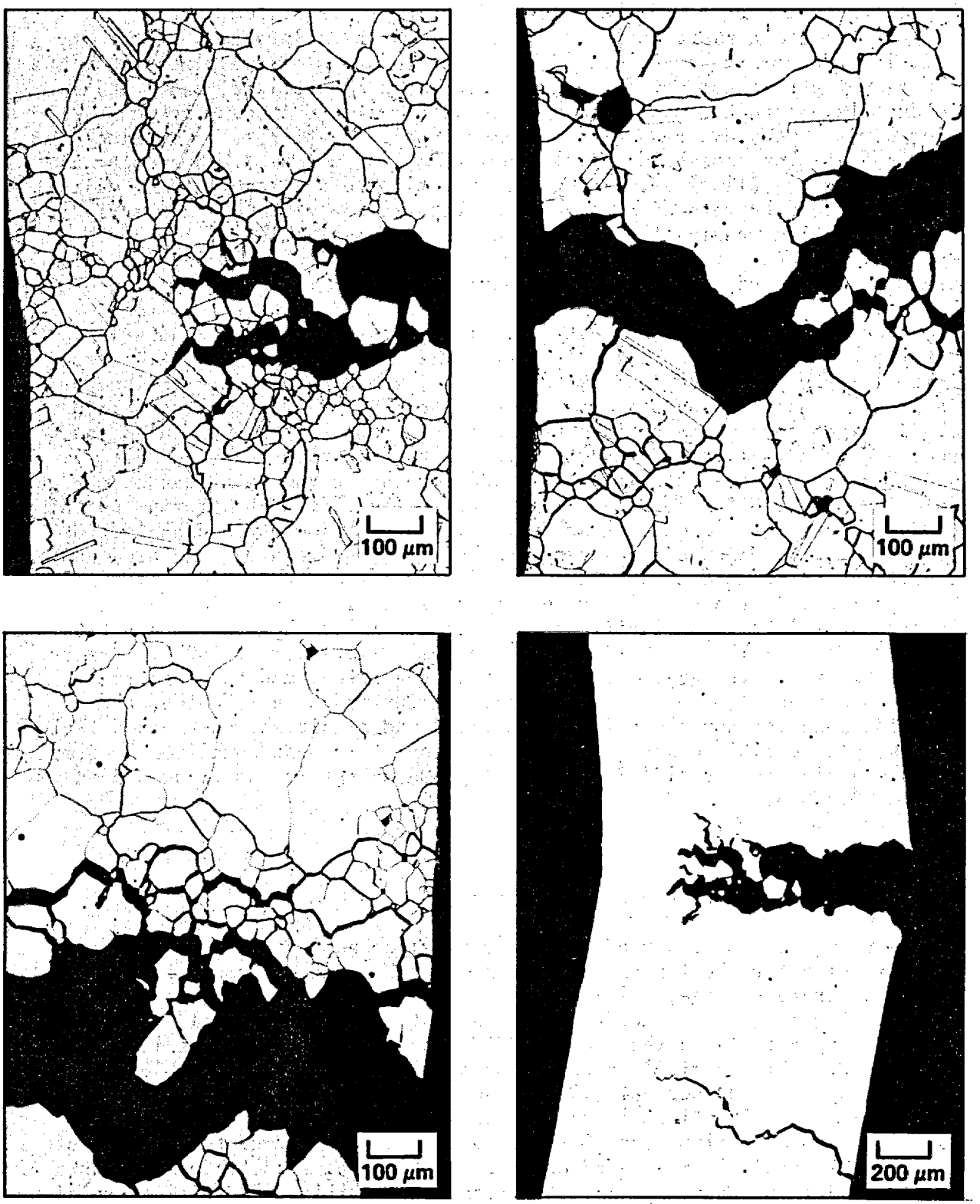

Figure 7-12. Metallographic cross sections of sensitized U-bend specimens of 304 stainless steel showing intergranular stress corrosion cracking. Modified from Juhas et al. (1984).

until fracture occurs and the fractured surface is examined, usually by scanning electron microscopy. A stress corrosion failure is indicated by a brittle fracture with evidence of grain facets and cleavage planes. In the absence of stress corrosion, the specimen fails by overload, and the failure is ductile, with characteristic plastic deformation. In many respects, the slow strain rate test resembles a common tensile test, but the specimens are strained at slow crosshead speeds (less than 1×10^{-4} s^{-1}). Straining at these low rates allows study of the competition between the rate of slip step emergence and the rate of environmental interaction with this new surface, the interaction causing the dissolution or the passivation of the new surface. Mechanisms of stress corrosion cracking in metals involve the transition from passive to active behavior.

Results of testing the austenitic materials in 150°C aerated well J-13 water are summarized in Tables 7-11 and 7-12 (Juhas et al., 1984). These initial tests were performed at this more elevated temperature to induce failure in some of the test specimens. The AISI 304 material contained 0.054 weight percent carbon and was tested in both the mill-annealed (as received from the vendor) condition and in the solution-annealed and sensitization-treated condition (1,050°C for 15 min and water quench, followed by 600°C for 24 h and air cooled). The AISI 304L material contained 0.024 wt. percent carbon and was tested in both the solution annealed (1,050°C for 15 minutes and water quenched) and the solution annealed and sensitization-treated condition (600°C for 10 h and air cooled). The AISI 304 specimens in the solution annealed and sensitized condition failed intergranularly with a significant drop in ductility when the strain rate was reduced from 1×10^{-4} to 2×10^{-7} s^{-1} in well J-13 water at 150°C. Cracks were found along the gage section of these specimens, and the fracture surfaces showed clear evidence of intergranular fracture. Neither the solution-annealed nor the solution-annealed and sensitization-treated AISI 304L samples exhibited stress corrosion under these test conditions. Similar tests are planned for AISI 316L and Alloy 825 materials, as discussed in Section 8.3.5.9.

7.4.2.5.3 Low temperature sensitization

Although the L grades of stainless steel do not appear susceptible to sensitization for the length of time the container might remain in the 500 to 800°C temperature range, a long-term, low temperature sensitization might occur during the tens to hundreds of yrs that the container will experience surface temperatures in the 100 to 270°C range after emplacement in the repository. This possibility of low temperature sensitization (LTS) was analyzed by Fox and McCright (1983), who concluded that heavily cold-worked AISI 304L SS (0.028 weight percent carbon) could develop a sensitized structure after as little as 10 yr at an isothermal surface temperature of 280°C. This analysis was based on extrapolating the results from the work of Briant (1982) in support of investigations on sensitized 300-series stainless steels under BWR environmental conditions. Reduction of the container surface temperature in the repository could cause a significant increase in the time required to develop a sensitized microstructure; for instance, the stainless steel in Briant's (1982) work would take 120 yr to sensitize isothermally at 250°C and 4,000 yr at 200°C (Fox and McCright, 1983). In

Table 7-11. Results of slow strain rate tests on AISI 304 stainless steel at 150°C[a]

Environment	Strain rate (s^{-1})	Reduction of area (%)	Elongation (%)	Yield strength (ksi)	Ultimate strength (ksi)
		MILL-ANNEALED SPECIMENS			
Air	$1x10^{-4}$	80.2	48.0	37.4	74.4
Air	$2x10^{-7}$	76.5	45.0	35.9	76.6
J-13[b]	$1x10^{-4}$	77.9	47.0	36.1	75.3
J-13	$1x10^{-4}$	79.6	46.0	36.3	74.9
J-13	$2x10^{-7}$	75.7	50.0	33.5	77.5
J-13	$2x10^{-7}$	76.4	47.0	35.1	77.0
		SOLUTION-ANNEALED AND SENSITIZATION-TREATED SPECIMENS			
Air	$1x10^{-4}$	72.2	50.6	21.9	68.0
Air	$1x10^{-4}$	66.5	51.5	26.0	68.8
J-13	$1x10^{-4}$	75.5	53.5	23.5	68.8
J-13	$1x10^{-4}$	74.9	51.0	23.5	69.0
J-13	$2x10^{-7}$	50.9	ND[c]	22.0	70.1
J-13	$2x10^{-7}$	26.4	ND[d]	20.7	64.5

[a]Source: Juhas et al. (1984).
[b]Air-sparged well J-13 water.
[c]ND = not determined.
[d]Broke at gage mark.

reality, the container surface will cool continuously. Therefore, predictions based on isothermal conditions are very conservative. A subsequent analysis (Oversby and McCright, 1984) indicated that with a peak surface temperature of 250°C followed by cooling at a rate predicted from a heat transfer code under certain reference waste package conditions (Hockman and O'Neal, 1984), even the high carbon, heavily cold-worked AISI 304L SS used in Briant's (1982) work would not sensitize (Fox and McCright, 1983). Results of this analysis are illustrated in Figure 7-13.

Development of LTS can be retarded in other ways beside reduction of the peak surface temperature of the container. The mechanism for development of LTS is discussed by Povich (1978) and requires a highly cold-worked structure for nucleation of subcritical carbide precipitates that are formed in the usual sensitization temperature range (above 500°C) but are not discernible by any of the American Society for Testing and Materials (ASTM) tests. These

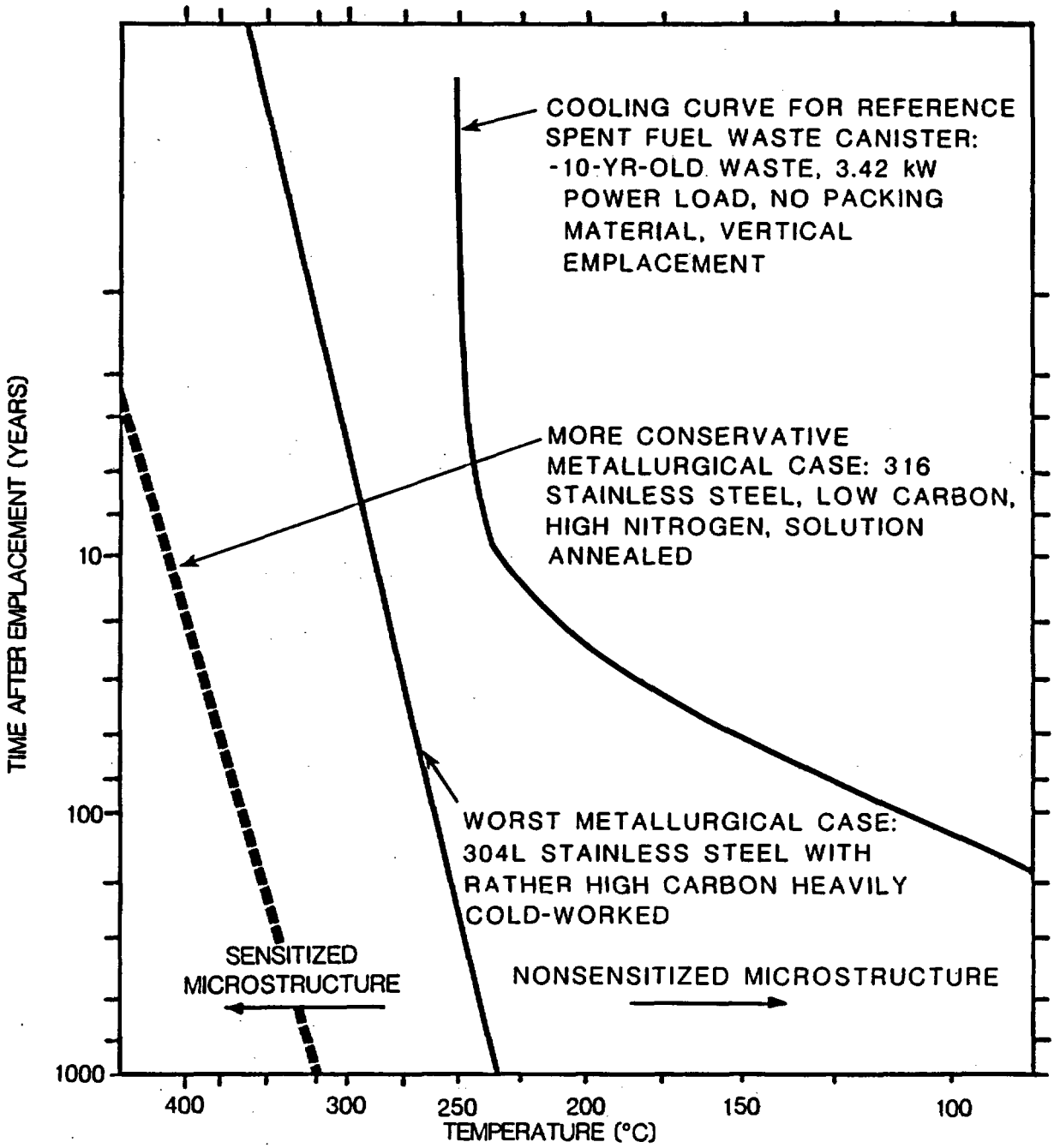

Figure 7-13. Relationship between thermal history of emplaced nuclear waste containers and long-term sensitization of austenitic stainless steels. Modified from Oversby and McCright (1984)

Table 7-12. Results of slow strain rate tests of AISI 304L at 150°C[a]

Environment	Strain rate (s^{-1})	Reduction of area (%)	Elongation (%)	Yield strength (ksi)	Ultimate strength (ksi)
		SOLUTION-ANNEALED SPECIMENS			
J-13[b]	$1x10^{-4}$	80.5	54.0	25.8	68.4
J-13	$1x10^{-4}$	78.4	52.0	27.1	68.2
J-13	$2x10^{-7}$	68.7	48.0	28.4	67.7
J-13	$2x10^{-7}$	72.9	46.3	26.7	68.2
		SOLUTION-ANNEALED AND SENSITIZATION-TREATED SPECIMENS			
Air	$1x10^{-4}$	73.7	49.0	29.4	68.6
J-13	$1x10^{-4}$	72.2	49.6	ND[c]	ND
J-13	$1x10^{-4}$	74.8	51.6	29.6	69.1
J-13	$2x10^{-7}$	76.0	49.0	26.6	68.8
J-13	$2x10^{-7}$	70.4	48.0	27.2	68.8

[a]Source: Juhas et al. (1984).
[b]Air-sparged well J-13 water.
[c]ND = Not determined.

subcritical precipitates then grow when the specimen is exposed to temperatures below 500°C for prolonged periods. Obviously, reduction of the amount of cold work in the specimen vitiates development of LTS.

Work performed in response to the concerns of intergranular stress corrosion cracking (IGSCC) in BWR piping indicates that the molybdenum-bearing AISI 316L SS is considerably more resistant to LTS (Briant et al., 1982; Mulford et al., 1983). The same group also tested special grades of 316 and 304 SS with extra low carbon (<0.02 weight percent) and with intentionally high nitrogen contents (>0.06 weight percent) and found that these compositions produced beneficial effects. Special nuclear grades of 316 SS with high nitrogen and low carbon are recommended as replacement materials for 304 SS piping in BWRs (Proebstle and Gordon, 1982; Danko, 1984). It appears that the molybdenum and nitrogen additions impede the diffusion of carbon atoms in austenitic stainless steels so that the growth rates of carbide nuclei are slowed, and materials containing these alloy additions are considerably more resistant to sensitization both above and below 500°C.

Some additional factors need to be considered to assess the possibility of developing a sensitized microstructure and resulting intergranular corrosion cracking (IGA) and IGSCC. With sufficient time and temperature, chromium could rediffuse from the bulk to the depleted regions and restore a uniformly high chromium content throughout the alloy. This condition would eliminate any preference for localized attack due to the lack of chromium and instability of the protective film at these locations. The activation energy for chromium diffusion is considerably higher than that for carbon diffusion so that the restoration process is slow (chromium rediffusion is indicated in the series of curves on the top-right side of the time-temperature sensitization curves (Figure 7-11)). At very long times at lower temperatures (200° to 300°C), it is possible that the series of curves bounding the sensitized region on the bottom and left in Figure 7-11 would meet those bounding this region on the top and right. Physically, this would mean that the carbide precipitates would be nucleated, but the growth of these precipitates would be so slow that the chromium content would never be locally depleted. This situation would not produce a sensitized microstructure.

On the other hand, situations that would enhance carbon diffusion at lower temperatures (such as movement of carbon atoms along dislocation pipes) could readily favor sensitization. Diffusion along dislocations is relatively more significant at lower temperatures where matrix diffusion of atoms is very slow. This competition of different mechanisms was considered by Logan (1983), who applied a finite element analysis and concluded that AISI 304L SS would not sensitize under the projected repository thermal conditions. However, his analysis did not consider the full range of reported activation energies for the different diffusion processes. Figure 7-13 indicates that if sensitization were to occur at all, it would be evident in a few yrs at temperatures in the range 200° to 300°C. This time period lies within the realm of experimental practicality, and experiments of this duration will provide an important way to determine the predominance of either a potentially beneficial or potentially detrimental effect. Plans for this type of testing are described in Section 8.3.5.9.

7.4.2.5.4 Environmental effects on intergranular stress corrosion cracking susceptibility

A sensitized microstructure is considered as being necessary for intergranular stress corrosion cracking (IGSCC) to occur. The chemical environmental conditions are also important. The phenomenon has been studied mostly under the thermal and chemical environmental conditions relevant to BWR coolant (250° to 300°C high-purity water of the order of 1 Mohm-cm resistivity, under pressure, with varying oxygen contents usually ranging from 2 to 8 ppm). The general conclusion from this work is that the stronger the oxidizing potential of the environment, the greater the susceptibility for IGSCC in sensitized materials. The work of Fujita et al. (1981) indicated that gamma radiation (4.5×10^4 rads/h) further increased the stress corrosion susceptibility of sensitized AISI 304 SS in high-purity water. They used the slow strain rate test to determine the stress corrosion cracking (SCC) susceptibility and found that the fractures were all intergranular.

It is not clear whether the ionic content of the water has any effect on susceptibility of stainless steels to IGSCC. Unlike other corrosion degradation modes on stainless steel, susceptibility toward IGSCC is probably not so strongly affected by the chloride ion. However, it is difficult to divorce all effects of the ions and the ionic strength of the solution from the processes of initiating and propagating a stress corrosion crack. Many theories of SCC consider a surface pit or crevice to be the site of initiation and the electrolyte content is important in establishing these sites (Staehle, 1971). It is also difficult to make clearly valid extrapolations of results obtained in the BWR environment to predict the behavior of waste package containers in the repository environment.

The analysis of Fox and McCright (1983) considered some of the mitigating effects that the environment might have, even on a sensitized stainless steel. First, the dominant environment for tens to hundreds of yrs after emplacement would be unsaturated steam at temperatures above 97°C. During this period, the gamma radiation field would be at its highest level; but without an electrolyte present, there would be high electrical resistance between local anodes and cathodes and, consequently, slow kinetics of oxidation. Mechanisms for aqueous corrosion become operable when a continuous moisture film is present, which appears to occur only at or below the boiling point and at relative humidities greater than 50 to 60 percent (Shreir, 1976). By the time the container surface temperature cooled to where condensation is possible, the radiation field for most of the packages would be a few rad/h. At this level of radiation, radiolytically induced changes in the aqueous environment may not have significant effects on corrosion. Experimental work thus far completed has not indicated any intergranular stress corrosion initiation in the wet simulated repository environment for the low-carbon austenitic stainless steels (McCright et al., 1983; Juhas et al., 1984).

7.4.2.5.5 Stress effects in intergranular stress corrosion cracking susceptibility

Stress is also an important factor in assessing stress corrosion susceptibility. Work performed in regard to stress corrosion cracking (SCC) of AISI 304/SS piping in BWR environments characteristically has shown that a threshold stress on the order of 70 percent of the yield strength is needed to initiate SCC, the actual threshold stress being a function of temperature, ionic concentrations, and degree of sensitization (Bruemmer and Johnson, 1984). The waste container body, including any assembly welds, could be annealed after forming to reduce residual stress. Reduction of the residual stress would also decrease the tendency for low temperature sensitization to occur during prolonged exposure to the thermal conditions of the repository, because the annealing or stress relief process on the container would have eliminated many potential high-diffusivity paths for carbide growth and chromium depletion. Any annealing or stress relieving to be performed after the final closure weld was made would probably be impractical, and this region might retain a residual stress approaching the yield strength of the material. However, different processes leave the weld and heat-affected zones in different states of stress, and it is possible to choose a process

that would leave at least the outside surface of the container in compression, to minimize the possibility of initiating SCC. The effects of different welding processes on increasing the resistance to SCC of AISI 304 SS in the BWR environment have been discussed by Iwasaki (1982). A leading process is to inductively heat the weld on one side and cool it on the other to superpose a favorably oriented thermal stress on top of the weld stress so that the surface that is exposed to the SCC causative environment is compressed. The ready accessibility of the container assembly welds is expected to be amenable to nearly any process required to demonstrate a high level of assurance that SCC will not occur. However, the closure weld presents limitations on the choice of processes that can alleviate stress corrosion concerns. This is discussed further in Section 7.4.2.7.

7.4.2.5.6 Alloying effects on intergranular stress corrosion cracking susceptibility

Another approach to minimizing sensitization is the use of the stainless steel grades with additions of alloying elements to stabilize the carbides. Recent alloy developments combine the best features of the low-carbon grades with those of the stabilized grades of stainless steels (Abe et al., 1982). The high alloy content of Alloy 825, its low carbon content, and titanium stabilization of the carbides confer a very high degree of resistance to sensitization.

7.4.2.5.7 Summary of testing and analysis to date

In summary, experimental work performed as of June 1986 has not shown any tendency for the L grades of stainless steels to stress corrosion crack intergranularly even when specimens are stressed to and beyond the yield strength and are given heat treatments that favor carbide precipitation. Exposure conditions have also been severe, including irradiated water and saturated moist air where moderately to strongly oxidizing conditions are obtained. An analysis aimed at determining whether low temperature sensitization could occur in nuclear waste containers indicated that heavily cold-worked AISI 304L SS might sensitize given the expected fabrication, welding, and storage in the thermal environment of the repository if temperatures were higher than the reference case. Viable alternatives to AISI 304L SS would be AISI 316 SS, with extra low carbon and high nitrogen modifications, and Alloy 825. Reduction of the peak surface temperature and stresses in the container would also alleviate intergranular stress corrosion susceptibility. This can be accomplished by reducing the residual stress arising from fabrication and welding of the container and also by reducing the peak temperature of the containers by appropriate design of the waste package and arrangement of waste packages in the repository. (It is advantageous to maintain the container surface temperature above the boiling point for as long as possible for overall corrosion considerations; however, from the point of view of retarding sensitization, it is advantageous to keep the surface temperature below approximately 250°C for the more susceptible materials.)

If the low-carbon grades of stainless steel were to become sensitized, the sensitization would likely be partial in that only some of the grain boundaries would be continuously depleted in chromium. Furthermore, the areas most likely to sensitize are confined to the region around the final closure weld in the container. These points are discussed more fully in Section 7.4.2.8.

A model to predict sensitization in austenitic stainless steels and an extension of this model to high-nickel materials, such as Alloy 825, are being developed. The essential feature of this model is consideration of the chromium diffusion rate as established by the chromium thermodynamic activity gradient between the activity of chromium in the bulk and that at the carbide-austenite interface. This model considers temperature, strain, and compositional effects in materials (Mozhi et al., 1985). Plans for further development of this model are discussed in Section 8.3.5.9.

7.4.2.6 Pitting corrosion, crevice corrosion, and transgranular stress corrosion cracking

These three corrosion degradation modes are governed principally by the composition of the aqueous environment when the concentration of certain ionic species in water exceeds some threshold amount. But just as the attack itself is localized, the causative environment may be localized and considerably different from the bulk environment. In most instances, the susceptibility to these degradation modes is dependent on the chloride ion concentration in the environment. A review paper by Nuttall and Urbanic (1981) discussed the levels of chloride ion needed to initiate pitting, crevice, and transgranular stress corrosion attack in AISI 304 SS. Much of their documentation on critical chloride levels (as sodium chloride) was based on the observations of Truman (1977). Figure 7-14 was adapted from their work and the chloride content of well J-13 water (approximately 7 ppm) was juxtaposed. The low level of chloride in well J-13 water suggests that AISI 304 SS would be safe from attack by these degradation modes and that a several-fold increase in the concentration would be needed before these kinds of corrosion attack would initiate. Because of the similarity in composition of major alloying elements, Type 304L is expected to behave similarly to Type 304 SS. AISI 316L and Alloy 825 are markedly more resistant to chloride-induced corrosion degradation modes, because higher thresholds of chloride ion concentration are required to initiate and propagate the corrosion attack.

Although these degradation modes have some features in common, there are important differences, particularly in the initiation phase of each mode. A brief discussion is presented here because the testing and analyses are based on aspects of the causative mechanisms; greater detail can be found in the reference text Fontana and Greene (1978).

Crevice corrosion is favored when differential concentration cells are established on a metal surface, particularly on a metal that shows active-passive behavior, as do stainless steels in many environments. The creviced area is starved for oxygen, and the passive film breaks down and cannot readily reform. Dissolution of the metal occurs at this resulting local anode, the metal ions hydrolyzing with the water to form a more acidic

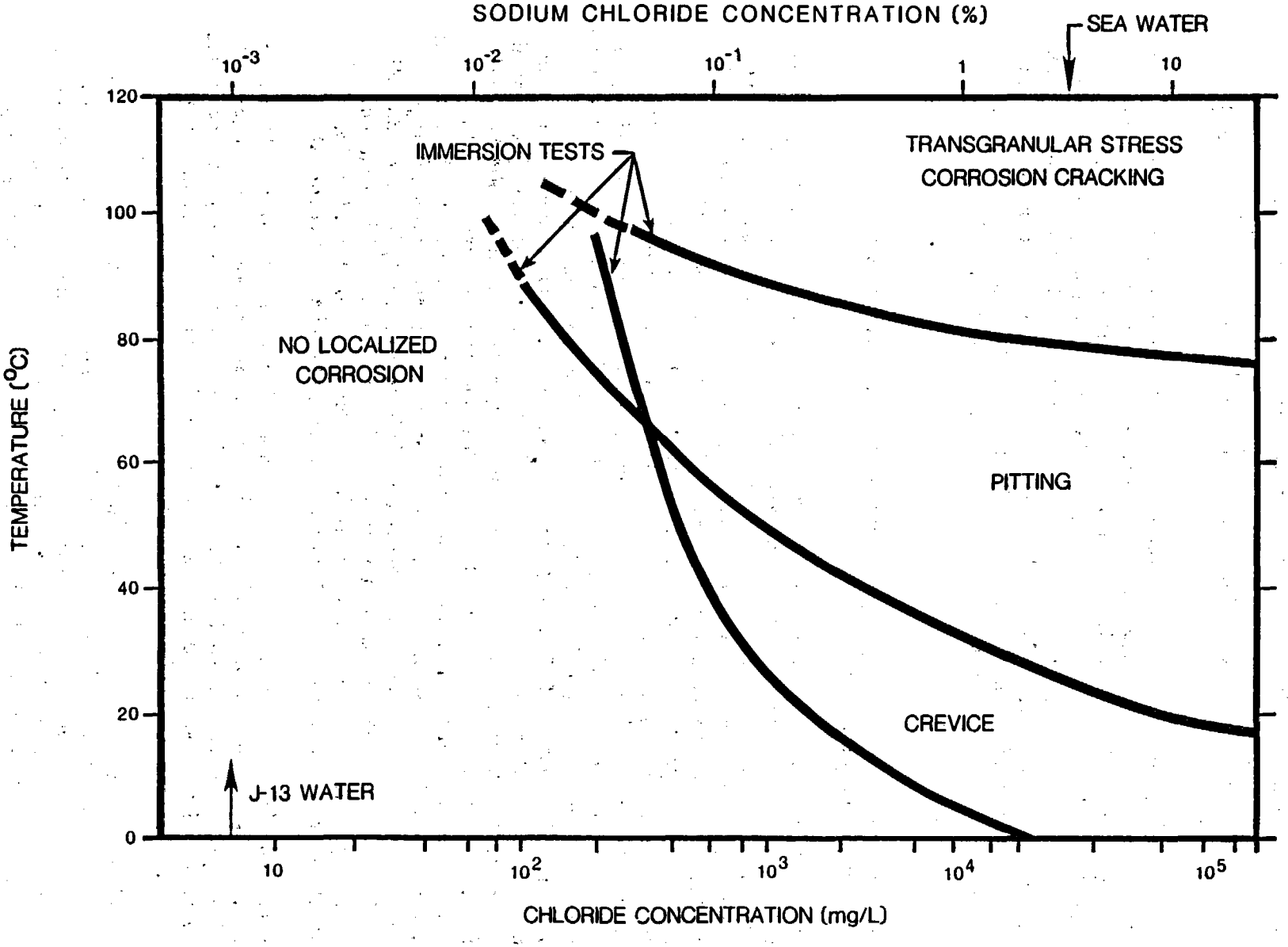

Figure 7-14. Temperature-chloride concentration thresholds for initiation of localized corrosion phenomena in sodium chloride solutions. Crevice, pitting, and transgranular stress corrosion cracking initiate to the right of their respective threshold curves as determined by immersion corrosion tests. For comparison purposes, the chloride ion concentration of well J-13 water is indicated. Modified from Nuttall and Urbanic (1981).

environment than the bulk environment. Anionic species, especially the mobile chloride ions, migrate to the anode and generally increase the ionic strength in the local environment. The local pH in the crevice region decreases, and the concentration of anionic species (such as chloride) increases. These conditions do not favor repassivation of the alloy, and a high dissolution rate of the metal in the creviced region continues.

Pitting corrosion is initiated at weak points in the passive film. Pits form preferentially at locations such as inclusions (especially certain sulfide-rich inclusions) on the exposed metal surface where the film readily breaks. Electrochemical differences between the inclusion and the bulk material stimulate local currents, and dissolution of the inclusion creates a local chemical difference that is aggressive toward the metal. Propagation of the pit occurs because of locally intense metal dissolution. The larger area of the metal surface remains passivated and cathodic. Many features of the propagation phase in pitting corrosion are similar to those for crevice corrosion.

Transgranular stress corrosion cracking (TGSCC) is due to the conjoint action of very localized anodic dissolution and applied or residual stress. The cracking frequently appears to initiate around a crevice or pit, and intense dissolution occurs at the crack tip while most of the crack wall acts as a cathode. Resistance to this kind of corrosion is obtained by adding alloying elements that decrease the electrochemical difference between "bare" areas (where the strain has transiently broken the protective passive film) and the areas still covered and protected by the film. Unlike the intergranular kind of stress corrosion cracking (SCC) discussed in Section 7.4.2.5, these cracks propagate transgranularly, and the propagation is not affected appreciably by sensitization of the material. In high chloride solutions (on the order of a few percent chloride ion), stresses on the order of 10 percent of the yield stress sustain cracking. The threshold stress decreases with increasing chloride ion concentration.

Pitting, crevice, and TGSCC are most significantly affected by the alloy composition (particularly the major alloying constituents of chromium, nickel, and molybdenum and to some extent the minor constituents of sulphur, phosphorus, nitrogen, and manganese) and the environmental composition. These degradation modes are particularly favored in concentrated ionic environments, since the high ionic strength of these environments support the electrochemical currents between local anodes and cathodes. Furthermore, species that tend to acidify the environment and species that cause breakdown of passive films favor these forms of corrosion. The primary role of the beneficial alloying additions is probably their effect on increasing the rate of film repassivation (Latanision and Staehle, 1969).

7.4.2.6.1 Electrochemical testing to determine localized corrosion occurrence

A preliminary study by Glass et al. (1984) surveyed electrochemical parameters relating to general corrosion (e.g., corrosion potential and corrosion current) and to pitting and crevice corrosion (e.g., pitting potential and protection potential). These parameters were measured for the

candidate materials in aqueous solutions believed to be characteristic of the repository site. In addition to using well J-13 water, certain intentional additions were made to study the effect of chloride ion and, in some instances, the ionic species in well J-13 water were concentrated by boiling down. Test procedures and details are discussed by Glass et al. (1984). The principles and theory of electrochemical techniques for evaluating corrosion susceptibility of metals are described by Barnartt (1977), Mansfeld (1977), and Verink (1977).

To assess the susceptibility of the candidate materials to localized corrosion (pitting and crevice attack) in well J-13 water at different temperatures, cyclic anodic polarization curves were obtained. The potential of the working electrode (which is the candidate material of interest) was scanned by enforcing potentials anodic to the corrosion potential (E_{corr}) and then reversing the direction of the scan back to more negative values. (Note that the corrosion potential is the potential that the material naturally assumes in the solution as a result of corrosion processes, without having a potential artificially impressed upon it.) The scan rate was 1 mV/s (to ensure very nearly steady-state conditions), and potentials were measured relative to a saturated calomel electrode (SCE) at room temperature. Current flowing through the working electrode was continuously monitored during the scan. Such a scan, whose waveform is triangular when the impressed potential versus time is plotted, yields electrochemical values of interest such as the pitting potential (E_{pit}) and the protection potential (E_{prot}). The pitting potential is the potential above which pits spontaneously initiate and grow. The protection potential is the potential below which previously initiated pits repassivate and no new pits form. At potentials between the pitting and protection potential, new pits are not initiated but any previously initiated pits continue to grow. The values of the pitting and protection potential relative to the corrosion potential are indicative of the pitting susceptibility of the tested alloy in the testing environment.

The values of E_{pit}, E_{prot}, and E_{corr} depend on the technique used (particularly the potential scan rate). Slow scan rates approach the truly steady-state potentiostatic condition, and the pitting potential is usually observed to decrease at the slower scan rate values. For example, the pitting potential of AISI 316L SS in a 0.2 M NaCl solution is 0.429 V (SCE) at a potentiodynamic scan rate of 10 mV/s. The pitting potential decreases to 0.397 V (SCE) at a rate of 1 mV/s and to 0.391 V (SCE) at a rate of 0.1 mV/s (McCright et al., 1987). Projections of localized corrosion performance are best made on the basis of the potentiostatic determination (that is the scan rate approaching zero) of the pitting potential as well as the other important electrochemical parameters.

A typical anodic polarization curve for 304L stainless steel in 90°C well J-13 water is shown in Figure 7-15. The curve displays features common to all polarization curves obtained in well J-13 water. The important electrochemical parameters are identified on the figure. When the stainless steel is scanned anodically (to higher potentials) starting from E_{corr}, the 304L SS remains passive until the pitting potential is reached. At this characteristic potential, wholesale breakdown of the passive surface occurs and the anodic current density increases markedly by several orders of magnitude. The closer E_{pit} is to E_{corr}, the more susceptible the alloy would be to pitting in the event that an increase in the oxidizing potential of the

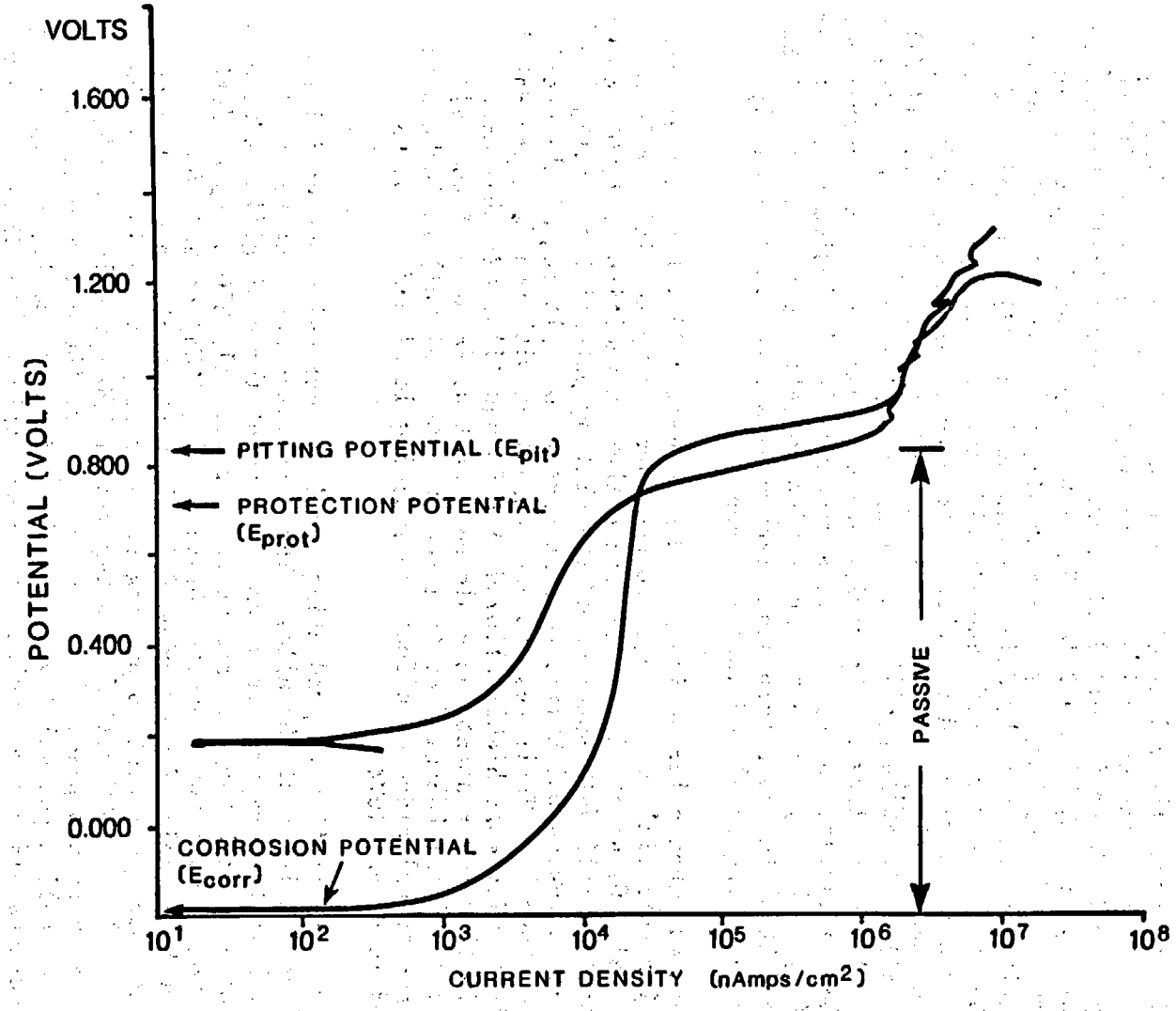

Figure 7-15. Potentiodynamic anodic polarization curve for AISI 304L stainless steel in well J-13 water at 90°C. Scan rate was 1 mV/s. Scan starts from E_{corr}. Line marked passive indicates that stainless steel remains passive until the pitting potential is reached. Modified from Glass et al. (1984).

environment occurred. This might occur, for example, in a radiation field where radiolysis products would shift E_{corr} to more positive values. From plots like that in Figure 7-15, tabulations of electrochemical parameters for some of the prospective container materials were made. The parameters for 304L SS, 316L SS, and Alloy 825 were all quite similar (Glass et al., 1984). Figure 7-16 summarizes the data for 304L SS. Over the range tested, no clear temperature dependence was found.

In all instances, the values of the pitting potential are sufficiently removed from those of the corrosion potential that no spontaneous pitting of these alloys should occur in well J-13 water. This result is the expectation from the summary figure, Figure 7-14. The other ionic species present in the well J-13 water, if they have any effect at all, would tend to retard pitting as the quantitative analysis by Szlarska-Smialowska (1974) has indicated. Although the halide ions chloride and fluoride increase the pit propagation rate, ions such as nitrate and bicarbonate tend to retard the propagation rate. The parameter ($E_{pit} - E_{prot}$) has been used previously by Wilde (1974) to evaluate alloys in terms of crevice corrosion resistance. As the value of ($E_{pit} - E_{prot}$) becomes larger, the resistance to crevice corrosion decreases. Also, greater difficulty in repassivating growing pits is indicated by larger values of ($E_{pit} - E_{prot}$). When the protection potential moves closer to the corrosion potential on the return scan, the metal surface is less easily repassivated allowing localized attack to continue.

As expected, when chloride ion is added to well J-13 water, the pitting and protection potentials move closer to the corrosion potential for 304L stainless steel. Glass et al. (1984) showed that an addition of 1,000 ppm by weight of NaCl to well J-13 water moved the pitting potential to within 100 mV of the corrosion potential, so that spontaneous pitting of the specimen could be observed. Their results are consistent with the data presented in Figure 7-14. The more highly alloyed 316L SS and Alloy 825 show more resistance in this environment, as would be expected, because of the well-documented role of molybdenum (and to a lesser extent nickel) in increasing the resistance to chloride-ion effects on inducing localized corrosion (Pessall and Nurminen, 1974).

Another consideration in predicting localized corrosion susceptibility is the surface condition of the alloy. The containers are expected to experience a high-temperature air/steam environment for a significant time after emplacement, with temperatures up to approximately 250°C (spent fuel packages). Some preliminary results (Glass et al., 1984) on 304L SS specimens with thermally formed oxide films indicate that these specimens were somewhat more resistant to pitting (lower current densities near the pitting potential) in 90°C well J-13 water with 1,000 ppm chloride addition than those that were not preoxidized. However, once these specimens started to pit and the applied potential was then shifted cathodically, the thermally oxidized specimens did not repassivate any more rapidly than those that were not previously oxidized; thus, the beneficial effects can be lost once pitting initiates. The work of Bianchi et al. (1974) indicates that at some temperatures oxides are formed that are more susceptible to pitting corrosion because of changes in the semiconducting properties of the oxide. Additional work is needed to resolve the effects of thermally grown films on the subsequent localized corrosion susceptibility. Plans for this work are outlined in Section 8.3.5.9.

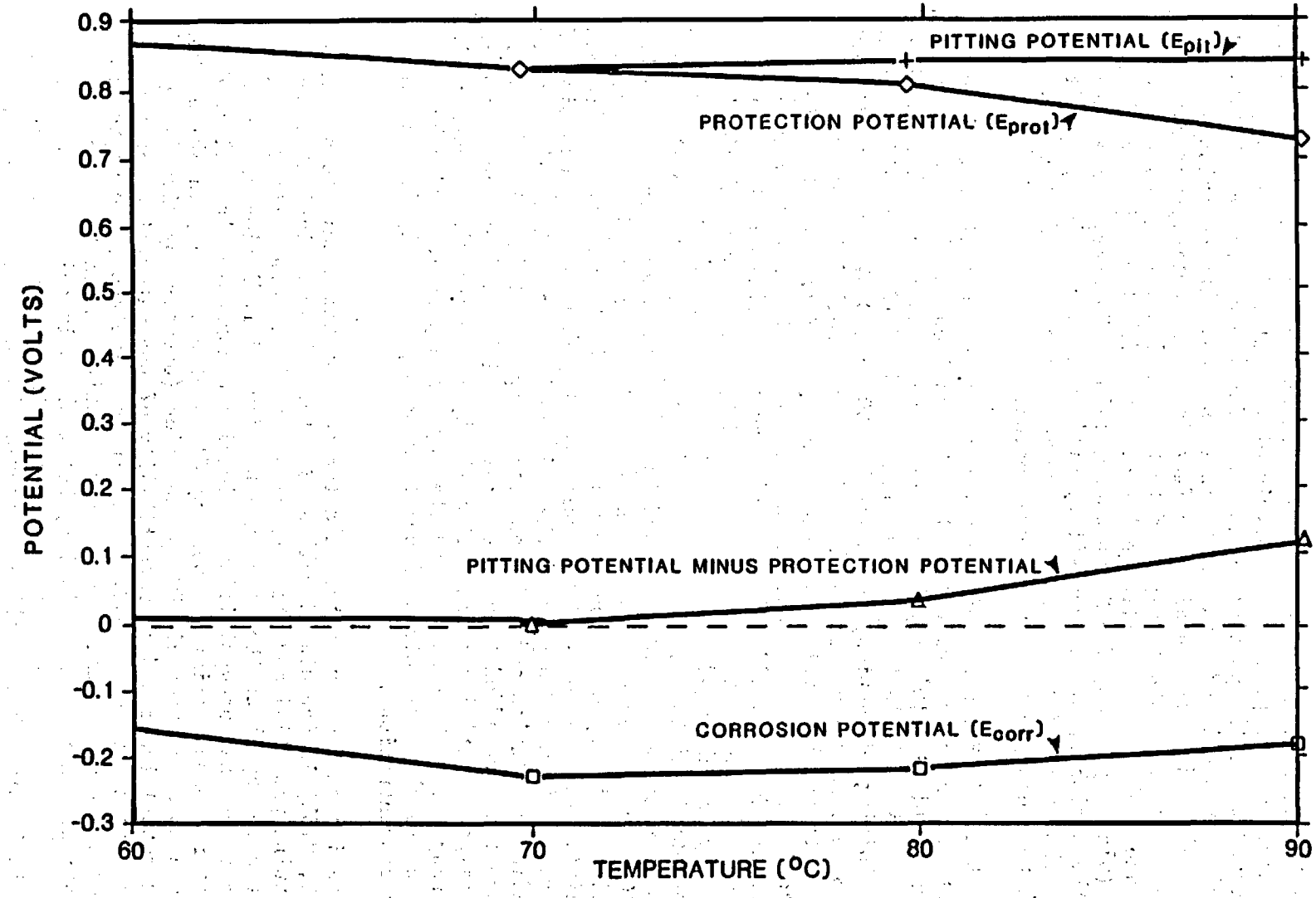

Figure 7-16. Electrochemical parameters for AISI 304L stainless steel in tuff-conditioned water from well J-13 as a function of temperature. All potentials are referenced to a saturated calomel electrode at 25°C. Modified from Glass et al. (1984).

7.4.2.6.2 Localized corrosion testing in gamma-irradiated environments

The combination of a concentrated aqueous environment and a sufficiently high gamma dose rate to promote radiolysis of the water is potentially one of the most demanding of the possible conditions for the container. Relatively little previously published work exists in this area. The co-existence of a high gamma field and a wet container surface is not an anticipated condition, because the gamma dose rate is expected to be at a low level when the container surface cools to the boiling point of water for the majority of the containers (Glassley, 1986; Van Konynenburg, 1986). However, waste packages placed at the periphery of the repository will cool more rapidly, and it is conceivable that some of these would become wet while the radiation level was high enough to radiolyze the aqueous environment.

Glass et al. (1985) measured the corrosion potentials of austenitic stainless steels in irradiated well J-13 water environments. Upon imposition of the gamma field (3×10^6 rad/h), the corrosion potentials of both 304L and 316L SS in a series of electrolytes related to well J-13 water shifted in the positive (oxidizing) direction, typically by 150 to 200 mV. The results for AISI 316L SS in a solution prepared by boiling down well J-13 water to one-tenth of its original volume are shown in Figure 7-17. In this figure, on refers to lowering the test cell into the center of the gamma source assembly (cobalt-60), and off refers to raising the cell about 1.5 m above the source assembly where the cell is shielded by the water in which the source assembly is submerged. Several on/off cycles are shown. Similar positive potential shifts upon imposition of the gamma field were observed for 316L SS in plain well J-13 water and in well J-13 water concentrated by a factor of 100, as well as for 304L SS in well J-13 water and in its concentrated versions. As expected, the gamma radiation field made the environment more oxidizing. This was shown to be very probably due to the production of hydrogen peroxide from radiolysis of the well J-13 water. Chemical analysis of the irradiated solution and a demonstration experiment in which drops of hydrogen peroxide were added to a fresh solution with simultaneous monitoring of the corrosion potential confirmed that the hydrogen peroxide concentration was in the range of 0.14 to 0.49 M and that hydrogen peroxide added by dropping produced the same potential shift as that produced by irradiation for similar concentrations.

Polarization curves were determined for some of the candidate stainless steels (304L, 316L) in irradiated well J-13 water. Results indicated that both the pitting potential and the corrosion potential were shifted in the positive direction by about the same amount. Thus, irradiation does not appear to increase the susceptibility to localized corrosion in unaltered well J-13 water. Some preliminary work by Glass et al. (1985) in which 316L SS was exposed to a solution of 650 ppm chloride (prepared by dissolving NaCl in deionized water) indicated a susceptibility of the material to pitting and crevice corrosion under those conditions. In this instance, the protection potential (on the reverse scan) lay at more negative values than the corrosion potential. In the same solution, but without irradiation, the protection potential lies at more positive potentials than the corrosion potential, a situation indicating that localized corrosion is not predicted. These polarization curves are depicted in Figure 7-18. These curves were obtained in deionized water with NaCl additions; the mitigating ionic species normally present in the well J-13 water were absent. This kind of work is being

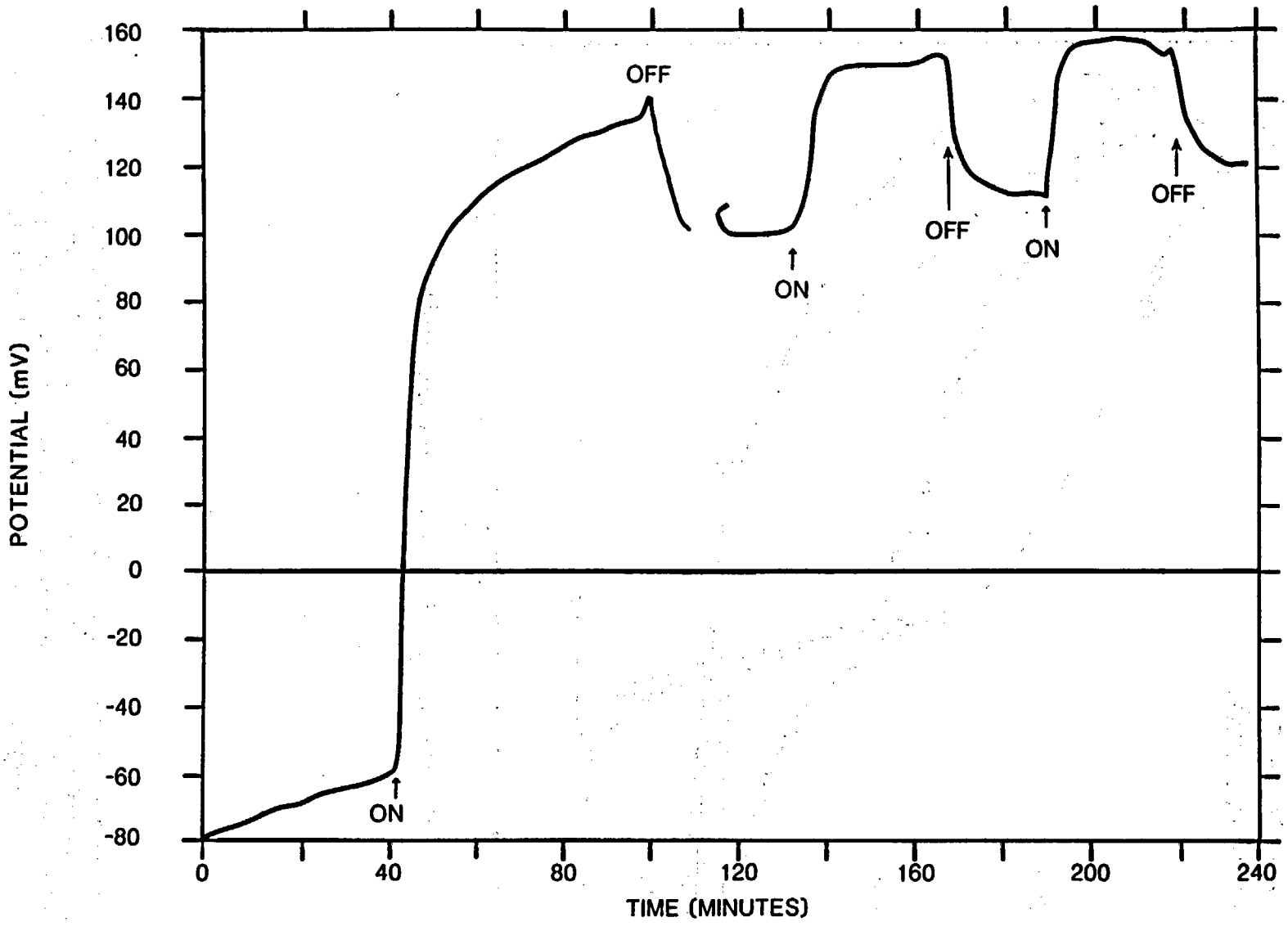

Figure 7-17. Corrosion potential behavior for AISI 316L stainless steel in water from well J-13 concentrated 10 times and under gamma irradiation. All potentials are references to a saturated calomel electrode. (The solution was not exposed to irradiation before the initiation of the first on/off irradiation cycle.) Modified from Glass et al. (1985).

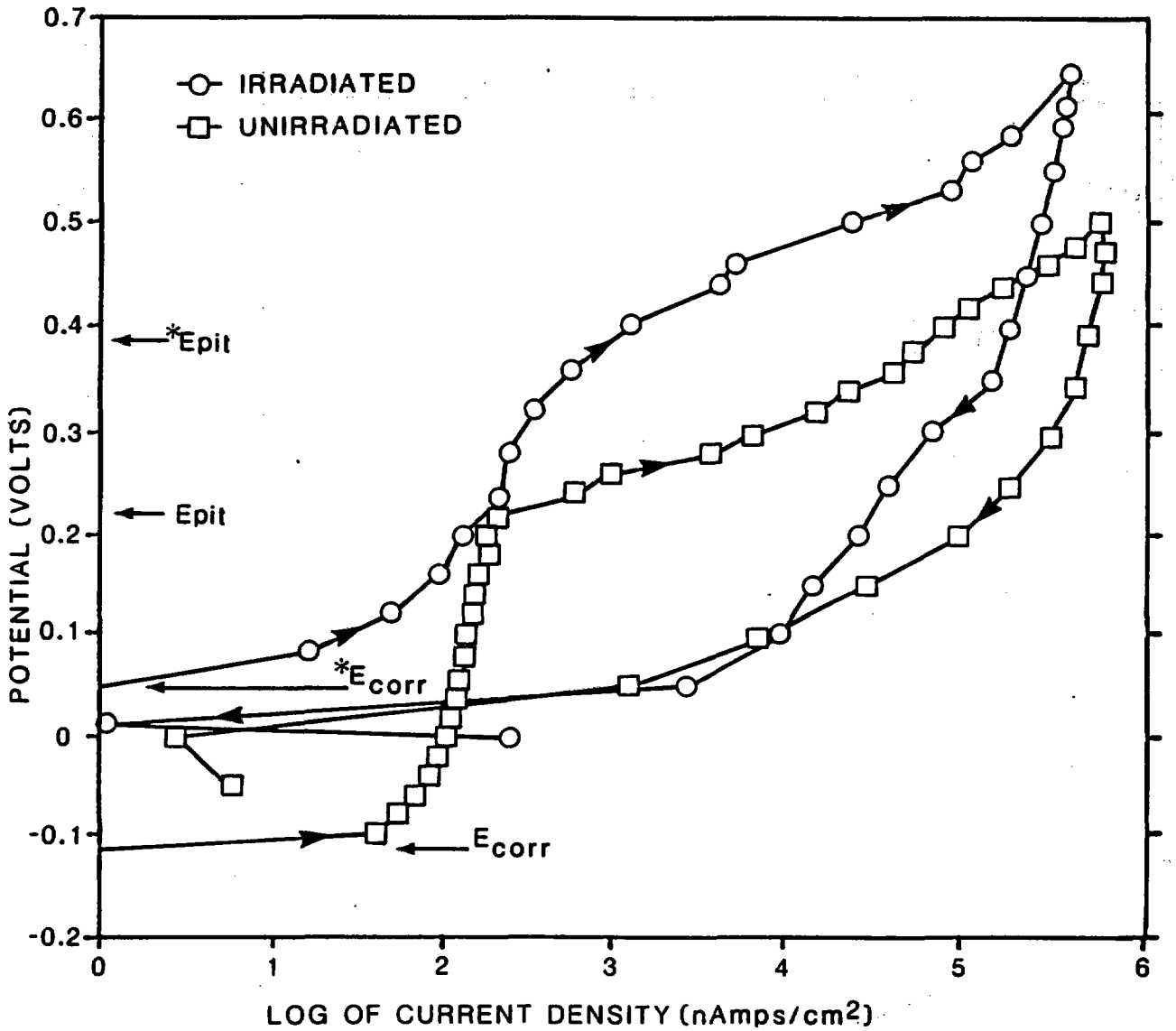

Figure 7-18. Comparison of the potentiostatic anodic polarization behavior for 316L stainless steel in 650 ppm chloride solution in deionized water with and without gamma irradiation. All potentials are referenced to a saturated calomel electrode. (The polarization curves were scanned anodically starting from the corrosion potential in each case. Upon reaching the anodic limit, the scans were reversed to more negative potentials. In this figure, E_{corr} and E_{pit} represent values of the corrosion potential and pitting potential, respectively, for the nonirradiated case. The corresponding values for the irradiated experiment are indicated on the figure as $*E_{corr}$ and $*E_{pit}$). Modified from Glass et al. (1985).

continued on other materials and at different concentrations and temperatures. Plans are outlined in Section 8.3.5.9.

An important benefit of the work described in this section is its application to conducting long-term tests at predetermined, controlled potentials. The goal of these tests is either to accelerate or to retard localized corrosion, depending on the choice of the controlled potential and its position relative to the critical pitting and protection potentials. This is an important part of the modeling effort for localized corrosion. It is discussed in greater detail in Section 8.3.5.9. This effort also relates to the work discussed under general corrosion (Section 7.4.2.4), where a model to predict the long-term changes in the corrosion potential is being developed. The chemical effects of gamma radiation can then be related to the change in corrosion potentials and critical potentials. Future work is needed at different gamma dose rates and temperatures to define the ranges of these electrochemical parameters. Plans for this work are given in Section 8.3.5.9.

7.4.2.6.3 Localized corrosion testing with creviced specimens

Metal-Teflon™-metal sandwich-type creviced specimens are being exposed for long periods of time to well J-13 water and to its concentrated versions with and without irradiation. The electrochemical polarization approach is useful to identify metal-environment combinations that might induce localized forms of corrosion, but confirming tests such as these are needed. Further, the initiation phase can require long exposure times in rather benign environments (such as what well J-13 water appears to be). An example of the type of testing used is found in Glass et al. (1984). They exposed (without any applied potential) 5 by 5 cm plates of stainless steel, bolted together with Teflon™ shims as spacers, for 54 d at 35°C in water with 10,000 ppm chloride. They found an average of 7.7 percent of the area of 304L SS specimens was attacked and 1.3 percent of the area of 316L SS specimens was attacked. The penetration depth was irregularly distributed over the attacked area and was not measured.

Along with the general corrosion tests, discussed in Section 7.4.2.4, Teflon™-metal crevices were created to observe whether preferential attack would occur there. These crevices were created with slotted washers that were used with the fastener assembly to support the coupons in the test environment. The data obtained so far (McCright et al., 1987) indicate that a tarnishing phenomenon is occasionally observed around the creviced area. After more than 10,000 h, the deepest attack in a crevice on 304L SS occurred in 90°C well J-13 water and was estimated at 0.3 micrometer while that for 316L SS occurred at 70°C and was estimated at 0.5 micrometer. Pitting attack as measured on the bold (uncreviced) surface was even less extensive than the crevice-tarnish attack. The aspect ratio (ratio of the depth of attack to the width of attack) was less than one. In true pitting of stainless steel the aspect ratio is significantly greater than one. Expressed on an annualized basis, these localized corrosion rates are of comparable magnitude to the general corrosion rate and are consistent with the conclusions drawn from the electrochemical polarization work. No enhancement of localized corrosion

appears to occur in the unmodified well J-13 water under the conditions so far tested (McCright, 1985).

7.4.2.6.4 Activities to determine transgranular stress corrosion cracking susceptibility

In the discussion on intergranular stress corrosion cracking (IGSCC), (Section 7.4.2.5), it was reported that some of the U-bend specimens exposed to irradiated well J-13 water and saturated moist air showed transgranular cracking. Although this particular test had been designed primarily to show IGSCC susceptibility, broken specimens were examined to determine the crack propagation path. Test conditions are given in Section 7.4.2.5. After 14 mo of exposure in the 90°C test, two specimens of 304L SS that had been given a sensitizing heat treatment showed transgranular cracking. One of the cracked specimens was located in the moist air only zone, and the other was located in the moist air and rock zone. Subsequent inspections (after 23 mo of exposure) revealed that other specimens of both sensitization treated 304 and 304L SS and annealed 304 and 304L SS cracked transgranularly in the 90°C test. No specimens cracked transgranularly in the 50°C test, although intergranular cracking was noted for sensitized 304 material in this test. These observations are discussed in greater detail by Westerman et al. (1987).

Three major points, however, should be made before considering the results. First, when the research began, the tuff available was from the Bullfrog surface outcropping. Rock-water interaction studies by Oversby and Knauss (1983) show that this rock contains soluble salts (caliche or evaporite material) as a result of its location on the surface. The tuff taken from the depth proposed for the repository, however, did not contain such material (Oversby, 1985). Consequently, the electrolyte concentrations present in these tests (peak chloride concentration of 600 ppm) were considerably higher than would be expected in the proposed repository. This is particularly important in the case of chloride because of its role in stress corrosion cracking (SCC).

Second, these tests were viewed as corrosion tests rather than chemical experiments, and emphasis was placed upon maintaining an open system, sparged daily with fresh air, to simulate repository conditions. Attempts were not made to keep track of the total amount of water added or the final volumes of solution remaining.

Third, the temperature control in the intended 90°C experiment was unsatisfactory for the first month, which led to repeated boil-off of the solution and plugging of the access line. The temperature and the time history of the physical state of the corrosion medium are therefore uncertain for this period.

In view of these factors, it appears that these tests were considerably more severe than the repository application would be. Nevertheless, they provide information for comparison.

It appears that the transgranular stress corrosion cracking (TGSCC) resulted from the presence of a more concentrated electrolyte on the metal

surface. In addition to purging the system of the radiolytically produced hydrogen and oxygen gas, it might be that the sparging (depending on how high a flow rate was used) blew the liquid up into the vapor space or produced aerosols of the dissolved solutes, which then deposited on the metal sample surfaces located in the vapor phase.

By whatever means the chloride concentrated (assuming that chlorine is the species responsible for the cracking), the effect of chloride ion in initiating cracking is increased when the environment becomes more oxidizing. Gamma radiation makes the environment more oxidizing. It is well established that the threshold levels of chloride to initiate cracking in 18-8 types of austenitic stainless steels are lowered when the environment is made more oxidizing. Williams (1957) showed that chloride levels as low as 2 ppm initiate TGSCC when the oxygen content is high (20 ppm) and that higher chloride concentrations are required to initiate cracking when the oxygen content is lower. However, his work was performed in a boiling situation of wet steam with intermittent wetting; therefore, it is likely that the real causative levels of chloride-induced cracking were higher.

In another experiment, a series of 40 U-bend specimens of 304 and 304L stainless steel, both in the solution-annealed and sensitization-treated condition, were exposed to unirradiated well J-13 water at 200°C in an autoclave (Westerman et al., 1987). The autoclave was cycled so that the specimens were exposed to the hot liquid water under pressure for 1 wk; then the liquid was allowed to boil to dryness by reducing the pressure while maintaining the same temperature. New water was then added and the system was returned to pressure and the cycle repeated. The intent of this experiment was to allow concentration of ionic species in well J-13 water to accumulate on the metal specimen surfaces. After 50 cycles (1 yr) of alternate wetting and drying, only the sensitization-treated 304 specimens had cracked, and these had cracked intergranularly, even though the experiment was planned primarily as one for investigating and accelerating transgranular cracking. Water analyses showed that, after 1 yr, the chloride content had reached 90 ppm and the fluoride content had reached 19 ppm in the water. The expectation is that some of the 304 and 304L SS specimens will eventually show TGSCC as the experiment continues, particularly those in the annealed condition.

Although rather extreme (in contrast to the expected) environmental conditions are needed to reveal localized corrosion tendencies of the candidate materials, recent publications (Bandy and van Rooyen, 1985) indicate that nitrogen additions to stainless steel and nickel-based materials combat localized corrosion. These additions are also beneficial in increasing the resistance to sensitization, and they combat forms of corrosion associated with that phenomenon.

The experiments just described were conducted in environmental conditions that are not anticipated in the Yucca Mountain repository; in particular, a concomitant high radiation field and an aqueous environment are not expected. However, the susceptibility of 304L SS to cracking due to either an increase in the electrolyte concentration or to increase in the oxidizing potential of the environment does need to be determined. Thus, testing of 316L SS and Alloy 825 to discern comparative susceptibility to TGSCC under similar accelerating conditions is planned. Future work also involves use of

precracked specimens to eliminate the apparently long incubation time needed to initiate cracking in well J-13 water or in the concentrated, boiled-down modification of this water. Some of these precracked specimens will be maintained at constant applied potentials either to accelerate or to retard crack growth. Plans for this work are given in Section 8.3.5.9.2.

7.4.2.6.5 Environmental considerations in localized corrosion initiation

As discussed in Section 7.4.1, the amount of water that could enter into the near-waste-package environment is expected to be small because of the low amounts of precipitation in the Nevada desert and the small fraction of the precipitation that actually percolates to the depth where the repository would be located. The heat generated from the radioactively decaying waste would vaporize incoming water when the package environment was above 97°C. During this period, it is possible that repeated evaporative processes (i.e., a refluxing operation) could leave behind salt deposits at or near the 97°C isotherm in the rock that would later be dissolved by water at a lower temperature as the isotherm moves toward the container. Surface tension effects may locally elevate the boiling point. The result would be that water with higher concentrations of ionic species could contact the metal container. Another scenario for concentrating ionic species directly on a container would be repeated dripping on the hot container surface from a fracture located above the container so that a highly ionic residue is left on the container to become wetted at some later time. Although even more unlikely than the preceding scenarios, it is possible that flooding of a portion of the repository could occur by a series of events such as a fracture admitting a surge of water to the waste package environment combined with plugging of the fractures below the container (a bathtub effect), with consequent boiling away of the water and concentration of the ionic salts. Repeated occurrences of this event would be required to build up a significant concentration of the important species affecting metallic corrosion. Although the events that can produce concentrating effects are the subject of study discussed in other parts of this site characterization plan, performing corrosion tests in these concentrated environments is important in selecting container materials.

One analysis that has been conducted in this regard is that of Morales (1985). This analysis considered that the "dripping water on the hot metal surface" scenario could not realistically occur in the repository, because the thermal output from the container would evaporate any liquid water at a distance well away from the container. With regard to the scenario of repeated evaporation of downward infiltrating water and eventual resaturation of this water when the boiling point isotherm has moved to the container surface, this analysis concluded that as a conservative maximum a solution with 20 times the salt concentration of well J-13 water could reach the containers as a burst, or the more gradual redissolution of the accumulated salt in the rock over a longer period of time could result in a slightly more concentrated salt solution than well J-13 water reaching the containers.

To project the numbers of containers that could eventually perforate by localized corrosion attack or TGSCC, models will be built around the rates of attack for different concentrations of salt in groundwater of the well J-13

type. It is recognized that eventual cooling of the repository will allow for hydration of the environment with potential for access of the aqueous environment to the container surface. However, this does not appear to be possible until several hundred yrs after the repository closure. A more precise statement of the time depends on many features of the waste package and repository design and the thermal projections based on these designs.

7.4.2.6.6. Summary of testing for pitting, crevice, and transgranular stress corrosion cracking

In summary, the candidate stainless steels appear to be sufficiently resistant to pitting, crevice attack, and transgranular stress corrosion cracking in the unmodified and irradiated well J-13 water and in steam generated from the water. Even if the highest measured nonstress assisted corrosion rate is added to the general corrosion rate, container service life far exceeds the maximum containment requirement. However, if concentration of the ionic species in the water could occur, these would possibly result in much more aggressive environmental conditions in which the candidate stainless steels would show quite different behavior. It appears that the combination of concentrated electrolyte and irradiation is the most severe environment so far tested and even 316L SS may pit and crevice corrode under these conditions. Scenarios that could result in such environmental conditions are unlikely; however, assessing container behavior under unanticipated processes and events is necessary to develop radionuclide source term estimates for low probability scenarios.

7.4.2.7 Phase stability and embrittlement

In this section, the stability of the austenitic structure over long periods of time is discussed. Possible phase transformations of concern include the formation of ferrite, martensite, and sigma phase in some of the candidate stainless steels. The concern is whether these phases could adversely affect long-term fracture toughness and result in a more brittle structure (and in some instances less corrosion resistant) than the parent structure. Some transformation products, such as martensite, are more susceptible to hydrogen embrittlement when exposed to environmental situations where atomic hydrogen is produced. Many of these phase instability concerns are closely related to microstructural features of the weld and heat-affected zones and, thus, the processes used for fabricating and welding the container material structure.

7.4.2.7.1 Phase stability

Many austenitic stainless steels have a tendency for transformation of some austenite to ferrite. The austenite-stabilizing alloying elements are balanced against the ferrite-stabilizing elements in alloy development. The presence of delta-ferrite in the weld microstructure to prevent hot cracking can be detrimental to corrosion resistance over long periods of time or with

high temperatures. According to some researchers, carbides that may have grown due to low-temperature sensitization will most likely reside at austenite-ferrite boundaries (Duhaj et al., 1968; DaCasa et al., 1969). Whether retained delta-ferrite or subsequent transformation of austenite to alpha-ferrite would be harmful to the corrosion performance of a stainless steel nuclear waste container has not yet been determined. A further concern with retained ferrite is its possible transformation to hard, brittle sigma phase when held at moderately elevated temperatures. Although most studies show the nucleation time of sigma phase from delta-ferrite to be quite long, some sigma phase nuclei have been observed after exposure at 750°C for only about 5 min (Wegrzyn and Klimpel, 1981). As with the study of low temperature sensitization, the expected prolonged exposure of the container to temperatures in the 100 to 280°C range in the repository raises the question of whether a small amount of sigma phase would form at these relatively elevated temperatures for very long times (hundreds of years). A content of just 2 weight percent sigma phase reduces the fracture toughness (impact strength) of stainless steel by one-half. Fracture toughness is most important as a material property for the first 50 yr when retrievability of the waste package is a requirement; impact loads on the container during retrieval could conceivably rupture an embrittled material. Molybdenum additions (ferrite stabilizer) as in 316L stainless steel slightly increase the tendency toward sigma-phase formation (and also enhance formation of brittle chi and Laves phases). Thus, the beneficial qualities offered by the 316 stainless steel series in improving resistance to localized corrosion, and resistance to sensitization effects may be offset by a greater tendency to form brittle phases over long periods of time. These factors need to be addressed in future work. Also, cold deformation appears to speed up the kinetics of sigma-phase transformation. Although most of the container surface could be stress relieved, the area around the final closure weld would appear to be subject to retention of residual stress.

Residual cold work in the container could also favor transformation of the austenite to martensite with attendant loss in fracture toughness. As in sigma phase formation, this transformation would be expected to occur at a local level. Further, a martensite transformation would allow more carbon to become available for chromium carbide formation, and subsequent sensitization would be more likely to occur. Generally, the molybdenum-bearing stainless steels are more resistant to martensite transformations; therefore, in this situation, the 316 series would be more resistant than the 304 series. This transformation could be avoided if the cold-worked container were annealed.

7.4.2.7.2 Hydrogen embrittlement

Although the face-centered cubic austenitic structures are ordinarily regarded as highly resistant to hydrogen-embrittling effects, the long-term interaction with a hydrogen-producing environment must be considered a possible degradation mode. Martensite transformation from the austenite results in a phase that is much more susceptible to hydrogen embrittlement, and strain-induced martensite could form in a heavily cold-worked 304L material. As discussed earlier, a source of hydrogen is the radiolytic decomposition of water vapor (during the containment period, when the radiation field is high) or the electrochemical decomposition of water resulting

from corrosion reactions on a container surface. The former source would only be possible if the environment becomes saturated while the radiation field is high, which is not likely for the majority of the packages as discussed previously.

Of the candidate materials, 304L SS is the most susceptible to martensite formation if the material is highly strained. A rough calculation of the temperature at the beginning of deformation of martensite transformation, at 30 percent strain for a typical 304L SS composition, indicates that martensite could start forming when the temperature drops to approximately 85°C. This calculation was based on the expression given in the review article by Novak (1977). Higher strains will elevate the temperature, and alloying additions will lower the temperature. This result suggests that hydrogen embrittlement of a martensitic structure would be of concern at a later period when the container surface had cooled to below this critical temperature and when an aqueous environment could access the container surface. It therefore is not of concern with respect to retrieval.

One potential problem area that has not yet been explored is hydrogen embrittlement in the duplex structure of weld metal for austenitic stainless steels. The ferrite phase has the potential for trapping hydrogen. In this instance, no martensite transformation is required as a prerequisite condition. Although hydrogen could enter the stainless steel from radiolytic decomposition of the water vapor, the relatively high temperatures would tend to mitigate against trapping effects (the hydrogen could diffuse out as readily as it diffuses in). Also, the oxidizing nature of the environment will tend to combine oxidizing radicals with atomic hydrogen as it is produced. One possible source of hydrogen produced by radiolytic decomposition of water vapor could develop inside the waste package container from water-logged spent fuel rods. Because the spent fuel waste packages will be filled with an inert gas (e.g., argon) and zircaloy may serve as an oxygen getter, atomic hydrogen may have a longer lifetime in this type of environment. Thus, there exists the possibility that this hydrogen could enter and permeate into the metal container. However, these effects will need to be investigated to determine whether significant concentrations of hydrogen atoms are produced in the gas phase and whether they can permeate into the metallic structure. Studies to address this question are discussed in Section 8.3.5.9.

7.4.2.7.3 Welding considerations

The integrity of the weld region of the container and the propensity of weld-processing variables for producing microfissures in the weld require evaluation of the state-of-the-art techniques for nondestructive postweld inspection of the container.

In welding processes using filler materials, a certain amount of delta ferrite (e.g., 3 to 5 weight percent) is generally sought in the fusion zone to mitigate against hot cracking. For this reason, the higher chromium content AISI 308L SS is often specified for the filler material in welding AISI 304L SS. However, the intentional presence of delta ferrite in the weld microstructure can be detrimental to long-term corrosion resistance. Whether

the presence of delta ferrite would adversely affect container performance in the anticipated repository environment needs to be determined.

Molybdenum additions (such as those made to AISI 316L SS) slightly increase the tendency to form brittle phases such as sigma. Thus, the beneficial qualities of AISI 316L SS (including improved resistance to localized corrosion and sensitization) may be somewhat offset by the greater tendency to form brittle phases over long periods of time. These factors need to be addressed in future work. Also, cold work appears to speed up the kinetics of sigma formation. Although most of the container could be stress relieved, the area around the final closure weld would appear to be subject to retention of residual stress.

Care must be taken in welding Alloy 825. This alloy is purely austenitic and lacks the formation of delta-ferrite in the weld zone; the advantage of delta ferrite is to soak up harmful impurities (such as sulfur) that cause hot cracking. This means that more careful control of the alloy chemistry (and filler material if a weld process using filler material is eventually selected) is required. The higher-nickel materials are sufficiently unlike the austenitic stainless steels that different welding parameters must be used to ensure sound welds.

7.4.2.7.4 Summary of work on phase instability and embrittlement

Relatively little work has addressed issues of phase instability for some of the candidate materials and problems of embrittlement that may be associated with the phase instability. The embrittlement may be purely mechanical due to the loss of fracture toughness by formation of sigma phase or other brittle intermediate phases, or the embrittlement may be due to hydrogen produced by the environment, the hydrogen favoring martensite, and possibly ferrite and causing embrittlement in those phases. If the embrittled phase is continuous, then the structure suffers from a severe loss of fracture toughness. Further study of the long-term physical metallurgical stability of the different grades of austenitic stainless steels in repository-relevant thermal and chemical environments is needed. The high-nickel Alloy 825 is apparently immune to transformation of austenite, but the possibility (probably remote) of detrimental hydrogen embrittlement would need to be addressed. Phase stability and embrittlement is addressed in more detail in Section 8.3.5.9.

7.4.2.8 Projections of containment lifetimes (austenitic materials)

The purpose of this section is to project a lifetime for the container based on corrosion data obtained to date. The performance assessment of the container is a composite of the individual assessments of each potential mode of degradation. These individual assessments are generally not additive; environmental or metallurgical conditions will determine which mode is operative (and exclusive to the others), and, as these conditions change, different degradation modes may become operative.

7.4.2.8.1 Time periods and relevance of degradation modes

As discussed in Section 7.4.2.1, the function of the metal container depends on the time period (e.g., the period during which the repository is in operation) and the various time periods following permanent closure of the repository.

Thus far, oxidation is the only experimentally measurable degradation mode for the candidate stainless steels under anticipated environmental conditions that is expected to be significant during the minimum containment period. General aqueous corrosion will occur when the container surfaces become wet; as discussed in Section 7.4.2.4. As discussed in Glassley (1986), this condition is not expected during the minimum containment period, but it may develop around some of the containers during the succeeding post-closure period. The time for hydration of the rock to occur will depend strongly on the configuration of containers in the repository and on the average thermal loading per container and the areal power density maintained for the configuration. Typical corrosion rates in unsaturated steam are 0.07 micrometers per yr, and these increase to 0.10 micrometers per yr in saturated steam and to 0.15 micrometers per yr in water immersion. Even with full water immersion during the entire maximum containment millenium, the projected amount of metal wastage would predict complete containment for container lifetimes (assuming 10,000 micrometers thickness) in excess of 10,000 yr. If the high value of 0.51 micrometers per yr (measured on 304L SS in irradiated well J-13 water at 150°C) were used, and a high crevice corrosion rate of 0.5 micrometers per yr were coupled to this, the projected wastage would be only one-tenth of the container thickness for the 1,000 yr containment period. Sustained localized corrosion rates of several micrometers per yr would be needed before this form of corrosion would seriously limit the containment objectives. Rates of this magnitude would not be expected to occur in unsaturated steam. Because sustained immersion of substantial areas of the containers appears to be highly improbable, higher corrosion rates are not expected.

One of the nonuniform modes of corrosion that does appear to offer some limitations on containment life is development of a sensitized microstructure during the containment period and subsequent wetting of the affected area to produce intergranular stress corrosion cracking. The time-to-sensitization decreases substantially with an increase in the peak temperature of the container, a heavily cold-worked 304L SS (with 0.028 percent carbon) is predicted to sensitize in as little as 120 yr at isothermal conditions of 250°C, and in 4,000 yr at 200°C. AISI 304 stainless steel did exhibit intergranular cracking in irradiated well J-13 water and saturated vapor; the question remains as to whether the lower carbon content in the L grades can confer immunity or at least a high resistance to the phenomenon. Proper selection of the thermomechanical processing of the containers can confine this phenomenon to the area around the final closure welds; proper selection of the alloy, its physical microstructure, and control of its micro-constituents can further reduce the susceptibility, until a situation compatible with substantially complete containment is achieved with a high level of assurance.

The metastability of austenite in the 300 series candidate austenitic materials may be a second issue of concern during the containment period

since sigma (or another brittle) phase might form from either the austenite or from retained delta ferrite in the duplex weld material. A further embrittlement problem during the containment period might be hydrogen embrittlement at the austenite-ferrite interface or in the ferrite phase, if sufficient hydrogen forms from radiolysis of the environment and permeates the metallic structure during this time period.

The next most likely degradation modes to consider as limiting containment would be transgranular stress corrosion cracking (TGSCC), pitting, and crevice corrosion. These modes would only occur if some unusual event happened during the minimum containment period when the container was above the boiling point of the vadose water. Their occurrence becomes considerably more probable when aqueous conditions arise by eventual water infiltration to the cooling container surface in the later periods. These modes would be promoted by lengthy immersion time (to build up and sequester electrolyte concentration in the local geometry) or influx of a more concentrated electrolyte than the reference well J-13 water environment, neither of which are expected conditions for a Yucca Mountain repository.

Alloy 825 is considered to be the most resistant of the candidate materials to virtually every form of corrosion that might occur in a geological repository in tuff. The alloy is low in carbon and titanium- stabilized to render it highly resistant to sensitization. The austenitic structure is stable at all temperatures. The alloy is resistant to chloride-induced pitting, crevice attack, and TGSCC (except in very aggressive solutions that are low in pH, high in chloride, and strongly oxidizing (such as 10 percent $FeCl_3$ solutions)). Although the metallurgical stability and the chemical stability in the Yucca Mountain environment all appear to be quite favorable to Alloy 825 as a container material, some developmental work would be needed to ensure its good weldability, should this material be selected for the advanced designs.

7.4.2.8.2 Long-term performance projections and selection of container materials for advanced designs

Understanding the governing mechanisms for the different corrosion processes is the basis for any long-range predictions of performance. To this end, estimates of the changes in the corrosion potential for the different candidate stainless steels are modeled to result from changes in environmental conditions. Models of mechanisms for localized and stress-assisted forms of corrosion are based on the corrosion potential exceeding a characteristic critical potential (for each form of corrosion) that corresponds to the threshold causative environmental conditions for that particular corrosion mode. When the corrosion potential is at or above this critical potential, then the particular form of localized or stress corrosion is operative. If the corrosion potential lies below the critical potential, then general corrosion is the operating mode. In Section 7.4.5, the performance assessment of the waste package is discussed in terms of individual performance assessment models for the different waste package components. The overall "corrosion model" for the waste package container is based on which particular corrosion model (general, pitting, crevice, stress, etc.) operates for a given set of environmental conditions. During the entire

10,000-yr period of concern for characterization of the corrosion performance of container materials, different individual corrosion models can operate according to the particular environmental conditions, and the overall corrosion model will account for the situations where individual models are operative. Performance predictions ultimately will involve a mapping activity between the phenomenology observed during the testing activities and an understanding of the mechanisms that govern the phenomenology.

The research and development effort on metal barriers is driven by the need to select a container material that will provide substantially complete containment for the requisite time period. Thus, a large effort is placed on assessing the chemical stability of the different candidate metals in the projected thermal and geochemical environment of the repository, and failure of these candidate materials is assumed to occur by corrosion. A good deal of effort has been placed on the particular corrosion effects in and around the welds, and some of the special limitations imposed by making the final closure weld by remote processes.

When sufficient information has been gathered on the six candidate materials, an assessment will be made to reduce the number of candidate materials to one or two. This assessment will be made on the basis of weighted selection criteria. Additional experimental work will be done to provide model verification for the appropriate degradation modes. This work is discussed in more detail in Section 8.3.5.9.

7.4.2.9 Alternative alloy system

Copper and certain of its alloys are under consideration as a completely alternative alloy system. Copper and its alloys have many of the same advantages as the austenitic stainless steels and also offer certain unique advantages. Copper and its alloys are, like the stainless steels, ductile materials that are readily fabricable by a variety of processes. Copper, alone among the engineering materials, can thermodynamically coexist with aqueous environments under certain conditions. Thermodynamic stability may be an important argument in demonstrating that the selected waste package container material can attain the long-term performance objective. The existence of copper artifacts from earlier civilizations, as well as native copper, indicates that copper can survive for at least a thousand yrs under some environmental conditions. However, under particularly oxidizing aqueous conditions, copper readily corrodes because the various copper oxides or cations are the thermodynamically stable species under these conditions. The aerated steam that is expected to dominate the waste package environment is moderately oxidizing, as would be the vadose water. Irradiation of these environments would likely make them more oxidizing. As with the stainless steels, the question is whether copper or a copper-based alloy would passivate or corrode actively for a given environmental condition. If the metal were attacked, would the pattern of attack be substantially uniform or highly localized? The review of Nuttall and Urbanic (1981) considered the different possible degradation modes of copper in repository environmental settings but concluded that experimental work is needed in site-specific environments.

7.4.2.9.1 Candidate materials and test plan

The NNWSI Project plan for testing copper essentially parallels that for the austenitic stainless steels. The fundamental thesis for testing and selecting materials is similar, namely, certain alloys are more resistant to specific forms of corrosion and their use would be pursued if testing revealed that the less alloyed (and less costly) material were susceptible. The candidate copper-based materials, their nominal compositions, and their mechanical properties are given in Section 7.3.2.2. The materials are CDA 102 (high-conductivity copper), CDA 613 (aluminum bronze), and CDA 715 (70-30 copper-nickel). CDA 102 is the reference material in this alternative alloy system. Pure copper is a relatively weak material when fully annealed. A thicker container wall than that specified in the reference waste package designs (1 cm) is expected to be needed for a pure copper container. The copper alloys are inherently stronger materials than pure copper, and their use would probably not require much, if any, change in the dimensions of the reference designs. If copper or a copper alloy were selected for the container, required fabrication techniques may be quite different from those contemplated for stainless steel.

The test plan, candidate materials, and expected degradation modes for copper were discussed by McCright (1985). To expedite the copper testing plan, NNWSI Project staff members consulted with representatives from the copper industry on the suitability of different alloys for use in nuclear waste containment. The Copper Development Association Inc. and International Copper Research Association, Inc. recommended the alloys being considered.

7.4.2.9.2 Possible degradation modes for candidate copper and copper-based alloy materials

The types of corrosion that may develop in the tuff repository are uniform corrosion, pitting corrosion, crevice corrosion, intergranular corrosion, selective leaching, and stress corrosion cracking. Uniform corrosion is considered the most likely degradation mode. Pitting corrosion is also possible, especially because of the irradiated environment.

A review of the literature was discussed by McCright (1985). The review summarized the known oxidation and corrosion behavior of the three candidate materials in air, steam, and a variety of aqueous solutions between ambient and 300°C. The experimental program based on that review consisted of several parts: (1) electrochemical studies, (2) long-term phenomenological experiments under gamma irradiation, and (3) modeling studies. The experimental program is discussed in detail in the work of Acton and McCright (1986).

The experimental test plan for copper-based materials is based on an initial survey of the different kinds of corrosion that may occur in both the expected and the possible but not expected environmental conditions in the tuff repository. Many of the same kinds of tests, as discussed in Sections 7.4.2.5 and 7.4.2.6 are under way for the copper-based materials. The NNWSI Project has completed a 2-yr feasibility study in response to a congressional directive on whether copper or one of its alloys could be used under the

environmental conditions anticipated for a tuff repository. This study was completed in September 1986. At this time, copper and its alloys have not been shown to be infeasible, based on the limited experimental work done in repository-relevant conditions. It is expected that the NNWSI Project will further test any selected material, as discussed in Section 8.3.5.

7.4.2.10 Borehole liner materials

This section is concerned with the performance of a borehole liner that can be designed to achieve approximately 100-yr service life after emplacement of the waste packages for possible retrieval of the waste packages, as required in 10 CFR 60.111. The borehole liners are discussed in Chapter 6 (repository design). In the current conceptual design, a partial liner is planned for use in the vertical-emplacement boreholes. A liner is planned for use in the entire length of the horizontal emplacement boreholes. One concern is the effect that the presence of the borehole liner could have on the integrity of the waste container. This effect could be favorable (assuming that the liner would sacrificially corrode and protect the container or resist loads that might otherwise be imposed on the waste container) or unfavorable (soluble corrosion products might migrate to the container surface and intensify the attack on this component). The effect of liner corrosion products on radionuclide transport properties is of concern. Although these effects are not included in the designed functions of the liner, its presence in the waste package environment could influence the ultimate performance of the container.

As a way of reducing the number of possible interactions among the waste package and repository components, the current NNWSI Project plans are to use a borehole liner made from a material of the same alloy family as the waste container. In this consideration, the liner material would not, however, need to be fabricated from exactly the same material as the container. This approach is discussed further in Sections 8.3.5.9 and 8.3.5.10 under Issues 1.4 and 1.5 and in Section 8.3.4.2 under Issue 1.10.

7.4.3 WASTE FORM PERFORMANCE RESEARCH AND TESTING

The waste forms being studied by the NNWSI Project to establish their expected performance in a repository sited at Yucca Mountain are of two types. The first is spent fuel from commercial power reactors. This waste form is expected to represent the majority of the waste to be disposed of in the first high-level waste repository, based on present inventories of waste and the absence of any commercial waste reprocessing plant coming on line in the foreseeable future.

The second waste type is the product of solidification of high-level waste solutions produced during the reprocessing of spent fuel. Reprocessing wastes exist in four locations in the United States (Manaktala, 1982). Three of these locations are defense facilities located at Savannah River, South Carolina; at Hanford, Washington; and at Idaho Falls, Idaho. The Savannah

River Plant has chosen a final waste form (Baxter, 1983) and is in the process of constructing the Defense Waste Processing Facility (DWPF) to convert its waste into borosilicate glass. Final choices of waste form have not yet been made for the other two facilities. The fourth site where liquid waste is located is at West Valley, New York. The solidification of this waste is controlled by the West Valley (WV) Demonstration Project. The exact formulation of the final waste form for West Valley waste has not yet been chosen, but it will be a borosilicate glass similar in composition to the DWPF glass (Oversby, 1984b; Eisenstatt, 1986).

To determine the anticipated performance of these waste forms in a repository at Yucca Mountain, an assessment must be made of the physical and chemical environment of the waste form after disposal (Section 7.4.1), the expected performance of the waste container (Section 7.4.2), and the emplacement configuration. For a repository in the unsaturated zone, the emplacement configuration may govern the geometry of the waste form-water contact. The detailed discussions of waste performance in Sections 7.4.3.1 and 7.4.3.2 are predicated upon these assessments. Most radionuclides can only be removed from the engineered barrier system through the action of water. (The principal exception is carbon-14, which could also leave a breached container in gaseous form (Van Konynenburg et al., 1986)). Even though extremely little water is expected to be available to contact the waste, waste form testing is done using various water volumes and contact mechanisms to understand how radionuclide release could occur. The results of these studies can be applied to performance assessment by calculating the fractional number of containers in which the waste will be exposed to water under those conditions.

For the purposes of designing waste form tests and calculating expected releases from the waste form, the reference container material and designs have been used. It has been assumed that the geometry of the container would be maintained throughout the 10,000-yr isolation period. The predicted uniform corrosion rate, based on presently available data, is sufficiently low that there should be a substantial thickness of stainless steel container remaining in essentially the original emplacement geometry for at least 10,000 yr. It is further assumed that some fraction of the containers would have developed perforations in the heat-affected zones around welded regions of sufficient size to allow water, if present, to flow freely through the perforations. The most likely failure mechanism for the metal container under Yucca Mountain tuff repository conditions after the containment period is stress corrosion cracking (SCC), probably of a welded or heat-affected zone. Failure by pitting or crevice corrosion would also produce localized penetrations in the container. Two emplacement configurations are under consideration by the NNWSI Project: (1) vertical, which is the reference mode, and (2) horizontal, which is an alternative mode. Waste form testing has been designed to cover the possible types of waste form-water contact that might result from both of these emplacement geometries with the waste held in a perforated, but essentially intact, container.

An essentially intact container throughout the isolation period provides a means for water to interact with the waste form for extended periods of time. This is a more realistic model for the unsaturated zone than one that assumes that the container is absent following breach. Absence of the container in the unsaturated zone would mean that water could drain away from

the waste form; thus, contact times would be short and degradation of the waste form would be minimized under these conditions compared with the same amount of water being held in contact with the waste for a longer period of time. Depending on the location and number of container perforations and on the water flow regime in the borehole region, water contact with the waste could vary from none to water dripping on the waste and immediately running off to water accumulating in the container up to the level of the perforation and interacting with the waste for long periods of time.

Spent fuel canisters will contain either assemblies or consolidated rods from assemblies. In either instance, there would be a significant amount of free space distributed rather uniformly throughout the container. For a vertically oriented container with perforations in or around the top circumferential weld, water could potentially accumulate inside the container up to the level of the perforations. Testing related to this geometry forms the basis of the NNWSI Project spent fuel testing to date: spent fuel in varying conditions of degradation has been tested under semistatic conditions where the fuel is completely covered with water. For a container with perforations at different levels, the geometry for fuel dissolution and degradation is unchanged, but the volume of water in the container would be limited to that which could accumulate in the region up to the lowermost perforation. If the perforations occurred only at the bottom of the container, liquid water would probably not be able to enter the container; however, water vapor might enter the container and condense, providing a means for limited radionuclide release.

Spent fuel containers emplaced horizontally would provide similar degradation geometries. The only configuration that would provide for a significantly different waste form-water interaction mode would be that present if there were perforations in both the upper and the lower sections (as emplaced) of the container. In this instance, water could drip through the upper perforations, flow past various fuel rods, and flow out the lower perforations in the container. The unsaturated test method used for glass waste forms is being modified to use with spent fuel to test the results of water interaction under these conditions.

Containers of glass waste would have a decidedly different waste form-water interaction geometry because of the stainless steel pour canister inside the container and the presence of significant open space only at the top of the container and pour canister. Currently, the simplifying assumption is made that the inner canister provides no restriction on water access to the waste and no control on the geometry of contact. When more data are available from the metals testing program on the effects of residual stress and sensitization on canister failure rates and mechanisms, water interaction scenarios can be improved to include the effects of the inner canister on control of release. This will not change the available water contact mechanisms; it will only affect the proportion of waste packages in which there is access for water to the waste.

The location of perforations in the container would have a large effect on the geometry of water contact with glass waste forms. If perforations occurred in the container at any location below the top surface of the waste form, the ability of water to contact the waste form would be severely limited. Only perforations occurring above the glass surface would allow

prolonged contact of significant amounts of water with the glass. In this instance, the headspace between the top surface of the glass and the perforation could eventually fill with water to the level of the perforation. This would result in a period of glass-water interaction without any release from the container until the water level reaches the perforated region. After this occurs, the water could potentially flow through the container at a rate up to the water flux passing the outside of the container. This scenario would provide the maximum water flux and contact time and minimum ratio of surface area of glass to volume of liquid. Glass degradation occurring under these conditions would provide an upper limit on the release rate of radionuclides from the glass.

For horizontally emplaced glass containers with perforations occurring in the upper and lower (as emplaced) regions of the top container weld, the glass-water interaction would occur as a combination of dripping water and vapor phase alteration. This type of dripping-water contact could occur in any situation where the container is perforated at two levels, but the extent of possible water flow inside the pour canister along the glass-steel interface or long cracks in the glass has not yet been determined. The NNWSI Project Unsaturated Test Method (Bates and Gerding, 1985) was developed to address these scenarios where water can enter the container, flow over the glass while reacting with it, and then leave the container.

These water contact scenarios form the basis of the NNWSI Project waste-form testing program. Significant emphasis is placed on testing corresponding to a perforated container filling with water because this would provide for the greatest waste-form degradation. For purposes of estimating release rates, it will initially be assumed that the container does not impede access of water to the waste-form except by the location of the perforations. This assumption places the burden of achieving the performance objective on control or release solely on the waste form when long time periods are considered, if one assumes that all containers will eventually develop penetrations and will have equal water fluxes. Short-term control may be provided by the containers since they are not expected to all fail at once; however, the rate of perforation initiation and growth may be difficult to establish with a high degree of confidence. Therefore, the release rate from perforated containers will be combined with the anticipated water flux in the borehole to demonstrate that the performance objective for control of radionuclide release has been met.

7.4.3.1 Spent fuel performance research and testing

The spent fuel presently in storage consists of boiling water reactor fuel discharged since 1969 and pressurized water reactor fuel discharged since 1970. The characteristics of the fuel have been summarized by Oversby (1984b) to provide a reference spent fuel composition for the NNWSI Project testing program. Before use, the fuel rods consist of a stack of uranium dioxide (UO_2) pellets encapsulated in a metal tube, which is called the cladding. Most fuel is clad in Zircaloy; however, four reactors use fuel clad in stainless steel.

The fuel rods are arranged into assemblies for insertion into the reactor. The detailed geometry of the rods and of the assemblies depends on the reactor in which they have been used. Woodley (1983) has described the variation in rod and assembly characteristics and also the evolution in rod design to improve performance of the fuel in the reactor. He also has summarized the available literature on the physical and chemical characteristics of spent fuel that are of significance to waste package design. The discussion that follows is based on his summary unless otherwise noted.

During irradiation, the physical and chemical nature of the fuel is changed. The chemical changes are caused by the fission of uranium, the production of higher atomic-number actinides by neutron capture reactions, and the production of activation products by neutron capture. The activation products are located in the fuel itself, in the cladding, in deposits on the cladding, and in the assembly parts. Since some of the activation products are in the cladding and assembly parts (such as carbon-14, a radionuclide whose release rate must be controlled to within the NRC and EPA specified limits), the waste form for spent fuel is the entire assembly (if disposed of intact) or the clad fuel rods and disassembled nonfuel hardware (if disposed of as consolidated rods).

Oversby (1986) reviewed the constraints on the release rates specified by the NRC and EPA regulations and established a list of radionuclides for which data on dissolution rates are necessary. The simplest case, which maximizes the number of such nuclides, results in the identification of 17 chemical elements for which dissolution data are needed for performance assessment. Of these, americium and plutonium are the most important; other actinides, carbon, and nickel are also important.

The abundance and spatial distribution of new chemical species formed during irradiation depends on the operating conditions to which the fuel rods are exposed. The abundance of fission products depends principally on the burnup of the fuel, that is, the amount of energy produced per unit weight of initial uranium. Burnup is usually expressed in megawatt-days per metric tons of uranium (MWd/MTU). The abundance of activation products depends on the composition of the starting materials, particularly with respect to trace impurities such as nitrogen in the fuel and cladding, and on the neutron fluence and spectrum. The transuranic actinide content will depend on burnup and on the neutron fluence and spectral conditions in the fuel (Roddy et al., 1985).

The spatial distribution of fission products in spent fuel depends on the chemical interactions between the matrix and the fission products and on the reactor operating conditions, which can strongly affect the ability of fission products to segregate from the matrix. Gaseous fission products (krypton and xenon) accumulate in the matrix as small gas bubbles (Baker, 1977; Woodley, 1983). If temperatures become high enough, the gases can diffuse to grain boundaries or to the gap between the pellets and the cladding. The degree of migration that has occurred for a given spent fuel rod can be determined by sampling the gas contained in the pellet-cladding gap. This is referred to as fission gas release and is usually expressed as a percentage of the inventory calculated to be present in the rod.

During reactor operation, the centerline temperature of the fuel rods can be between 800 and 1,600°C. Some of the other fission products that are not gaseous at lower temperatures will be volatile at the higher temperatures. Elements that have been identified as mobile under reactor operating temperatures include cesium and iodine (Johnson et al., 1983a). These elements migrate to grain boundaries and from there to the pellet-cladding gap. Other fission products are metallic under the oxidation-reduction conditions inside the fuel rod and form metallic segregations. These may be located within the grains or at the grain boundaries. The degree of fission gas migration was large in early designs that allowed the fuel to reach very high temperatures. Fission gas release of 15 to 25 percent has been measured for spent fuel from several reactors. Improved fuel rod and assembly design has resulted in lower operating temperatures for the fuel and much lower fission gas release. Gas release for modern fuels is generally less than one percent.

Migration of fission products can occur by volume and grain boundary diffusion at operating temperatures if they are sufficiently high. However, measurements of internal pressure in an instrumented assembly indicate that most of the migration occurs during reactor power changes, when the rapid temperature changes stress the fuel and induce cracks, thereby allowing enhanced migration of volatile species. Thus, the number of shutdowns and the rates of power changes during operation can influence the gas release for a fuel rod.

The temperature in the central portion of a fuel rod during irradiation may be high enough for grain growth to occur by a mechanism analogous to sintering. This phenomenon in fuel is referred to as restructuring and is accompanied by segregation of insoluble fission products such as metals into secondary phases. Operating temperature and starting grain size are both important factors determining the degree of restructuring. Extensive restructuring does not usually occur in LWR fuels because most fuel operates with a centerline temperature less than 1,300°C. Extensive restructuring is observed above 1,500°C and is common in liquid metal fast-breeder reactor (LMFBR) fuels that have peak center-line temperatures of approximately 2,000°C; fission product elements that may show larger early releases during the leaching of highly restructured fuels include cesium, iodine, selenium, strontium, and technetium (Wilson, 1985a; Olander, 1976).

Physical examination of fuel after irradiation shows that the pellets are extensively cracked. If fuel is removed from its cladding, a wide range of particle sizes is obtained, including some very fine fragments (Katayama et al., 1980). Zircaloy cladding develops an oxidized layer on the outer surface during reactor operation. Some materials precipitated from the water during operation may be present on the cladding surface; these deposits are called "crud." Some fuel rods may have small defects such as pinholes or cracks in the cladding. Approximately 1 percent of the rods developed defects in the cladding during reactor operation in the United States from 1969 to 1972. Improvements in fuel rod design and in reactor operating procedures have reduced the rod failure rate for modern fuels to less than 0.1 percent (Woodley, 1983).

The information on spent fuel characteristics just described and the data obtained by the Swedish (KBS) and Canadian (AECL) workers on the release

of radionuclides from spent fuel in ground waters of composition similar to well J-13 water were used as the basis for planning the NNWSI Project spent fuel testing program. The results from both the KBS and AECL programs showed that the release rate of some elements from spent fuel pellets in contact with water would be very rapid during the first few months of contact with water (Ekland and Forsyth, 1978; Johnson et al., 1982). The initial release of cesium from spent fuel correlates with gas release, which itself is a function of linear heat generation rate in the fuel. Even for fuel with low power rating and low gas release (Johnson et al., 1983a), several tenths of a percent of the cesium inventory was released within a few days of leaching with air-saturated distilled water.

Other fission products that migrate to the pellet-cladding gap or accumulate on grain boundaries within the fuel, such as iodine-129, might also be expected to show a similar initial release pulse. The release amounts, the rapid nature of the release, and the high solubility of the elements under expected NNWSI Project disposal conditions led to a consideration of the role of the cladding material in providing control of release of radionuclides from the spent fuel pellet and gap inventories. The review by Woodley (1983) indicated that only a small fraction of spent fuel rods delivered to the repository would have defects in their cladding. If the intact condition of the cladding were to continue throughout the disposal period of concern with respect to control of release rates, then the rather large initial cesium release could be controlled easily to a maximum population-averaged release rate of less than 1 part in 100,000 per year. A 1 percent per year release rate of cesium from breached fuel rods could be tolerated provided that no more than 0.1 percent of rods contained breaches. The rapid release fraction of cesium is exhausted after a few months (Johnson et al., 1982; Forsyth et al., 1985). Thus, the cladding could provide a control on cesium release even if it were to develop defects after disposal, as long as the rate of defect generation is low and cladding failure does not occur nearly simultaneously in all rods.

Based on these considerations, a three-part testing program for spent fuel was established. The heart of the program is a series of fuel dissolution tests that examine the rate of release of radionuclides from bare spent fuel, fuel segments with intentionally defected cladding, and segments with intact cladding. Series 1 tests (Wilson, 1985a,b) used deionized water and ambient hot cell temperature (≈25°C); series 2 tests used well J-13 water and ambient hot cell temperature. The test vessel and experimental configuration of the series 1 and 2 tests are shown in Figure 7-19. Results of the series 1 and 2 tests are given in the reports by Wilson (1985a,b, 1987). Series 3 tests used well J-13 water and sealed stainless steel vessels at 85°C. Details of the test plan are described in Wilson (1986). At the time of this writing (August 1987), the series 3 tests are still in progress and published results are not yet available.

The second area of testing related to spent fuel is an experimental study of the rate of oxidation of spent fuel under repository disposal conditions. When uranium oxidizes, there is a large volume increase at the stage when uranium oxide (U_3O_8) is formed. This has been the cause of large-scale rupture of cladding that originally contained only small defects. The available data on oxidation rates of spent fuel were obtained at higher temperatures than those relevant for long-term disposal conditions. Data are needed

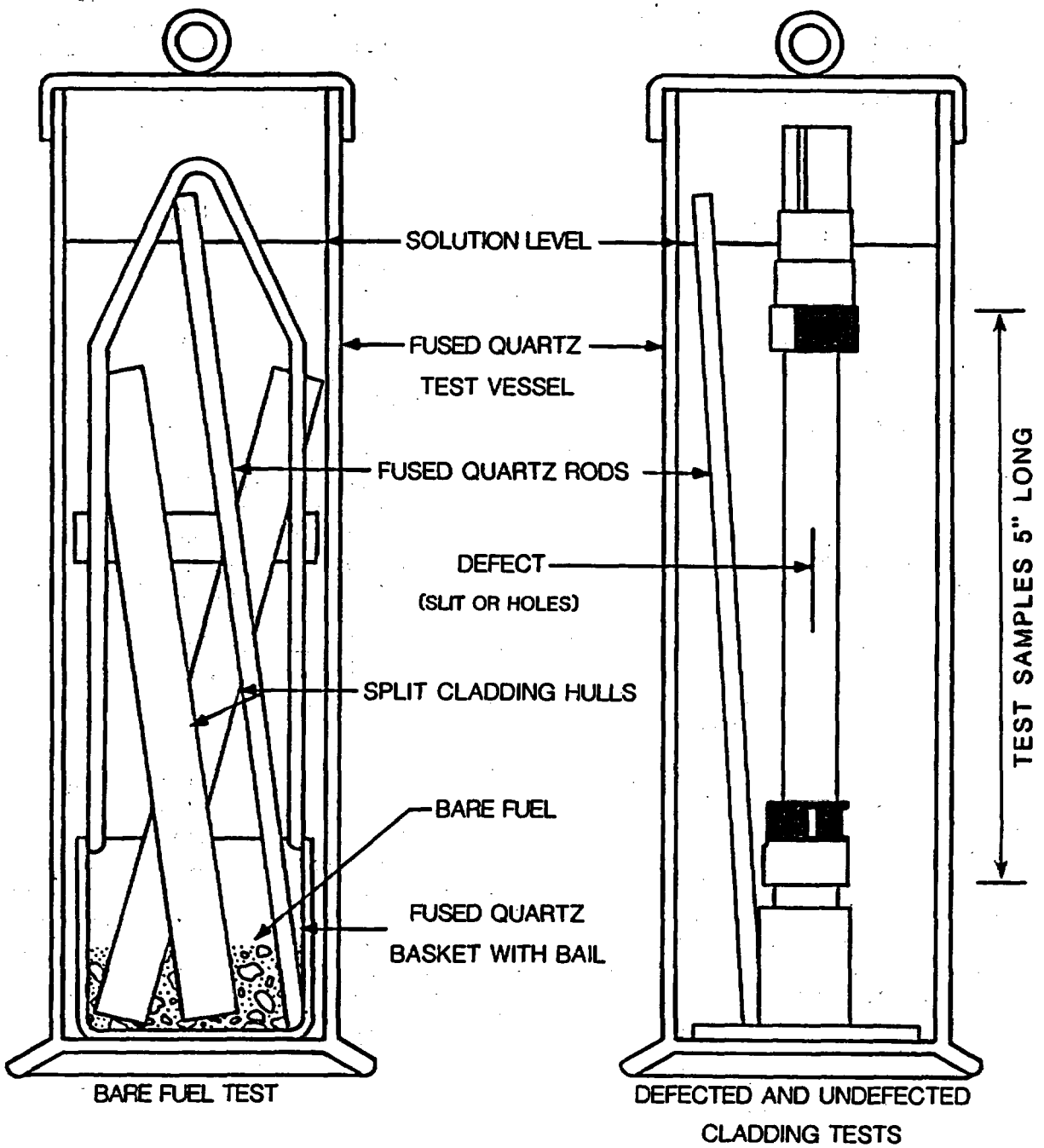

Figure 7-19. Test vessel and experimental configuration for spent fuel dissolution experiments at ≈ 25°C. Modified from Wilson (1985a,b).

at lower temperatures to determine whether the rates extrapolated from the high temperature data are valid at low temperatures and whether the oxidation mechanism is the same at the lower temperatures. Einziger and Woodley (1985a) have evaluated the potential for oxidation of spent fuel to occur under NNWSI Project disposal conditions. Their evaluation has led to development of a testing program (Einziger, 1985) that combines thermogravimetric analysis (TGA) studies for short periods (Einziger and Woodley, 1985b; 1986) with longer conventional oven-soak oxidation measurements (Einziger, 1986). The TGA studies allow continuous monitoring of weight changes, thereby providing detailed information about the oxidation mechanism and rate. The oven oxidation studies complement the TGA work by allowing longer experimental runs with multiple samples that are larger than those used in the TGA apparatus.

The rate of corrosion and degradation of Zircaloy under disposal conditions will have a profound influence on the ability of the cladding to control the release rate of nuclides from the interior of the fuel rods. An examination of the available information on corrosion of Zircaloy suggested that cladding would not develop a large number of defects under NNWSI Project disposal conditions (Rothman, 1984). A few areas were identified where further work on Zircaloy corrosion is needed to determine the expected rate of defect generation under repository conditions. Accordingly, a program of corrosion testing for irradiated Zircaloy cladding was initiated. At present, scoping experiments and tests are being conducted on two potential modes of cladding failure: electrochemical corrosion and stress corrosion cracking (SCC). An overview of the planned experiments is given in the report by Smith (1985), and the criteria used in the choice of samples for these experiments is discussed in Smith (1984b). Test plans for the initial electrochemical corrosion scoping experiments at 90°C and one atmosphere, and additional tests at 170°C and 0.83 MPa (120 psia) water are given in Smith (1984a, 1986a). Preliminary observations from the 90°C corrosion experiments are given in Smith and Oversby (1985). The test plan for the initial scoping experiments on SCC is presented in Smith (1986b).

In the discussion that follows, the work done on spent fuel dissolution by the NNWSI Project is described and the results are compared with those in the published literature. The oxidation of spent fuel both in solution and in air is discussed. A brief discussion of Zircaloy corrosion follows. The section closes with a description of the release rate model being developed for spent fuel.

7.4.3.1.1 Spent fuel dissolution studies

The purpose of the NNWSI Project testing is to determine the fraction of the sample inventory mobilized under test conditions and the physical nature of the mobilized components. That information will then be related to expected release rates at the end of the containment period. These release rates are referenced to the inventory present at 1,000 yr after repository closure. Table 7-13 gives the calculated inventory of radionuclides in PWR spent fuel at 1,000 yr for all isotopes with activity greater than or equal

Table 7-13. Radionuclide inventories at 1,000 years postclosure for pressurized water reactor spent fuel assemblies[a,b]

Radionuclide[c]	Percentage of total 1000-yr activity	Cumulative percentage
Am-241	51.84[d]	51.84
Am-243	1.75	53.59
Pu-240	26.87	80.46
Pu-239	17.37	97.83
Pu-242	0.1	97.93
Pu-238	0.06	97.99
Tc-99	0.77	98.76
Ni-59	0.252	99.01
Ni-63	0.021	99.03
Zr-93	0.181	99.21
Nb-94	0.074	99.28
C-14	0.076[e]	99.36
U-234	0.113	99.47
U-238	0.018	99.49
U-236	0.015	99.64
Np-237	0.058	99.70
Sn-126	0.045	99.74
Se-79	0.023	99.76
Cs-135	0.022	99.78
Sm-151	0.013	99.79
Pd-107	0.006	99.80
I-129	0.0018	99.80

[a]Source: Wilson (1987)

[b]Based on ORIGEN data reported in Alexander et al. (1977) pressurized water reactor assemblies with 33,000 MWd/MTU burnup.

[c]Radionuclides with 1,000-yr activity less than iodine-129 or half-life less than 1 yr omitted.

[d]Includes activity of neptunium-239 daughter products.

[e]Carbon-14 activity may vary considerably depending on as-fabricated nitrogen impurities.

to that of iodine-129. The nickel activity is mainly associated with stainless steel and Inconel assembly parts that were not part of the NNWSI Project test apparatus.

The spent fuel samples used in the NNWSI Project testing program have come from two PWR reactors, Turkey Point Unit 3 and H. B. Robinson Unit 2. Detailed characterization data are available for sibling rods from the same assemblies that these materials were obtained from in the cases of H. B. Robinson fuel (Barner, 1984) and from the same rods in the case of Turkey Point (Davis and Pasupathi, 1981). The Swedish testing program has used fuel sections from the Oskarshamn I BWR (Forsyth et al., 1984). The Canadian testing program uses CANDU natural uranium spent fuel (Johnson et al., 1982). In the CANDU reactor, where bundles of single enrichment natural UO_2 are irradiated in an array of process tubes extending through the core, greater variations in fuel rod linear power and fuel operating temperatures occur than in LWR reactors, which use variable enrichments and have more uniform neutron flux across the core. As a result, fission gas release, fuel restructuring and segregation of fission products from the oxide fuel matrix generally occur to a greater extent in CANDU fuels than in LWR fuels. A summary of the characteristics of the spent fuel samples used in the three testing programs is given in Table 7-14.

The three testing programs also use different ground-water compositions for the leaching solutions. Although the compositions are similar, differences in some components might affect fuel leaching. The Canadians have used a water composition, referred to by them as KBS ground water, which is higher in dissolved carbon species than that reported by Forsyth et al. (1984). To distinguish between the two, the Swedish composition will be designated KBS and the Canadian composition will be designated AECL-KBS. The Canadians also use a composition called "granite groundwater," which will be referred to as AECL-GR. The compositions of these three waters and the possible effects on spent fuel dissolution of solution composition differences are discussed in Oversby and Shaw (1986). The composition of well J-13 water is discussed in Section 7.4.1.

Laboratory testing cannot be done under repository conditions because the water-flow rates required are too low to obtain measurable results in the time period available. To overcome this experimental limitation, dissolution testing uses a higher ratio of water to fuel than is expected under repository conditions. The spent fuel dissolution testing procedure is a semi-static one in which samples of fluid are periodically taken for analysis. The fluid volume is then returned to the starting volume by adding sufficient fresh leachant to make up for the sample taken and for any evaporative losses. In this respect, the test resembles a slow flow-through test. Each test series consists of several cycles. This is done so that the size of the rapidly released gap and grain boundary inventory of fission products can be assessed. These nuclides are released very quickly in the first cycles and the levels attained in subsequent cycles show a progressive decrease. At the end of each cycle, the spent fuel specimens are rinsed and transferred to clean leaching vessels and the test restarted for the next cycle using fresh leachant. After the remaining leach solution is removed at the end of each cycle, the used leaching vessels are rinsed with leachant and stripped with 8 M nitric acid to remove any solid, precipitated, or adsorbed material. Series 1 and 2 tests were conducted in loosely covered, fused quartz vessels

Table 7-14. Characteristics of spent fuel samples used in release rate testing[a]

Characteristic	NNWSI Project		Sweden	Canada
	Turkey Point unit 3	H. B. Robinson unit 2	(Oskar-shamn I)	(CANDU)
Fuel type	PWR 15 x 15	PWR 15 x 15	BWR	BWR Natural U
Cladding	Zircaloy-4	Zircaloy-4	Zircaloy	Zircaloy-4
Sample weight UO_2 (g)	43	80	16	72
Estimated burnup (MWd/kgU)	27	31	42	7.9
Initial enrichment (wt%)	2.559	2.55	--[b]	0.71
Fission gas release (%)	0.3	0.2	0.7	1 to 9
Peak linear heat generation rate (kW/m)	32.7	32.7	<30	42 to 58
Initial pellet density (% Total density)	92	92	--	97
Pellet diameter (cm)	0.9	0.9	--	1.4
Grain size (μm)	25	6	--	7 to 10
Discharge date	11/25/75	5/6/74		

[a]Data from Johnson (1982), Barner (1984), Johnson et al. (1983a), Forsyth et al. (1984), and Wilson and Oversby (1985).
[b]No data.

at approximately 25°C. The series 1 tests were conducted using deionized water as the leachant and in the series 2 tests well J-13 water was used. These tests also included fused quartz rods, which were removed at intervals to monitor plate-out. Series 3 differs from the previous two in that the tests are being conducted in sealed 304 (cycle 1) or 304L (cycle 2) stainless steel vessels at a higher temperature (85°C). The leachant used in series 3 is well J-13 water. One bare fuel specimen at 25°C is included in series 3 so that the results from the series 2 tests can be compared and so that the effect of changing the experimental vessel on the observed release of radionuclides, exclusive of any temperature effect, can be evaluated.

Each test series includes several types of test specimens, each a 5-in. segment cut from a full-sized rod: (1) bare fuel with the emptied cladding hulls, (2) fuel rod segments fitted with watertight end caps and with laser-drilled holes through the cladding, (3) fuel rod segments with watertight end caps and with a machined slit through the cladding, and (4) undefected fuel

rod segments with watertight end caps. These various specimen types approximate fuel rods with differing degrees of cladding failure. The end caps prevent accidental access of water to the fuel by means other than the induced defect. The exterior surfaces of all specimens are cleaned of radioactive contamination before used in a test. Series 1 tests used spent fuel from the Turkey Point Unit 3 reactor. Series 2 and 3 used spent fuel from two sources: fuel from the H. B. Robinson Unit 2 reactor obtained from the Pacific Northwest Laboratory Materials Characterization Center and designated as ATM-101 (Barner, 1984) and fuel from the Turkey Point reactor. The two fuels are similar PWR fuels from the same vendor and are of approximately the same vintage. As can be seen from Table 7-14, both fuels have low gas release and similar burnup. The grain size of the Turkey Point fuel, however, is significantly larger than that of the H. B. Robinson fuel.

Data were obtained on all samples for americium isotopes, plutonium isotopes, curium-244, uranium, and cesium isotopes. Cobalt-60 was measured in most test solutions. Selected samples were analyzed for technetium-99, strontium-90, neptunium-237, selenium-79, carbon-14, and iodine-129. In addition, selected samples were analyzed in three fractions: (1) unfiltered, (2) filtered through 0.4 micron filters (Nucleopore 110407 polycarbonate), and (3) filtered through 1.8 nm filters (Amicon CTS-1 membrane cone centrifuge filters).

The following discussion concentrates on the results of the series 2 tests (Wilson, 1987) because they are the most relevant data available for the conditions in the NNWSI Project proposed repository. Significant differences were noted in the behavior of spent fuel in the series 1 and 2 tests because of the use of well J-13 water in series 2. These differences are discussed when they provide insight into the dissolution process or release mechanism. Complete results for the series 1 tests are contained in Wilson (1985b).

Figure 7-20 shows the H. B. Robinson uranium data for unfiltered solutions for series 2, cycles 1 and 2. Data points with a downward pointing arrow are data reported as below detection limits. The line marked 10^{-5} inventory is the solution concentration that would result if 1 part in 100,000 of the test specimen were to dissolve in the leachant. This level is indicated in the figures and tables simply as a convenient reference point for comparing the release of various radionuclides from specimens of different sizes and for comparing the release of radionuclides normalized to their abundance in the fuel. This value cannot be directly related to the NRC release rate limit of 1 part in 100,000 per year of the 1000-yr inventory.

Conversion of solution concentrations to release rates requires a model for spent fuel dissolution in the repository setting. This is discussed in more detail below and in Section 8.3.5.10.

Solution uranium concentrations reached relatively stable levels after a few days. The H. B. Robinson cycle 1 bare fuel test, which required more than 60 d to reach a stable level, was a notable exception to this. Uranium concentration data for the bare fuel tests are plotted on a linear scale in Figure 7-21. The H. B. Robinson cycle 1 test peaked at 4.5 micrograms per milliliter on day 6 and decreased to 1.2 micrograms per milliliter at the

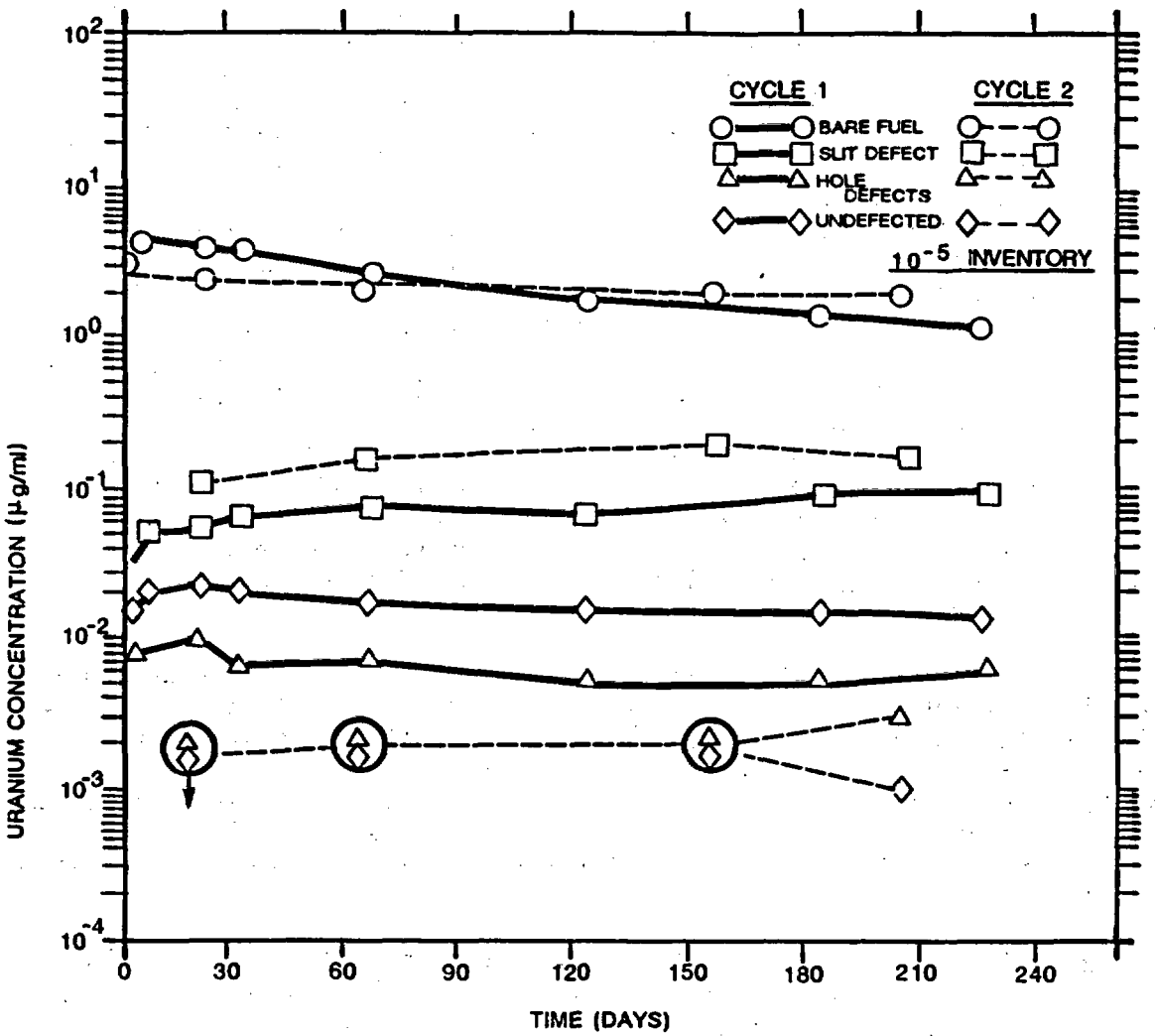

Figure 7-20. Uranium concentrations in unfiltered solution samples, series 2, cycles 1 and 2 (25°C, well J-13 water) H. B. Robinson unit 2 fuel. Circled data points have identical reported values but are offset for clarity. Modified from Wilson (1987).

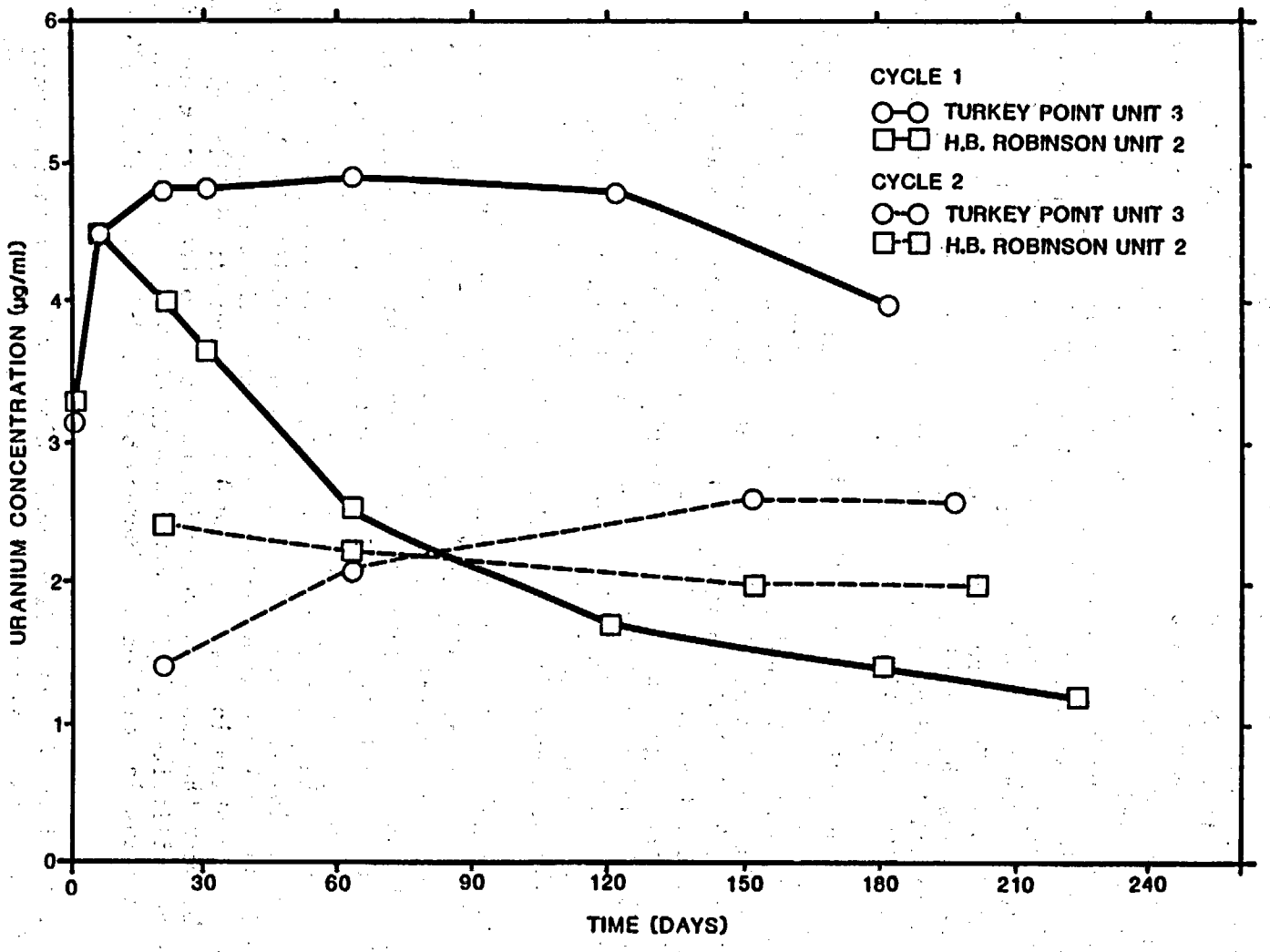

Figure 7-21. Uranium concentrations for bare fuels in well J-13 water, linear scale, series 2, cycles 1 and 2 (25°C, well J-13 water). Modified from Wilson (1987).

termination of cycle 1 as the solution apparently equilibrated with a phase having lower solubility than that initially present on the fuel surface. Uranium in the cycle 1 Turkey Point test began to decrease only after 120 d dropping from a peak value of 4.9 micrograms per milliliter on day 30 to 4.0 micrograms per milliliter at the cycle termination, suggesting that more of a higher solubility phase was initially present. The greater amount of a high solubility phase in the Turkey Point fuel may be related to this fuel's greater exposure to air before testing, which may have resulted in a more extensively oxidized fuel surface. During cycle 2, the solution concentration levels of uranium were similar for both fuel types. Uranium concentration dropped from a peak of 2.4 micrograms per milliliter in the day 20 sample to 2.0 micrograms per milliliter in the H. B. Robinson bare fuel test. In the Turkey Point test, uranium concentration peaked at 2.6 micrograms per milliliter in the day 154 sample and dropped to 2.4 micrograms per milliliter in the final sample. Data from day 224 of the third test cycle (not shown) for these specimens show uranium concentrations dropping to 1.4 micrograms per milliliter and 1.2 micrograms per milliliter for the H. B. Robinson and Turkey Point fuels, respectively (Wilson, 1987).

Table 7-15 summarizes the uranium release results for series 2, cycles 1 and 2 of the spent fuel dissolution tests. These data show that the uranium release for the bare fuel specimens was greater than that of any of the defected cladding specimens. The higher fractional release from Turkey Point fuel relative to H. B. Robinson fuel in the three defected cladding configurations may reflect the presence of a more highly oxidized fuel surface on the Turkey Point fuel. Higher uranium concentrations in the undefected test versus the drillhole defect test for H. B. Robinson cycle 1 specimens is likely due to the presence of residual contamination on the cladding exterior of the undefected specimen; in cycle 2, the uranium concentrations were more nearly the same for the drillhole defect and the undefected specimens.

The uranium solubility behavior observed in the series 2 tests using well J-13 water was significantly different from that seen in the series 1 tests that used deionized water. In series 2, essentially all the uranium measured in the unfiltered solution samples passed through the 0.4 micrometer and 1.8 nm filters, indicating that the uranium was in true solution. In contrast in series 1, much of the uranium was trapped on the 0.4 micrometer filter, indicating that much of the uranium in the aqueous phase was in a particulate or colloidal state. The real uranium solubility in the deionized water used in series 1 was at or below the detection limit of the technique used to measure uranium in that test ($\approx$0.001 microgram per milliliter). The difference between the two test series is attributed to the presence of $\approx$120 micrograms per milliliter of bicarbonate ion in the well J-13 water that complexes with uranium in solution and increases its solubility (Wilson, 1985a; 1987).

Table 7-16 lists the total fractional release of the actinides measured in the series 2 tests along with the percentage of the release accounted for by the activity present in the aqueous phase (unfiltered solution activity). Because of the very low activities in solution, reliable neptunium data were not obtained for most of the sample configurations; however, the data are consistent with the results for the other actinides.

Table 7-15. Uranium release data for series 2, cycles 1 and 2 experiments with H. B. Robinson unit 2 and Turkey Point unit 3 fuels (25°C, well J-13 water). Units are micrograms unless otherwise noted[a] (page 1 of 2)

Parameter	Bare fuel		Slit defect		Hole defect		Undefected	
	HBR[b]	TP[c]	HBR	TP	HBR	TP	HBR	TP
				CYCLE 1				
Solution samples	253	351	6.59	35.8	0.63	2.27	1.67	0.76
Final solution	300	1,000	23.80	212.5	1.50	7.25	3.25	2.00
(ppm U)	(1.2)	(4.0)	(0.09)	(0.85)	(0.006)	(0.029)	(0.013)	(0.008)
Rod samples	36	15	0.31	0.54	<0.18	<0.19	<0.22	<0.10
Rinse	660	366	1.80	10.2	0.60	<0.60	<0.60	<0.6
Acid strip	2,700	960	1.50	15.9	0.60	2.70	0.6	<0.3
Total release	3,949	2,692	34.00	274.9	3.51	<13.01	<6.34	<3.76
x 10^5 inventory	5.66	11.67	0.047	0.662	0.005	<0.030	<0.009	<0.009[d]
% in aqueous phase	14.00	50.19	89.38	90.32	60.86	73.17	77.60	--
				CYCLE 2				
Solution samples	142	135	10.15	22.1	<0.13	0.22	<0.13	0.18
Final solution	500	600	40	125.0	0.75	1.00	0.25	0.75
(ppm U)	(2.0)	(2.4)	(0.16)	(0.50)	(0.003)	(0.004)	(0.001)	(0.003)
Rod samples	18	3	<0.08	0.054	<0.06	<0.05	<0.06	<0.05
Rinse	102	39	1.20	3.6	0.60	<0.60	0.60	<0.06
Acid strip	300	156	1.20	0.3	4.50	0.30	--	<0.3
Total release	1,062	933	52.63	151.0	6.04	<2.17	<1.04	<1.88
x 10^5 inventory	1.54	4.13	0.073	0.363	0.008	<0.005	<0.0015	<0.004
% in aqueous phase	60.45	78.78	95.29	97.42	14.57	56.22	36.54	--

Table 7-15. Uranium release data for series 2, cycles 1 and 2 experiments with H. B. Robinson unit 2 and Turkey Point unit 3 fuels (25°C, well J-13 water). Units are micrograms unless otherwise noted[a] (page 2 of 2)

Parameter	Bare fuel		Slit defect		Hole defect		Undefected	
	HBR[b]	TP[c]	HBR	TP	HBR	TP	HBR	TP
			SUMMARY, CYCLES 1 and 2					
Total release	5,011	3,625	86.63	425.9	9.55	<15.1	--	<5.64
x 10^5 inventory	7.20	15.80	0.120	1.025	0.013	<0.035	<0.010	--

[a]Source: Wilson (1987).
[b]H. B. Robinson unit 2.
[c]Turkey Point unit 3.
[d]-- = Not applicable.

Table 7-16. Summary of the measured fractional release for series 2, cycles 1 and 2 experiments with H. B. Robinson unit 2 and Turkey Point unit 3 fuels (25°C, well J-13 water). Units are parts per 100,000 unless otherwise noted[a] (page 1 of 2)

Parameter	Bare fuel		Slit defect		Hole defect		Undefected	
	HBR[b]	TP[c]	HBR	TP	HBR	TP	HBR	TP
Uranium								
Cycle 1	5.66	11.67	0.047	0.662	0.005	0.030	0.0090	<0.009
Cycle 2	1.54	4.13	0.073	0.363	0.008	0.005	0.0015	<0.004
Sum	7.20	15.80	0.120	1.025	0.013	0.035	0.0105	<0.013
% in aqueous phase:								
Cycle 1	14.00	50.19	89.43	90.32	60.68	73.17	75.69	--[d]
Cycle 2	60.45	78.78	95.29	97.42	14.57	56.22	60.58	--
Both Cycles	23.96	57.66	93.02	92.85	32.30	70.80	73.53	>66.04
Pu-239 + Pu-240								
Cycle 1	7.18	7.31	0.009	0.1090	0.002	0.022	0.0020	<0.005
Cycle 2	1.28	1.57	0.008	0.0147	0.012	0.004	0.0008	<0.002
Sum	8.46	8.88	0.017	0.1237	0.0157	0.0255	0.0028	<0.007
(Sum Pu)/(Sum U)	1.17	0.56	0.14	0.11	1.21	0.73	--	--
% in aqueous phase:								
Cycle 1	1.56	12.61	17.10	6.25	48.57	8.01	23.15	≈13
Cycle 2	4.12	19.84	11.62	47.31	1.20	17.15	23.35	≈22
Both Cycles	1.95	13.89	14.52	11.13	14.05	9.40	23.21	>13.70
(aq[e] Pu)/(aq U)[d]	0.10	0.13	0.02	0.01	0.53	0.10	--	--
Am-241								
Cycle 1	8.04	6.88	0.009	0.126	0.0028	0.023	0.0031	<0.003
Cycle 2	0.77	1.33	0.005	0.010	0.0138	0.004	<0.0003	<0.002
Sum	8.81	8.21	0.014	0.136	0.0166	0.027	<0.0034	<0.005
(Sum Am)/(Sum U)	1.22	0.52	0.12	0.13	1.28	0.77		
% in aqueous phase:								
Cycle 1	1.57	14.04	20.53	6.16	47.95	5.86	--	--
Cycle 2	1.00	5.15	2.00	17.35	<0.66	13.65	--	--
Both Cycles	1.52	12.60	13.68	6.95	≈8.63	6.96	≈14.69	≈19.77
(aq Am)/(aq U)	0.08	0.11	0.02	0.01	0.34	0.08	--	--

Table 7-16. Summary of the measured fractional release for series 2, cycles 1 and 2 experiments with H. B. Robinson unit 2 and Turkey Point unit 3 fuels (25°C, well J-13 water). Units are parts per 100,000 unless otherwise noted[a] (page 2 of 2)

Parameter	Bare fuel		Slit defect		Hole defect		Undefected	
	HBR[b]	TP[c]	HBR	TP	HBR	TP	HBR	TP
Cm-244								
Cycle 1	8.64	7.79	0.010	0.137	0.0018	0.027	0.0024	0.0045
Cycle 2	1.61	1.42	0.010	0.010	0.0170	0.003	<0.0012	<0.0014
Sum	10.25	9.21	0.020	0.147	0.0188	0.030	<0.0036	<0.0059
(Sum Cm)/(Sum U)	1.20	0.58	0.16	0.14	1.45	0.87	--	--
% in aqueous phase:								
Cycle 1	2.29	18.13	19.23	7.34	60.29	5.05	11.20	7.87
Cycle 2	1.04	6.73	2.19	24.44	0.19	3.35	--	--
Both Cycles	2.09	16.37	10.71	8.50	5.94	4.86	>8.70	>6.83
(aq Cm)/(aq U)	0.12	0.17	0.02	0.01	0.27	0.06	--	--

[a] Wilson (1987).
[b] HBR = H.B. Robinson, unit 2.
[c] TP = Turkey Point, unit 3.
[d] -- indicates no data.
[e] aq = aqueous.

The H. B. Robinson bare fuel test yielded total fractional releases (summed over both cycles of the test) of approximately 8 to 10 parts in 100,000 of the inventory for all the actinides, including uranium. The analogous Turkey Point specimen yielded similar releases for the higher (i.e., transuranic) actinides but had a uranium release approximately twice that of the other actinides. As noted previously, this may be due to the presence of a more extensively oxidized surface on the Turkey Point fuel.

As for uranium, the fractional release of higher actinides in the bare fuel test was much greater than for any of the other sample configurations. The results listed in Tables 7-16 indicate that for each defected specimen type, the release of the higher actinides occurred congruently, with the Turkey Point specimens having fractional releases from 2 to 10 times that observed for the analogous H. B. Robinson specimens. The total fractional uranium release for both hole defect specimens is similar to that observed for the other actinides. In the slit defect specimens, the fractional release of uranium was approximately 8 to 10 times the release of the other actinides for both fuel types.

The fractional releases just discussed above refer to all the material mobilized from the test specimens and include material plated out on the quartz rods and on the test vessel walls, recovered by acid stripping the vessel. Of greater interest is the portion of the material present in the aqueous phase since it is this radioactivity that has the potential to be transported from a failed disposal container by fluid entering and leaving the container. This material may be either in true solution or present as suspended particles or colloids; thus the entries in Tables 7-16 for the percentage in the aqueous phase are based on unfiltered solution analyses. The percentages of the higher actinides that were in the aqueous phase were approximately the same for each specimen type; however, there were significant differences between the different specimens. These differences do not appear to be systematically related to either the cladding configuration or the fuel type. In all instances, the fraction of the uranium in the aqueous phase significantly exceeded that of the other actinides. Higher actinide to uranium ratios (normalized to the same ratio in the fuel) in the aqueous phase ranged from 0.06 to 0.43. It appears that uranium has the potential to be transported from a failed disposal container preferentially to the other actinides.

Most of the aqueous phase activity due to the higher actinides was also measured in the 0.4 micrometer-filtered fractions (58 to 96 percent). Much of the plutonium activity also passed through the 1.8 nm filter (30 to 76 percent); however, the majority of the americium and curium was stopped by this filter (only 3 to 12 percent of the unfiltered activity was found in the 1.8 nm filtrate). The americium and curium may have been present as large complexes or colloids, preventing them from passing through the finer filter. Alternatively, the concentrations of americium and curium were only ≈100 pg/g and ≈3 pg/g, respectively. At such low concentrations, these elements may have been removed from solution by adsorption onto the 1.8 nm filters.

The fission product cesium, which is partially released from the oxide fuel matrix during irradiation, segregates to the grain boundaries and the fuel-cladding gap. This gap and grain boundary inventory dissolves immediately upon contact with water. As shown in Figure 7-22, cesium was rapidly

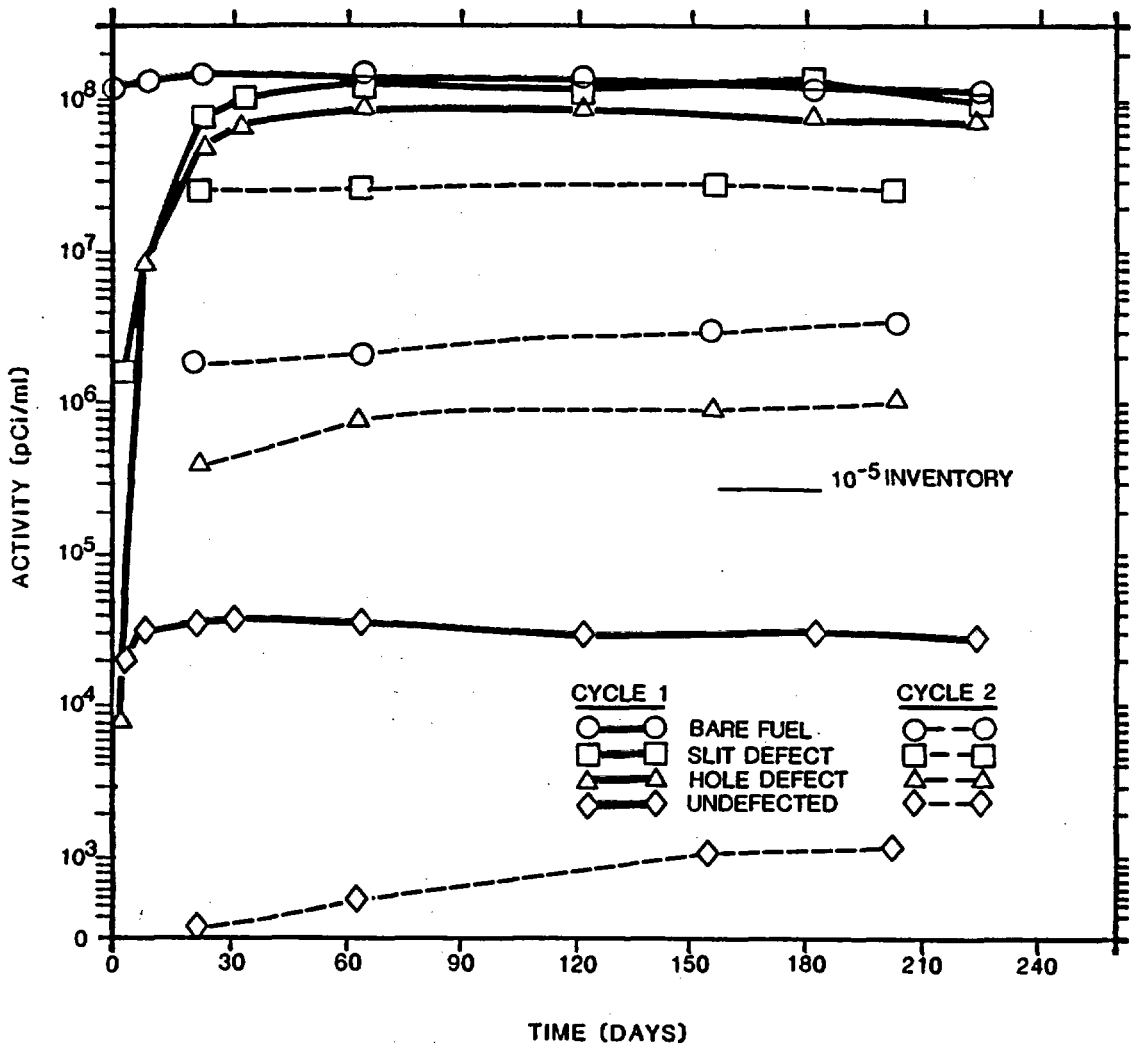

Figure 7-22. Cesium-137 activities in unfiltered solution samples for series 2. cycles 1 and 2 experiments with H. B. Robinson unit 2 fuel (25°C. well J-13 water). Modified from Wilson (1987)

released in the NNWSI Project series 2 dissolution tests. Relatively constant solution levels followed this initial release. Most of the release occurred in cycle 1 (Table 7-17 and Figure 7-22), and the mobilized cesium was retained in solution. For the defected cladding configurations, more than 97 percent of the cesium released was in the aqueous phase. Slightly lower percentages for the bare fuel tests (Table 7-17) probably reflect the mobilization of small fuel particles that quickly settle. Unlike the case of the actinides, the presence of defected cladding did not act as a significant barrier to the release of cesium. The Turkey Point hole defect test was a exception to this; the fractional release of cesium for this test (< 0.01 percent) was much lower than expected and is not currently understood.

Fractional cesium releases for the Turkey Point bare fuel and slit defect tests were 0.3 and 0.2 percent, respectively. This is close to the reported fractional fission gas release for this fuel (Table 7-14). Fractional releases for the H. B. Robinson bare fuel, slit, and hole defect specimens were 0.8, 0.8, and 0.4 percent, respectively. The reported fractional fission gas release for this fuel is only 0.2 percent. The ≈250 percent greater fractional cesium release for the H. B. Robinson fuel compared with the Turkey Point fuel is thought to be a reflection of the much smaller grain size of the former. The larger grain boundary area and shorter diffusion path lengths to grain boundaries likely results in a greater grain boundary cesium inventory as cesium is transported along grain boundaries during reactor operation. Given the similarities in the fuels (same manufacturer, same vintage, similar burnup, similar gas release), the difference in cesium release clearly shows that more work will be needed to establish the factors that control cesium distribution in the fuel before general conclusions regarding cesium release can be substantiated.

The behavior of cesium in well J-13 water was similar to that observed in deionized water. The main difference in behavior in the two leachants was that no decrease in cesium levels in the aqueous phase occurred with well J-13 water. In the series 1 test, cesium levels over bare fuel began to decrease after 60 d. This was thought to be due to the precipitation of some cesium salt, possibly $Cs_2U_2O_7$, the cesium analogue of a sodium salt that has been suggested by Johnson (1982) to be the solubility control for uranium in solutions over spent fuel. The well J-13 water contains a significant amount of sodium (50 ppm); this may cause sodium uranate to form at the expense of cesium uranate, leaving the cesium in the solution phase. To date, neither of these alkali uranate phases has been identified during post-test examination of the specimens.

The release of technetium is of particular interest since the pertechnetate ion is expected to be quite soluble in the mildly oxidizing ground water at the NNWSI Project candidate repository. Like cesium, technetium tends to separate from the oxide fuel matrix during reactor operation. Technetium should exist as a metal at the oxygen fugacity present in fuel during irradiation. Hence, it is associated with other phase-separated metallic fission products in spent fuel.

The detection limit of the radiochemical procedure used for the technetium analyses is just adequate to detect 1×10^{-5} of the specimen inventory in solution. Significant activities of technetium-99 were measured in most solution samples taken from the bare fuel and slit defect tests (Table 7-17).

Table 7-17. Summary of the measured fractional release of Cs, Tc, and I for series 2, cycles 1 and 2 experiments with H. B. Robinson and Turkey Point fuels (25°C, well J-13 water). Units are in parts per 100,000 unless otherwise indicated[a] (page 1 of 2)

Parameter	Bare fuel		Slit defect		Hole defect		Undefected	
	HBR[b]	TP[c]	HBR	TP	HBR	TP	HBR	TP
Cs-137 + Cs-134								
Cycle 1	776	308	664	144	425.0	7.8	0.19	0.11
Cycle 2	19	16	140	75	5.2	1.5	ND[e]	ND
Sum	796	324	804	219	430.2	9.3	--[f]	--
(Sum Cs)/(Sum U)[d]	110.55	20.50	6700.00	213.66	33092	264.8	--	--
% in aqueous phase								
Cycle 1	94.88	81.52	98.97	96.95	98.80	98.01	95.88	92.90
Cycle 2	92.80	89.31	98.90	98.05	97.77	98.09	ND	ND
Both cycles	94.84	81.95	98.96	97.33	98.79	98.02	95.88	92.90
(aq Cs)/(aq U)	438.0	28.6	7127.7	224.0	101196	367	24	ND
Tc-99								
Cycle 1	≈23	≈32	≈2.8	<15.3	ND	ND	ND	ND
Cycle 2	<8.6	<8.3	<2.1	<6.6	ND	ND	ND	ND
Sum	32	41	<4.9	<22	ND	ND	ND	ND
(Sum Tc)/(Sum U)	4.44	2.59	≈40.83	≈21.46	ND	ND	ND	ND
% in aqueous phase								
Cycle 1	77.00	79.32	≈43	--	ND	ND	ND	ND
Cycle 2	>86.49	>63.13	--	--	ND	ND	ND	ND
Both cycles	>79.55	>75.98	>48.70	>84.47	ND	ND	ND	ND
(aq Tc)/(aq U)	14.66	3.40	21.11	19.50	ND	ND	ND	ND
I-129								
Cycle 1	10.5	29.2	5.4	7.9	ND	ND	ND	ND
Cycle 2	7.5	12.0	0.7	5.7	ND	ND	ND	ND
Sum	18	41.2	6.1	13.6	ND	ND	ND	ND

Table 7-17. Summary of the measured fractional release of Cs, Tc, and I for series 2, cycles 1 and 2 experiments with H. B. Robinson and Turkey Point fuels (25°C, well J-13 water). Units are in parts per 100,000 unless otherwise indicated[a] (page 2 of 2)

Parameter	Bare fuel		Slit defect		Hole defect		Undefected	
	HBR[b]	TP[c]	HBR	TP	HBR	TP	HBR	TP
(Sum I)/(Sum U)	2.45	2.61	50.8	13.27	ND	ND	ND	ND
% in aqueous phase	ND	ND	ND	ND	ND	ND	ND	ND
Cycle 1	ND	ND	ND	ND	ND	ND	ND	ND
Cycle 2	ND	ND	ND	ND	ND	ND	ND	ND
Both cycles	ND	ND	ND	ND	ND	ND	ND	ND

[a] Wilson (1987).
[b] H. B. Robinson, Unit 2.
[c] Turkey Point, Unit 3.
[d] See Table 7-16 for uranium values.
[e] ND = no data.
[f] -- = not available.

As with cesium, most of the technetium release occurred during the early part of cycle 1. More than 75 percent of the mobilized technetium was in the aqueous phase, consistent with the solubility expectations. The release of technetium from the H. B. Robinson specimens was greater than for the Turkey Point specimens. This is again likely due to the finer grain size of the H. B. Robinson fuel.

Iodine-129 was measured on selected solution samples. A summary of the data, given in Table 7-17, shows that the apparent release of iodine was much less than that of cesium. It is possible, however, that iodine was lost to the air since these tests were run in unsealed vessels; however, since Johnson et al., (1983b) found high concentrations of iodine in tests conducted under conditions similar to the NNWSI Project tests, it is likely that iodine loss from solution to the air is a minor effect. The series 3 tests, run in sealed vessels, should provide better data on iodine release. Nevertheless, if one assumes that iodine loss was negligible, the iodine measured in solution correlates better with the uranium total release than with either cesium or technetium. Since iodine should be present in solution as iodide, it should not plate out on the stainless steel vessel. There is some evidence that iodide is sorbed by the Zircaloy cladding present in these tests (Johnson et al., 1985). A check for plate-out components was made at the termination of the second run by measuring the iodine-129 activity in a acid strip of the test vessel; only $\approx 1.3 \times 10^{-8}$ of the specimen inventory was recovered in this manner. However, since the vessel strip used nitric acid, iodine may have been lost to the atmosphere from the strip solution. Note that only the vessel and basket were stripped; the Zircaloy cladding was not. The data suggest that iodine-129 is being mobilized from the bare fuel at a rate similar to the matrix components and not at the much higher rate exhibited by cesium. The slit defect sample shows a clear enhanced release of iodine relative to the actinides and probably represents a gap inventory release. The amount of release, however, is still two orders of magnitude below the fractional release of cesium from slit defect samples.

Technetium is released at a rate somewhat higher than the matrix dissolution rate and higher than that of iodine-129 in bare fuel. For the slit defect case, the releases of iodine and technetium are comparable.

Wilson (1987) reports the results of carbon-14 analyses for some of the series 2 solution samples. No correlation was found between defect severity and release for either the H. B. Robinson or Turkey Point samples, suggesting that the carbon-14 was released from the cladding rather than from the fuel. Carbon-14 was radiochemically separated and measured on fuel and cladding for two samples of the H. B. Robinson fuel rod used for the series 2 specimens. The average of the analyses was 0.53 microcuries per gram for the cladding and 0.49 microcuries per gram for the fuel. In general, 30 to 60 percent of the carbon-14 in the spent fuel waste form is in the nonfuel components such as the cladding. The exact amount depends on the nitrogen impurity levels in the cladding and in the structural materials. By using the measured carbon-14 inventories in H. B. Robinson spent fuel, the carbon-14 release in the H. B. Robinson bare fuel tests was estimated to represent $\approx 1 \times 10^{-3}$ of the cladding inventory or $\approx 2 \times 10^{-4}$ of the fuel inventory in each of the cycles. These fractional inventory values are lower limits on the actual

release of carbon-14 since the test vessels used were capped with loose-fitting lids that may have allowed loss of carbon as carbon dioxide to the atmosphere.

The results of a test using a spent fuel assembly under an air atmosphere in a sealed container at 275°C showed that there is an initial release of approximately 0.3 percent of the carbon-14 inventory of the entire assembly (Van Konynenburg et al., 1984). The carbon-14 release occurred as carbon dioxide gas. Gas analyses of storage tests of spent fuel stored under inert atmospheres (helium and nitrogen) do not show significant releases of carbon-14. These results support the hypothesis that the observed release under oxidizing conditions is due to the removal of carbon as carbon dioxide from the outer surface of the Zircaloy cladding by reaction of the carbon with oxygen in the atmosphere (Van Konynenburg et al., 1986).

The test was continued with the air in the container pumped out and replaced several times to measure additional release. During the first part of the test, one of the fuel rods ruptured. This occurred after the initial carbon-14 release was measured. Despite the presence of a ruptured rod, the subsequent releases of carbon-14 were much lower than the initial release (Van Konynenburg et al., 1986). These data are still being analyzed; however, the observed carbon-14 release appears to be consistent with the fuel rod fill gas analyses reported by the Materials Characterization Center on similar fuel (Barner, 1984). Carbon-14 concentrations reported for the fill gas average 0.81 nCi/cm^3 (STP), which is equivalent to an average activity per fuel rod of approximately 0.3 microcuries. This is more than three orders of magnitude lower than the observed initial release reported by Van Konynenburg et al. (1984), supporting their conclusion that the initial carbon-14 release came from the cladding or metal components of the assembly rather than from the fuel.

There is presently only one data set for dry oxidative release of carbon-14 from spent fuel (Van Konynenburg et al., 1984, 1986). Additional experiments are planned to determine the release rate and fraction released under conditions expected at long times. Work is also in progress to determine the spatial distribution of carbon-14 in the cladding by means of controlled etching of the cladding surfaces. A description of the planned tests is in Section 8.3.5.10.

Four types of solids characterizations were performed at the end of series 2: (1) scanning electron microscope (SEM) examination of small, fractured fuel particles; (2) SEM examination with energy dispersive x-ray (EDX) microanalysis of the filters used to filter the sample solutions; (3) SEM and EDX analyses of residues from bare fuel rinse solutions; and (4) posttest radiometallurgical examination of polished sections from test specimens (Wilson, 1987).

The SEM examination of fuel particles did not reveal any significant change in fuel structure caused by the test. As is typical of spent fuel, the fracture surfaces of the fuel particles tended to follow grain boundaries. This contrasts with the behavior of nonirradiated fuel, which is a hard ceramic material that exhibits transgranular cleavage when fractured. Areas of mixed cleavage and grain boundary fracture were observed in some spent fuel particles thought to be from near the outer radial regions of the

fuel pellet. Irradiation temperatures are lower, and less fission product migration to grain boundaries occurs in these areas as compared with the center of the pellet; thus, there is less change in the fracture properties in these regions during irradiation.

An SEM image of one of the larger particles obtained from the cycle 1, H. B. Robinson rinse residues is shown in Figure 7-23. The particle is a small fuel fragment, partially coated with a surface layer of material that EDX analyses show to be primarily silicon or silica (the EDX method does not detect oxygen or other light elements). The layer appears to be a layer of silica gel ranging in thickness from 10 to 25 micrometers. Similar layers were observed on other H. B. Robinson particles as well as on Turkey Point fuel particles. The quantity of silicon involved in the layers appears to be a significant portion of the ≈7.5 mg of silicon contained in the 250 ml of well J-13 water used in the tests. The effect of this layer on the dissolution rate of spent fuel is not known. An H. B. Robinson bare fuel specimen is being tested at 25°C in a stainless steel vessel in the series 3 tests. This specimen was included to examine the effects, if any, of the test vessel material on the results of the test. The test being conducted in the stainless steel vessel is a closer representation of the repository case.

SEM and EDX analyses of selected filters used in series 2 commonly revealed extremely small particles composed dominantly of silicon. These probably represent colloidal silica flocs.

Metallographic examination of polished, mounted fuel fragments recovered after the series 2 tests did not reveal any significant evidence of grain boundary dissolution. Particular attention was given to the examination of the particle edges; however, no unusual features were noted in the post-test samples. These observations differ from those made on the posttest series 1 fuel fragments. Significant grain boundary dissolution was noted in the series 1, H. B. Robinson bare fuel particles. This difference is probably due to the more aggressive action of the deionized water used in the series 1 tests (Wilson, 1987).

Metallographic examination of the fuel at the pellet-cladding gap in the slit defect specimens of both fuel types did not reveal any unusual features that could be related to fuel dissolution.

Solution analyses for nonradioactive components were performed on the starting well J-13 water and on selected periodic solution samples (Wilson, 1987). The solution chemistry data indicate that there was little change in the composition of the leachant over the course of the tests. The only consistent change was a shift to more basic pH during cycle 1. The barrel of well J-13 water used for these tests also shifted during this time, and the change is attributed to equilibration of the well J-13 water with the atmosphere. Silicon levels in solution were of interest since the tests were run in fused silica vessels. Except for a 20 to 30 percent drop in silicon in the 30- and 120-d cycle 1, H. B. Robinson samples, the silicon concentrations remained relatively constant. SEM characterization of residues rinsed from the fuel specimens revealed a deposit of silica on the fuel surface. Apparently, the silica lost by precipitation was replaced at approximately the same rate by dissolution of the vessel; thus a constant silica concentration was maintained in solution. Another minor change in solution chemistry was

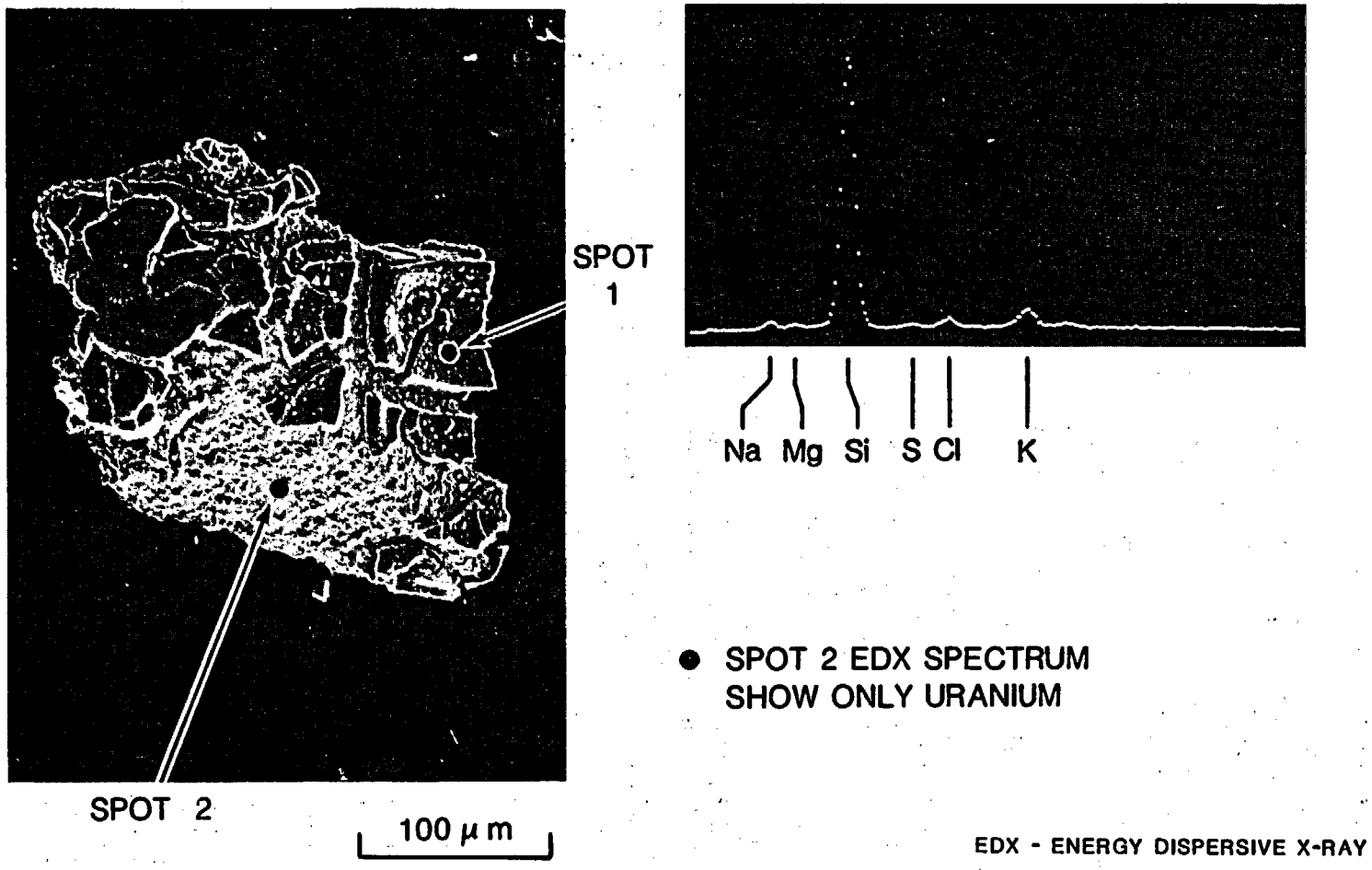

Figure 7-23. Fuel particle from the series 2, H. B. Robinson bare fuel test showing remnants of a silica layer deposited on the particle surface during the test. Modified from Wilson (1987).

the conversion of some of the initial nitrate to nitrite by radiolysis. The source of the nitrite is thought to be primarily nitrate rather than dissolved air because the measured concentrations of nitrate and nitrite in solution show an inverse correlation.

The link between the laboratory data and the expected repository performance comes through geochemical modeling calculations. The EQ3/6 geochemical modeling code is being used for this purpose. For geochemical modeling calculations to be meaningful, the solid phases that control the solution concentrations and the solubility of those phases under appropriate conditions must be identified. If the relevant thermodynamic properties of the solids are known, the solubility data obtained under one set of conditions can be used to calculate solubilities under a range of other conditions of interest. For many of the elements of interest in spent fuel dissolution, solubility data are not available for the solids that are predicted to be important in limiting solution concentrations of radionuclides.

The peak concentration of uranium in dissolution tests in well J-13 water was less than 5 ppm, and the solutions for cycle 2 of the tests were 2 to 2.6 ppm. For plutonium, the peak concentration was 5 ppb. These concentrations are much lower than the values of 50 ppm and 430 ppb, respectively, used by Kerrisk (1984) in his study of dissolution rates and solubility limits of radionuclides in a tuff repository.

Other data also point to a much lower actinide solution concentration than that predicted by the current geochemical codes. The data obtained by Forsyth et al. (1984, 1985) have a range of uranium concentrations of 0.1 to 2 ppm, with an average value of 0.8 ppm in KBS water. Forsyth et al. (1985) report a plutonium saturation value of ≈1 ppb under the same conditions. Johnson (1982) found uranium concentrations of 1.2 to 4.5 ppm in the AECL-KBS water (higher bicarbonate than well J-13 water) and 0.2 to 3 ppm in AECL-GR water. The experimental data were obtained at fuel-weight to water-volume ratios that ranged from a low of 8 g/100 ml for the Swedish tests to 72 g/100 ml for the Canadian tests. There is no indication of a correlation between solution concentration of uranium and fuel-to-water ratio. There is a weak correlation with bicarbonate content, as might be expected. Some of the variation among the three sets of results may be due to intrinsic differences in the spent fuels. Nevertheless, despite the scatter and uncertainties, th re is remarkably good agreement among the maximum solution concentrations in the three data sets. The agreement among the three sets of data with respect to uranium and plutonium solution concentrations suggests that these values represent a better estimate of the solubility of uranium and plutonium over spent fuel than the estimates obtained by calculation. This, in turn, suggests that either the phases responsible for limiting the concentration of plutonium and uranium in the system were not represented in the data base used in the calculations or the thermodynamic properties for the phases were not correct. To extrapolate the results of laboratory testing of spent fuel to the time scales relevant to repository disposal, it is necessary to develop an understanding of the dissolution mechanism for spent fuel. Detailed determination of the mechanism will require the analysis of alteration products on the surface of fuel that has undergone dissolution. Identification of the alteration products on the surface of the fuel and of any

secondary phases formed by precipitation from solution will allow the development of a model that will describe both the solid and solution phases during interaction of spent fuel with solutions.

Oversby and Shaw (1986) have reviewed the published work on spent fuel and unirradiated uranium dioxide (UO_2) dissolution in waters similar in composition to well J-13 water and in deionized water. The following discussion will summarize their analysis.

The methods used by the various workers for reporting the results of leach tests can cause confusion and apparent inconsistencies between data sets, especially when the solution concentrations are limited by the solubility of a sparingly soluble phase. If solution concentrations are constant and data are reported as leach rate per unit time, then the calculated rate will depend on the length of the test. Short tests will give high leach rates and long tests will give low leach rates. The ratio of fuel to liquid will also affect the calculated leach rate since, for concentrations in solution that are controlled by solubility of a phase, the amount in solution depends on the volume of solution and not on the amount of solid in the system. Thus, a fuel-to-water ratio of 10 g/100 ml will give a calculated leach rate 10 times higher than a fuel-to-water ratio of 100 g/100 ml if the rates are reported as fractional release per unit time.

To compare release rates determined under different experimental situations, the data must be normalized to a common set of conditions. Unfortunately, published results frequently do not contain all the information that is needed to reduce the data sets to a common basis. Johnson (1982) acidified solutions before he removed them from the leach container; therefore, he measured the sum of the solution plus plate-out component. Forsyth et al. (1984, 1985) decanted the solutions from the leach vessel, filtered a fraction of the sample to determine colloidal material, rinsed the vessels, and then stripped the leach vessel with acid to measure the plate-out component. The NNWSI Project solution analyses can be directly compared with those of Forsyth et al. (1984, 1985), but because they did not report the amount of material recovered in the rinse or acid-strip solutions, total release values cannot be directly compared. (They believe that all the material in the acid-stripping solution was due to fine particles of fuel and that it was inappropriate to include that material in the total release. Their interpretation is probably correct, but because of the possibility of particulate transport in a repository, it is necessary to determine the total amount of material mobilized during the test even if mobilization occurs as very fine solids.)

The procedures used for testing of spent fuel may also cause differences among the three sets of results. Johnson (1982) conducted tests using a modification of the International Atomic Energy Agency (IAEA) test. He used 100 ml of solution in a polypropylene bottle with an open-ended slice of CANDU fuel plus cladding, leaving the fuel sample in the solution for a fixed period of time. He determined that the solution had unimpeded access through the pellet-cladding gap, and so his tests are most nearly equivalent to the bare fuel tests carried out in the NNWSI Project studies. After the end of the leaching period, the fuel sample was transferred to a fresh bottle of solution, and the leaching was continued. Leachate solutions were acidified in the bottle before removal; so any plated-out material was dissolved and

included in the analysis. (This should not matter for uranium in the bicarbonate-rich ground waters but will have a significant effect on the other actinides.) Johnson conducted sequential tests for periods ranging from a few days to more than 100 d, with a total leaching time of nearly 3 yr.

The Johnson tests (1982) were conducted in granite ground water and measured cesium-137, strontium-90, technetium, uranium, and plutonium. Release rates were found to decrease for the first 6 months of the test and then to level out for all elements, including cesium. The range in release rates is nearly two orders of magnitude for the samples taken at 200 to 800 d into the test, with cesium, strontium, and technetium release all higher by a factor of 5 to 10 than the uranium release rate of a few parts in 10^8.

Katayama et al. (1980) reported results of the leaching of H. B. Robinson spent fuel in deionized water, 0.03M sodium bicarbonate ($NaHCO_3$), and three other leachants. They used the same general test procedure as did Johnson (1982) but used bare fuel fragments 2 to 5 mm in size, 15 g of fuel, and 300 ml of solution. This gives a fuel-to-solution ratio of 5 g/100 ml, more than 10 times lower than Johnson's. Katayama et al. (1980) acidified the solutions in the leaching vessel, as did Johnson (1982), and so they obtained data that were the sum of the solution component plus the readily soluble plate-out component which was retained in the solution due to acidification. They then did an acid stripping of the vessel and added the amount in the acid-stripping solution to the original solution value. This total was converted into a leach rate in g/cm^2,d. There is sufficient information in the report to back out the original total amount of each element that was mobilized during each sequential leaching step, but because the leach solution and acid-stripping data were added together (and never reported separately), it is difficult to compare their data meaningfully with any other group's data. They reported rather high uranium release in deionized water, which seems to conflict with Johnson's (1982) results; but since the data contained an indeterminate amount of plate-out material, there may be no inconsistency. In the series 1 NNWSI Project work, 99 percent or more of the uranium release in deionized water was recovered from rinsing the fuel sample (which may dislodge precipitated material) or from acid stripping the vessel or glass plate-out monitors.

Katayama et al. (1980) also reported data for sodium bicarbonate water leaching. The bicarbonate concentration was approximately 1,800 ppm, a level much higher than any of the ground waters used in fuel leaching. The data given in their report can be converted into solution concentrations if it is assumed that the bicarbonate concentration is sufficiently high to ensure that no uranium has plated out. The calculated concentrations range from 1 to 6 ppm uranium, a value that is in excellent agreement with the results for groundwater leaching of spent fuel discussed previously.

Forsyth et al. (1984, 1985) reported their data (1) as the fraction of the inventory in the aqueous phase (FIAP) and based their leach rates on FIAP or (2), in some instances, as solution concentrations. Therefore, their results for BWR fuel can be directly compared with the NNWSI Project solution analysis results for PWR fuel. They use a fuel-to-water ratio of 8 g/100 ml compared with the ratio of 32 g/100 ml used for the H. B. Robinson tests in well J-13 water. They found that the fraction of cesium released rapidly in

the tests was approximately 1 percent, slightly higher than the 0.7 percent fission gas release. Strontium was released at about one-tenth the rate of cesium release, and uranium release was lower than strontium release by a factor of 10. The concentration of uranium found was generally between 0.1 and 1 ppm for contact times up to approximately 3 yr. Johnson (1982) found that solution concentrations of uranium averaged 3 to 4 ppm for the 60-d leach solutions. There appears to be a real difference between the two sets of data, and the difference is probably due to the different concentrations of bicarbonate in the solutions used in the two studies. The bicarbonate content of well J-13 water is similar to the KBS water; the uranium concentrations in the NNWSI Project tests are intermediate between the other two data sets.

Johnson et al. (1983a) have established a general correlation between measured fission gas release from CANDU fuel and the fraction of rapidly released cesium found during a leach test. For very low gas release (about 0.07 percent xenon), the cesium release is approximately 10 percent of the gas release. For higher gas release, the fraction of cesium released is higher and is generally 50 percent of the gas release for all cases with more than 0.13 percent xenon release. This generally agrees with NNWSI Project results on the two low-gas-release PWR fuels. The BWR high-burnup fuel tested by Forsyth et al. (1984, 1985) showed cesium rapid release somewhat in excess of fission gas release.

Johnson et al. (1983b) have extended the study of mobile element release from CANDU fuel to include iodine. Iodine and cesium release were measured in distilled water at 25°C for up to 5 d. The same possibility of iodine loss to air as applies to the series 1 and 2 NNWSI Project iodine data also applies to this study because the Canadian tests were also run in unsealed vessels. Because Johnson et al. (1983b) found large amounts of iodine in tests conducted under conditions similar to the NNWSI Project fuel dissolution tests, the low levels of iodine found in the NNWSI Project tests are believed not to be due to loss of iodine from solution. In general, the gas release, iodine, and cesium rapid release are comparable, but differences of a factor of two or three are common. More recent data on iodine release from low-gas-release fuels shows a pattern similar to cesium release, with iodine release being about 10 percent of the gas release for gas release less than 0.1 percent (Johnson et al., 1985).

Johnson et al., (1985) found that iodine release was low if deionized water was used as a leachant. The effect was attributed to sorption of trace iodide onto the Zircaloy cladding. Most of their subsequent experiments used a solution with 0.2 g/L of potassium iodide to act as a carrier. Although this increased the reproducibility of their results, the relevance of the iodine release measured in these experiments to the release in ground water in the absence of large amounts of iodide in solution are questionable. (They do, however, provide a means of determining the location of the iodine-129 inventory within the fuel.) The low iodine-129 release rates observed in the NNWSI Project experiments may either reflect a lower gap inventory of iodine-129 in PWR fuel or the relative immobility of the iodine-129 in the absence of an iodide carrier.

Some data are available on the dissolution of spent fuel at higher temperatures. Results of testing CANDU fuel at 150°C are contained in the

report by Johnson et al. (1981), with a few additional data points for longer times being reported in Johnson et al. (1982). The experiments were conducted at 150°C in 1 L titanium autoclaves using 500 ml of granite ground water (Table 7-13), saturated with air. The runs were generally 8 to 10 d in length, with the fuel samples having been preleached at ambient temperature for 100 d to remove the readily soluble cesium fraction. During the run, the oxygen content of the system was thought to have decreased by a factor of 2 to 3. Experiments were also conducted using deionized water saturated with air.

The results gave similar uranium and plutonium concentrations for deionized water and granite groundwater, with an average concentration of 0.05 to 0.1 ppm for uranium and 0.1 ppb for plutonium. The uranium concentrations were much lower than those observed at ambient temperature. Data for leaching at 260 d gave a higher uranium concentration (0.2 ppm), which is still much lower than the ambient temperature results.

The NNWSI Project series 3 dissolution tests are being conducted at 85°C. Based on the results of Johnson et al. (1981, 1982), it is not expected that a substantial increase in matrix solubility will be observed.

Forsyth et al. (1985) have studied the effect of the intensity of the alpha radiation field on the dissolution rate of spent fuel. It is possible that the dissolution rate of uranium dioxide (UO_2) could be affected by changes in the redox state of the leachant due to alpha radiolytic decomposition of the water in contact with the fuel. They conducted leaching experiments using low-burnup (≈0.5 MWd/kgU) fuel that had a fission product activity similar in size (though different in composition) to that of fuel with more typical burnup. The inventory of alpha emitters was much less, however. The dissolution behavior of this fuel was significantly different from that of higher burnup fuel, but the observations could not be attributed to the difference in the alpha field. Rather, they believe that differences in microstructure and composition between the types of fuel are the reasons for the observed difference in leaching behavior.

The most detailed studies concerning oxidative dissolution of unirradiated UO_2 have been done as part of the Canadian program. They have used natural uranium in the form of sintered UO_2, which is the fuel material for the heavy-water CANDU reactors. Enriched uranium fuel pellets of the type used in light-water reactors generally have a lower density than the unenriched pellets (see Table 7-14 for comparison). This may affect the depth of penetration of surface oxidation and the surface area readily available for oxidation dissolution but should not alter the mechanism significantly.

Sunder et al. (1981) and Shoesmith et al. (1983) report the results of electrochemical studies using an electrode fashioned from fuel pellet material. They used potentiostatic and cyclic voltametric techniques to determine the mechanism for oxidation in solution of the surface of the uranium dioxide electrode. Sunder et al. (1981) used dilute Na_2SO_4 solutions in the pH range 6 to 11, and Shoesmith et al. (1983) used aqueous carbonate solutions with a range of 0.0001 to 0.5 mole/L total carbonate. The mechanism of dissolution has been found to be different in the two systems because of the ability of the carbonate ion to complex hexavalent uranium.

In the carbonate solutions, dissolution occurred from a layer of U_3O_7 at potentials of 0.1 V or less and from a layer of U_2O_5 at applied potentials of 0.15 and 0.2 V for solutions where the carbonate content was less than 0.001 mole/L (60 ppm). As the carbonate concentration was increased, dissolution of the electrode was enhanced and oxide film formation on the surface became less important. For total carbonate concentrations greater than 0.01 mole/L (600 ppm carbonate), the oxidation of the layer did not progress beyond U_3O_7 because uranyl ions were complexed by carbonate and taken into solution, thereby being unavailable for incorporation into the oxide layer for the next step in film formation. Thus, the mechanism of dissolution has been shown to be a function of both the potential applied to the electrode and the carbonate content of the system. It is probable that for the NNWSI Project tuff repository conditions, the surface from which dissolution occurs would be composed of U_3O_7 because of the combination of mildly oxidizing conditions and moderate bicarbonate concentrations.

Wang (1981) and Wang and Katayama (1982) reported the results of studies using single crystals of UO_2. They proposed a different mechanism than did the Canadians; however, their studies are much less detailed than those discussed above, and their results are correspondingly less certain. Experiments were conducted at 75 and 150°C in systems that were pressurized to give 200 ppm oxygen dissolved in the solutions. This level of dissolved oxygen is very high and may affect the oxidation mechanism for the samples and the nature of the alteration products. The studies done by the Canadians are more relevant to the NNWSI Project tuff repository conditions than is the work referred to in this paragraph.

In summary, the results of the several studies on the oxidative dissolution of UO_2 indicate that the mechanism by which uranium is liberated to solution is a multistage process that depends on both the chemistry of the solution (particularly the thermodynamic activity of CO_2) and the Eh or oxygen fugacity of the system. The effects of raising the Eh and of raising the activity of CO_2 oppose each other. At low activities of CO_2, the UO_2 surface oxidizes to U_3O_7, U_2O_5, and UO_3, with the higher oxides only forming at high Eh (high activity of O_2). Uranium is removed to solution from this oxide surface. At a constant Eh, as the activity of CO_2 increases to the levels present in ground water at the NNWSI Project candidate repository, the oxidation of the surface does not progress beyond U_3O_7. At these activities of CO_2, uranium appears to be removed directly from this surface, with no role played by higher uranium oxides.

Plans to develop the thermodynamic data base and additional information to support the fuel dissolution model needed for geochemical code development are discussed in Section 8.3.5.10. The latter includes studies to identify fuel-surface, alteration products and secondary phases formed by precipitation from solution and experiments to ascertain the effect of the initial oxidation state of the fuel matrix on release rates. The radioactivity present in the spent fuel interferes with most available surface analysis techniques. Because of the analytical difficulties involved, current program planning is being based on the assumption that the work of others on the dissolution mechanism of unirradiated UO_2 will be relevant to spent fuel and that the work on actual spent fuel can be limited to confirmatory studies.

7.4.3.1.2 Oxidation of spent fuel in air

Most spent fuel rods emplaced into a repository will consist of fractured UO_2 pellets enclosed by intact Zircaloy cladding. A small fraction of the rods (less than 1 percent) will have cladding defects, typically in the form of small splits or pinholes (Woodley, 1983). The fuel pellet retards the release of radionuclides when the leach rate is low, and the cladding provides an additional barrier that limits the ingress of water to the fuel. In the moist air atmosphere of the NNWSI Project candidate repository, the UO_2 fuel in a rod with defected cladding in a failed container will be oxidized to UO_3, given sufficient time. When it oxidizes, the UO_2 passes through several intermediate, metastable phases such as U_4O_9, U_3O_7, and U_3O_8. There is a large increase in the molar volume associated with the transformation to U_3O_8, and, if this oxidation state is reached, the fuel pellets swell and put a tensile hoop stress on the cladding, enlarging existing breaches and in some instances creating new ones (Novak and Hastings, 1983; Johnson et al., 1984; Einziger and Cook, 1984). Thus, if there is significant oxidation of the fuel, the ability of the waste form to retard release of radionuclides may be degraded, both by the disruption of the cladding and by the formation of uranium oxides with potentially higher leach rates than UO_2.

Most of the available data on the oxidation of UO_2 were obtained above 200°C and then extrapolated to lower temperatures. The data typically use the time to spallation as a measure of the time required for the onset of U_3O_8 formation; the data provide little insight into the rate of formation of intermediate oxides or which oxides form. Under conditions expected in the NNWSI Project candidate repository, the fuel temperature will be between 160 and 110°C in a container that fails between 300 and 1,000 yr. A time-dependent extrapolation of high temperature data (Einziger and Strain, 1984) indicates that insufficient oxidation of the fuel to U_3O_8 will occur to cause additional failure of the cladding. This calculation assumes that there are no operant oxidation mechanisms at low temperatures that are insignificant at the higher temperatures at which the data were obtained but which become dominant at the temperatures present in the repository.

The results of previous studies of spent fuel and UO_2 oxidation clearly indicated that there are substantial differences in the oxidation kinetics of various fuel types and especially between irradiated and nonirradiated fuel. Consequently, a program of spent fuel oxidation studies has been initiated to investigate oxidation under the conditions identified by Einziger and Woodley (1985a) as the most relevant to the NNWSI Project disposal conditions. The program goal is to obtain oxidation rate and mechanism data on spent fuel samples at temperatures as low as achievable on reasonable laboratory time scales. The work combines thermogravimetric analysis (TGA) of spent fuel oxidation with more conventional oven oxidation work on larger samples. Some of the larger samples will then be used in fuel leaching studies since the oxidation state of the surface of the fuel may affect its leaching behavior. The results of several runs using the TGA apparatus have been published (Einziger and Woodley, 1985b, 1986) and the work is continuing. The oven oxidation work is in progress and no published data are yet available. The following discussion is based on the existing TGA data.

Small samples (200 mg) of Turkey Point unit 3 PWR spent fuel have been used in NNWSI Project TGA studies at 200 and 225°C (Einziger and Woodley,

1985b). Tests at 140 and 175°C have been completed; the results are shown in Einziger (1986). Full test results will be published in the near future. The analytical system has been shown to have excellent stability over periods of up to 2,100 h with the ability to detect a weight change as low as 10 micrograms and the ability to control temperatures to ±1°C up to 300°C (Einziger and Woodley, 1985b). The test matrix for both the completed and the planned test runs is shown in Table 7-18, and TGA weight gain curves for the tests at 200° and 225°C are shown in Figure 7-24.

The effect of particle size was examined in the 140 to 225°C range by testing a single fragment versus pulverized fuel at the same temperature. Although the pulverized fuel showed a higher initial rate of oxidation due to the larger surface area, at temperatures above approximately 200°C the fuel fragment soon caught up and eventually exceeded the weight gain recorded by the pulverized fuel. At temperatures above 200°C, the particle size does not appear to influence the long-term oxidation rate (Einziger and Woodley, 1985b). In contrast, the data at 140°C indicate that surface area may be important at lower temperatures (Einziger and Woodley, 1986).

The results to date support a two-stage mechanism for the oxidation of spent fuel in air: (1) diffusion of oxygen along grain boundaries and oxidation of the grain surfaces and (2) bulk diffusion into the grains. At temperatures above approximately 200°C, grain boundary diffusion appears to be relatively rapid, allowing access of oxygen to most of the grains in the test specimen. This effectively increases the surface area available for bulk diffusion so that the initial surface area is relatively unimportant. This period is expressed in the weight gain curves as an early period of rapid weight change. At lower temperatures (140°C), the rate of grain boundary diffusion of oxygen appears to have slowed sufficiently so that the steady-state bulk diffusion stage was not reached during the 2,100-h test.

The effect of moisture content was examined by running tests at the same temperature but with two different levels of water vapor in the air, namely 3 and 16,000 ppm water at 225°C. The oxidation curves were virtually identical (Figure 7-24, curves 4 and 5; Table 7-18), indicating that moisture content does not seem to be an important parameter in the range tested. The data obtained by TGA were in good agreement with previous work on larger fuel samples, indicating that the small sample size is still representative of the bulk fuel (Einziger and Woodley, 1985b). This is fortunate because the continuous weighing characteristic of TGA allows the oxidation process to be followed in detail.

The rate constants obtained from the bulk diffusion portion of the TGA data can be fit to a straight line in an Arrhenius plot to obtain the activation energy of the diffusion-controlled oxidation. If the results from the 200 and 225°C runs are considered alone, they yield an activation energy of approximately 107 kJ/mole. Although there is considerable uncertainty in this determination because it is based on only two points, the value is in reasonably good agreement with literature values that generally range from 85 to 125 kJ/mole (Aronson et al., 1957; Hastings and Novak, 1984, 1986). If all the data from Figure 1 of Einziger (1986) are used, the value would be 171 kJ/mole, which is higher than that found in previous work. This value may be incorrect if the effects of grain boundary diffusion have not been

Table 7-18. Fuel oxidation test parameters for spent fuel thermogravimetic analyses[a,b]

	Test 1	Test 2	Test 3	Test 4	Test 5
			COMPLETED TESTS		
Temperature (°C)	225	224	200	225	225
Duration (h)	356	408	737	387	438
Atmosphere	air	air	(c)	air	air
Dew point (°C)	14.5	14.5	14.5	-69.8	14.5
Initial weight (mg)	195.2	228.5	227.6	214.5	211.5
Sample condition	Pulverized fuel	Single fragment	Single fragment	Two fragments	Four fragments
			TESTS IN PROGRESS OR PLANNED[d]		
Temperature (°C)	140	140	140	175	175
Duration (h)	2,200	830	300	2,150	2,150
Atmosphere	air	air	(c)	(c)	(c)
Dew point (°C)	14.5	14.5	14.5	-70	14.5
Initial weight (mg)	197.9	184.2	204.2		
Sample condition	Two fragments	Pulverized fuel	Pulverized fuel		
Temperature (°C)	175	155	155	155	
Duration (h)	2,150	2,150	2,150	2,150	
Atmosphere	(c)	(c)	(c)	(c)	
Dew point (°C)	-20	-70	14.5	-20	

[a]All tests carried out using Turkey Point spent fuel (Table 7-14).

[b]Source: Einziger and Woodley (1985b, 1986).

[c]Test conducted in a mixture of 80% N_2 + 20% $^{18}O_2$.

[d]Includes tests at 140 and 175°C that have been completed but for which complete results have not yet been published.

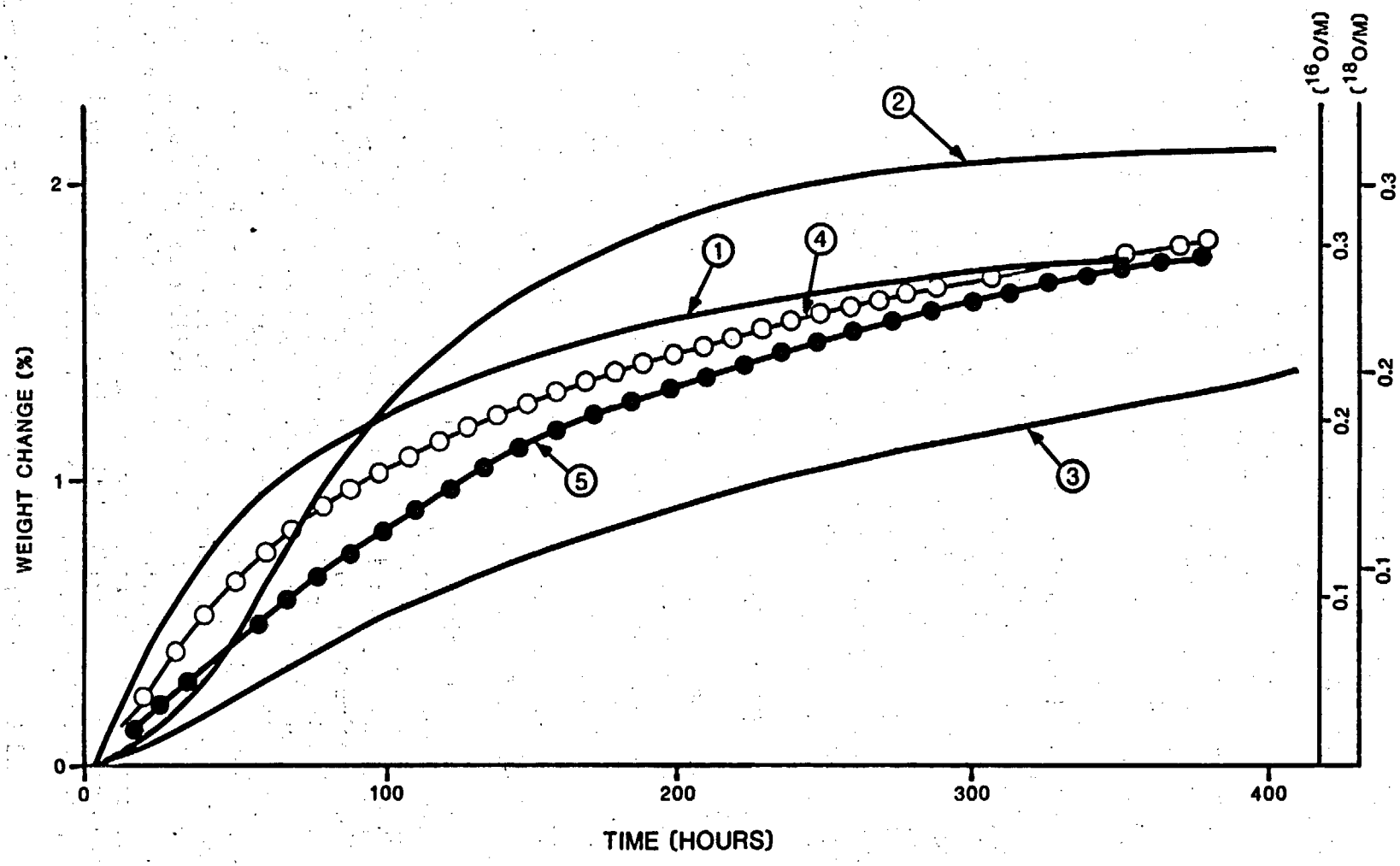

Figure 7-24. Thermogravimetric analysis test sample weight changes (percentage weight gain relative to starting weight). Numbers associated with the curves refer to the test numbers for the series of tests at 200 to 225°C in Table 7-18. Circles are actual data points. Modified from Einziger and Woodley (1985b).

accounted for adequately. The activation energy value will be refined as data from different temperatures are obtained.

A full understanding of the oxidation mechanism of spent fuel will depend on the identification of the phases formed during the process. Characterization of the posttest samples using optical microscopy, x-ray diffraction, electron diffraction, scanning electron microscopy, transmission electron microscopy, and ion microscopy (on samples oxidized in an oxygen-18 atmosphere) is planned (Section 8.3.5.10). Presently, it is not known whether the weight gains recorded in the TGA tests are caused by the formation of U_3O_8, U_3O_7, some other oxide phase, or a mixture of several oxide phases.

Other published work on the oxidation of unclad UO_2 is generally consistent with the data obtained from the NNWSI Project work. Hastings and Novak (1984, 1986) investigated the rate of oxidation of nonirradiated and irradiated CANDU pellet material in the range 175 to 400°C and found activation energies of 140 and 120 kJ/mole, respectively, for the two materials. Studies using spent fuel from the Bruce and Pickering reactors showed that the spent fuel oxidized 5 to 10 times faster than UO_2 at 215°C. They also presented data that suggested a correlation of decreasing fragment size with increasing oxidation rate; however, the scatter in the data is too large for the result to be conclusive.

White et al. (1984), from studies of nonirradiated UO_2 pellets, argue for a two-stage oxidation process with activation energy of 102 kJ/mol for the prespallation stage (corresponding to initial production of U_3O_8) and of 160 kJ/mole for the postspallation stage. There is considerable scatter in the data, and the argument for two stages is far from conclusive. If the activation energy were calculated as a single process, the result would be in reasonable agreement with that of Hastings and Novak (1984, 1986). They also tested Point Beach PWR spent fuel in gamma radiation fields of two intensities and found that the oxidation rate in a 10^5 rads/h field was less than that in a 10^3 rads/h field. This result is yet to be explained.

A large percentage of the work on oxidation of UO_2 has been done using clad fuel with induced cladding defects to study the rupture behavior of the cladding upon formation of U_3O_8. Johnson et al. (1984) have investigated the behavior of breached BWR fuel rods, which had been water logged before the start of the experiment, in air and argon atmospheres at 320°C for periods up to 2,100 h. This temperature is close to the design limit for fuel rod surface temperatures in the present NNWSI Project spent fuel container designs (350°C). They found no detectable change in the fuel rod held in the inert gas atmosphere, despite the presence of water in the system. On the other hand, the rod that was held in air oxidized extensively in the area near the original breach, which caused the cladding to split open. Before the start of the test, a drillhole was drilled near the plenum to allow moisture to escape from the rod. Air gained access to the top fuel pellet through that drillhole and oxidized the pellet, and the previously unbreached cladding split under the stress of the fuel expansion caused by oxidation.

Einziger and Cook (1984) also investigated the behavior of fuel rods in air and inert atmospheres. They used argon with 1 percent helium, a temperature of 229°C, and a test time of 5,962 h. They compared the behavior of

intact rods with those in which 0.8-mm-diameter drillholes had been drilled at two locations in the rod. One drillhole was drilled near the center of the rod, while the other was located near the top. No changes were found in any of the intact rods as a result of the test, nor were there any changes in the defected PWR rod in argon or in air. The BWR rod stored in air developed a split in the cladding at the location of the top defect, which was located at a pellet-pellet interface. The splitting was due to oxidation of the fuel in the vicinity of the defect, with the final product being U_3O_8. The center defect, located in the middle of a pellet, showed the start of oxidation from UO_2 to U_3O_8, but the degree of oxidation and stress on the cladding was not sufficient to result in splitting.

The difference in oxidation for the two defects in the BWR rod and the absence of any indication of extensive oxidation for the PWR rod held in air were interpreted by Einziger and Cook (1984) to be due to the location of the defects. The upper BWR defect was thought to allow greater access of air to the interior of the rod due to the location of the defect at a pellet-pellet interface, allowing more extensive oxidation to occur. As oxidation progressed and the fuel swelled, the access of air was impeded until the stress was large enough to split the cladding. For the central defect, located in the middle of a pellet, oxidation probably closed the space available for air to enter the rod, thus slowing the rate of oxidation. Because of the relatively low temperature at which the oxidation and cladding split occurred, Einziger and Cook (1984) recommended that dry storage of spent fuel use an inert atmosphere. That recommendation for the atmosphere of disposal containers has been adopted by the NNWSI Project to help preserve the integrity of the cladding during the early high temperature phase in the repository.

Einziger and Cook (1984) used their data to estimate the velocity of the oxidation front inside the breached fuel rod. Their results are in good agreement with the early data on the oxidation of irradiated CANDU fuel. At the velocity calculated (2 to 3×10^{-5} cm/min), the fuel cladding would split from end to end in 17 yr at 230°C.

Novak et al. (1983) reported results of testing of irradiated CANDU fuel elements into which drillholes have been drilled. The specimens had either one centrally located 0.8-mm diameter hole or 4 drillholes clustered near the center and one hole near each end of the element; control samples with no defects were also tested. They found cladding splitting in the case of the cluster of 4 defects for the element, with 6 total defects tested at 250°C, but no splitting at the site of the single defects in that element. The splitting, which was inferred to be due to U_3O_8 production, occurred after 208 h at that temperature. The single defect at this temperature showed 2 percent strain at the defect site but no splitting. The control sample with no defect was unchanged.

At 230°C, no cladding split was seen by Novak et al. (1983) for any configuration, and the largest change was 0.7 percent swelling at the site of the cluster of 4 defects after 600 h. The oxidation product was determined to be U_3O_7 by measurement of the O:U ratio. The single defect locations showed lower strain, indicating that access of oxygen to the fuel was controlled by the defect geometry. The extent of oxidation was shown to be limited to the region very close to the defects, and the oxidation front was calculated to move at 2×10^{-5} to 3×10^{-5} cm/min at 230°C, which is in

excellent agreement with the results of Einziger and Cook (1984). Novak et al. (1983) also measured the oxidation rate of defected nonirradiated fuel elements. Their results showed large differences between irradiated and nonirradiated fuel, a phenomenon noted by other workers studying fuel oxidation of pellets or fragments of fuel as well as defected rods (Hastings and Novak, 1984, 1986; White et al., 1984). This phenomenon may be due to the opening of grain boundaries during irradiation, allowing access of oxygen to the interior of the fuel pellets. The weight gains found by Novak et al. (1983) are 2 to 4 times less than those measured by Einziger and Woodley (1985b) for equivalent temperatures and exposure times. This phenomenon may also be a reflection of grain boundary versus bulk diffusion effects.

The short-term oxidation rate of spent fuel at intermediate temperatures of interest to the repository disposal conditions may depend on sample condition because the oxidation process occurs first by diffusion of oxygen along grain boundaries and then by bulk diffusion into the grains. For the time periods of interest in the repository, bulk diffusion should be the rate-limiting step. When measuring oxidation rates in the laboratory, care must be taken to ensure that the period of oxidation is long enough so that the grain boundary diffusion process is complete and the rate measured is that for bulk diffusion of oxygen controlling the oxidation process. Plans for work by the NNWSI Project to determine the rate of oxidation of spent fuel under conditions relevant to a repository at Yucca Mountain are given in Section 8.3.5.10, under Issue 1.5.

7.4.3.1.3 Zircaloy corrosion

Most spent fuel to be placed in a repository is clad with either Zircaloy-4 or Zircaloy-2. A small fraction of the spent fuel is clad in stainless steel (fuel from four reactors). The current NNWSI Project work on cladding involves only Zircaloy. Future work may include tests on stainless steel cladding (Section 8.3.5.10).

When considering the results of spent fuel dissolution studies, it is clear that some elements would be released into water at rates in excess of one part in 100,000 per year if the interiors of all the fuel rods were to be simultaneously contacted with water. The rapid release of cesium and associated elements would be confined to a short period and would involve the gap and grain boundary inventory of those elements. Since it will take many years for water to fill a breached container under the conditions expected at Yucca Mountain, rapid release of the gap and grain boundary inventory to water does not necessarily equate to rapid release from the waste package. If the Zircaloy cladding were to maintain its integrity for long periods of time and if cladding failure after disposal were to occur over an extended period of time rather than as a single catastrophic event, then the release of elements such as cesium would be further controlled. Preservation of cladding integrity would also prevent oxidation of the fuel to states that might be more leachable once water contact occurs.

The potential causes of failure in spent fuel rods that were intact at the time of disposal (or storage, in the case of studies conducted in support of the dry storage program) have been considered by Einziger and Cook (1984),

Johnson and Gilbert (1984), and Rothman (1984). Spent fuel containers for the Yucca Mountain repository would be filled with an inert gas to prevent the oxidation of fuel contained in failed rods placed in the container. Oxidation of the cladding would occur only after the container was breached, at which time temperatures would be relatively low. The mechanism of oxidation and generalized corrosion of Zircaloy appears to be the same in air, steam, and pure liquid water environments (Rothman, 1984). Predictions of the degree of oxidation, which depend on the model used to extrapolate the available laboratory data, show a range of about a factor of ten in the predicted oxide thickness formed due to isothermal oxidation at 180°C. The greatest thickness predicted was 53 micrometers after 10,000 yr of corrosion, a value that is less than 10 percent of the cladding thickness (Rothman, 1984). Johnson and Gilbert (1984) predicted an increase in thickness of the oxide layer of about 1 micrometer after 40 yr at 250°C compared with the typical thickness of 20 micrometers of oxidation layer found on fuel rods at the end of their reactor service life.

Corrosion of Zircaloy is enhanced by the presence of some elements in solution. Under expected NNWSI Project tuff repository conditions, none of the elements known to cause accelerated corrosion of Zircaloy is present in sufficient concentration to be of concern (Rothman, 1984). Of the species present under expected NNWSI Project conditions, only the fluoride ion appears to have the potential for significantly increasing the corrosion rate of Zircaloy. Even so, an increase in concentration of fluoride by approximately a factor of 10 would be necessary before any increase in corrosion rate would be expected. Nevertheless, because of the limited data base presently available, Rothman (1984) recommended that some work be initiated on the corrosion of Zircaloy in water having various fluoride concentrations. Such work is in the planning stages (Section 8.3.5.10).

Failure of Zircaloy can occur due to stress rupture when internal pressure from the gas inside the fuel rod exceeds the strength of the cladding material. Failure occurs after a period of time under stress and depends on the stress applied, which is a function of temperature. Einziger and Kohli (1984) have analyzed the data available on stress rupture and have shown that storage of fuel rods at temperatures of 305°C for 100 yr would produce a breach due to stress rupture in less than 5 percent of the rods. For a slightly lower temperature of 288°C, an isothermal period of 1,000 yr would be required before rupture would occur in a similar number of rods. The assumptions used in the analysis were extremely conservative. In particular, it was assumed that stress relief due to cladding creep does not occur and that all rods used in experimental testing are among the 5 percent of the population able to withstand rupture. Also, the rods tested at lower temperature were altered to allow overpressurization so that the test data were for pressure levels (and hence stresses) approximately twice the normal value. No test rods failed, and so the analysis is based on the assumption that the rods were just about to fail. These are also very conservative assumptions.

Rothman (1984) extended the stress rupture analysis to include the concept of life fraction. The time-to-failure at a particular temperature was calculated to represent cladding behavior for a time interval at that temperature under disposal conditions. The ratio of the time increment for that

temperature to the time-to-failure was determined. The process was repeated in steps to simulate the thermal decay curve for disposal conditions, and all the ratios were summed. If the results give a sum less than one, then failure by that mechanism is predicted not to occur. The analysis showed that a 10,000-yr period under disposal conditions is equal to only 0.1 percent of the time-to-failure by stress rupture under these conditions. Rothman (1984) concluded, therefore, that stress rupture was not a significant failure mode for fuel rods under the Yucca Mountain repository disposal conditions.

Analysis of the potential for failure by delayed hydride cracking showed that most of the data argued against this mechanism (Rothman, 1984). There is some concern that hydrides in the cladding, which are originally oriented in a circumferential direction, might reorient under storage or disposal conditions to a radial orientation. The radial hydrides might then accelerate cracking in the cladding (Einziger and Kohli, 1984). More data are needed on the statistics of crack properties in cladding and on the effects of slow cooling under storage or disposal conditions. Plans for work in the area of hydride reorientation effects are given in Section 8.3.5.10.

Stress corrosion cracking (SCC) is the final mechanism thought to be a potential cause of failure of Zircaloy under repository conditions. In an unbreached rod, SCC should be more likely on the inside than on the outside (Smith, 1985). There are two reasons for this: (1) the hoop stress due to gas pressure in the rod is greater at the inside surface than at the outer surface and (2) the chemical environment within the rod is much harsher (e.g., iodine) than that outside the rod. This is not to imply that the inside features of the fuel rod will not affect the behavior of the cladding exterior with respect to SCC. Indeed, chemical interactions within the rod could play a role in SCC from the exterior by creating inhomogenous stress distributions on the outer surface of the cladding.

Several analyses have been conducted to evaluate the potential for SCC of Zircaloy under repository conditions. Einziger and Cook (1984) concluded that SCC should not be a life-limiting degradation mechanism for fuel rods stored under dry storage or repository conditions at temperatures below 400°C. Miller and Tasooji (1984) agreed with this conclusion based on model calculation of crack propagation for typical fuel rods. They used an incipient crack depth of 20 percent of the cladding thickness and a fission gas release of one percent during reactor service and assumed a prepressurized PWR fuel rod. They found that their model predicted no failure due to SCC at any time for temperatures up to 400°C. They believed that their typical case represented 99 percent of fuel rods that are intact at the time of storage or disposal. For a worst case of 50 percent gas release (a very conservative figure), with the other parameters the same, they predicted that a crack would propagate to failure in 100 yr at 150°C. A somewhat lower, but still very large, gas release of 17 percent produced a predicted time-to-failure of 100 yr at 170°C. This is at the high end of the measured gas release fractions in reactor service for PWR rods.

Miller and Tasooji (1984) also presented an analysis of SCC based on linear elastic fracture mechanics. This analysis found a much higher limiting temperature of 290°C for an initial crack of 10 percent depth to propagate to failure in 100 yr. Below that temperature no failure would occur for cracks of that size, but larger cracks might propagate to failure.

Based on the preceding discussion, two types of information are needed with respect to Zircaloy corrosion. First, some general corrosion data for Zircaloy together with other components of the waste package in well J-13 water are needed to provide a baseline for further studies on the effect of water chemistry (especially fluoride content) on corrosion rates. Initial experiments were started in late 1984; a description of the work is contained in the reports by Smith (1984a, 1985). The preliminary results of this work are given in Smith and Oversby (1985). Initial evaluation of the test samples from the 90°C corrosion scoping experiment indicated no corrosion of Zircaloy-4 at a detection sensitivity of 1 to 2 micrometers of corrosion per year. Specimens that had been run for 2, 6, and 12 months showed no difference in appearance at that sensitivity. Work is planned to increase the sensitivity of these experiments (Section 8.3.5.10). By using STEM, electron diffraction on ion-milled specimens, and Auger surface analysis, corrosion on the scale of hundreds of angstroms can be studied.

Additional corrosion experiments at elevated temperature and pressure (170°C and 120 psia) are in progress (Smith, 1986a); data are not yet available for these experiments.

It has also been decided to investigate stress corrosion cracking using C-ring tests. An experimental apparatus has been built to allow remote testing of defueled cladding. The philosophy and execution of the tests are described in the reports by Smith (1985, 1986b). These tests are in progress and no published data are yet available (Section 8.3.5.10).

Zircaloy is also of concern because it is part of the waste form (i.e., it contains radionuclides whose release must be controlled). The most significant nuclide in Zircaloy cladding is carbon-14. The results of experiments to measure the release of this radionuclide by oxidation of the carbon in the cladding is discussed in Section 7.4.3.1.1.

7.4.3.1.4 Release model for determining the source term for the spent fuel waste form

Data from the experiments described previously and in Section 8.3.5.10 will be used to develop a model for the release of radionuclides from a waste package as a function of time. A distribution function, developed as part of the metal barrier task, will be used to determine the time-to-breach for containers under both anticipated and unanticipated conditions. The paper by Oversby and Wilson (1985) describes the methodology to be used in developing this model. Oversby (1986) examined the radionuclide inventory of the spent fuel waste form in light of EPA and NRC regulations and provides a basis for identifying which radionuclides are of the most concern.

The container breach-time distribution will give the starting point for radionuclide release from the waste package. The first radionuclide released will probably be carbon-14 from the outer oxidized skin of the cladding. This release may not require contact with water if the high temperature data are an indication of the release mechanism at lower temperatures. Following container breach, water may enter the container. The potential geometric configurations for water contact with the fuel rods are discussed in Section 7.4.3.

The source term for failed fuel rods will include five components:

1. Elements whose release is controlled by the matrix dissolution rate.

2. Elements enriched at grain boundaries and available for enhanced release.

3. Elements present in part in the pellet-cladding gap and available for rapid release.

4. Elements contained in stainless steel or in other fuel assembly components.

5. Elements contained in or on the fuel cladding.

The release of phase-segregated elements such as those present in metallic inclusions is accounted for by the first three items listed above.

The dissolution rate of the matrix will be determined using a fuel-to-water ratio that is as realistic as possible. The water volumes used in present testing for the NNWSI Project are approximately 10 times higher than those for a realistic repository ratio. The larger volume is needed to allow sampling of tests without disruption of conditions. As more data are gathered, future tests will involve less frequent sampling and higher fuel-to-water ratios. The overall dissolution rate will need to consider the distribution of the various fuel characteristics that affect the release of radionuclides such as burnup and grain size. To do this, good data on the irradiation histories and as-fabricated characteristics of the fuels to be emplaced into the repository will be needed.

The source term will include an estimate of both the number of rods initially emplaced with defected cladding and the degradation rate of the Zircaloy cladding. Distributing the breach rate of cladding over a range of time has a large effect on controlling the rate of release of elements such as cesium.

The data from each of the components of the source term will then be summed to determine the concentrations of radionuclides in solution within the container as a function of time. This information, combined with the infiltration rates for water, will then provide the maximum volume of water and amount of radionuclide that can be displaced from a breached waste package per year. At this time, it is not planned to use any restriction of flow provided by the breached container to show compliance with the release rate performance objective. The source term developed to describe spent fuel behavior will be used as input to the waste package performance analysis

subtask. Plans for development of the source term model and data are given in Section 8.3.5.10.

7.4.3.2 Glass waste form performance research

The goal of the NNWSI Project glass waste form performance research is to determine release rates for waste glasses under repository conditions. To accomplish this, testing is being done under conditions designed to measure glass leaching rates, to observe component interactions, and to determine the controlling factors in glass leaching under tuff repository conditions. In this summary, general results from glass testing, including NNWSI Project testing, are presented. These results are used to define important parameters for the NNWSI Project to study. Examples of some of the important effects observed are given from NNWSI Project studies. Following that, results from recent NNWSI Project testing are presented.

7.4.3.2.1 Glass waste forms and general principles of glass performance

Two glass-based waste forms are being considered for disposal by the NNWSI Project: Savannah River Plant (SRP) defense waste to be processed at the Defense Waste Processing Facility (DWPF) and reprocessed waste from the West Valley Demonstration Project. Any SRP waste will be made into a borosilicate glass based on Savannah River Laboratory (SRL) frit 165 (Baxter, 1983; Oversby, 1984b). The waste composition at West Valley falls approximately within the range of compositions found at Savannah River, and the glass is expected to be similar to DWPF glass (Eisenstatt, 1986; Oversby, 1984b). There is currently no commercial fuel reprocessing plant in the United States and therefore no glass-based waste form of commercial high-level waste (CHLW). The NNWSI Project has used glasses based on the Pacific Northwest Laboratory (PNL) 76-68 formulation (Oversby, 1984b) in studies of the effect of compositional variation on performance. This glass was originally designed as a CHLW glass.

The composition of waste glasses will vary depending on the composition of the waste. The compositions of a SRL frit 165 based glass and a PNL 76-68 glass, both made with simulated (nonradioactive) waste, are shown in Table 7-19. Samples of these glasses were supplied by SRL and PNL, respectively, and both were used in NNWSI Project tests (Section 7.4.3.2.2). Notable differences between the glasses are the higher silica (SiO_2) content of the SRL glass; the higher uranium, transition metal, and rare earth content of the PNL glass; and the absence of Li_2O in the PNL glass. Table 7-20 lists the projected composition of West Valley glass (Eisenstatt, 1986); no glass based on this formulation is yet available to the NNWSI Project for testing. Notable in the West Valley glass is the thorium and phosphorus content.

The radionuclide inventories of the Savannah River and West Valley facilities are summarized in Tables 7-21 and 7-22 (Aines, 1986), with each waste calculated separately so that their individual contributions to the

Table 7-19. Composition of two glasses designed for high-level waste with simulated (nonradioactive) waste components

Oxides	SRL 165[a] (wt %)	UO_2-spiked PNL 76-68[b] (wt %)
SiO_2	54.90 ± 2.1	42.00
Na_2O	11.40	12.70
Fe_2O_3	10.60 ± 0.7	9.56
B_2O_3	7.20	9.00
ZnO	--[c]	5.10
La_2O_3	--	4.10
UO_2	--	3.98
TiO_2	--	3.08
MoO_3	--	1.97
Nd_2O_3	--	1.40
Al_2O_3	5.13 ± 0.18	0.59
Li_2O	5.04	--
MnO_2	2.72 ± 0.13	--
CaO	1.51 ± 0.32	2.37
NiO	0.84 ± 0.24	0.23
MgO	0.72 ± 0.04	--
ZrO_2	0.66 ± 0.07	1.89
CeO_2	0.42	0.94
K_2O	0.14	--
SrO	0.10	0.40
RuO_2	0.036	--
CsO_2	0.0028	1.10
P_2O_5	--	0.80
BaO	--	0.55
Cr_2O_3	--	0.47

[a]A borosilicate glass formulated by Savannah River Laboratory (SRL) for defense high-level waste. Values with errors were measured by Bazan and Rego (1985); others are nominal values supplied by SRL.

[b]A glass formulated by Pacific Northwest Laboratory (PNL) for commercial high-level waste. Source of data: McVay and Robinson (1984).

[c]-- = not analyzed.

Table 7-20. Actual projected composition of West Valley WV 205 glass[a,b]

Oxide	Oxide (wt %)	Oxide	Oxide (wt %)
SiO_2	44.88	BaO	0.05
Fe_2O_3	12.16	CaO	0.60
FeO	--[c]	Cs_2O	0.08
Al_2O_3	2.83	K_2O	3.57
B_2O_3	9.95	MgO	1.30
Na_2O	10.93	SrO	0.03
Li_2O	3.03	P_2O_5	2.51
UO_2	0.56	SO_3	0.22
CoO	0.00	H_2O	--
Cr_2O_3,	0.31	ThO_2	3.58
CuO	0.00	CeO_2	0.07
MnO_2	1.31	La_2O_3	0.03
MoO_3	0.02	Nd_2O_3	0.12
NiO	0.34	Pr_6O_{11}	0.03
RuO_2	0.08	SmO_3	0.03
TiO_2	0.98		
Y_2O_3	0.02	Total	99.91
ZnO	0.00		
ZrO_2	0.29		

[a]Source: Eisenstatt (1986).
[b]Includes some radionuclides, but low concentration elements are not included.
[c]-- = no data.

Table 7-21. Important radionuclides in Savannah River Plant waste[a] (page 1 of 2)

Isotope	Half life (yr)	(Assumed) 1990 inventory[b] (Ci)	1,000 yr postclosure inventory[c] (Ci)	NRC release rate limit per year (Ci)	Ratio of release rate to 1 in 100,000 of 1,000 yr inventory[d]	
Ni-59[e]	76,000	1.5E+04[f]	1.5E+04	1.52E-01	1.00	
Ni-63	100	1.9E+06	1.2E+03	1.23E-02	1.00	
Se-79	65,000	8.0E+02	7.9E+02	7.86E-03	1.00	
Rb-87	4.89E+10	5.3E-02	5.3E-02	2.47E-03	4,600	
Sr-90	29	3.4E+08	3.4E-03	2.47E-03	73,000	
Y-90	0.0073	3.4E+08	3.4E-03	2.47E-03	72,000	
Zr-93	1.5E+06	8.7E+03	8.7E+03	8.70E-02	1.00	
Nb-93m	13.6	8.7E+03	8.7E+03	8.70E-02	1.00	
Nb-94m	20,000	7.2E+00	7.0E+00	2.47E-03	35.4	
Tc-99	2.13E+05	1.5E+04	1.4E+04	1.45E-01	1.00	
Pd-107	6.5E+06	7.2E+01	7.2E+01	2.47E-03	3.4	
Cd-113	9.5E+15	6.8E-11	6.8E-11	2.47E-03	**[g]	
Sn-121m	55	2.3E+02	3.6E-04	2.47E-03	**	
Sn-126	100,000	1.2E+03	1.2E+03	1.15E-02	1.00	
Sb-126	0.034	1.2E+03	1.2E+03	1.15E-02	1.00	
Sb-126m	0.001	1.2E+03	1.2E+03	1.15E-02	1.00	
Cs-135	3.0E+06	6.5E+02	6.5E+02	6.52E-03	1.00	
Cs-137	30.17	2.8E+08	7.5E-03	2.47E-03	32,000	
Ba-137m	0.001	2.8E+08	7.5E-03	2.47E-03	32,000	
Sm-151	90	1.9E+06	5.4E+02	5.37E-03	1.00	
Pb-210	22.3	0.0E+00	8.2E+00	2.47E-03	0.63	
Ra-226	1600	0.0E+00	1.1E+01	2.47E-03	0.67	##[h]
Ra-228	5.76	0.0E+00	5.3E-06	2.47E-03	**	##
Ac-227	21.773	0.0E+00	2.0E-01	2.47E-03	98.4	##
Th-229	7,300	0.0E+00	1.3E-02	2.47E-03	3,000	##
Th-230	75,400	0.0E+00	6.8E+01	2.47E-03	0.43	##
Th-232	1.4E+10	0.0E+00	1.4E-05	2.47E-03	**	##
Pa-231	32,800	0.0E+00	2.6E-01	2.47E-03	106.00	##
U-232	70	1.1E+03	2.8E-02	2.47E-03	8,700	
U-233	1.59E+05	1.3E-01	1.3E-01	2.47E-03	1,800	
U-234	2.45E+05	3.6E+03	6.4E+03	6.35E-02	1.00	
U-235	7.04E+08	1.2E+01	1.2E+01	2.47E-03	20.79	
U-236	2.34E+07	2.6E+02	2.6E+02	2.58E-03	0.97	##
U-238	4.47E+09	6.6E+01	6.6E+01	2.47E-03	.75	
Np-237	2.14E+06	6.8E+01	1.3E+02	2.47E-03	.71	##
Pu-238	87.74	7.9E+06	1.7E+03	1.68E-02	.00	
Pu-239	24,110	7.4E+04	7.2E+04	7.20E-01	.00	
Pu-240	6,560	4.7E+04	4.2E+04	4.20E-01	.00	
Pu-241	14.35	8.9E+06	3.3E-02	2.47E-03	7,500	
Pu-242	3.76E+05	6.5E+01	6.5E+01	2.47E-03	3.80	
Am-241	432	8.3E+04	7.0E+04	7.02E-01	1.00	

Table 7-21. Important radionuclides in Savannah River Plant waste[a] (page 2 of 2)

Isotope	Half life (yr)	(Assumed) 1990 inventory[b] (Ci)	1,000 yr postclosure inventory[c] (Ci)	NRC release rate limit per year (Ci)	Ratio of release rate to 1 in 100,000 of 1,000 yr inventory[d]
Am-242m	141	1.1E+02	5.8E-01	2.47E-03	427.71
Am-243	7,370	4.4E+01	4.0E+01	2.47E-03	6.17
Cm-243	28.5	4.3E+01	2.1E-10	2.47E-03	**
Cm-244	18.11	1.3E+03	2.1E-15	2.47E-03	**
Cm-245	8,500	5.1E-02	4.7E-02	2.47E-03	52,62.36
Cm-246	4,780	4.1E-03	3.5E-03	2.47E-03	70,459.20
Totals		1.26E+09	2.47E+05		

[a]Source: Baxter (1983); Aines (1986).
[b]An average age for waste in 1990 assumed.
[c]Assumed repository closure in 2050.
[d]For radionuclides that can be released at 0.1 percent of total release rate limit (2.47×10^{-3} Ci/yr), the column summarizes the extent to which the radionuclides can be released faster than 1 part in 100,000.
[e]Radionuclides with a release that must be controlled at 1 part in 100,000 of their own 1,000-yr-postclosure inventory are underlined.
[f]E indicates exponential notation.
[g]** = Ratio exceeds 100,000. The entire inventory could be released in one year and meet the regulation.
[h]## = Grow-in affects this ratio; values shown here are from Table 7-23 later in this section.

Table 7-22. Important radionuclides in West Valley waste[a] (page 1 of 2)

Isotope	Half life (yr)	1987 inventory[b] (Ci)	1,000 yr postclosure inventory[c] (Ci)	NRC release rate limit per year (Ci)	Ratio of release rate to 1 in 100,000 of 1,000 yr inventory[d]	
C-14[e]	5,730	1.4E+02[f]	1.22E+02	1.22E-03	1.00	
Ni-59	76,000	8.2E+01	8.12E+01	8.12E-04	1.00	
Ni-63	100	6.4E+03	4.04E+00	2.13E-04	5.28	
Se-79	65,000	3.7E+01	3.66E+01	3.66E-04	1.00	
Sr-90	29	7.4E+06	6.87E-05	2.13E-04	**[g]	
Y-90	0.0073	7.4E+06	6.87E-05	2.13E-04	**	
Zr-93	1.5E+06	2.3E+02	2.30E+02	2.30E-03	1.00	
Nb-93m	13.6	2.3E+02	2.30E+02	2.30E-03	1.00	
Tc-99	2.13E+05	1.6E+03	1.59E+03	1.59E-02	1.00	
Pd-107	6.5E+06	1.2E+00	1.20E+00	2.13E-04	17.7	
Sn-126	1.0E+05	4.0E+01	3.97E+01	3.97E-04	1.00	
Sb-126m	0.001	4.0E+01	3.97E+01	3.97E-04	1.00	
Sb-126	0.034	5.6E+01	3.97E+01	3.97E-04	1.00	
I-129	1.6E+07	3.6E-01	3.60E-01	2.13E-04	59.2	
Cs-135	3.0E+06	1.6E+02	1.60E+02	1.60E-03	1.00	
Cs-137	30.17	7.8E+06	1.94E-04	2.13E-04	**	
Ba-137m	0.001	7.3E+06	1.94E-04	2.13E-04	**	
Sm-151	90	2.1E+05	5.85E+01	5.85E-04	1.00	
Pb-210	22.3	0.0E+00	1.10E-02	2.13E-04	40.8	##[h]
Ra-226	1,600	0.0E+00	1.27E-02	2.13E-04	43.9	##
Ra-228	5.76	0.0E+00	1.17E+00	2.13E-04	10.0	##
Ac-227	21.773	0.0E+00	2.00E-03	2.13E-04	956	##
Th-229	7,300	0.0E+00	9.55E-01	2.13E-04	3.5	##
Th-230	75,400	0.0E+00	6.65E-02	2.13E-04	34.3	##
Th-232	1.4E+10	1.6E+00	1.60E+00	2.13E-04	13.34	
Pa-231	32,800	0.0E+00	2.23E-03	2.13E-04	1,000	##
U-233	1.59E+05	1.0E+01	9.95E+00	2.13E-04	2.1	
U-234	2.45E+05	4.6E+00	7.16E+00	2.13E-04	2.98	##
U-235	7.04E+08	1.0E-01	1.02E-01	2.13E-04	200	
U-236	2.34E+07	3.0E-01	3.40E-01	2.13E-04	62.70	
U-238	4.47E+09	8.5E-01	8.50E-01	2.13E-04	25.10	
Np-237	2.14E+06	1.1E+01	2.33E+01	2.33E-04	0.89	##
Pu-238	87.74	7.2E+03	1.60E+00	2.13E-04	13.33	
Pu-239	24,110	1.7E+03	1.65E+03	1.65E-02	1.00	
Pu-240	6,560	1.3E+03	1.22E+03	1.22E-02	1.00	
Pu-241	14.35	8.7E+04	8.12E+00	2.13E-04	2.63	
Pu-242	3.76E+05	1.7E+00	1.70E+00	2.13E-04	12.52	
Am-241	432	7.2E+04	1.36E+04	1.36E-01	1.00	
Am-242m	141	2.1E+01	1.12E-01	2.13E-04	190.6	

Table 7-22. Important radionuclides in West Valley waste[a] (page 2 of 2)

Isotope	Half life (yr)	1987 inventory[b] (Ci)	1,000 yr postclosure inventory[c] (Ci)	NRC release rate limit per year (Ci)	Ratio of release rate to 1 in 100,000 of 1,000 yr inventory[d]
Am-243	7,370	2.4E+03	2.17E+03	2.17E-02	1.00
Cm-243	28.5	1.7E+02	9.63E-10	2.13E-04	**
Cm-244	18.11	2.2E+04	4.40E-14	2.13E-04	**
Cm-245	8,500	1.0E+01	9.17E+00	2.13E-04	2.33
Cm-246	4,780	4.3E+00	3.68E+00	2.13E-04	5.79
Totals		3.03E+07	2.13E+04		

[a] Source: Baxter (1983); Aines (1986).
[b] From actual analysis of tanks by Eisenstatt (1986).
[c] Assumed repository closure in 2050.
[d] For radionuclides that can be released at 0.1 percent of total release rate limit (2.13×10^{-4} Ci/yr), this column summarizes the extent to which the radionuclides can be released faster than 1 part in 100,000.
[e] Radionuclides with a release that must be controlled at 1 part in 100,000 of their own 1,000-yr postclosure inventory are underlined.
[f] E indicates exponential notation.
[g] ** = Ratio exceeds 100,000 for this isotope. The entire inventory could be released in one year and meet the regulation.
[h] ## = grow-in affects this ratio; values shown here are from Table 7-24 later in this section.

repository release limits can be calculated and the relative importance of the radionuclides can be assessed. Table 7-21 is based on the projected operation of the DWPF. No actual analyses or estimates of the radionuclide content of the waste tanks at Savannah River are currently available. Aines (1986) estimated the inventories by assuming that 7,000 canisters of the reference waste described in Baxter (1983) would be produced at the DWPF and that the waste from which that glass will be produced would be present, and all of the same age, in 1990. This is equivalent to giving the waste one average age. Better estimates of the radionuclide inventory at Savannah River cannot be made until analyses of the existing waste are available. Currently available analyses, such as those given by Manaktala (1982) only list the radionuclides with the highest activity at the present time. These are all short-lived, and most of the radionuclides of interest at long times are not given. Table 7-22 is based on actual samples of the West Valley tanks (Eisenstatt, 1986). The contents of the tanks may be inhomogeneous, causing these analyses not to represent precisely the bulk average; but, the inventories obtained by analysis are consistent with the operating history of the facility (Eisenstatt, 1986).

Tables 7-21 and 7-22 give the calculated inventories (Aines, 1986) at 1,000 yr postclosure, assuming repository closure in year 2050. Full decay and grow-in were considered for all radionuclides. The release rate limit from the engineered barrier system is calculated separately for each waste type from 1 part in 100,000 of the individual 1,000-yr inventory, or as 1 part in 100,000,000 of the total 1,000-yr inventory. Both values are calculated from the assumed closure time since the emplacement times required to calculate the total release rate limit are not yet known. All radionuclides with a release that must be controlled at 1 part in 100,000 of their own 1,000-yr-postclosure inventory are underlined in the tables. Most short-lived (less than 1 yr) daughter nuclides are not significant to release rate limits and are not shown. All radionuclides reported by the waste producers and whose inventory is great enough that it could not be released in a single year are included.

The final column in Tables 7-21 and 7-22 gives the ratio of the release rate limit to 1 part in 100,000 of the inventory of the individual nuclides at 1,000 yr postclosure. For the radionuclides that can be released at 0.1 percent of the total release rate limit (given in each table), the final column summarizes the extent to which these nuclides could be released at a rate faster than 1 part in 100,000 of the total waste. This can be used to eliminate many radionuclides from further consideration; any radionuclide with a value greater than 100,000 in this column could have its entire inventory released in 1 yr. Most of these radionuclides have been excluded from the table, but radionuclides with large initial inventories and those involved in actinide decay chains are included even if the ratio in the last column exceeds 100,000. These radionuclides have a double asterisk in the final column to indicate that their release does not need to be controlled.

Several radionuclides in Savannah River waste grow in to significantly higher levels at 10,000 yr such that release of 1 part in 100,000 of the 10,000 yr inventory (beginning at 1,000 yr) would slightly exceed the allowed release. The radionuclides that grow in significantly and their 10,000-yr total inventories are shown in Tables 7-23 and 7-24. Radionuclides with a

Table 7-23. Radionuclides that grow in significantly in Savannah River Plant-Defense Waste Processing Facility waste glass[a,b]

Isotope	Half-life (yr)	1,000-yr postclosure inventory (Ci)	NRC release rate limit per year (Ci)	10,000-yr inventory grow-in (Ci)	Ratio of release rate limit to 1 in 10^5 of 10,000-yr total inventory
Pb-210[c]	22.3	8.2E+00[d]	2.47E-03	4.6E+02	0.53
Ra-226	1600	1.1E+01	2.47E-03	4.3E+02	0.57
Ra-228	5.76	5.3E-06	2.47E-03	1.7E-04	**[e]
Ac-227	21.773	2.0E-01	2.47E-03	2.5E+00	98.40
Th-229	7,300	1.3E-02	2.47E-03	8.0E-02	3,064.18
Th-230	75,400	5.8E+01	2.47E-03	5.5E+02	0.45
Th-232	1.400E+10	1.4E-05	2.47E-03	1.3E-04	**
Pa-231	32,800	2.6E-01	2.47E-03	2.3E+00	106.11
U-236	2.34E+07	2.6E+02	2.58E-03	2.7E+02	0.97
Np-237	2.14E+06	1.3E+02	2.47E-03	1.4E+02	1.71
Total		2.47E+05			

[a] Source: Baxter, 1983; Aines, 1986.

[b] Assumed repository closure in year 2050, 0.1 percent of total release rate, 2.47E-03 Ci/year.

[c] Radionuclides whose release must be controlled at 1 part in 100,000 of their own 1,000-yr-postclosure inventory are underlined.

[d] E indicates exponential notation.

[e] ** = Ratio exceeds 100,000.

release that must be controlled at 1 part in 100,000 of their own 1,000-yr-postclosure inventory are underlined in the tables. The 10,000-yr postclosure inventory is calculated assuming no release over that period. The NRC release rate limit is then compared with the release of 1 part in 100,000 from the 10,000-yr inventory. Under this assumption, the ratio of allowed release to 1 part in 100,000 (the last column in Tables 7-21 to 7-24) can drop below 1.00. For example, at 1,000 yr, postclosure release of lead-210 at 1 part in 100,000 of its inventory would be below the release rate limit by a factor of 30; but if all lead-210 were retained in the waste until 10,000 yr and then released at 1 part in 100,000 per year of its own inventory, it would exceed the allowed release rate limit by a factor of 2. This is not a physically realistic case, since the grown-in radionuclide's inventory could not actually increase to the point where 1 part in 100,000 would exceed the permitted rate until close to 10,000 yr after closure. The average release over that period would be much lower.

Table 7-24. Radionuclides that grow-in significantly in West Valley waste glass[a,b]

Isotope	Half-life (yr)	1,000-yr postclosure inventory (Ci)	NRC rate release limit per year	10,000-yr inventory grow-in (Ci)	Ratio of release rate limit to 1 in 10^5 of 10,000-yr total inventory
Pb-210	22.3	1.10E-02[c]	2.13E-04	5.22E-01	40.88
Ra-226	1,600	1.27E-02	2.13E-04	4.86E-01	43.90
Ra-226	5.76	1.17E+00	2.13E-04	213E+00	10.02
Ac-227	21.773	2.00E-03	2.13E-04	2.23E-02	956.85
Th-229	7,300	9.55E-01	2.13E-04	6.00E+00	3.56
Th-230	75,400	6.65E-02	2.13E-04	6.22E-01	34.31
Pa-231	32,800	2.23E-03	2.13E-04	2.07E-02	1030.81
U-234	2.45E+05	7.16E+00	2.13E-04	6.98E+00	2.98
Np-237[d]	2.14E+0	2.33E+01	2.33E-04	2.61E+01	0.89
Total		2.13E+04			

[a]Source: Baxter (1983); Aines (1986).
[b]Assumed repository closure in year 2050, 0.1 percent of total release rate, 2.13E-04 Ci/year.
[c]E indicates exponential notation.
[d]Radionuclides whose release must be controlled at 1 part in 100,000 of their own 1,000-yr-postclosure inventory are underlined.

Tables 7-21 to 7-24 do not reflect the actual release rate limits from the entire repository because they consider the glass wastes individually, but they may be used to assess the importance of the various radionuclides. All radionuclides whose release from the engineered barrier system must be controlled at 1 part in 100,000 of their own inventory (underlined in the tables) are of equal importance. Relatively less information is required about the minor radionuclides whose release is controlled at 0.1 percent of the calculated release rate limit; palladium-107, for instance, can be released three times faster than major radionuclides from SRP waste. Matrix dissolution in glass waste forms (discussion follows) will result in an upper limit to the release rate of all radionuclides (the matrix dissolution rate), which must correspond to less than 1 part in 100,000 because of the major radionuclides; therefore, the allowed greater release of palladium-107 has the effect that the relative uncertainty in the release of palladium-107 can be three times greater than that of major radionuclides.

The release rate of glass components during storage or testing of a waste form may be expressed in a number of different ways. The currently

accepted standard method is to report normalized elemental leaching (NL_i) for component i (Mendel, 1981; MCC, 1983). This corresponds to the time-integrated bulk leaching that would result if the entire sample were to dissolve at the same rate as the component i and is defined as

$$NL_i = \frac{M_i}{(f_i)(SA)} \tag{7-1}$$

where

M_i = mass of element i released from the waste form (g)
f_i = mass fraction of element i in the original sample
SA = surface area of the sample (m^2).

Alternatively, the leach rate (LR_i) may be defined as

$$LR_i = \frac{NL_i}{t} \tag{7-2}$$

where

t = time in days.

These expressions for leaching are useful because they do not involve the volume of the leachate, as does the concentration of element i. As such, the NL or LR values from laboratory tests may be scaled up to repository values directly; a NL value for a glass sample is the same regardless of the sample size. If a glass were to dissolve completely congruently, all components would have the same NL value, which would be equal to the total weight loss per square meter. The release may be calculated from the amount found in solution but is more meaningful if it includes particulate and adsorbed material on the test vessel and components. Uncertainty in NL values is a function of analytical uncertainty in both the glass analysis and the leachate-test vessel analysis.

The condition of the surface of a glass undergoing leaching can substantially change the observed leach rate simply by affecting the surface area of glass available to react with the leachant. There has been much confusion in the glass-leaching literature about rates and mechanisms as a result of this effect. Much of the initially high leach rate in static tests (Figure 7-25) may be attributed to rough, highly reactive surfaces (Mendel, 1984). This makes short-term laboratory experiments difficult to reproduce (Kingston et al., 1984). At longer times, the initial surface of the glass dissolves away and the results no longer depend strongly on the initial condition but can be affected by cracks. In 165 frit glasses, cracks can be the dominant regions where leaching occurs at short times (Mendel, 1984). Normalized loss data cited here use the geometric area of the sample, which can be measured accurately. The reproducibility of leaching results is

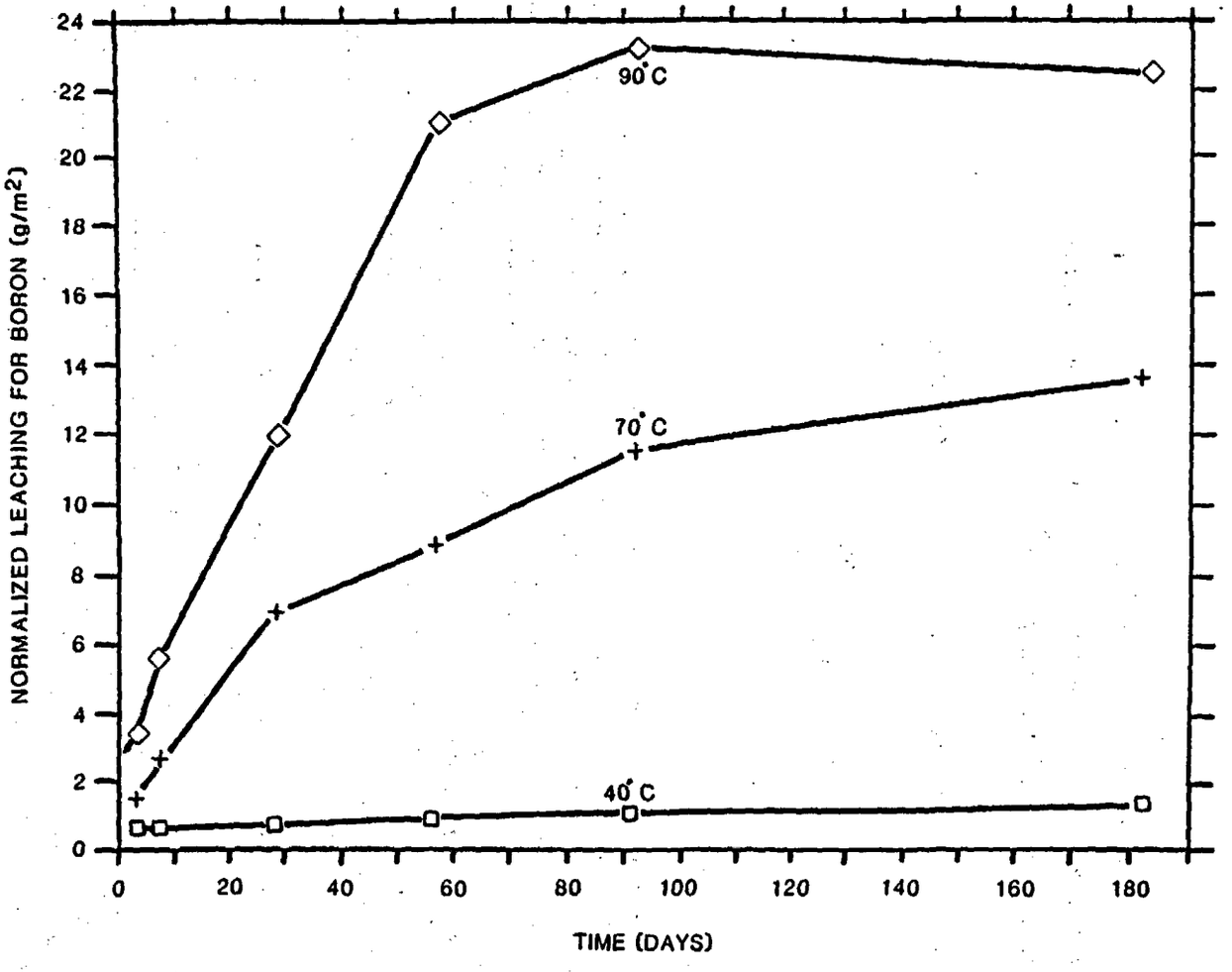

Figure 7-25. *Temperature effect on leaching of PNL 76-68 glass. MCC-1 static experiments in well J-13 water. Ratio of surface area to fluid volume (SA:V) = 10 m^{-1}. Replotted data from McVay and Robinson (1984).*

discussed by Kingston et al. (1984) and must be considered to be no better than 10 to 20 percent of the observed value due to the complexity of the tests and the compounding of uncertainties in calculating NL values.

The glass surfaces exposed after container and canister breach in a repository will be a combination of fractured and as-cast surfaces. Fracturing could increase the surface area by as much as a factor of 10 (Baxter, 1983), directly resulting in up to a factor of 25 increase in release if water comes in contact with fractured areas. NNWSI Project testing now includes the use of samples with as-cast surfaces and glass-304L SS surfaces formed by casting glass into stainless steel tubes. The extent of fracturing and other surface irregularities in DWPF full-scale canisters has not yet been determined. Tests reported by Bickford and Pellarin (1986) on sections cut from full-scale DWPF-type canisters indicate that the leach rate increased by up to a factor of two over the rate expected from uncracked glass. This experimental result is much less than the factor of 25 increase that might be predicted to result from surface cracking.

The second reporting method of interest is the concentration of leached elements, normally in milligrams per liter of water or milligrams per kilogram of water (ppm). This method is most useful when an element reaches a saturated concentration in the water; however, it does not normally take into account colloidal material although this can be differentiated by filtration. Solution results reported as concentrations have the advantage of not containing the compounded uncertainties inherent in NL calculations, which combine a number of individual measurements.

Current regulations regarding the release of radionuclides from the repository engineered barrier system are written in terms of individual nuclides. Therefore in NNWSI Project testing, an important goal is to determine release rates for the elements in Tables 7-21 through 7-24, which will be the major sources of radioactivity in leachate from 300- to 1,000-yr-old waste. Because of the large number of important radionuclides and their chemical diversity, it is desirable to know an upper bound on the release of any glass component. Extensive research on borosilicate glass leaching mechanisms has shown that such an approach is possible (Mendel, 1984).

The objective of the 3-yr defense high-level waste leaching mechanisms program was "to determine the dominant leaching mechanisms for defense waste glass and to evaluate the effects of some major environmental parameters upon the leaching mechanisms" (Mendel, 1984). The mechanisms involved are discussed below and are still subject to discussion in some aspects. However, it was shown that after an initial brief period of several months (depending on the leaching conditions) no element is released from borosilicate glasses at a rate in excess of the components of the frit that do not precipitate from solution under the test conditions. For PNL 76-68, molybdenum, sodium, and boron are such elements; for SRL 165 frit glass, boron, sodium, and lithium are such elements (Barkatt et al., 1983; Wallace and Wicks, 1983; Mendel, 1984). Their solubilities in water are very high under all reasonable test conditions.

Using this result, a very conservative statement can be formulated concerning the maximum leaching or leaching rate of any radionuclide: the NL_i or LR_i for any element will not exceed that of the most soluble element in the glass, commonly boron (or lithium in the case of SRL glass). Because of its conservatism, this statement should be used only as a guideline, and the NNWSI Project is therefore directly measuring individual radionuclide release values. In NNWSI Project testing, only one instance has arisen of a radionuclide having a larger long-term normalized loss than boron; in leach testing of the PNL 76-68-based glass ATM-8 inside a tuff reaction vessel, Bazan and Rego (1986) found technetium in solution at concentrations indicating that it was released at a normalized rate approximately 10 to 15 percent faster than boron and molybdenum. This may be caused by sorption of boron and molybdenum onto the tuff vessel or may be the result of an inaccurate analysis of the initial composition of the glass. If the Materials Characterization Center (MCC) analysis of the initial composition of ATM-8 is used instead of Bazan and Rego (1986), then boron, molybdenum, and technetium were released at the same rate within error.

To predict confidently the long-term behavior of waste glasses, it is essential to understand the mechanisms of glass leaching. A summary of results of current research and of theory on glass leaching has been prepared by the defense high-level leaching mechanisms program (Mendel, 1984). They determined that the important aspects of the leaching mechanism are the removal of highly soluble elements (e.g., sodium, boron, and lithium) from the glass surface, the buildup of layers of insoluble components (e.g., iron and zinc), and the gradual reprecipitation of slightly soluble components (e.g., calcium and silicon). The net result of these processes can be considered to be that the glass dissolves congruently (all elements simultaneously) but with many elements reprecipitating onto the glass or surrounding material (Strachan et al., 1984; Apted and Adiga, 1985; Barkatt et al., 1985; Grambow, 1985). This makes possible the use of a highly soluble element as an indicator of the maximum possible release.

The factors controlling the leach rate are the rate of removal of soluble species and the buildup of layers limiting that removal. These processes are dependent upon leachant chemistry; temperature; and, in particular, pH. Because the initial removal of soluble species is essentially a congruent process, restricting the solubility of the major glass component, silica, strongly limits the leach rate. The formation of surface layers may also restrict the leach rate. However, depending upon surface layers to protect glass from releasing radionuclides is a questionable practice because the layers may slough off, particularly after drying (Mendel, 1984). The most successful approach to modeling the dissolution rate of glass has been to apply transition state kinetic theory, using the dissolution of silica as the rate-limiting step. This method is described by Grambow (1984), and applications are given in numerous papers (Strachan et al., 1984, 1985; Freude et al., 1985; Grambow, 1985; Grambow et al., 1985). Although the rate of dissolution depends directly only on silica activity in solution in this modeling approach, many other factors affect that activity. The work to date indicates that many of the phenomena observed in glass leaching may be explained by this theory. The more important parameters of those phenomena are described in the following paragraphs.

Leach rates depend strongly on temperature. Results from NNWSI Project testing of PNL 76-68 glass leached at 40, 70, and 90°C in well J-13 water are shown in Figure 7-25 (McVay and Robinson, 1984). These data yield an activation energy of 16 kcal/mole, which is typical for borosilicate waste glasses (Bradley et al., 1983; McVay and Robinson, 1984; Mendel, 1984). This implies that there is an expected rate difference of about two orders of magnitude between glass leaching occurring at temperatures of 40 and 95°C, the range in which liquid water might be expected to contact the waste form under Yucca Mountain conditions (Section 7.4.1.2). Since leach rates are inevitably higher at higher temperatures, NNWSI Project tests are routinely performed at 90°C. Some future testing will also be conducted at 60°C (Section 8.3.5.10).

In glass leaching, the pH of the leaching solution is the most important parameter over which some control may be exercised in repository and waste form design. When the pH is controlled to within the range 5 to 9, leaching is at a minimum. Outside these limits, the leach rate increases dramatically. Figure 7-26 (after Plodinec et al., 1982) shows the relationship between pH and leaching in a previous SRL glass formulation, frit 131. This effect was first predicted by Paul (1977) and has since been found to occur widely in many glasses including nuclear waste glasses (Mendel, 1981; 1984).

The pH effect on leaching is subject to adjustment both by the glass and the leachant. In water in Yucca Mountain, the pH is initially buffered by the presence of dissolved CO_2 and silica. When reaction with glass occurs, the dissolved glass components will also buffer the pH of the water. The balance between acidic oxides (SiO_2 and B_2O_3) and alkaline oxides in the glass is a critical factor in determining the ultimate pH of a solution while it reacts with glass (Mendel, 1984). Proper glass formulation yields slightly more acidic oxides than basic oxides (by mole fraction), and the pH of the leachate remains near neutral and out of the rapid dissolution regime. Both SRL-165 frit-based glass and PNL 76-68 glass remain in the near neutral region during leaching. As was found by the defense high-level waste leaching mechanisms program (Mendel, 1984), however, a small increase in the amount of alkalis and a corresponding decrease in the silica content of a waste glass can lead to a large pH excursion (toward pH >10) and a concom-itant large increase in the leach rate. The buffering capacity of the ground water at Yucca Mountain would not be able to control a large excursion; glass composition must be carefully controlled to keep the pH from rising into the rapid dissolution range.

Self-irradiation of waste glass and irradiation of leaching fluids may affect release rates. However, considerable research on radiation effects on glass leaching has revealed few demonstrable effects, the most notable being acidification of heterogeneous air-water systems by intense gamma-ray fluxes. Alpha-decay damage within waste glasses produces little change in leaching behavior even at doses well in excess of that anticipated in waste glasses; alpha-radiolysis of water and dissolved components may affect leach rates by a factor of two but would be dependent upon repository interactions (Mendel, 1984; Burns et al., 1982). This type of interaction is being tested by the NNWSI Project by leaching radioactive glasses.

The radiolytic production of nitric acid from air in the presence of water can cause substantial effects (Burns et al., 1982). The effect on

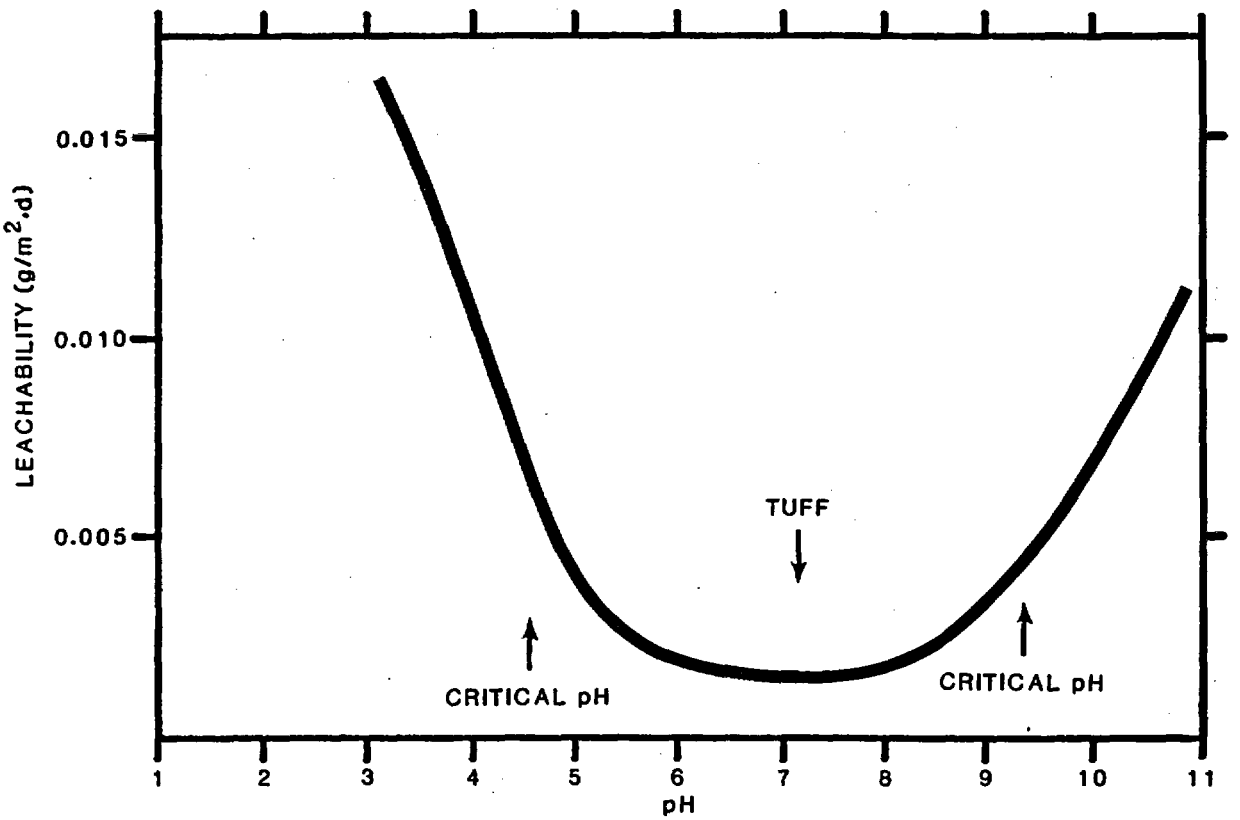

Figure 7-26. Leachability of an SRL-131 frit glass as a function of pH. Five-day static tests. ratio of surface area to fluid volume (SA/V) = 1000 m^{-1}. 23°C. Modified from Plodinec et al. (1982).

glass leaching in a repository is unknown because of uncertainties in water contact mechanisms. The dose rate from a DWPF canister would initially be approximately 2.5×10^3 rem/h, but would decrease by more than three orders of magnitude at 300 to 1,000 yr (Baxter, 1983). In the postcontainment period, gamma-radiolysis would not be nearly as important as it would be in the event of a premature container and canister breach; results of NNWSI Project testing in the presence of radiation fields are discussed in Section 7.4.3.2.2.

The discussion has so far been limited to factors that are independent of the amount of water or its contact mechanism with the waste form. The effects of water volume in laboratory leaching experiments are primarily on the rate of leaching. In the presence of a large amount of water, a given glass sample will lose more material than it does in a small volume of water in which the solution becomes saturated. A scaling factor that correlates this behavior over a wide range of circumstances is the ratio of glass surface area (SA) to solution volume (V), SA:V. (References to SA:V in this section are given in units of m^{-1}.) Leach rates are lowest at high SA:V where surface layers form due to precipitation of silicates and transition metal compounds. They are low primarily because the dissolution of silica is inhibited by the rapid increase of silica in a relatively small solution in contact with a large surface area of glass. The release of soluble components (boron, lithium, and radionuclides that are soluble) is inhibited by the depth of undissolved glass matrix through which they would have to diffuse to reach the solution. These elements may initially diffuse out of the glass, giving a release rate higher than that of the overall glass breakdown rate; however, diffusional release eventually slows to less than that of the overall breakdown rate, and all elements are released congruently (although many immediately reprecipitate).

Over a wide range of SA:V ratios and times (t), it has been found that a given NL_i value for a glass is reached at a constant value of (SA:V)(t) (Pederson et al., 1983; Mendel, 1984). This behavior is apparently due largely to the onset of solution saturation, but in some instances it is found in solutions that are apparently saturated with respect to some glass components. The leaching of SRL-165 glass as a function of (SA:V)(t) is shown in Figure 7-27, from Bazan and Rego (1985). Using (SA:V)(t) scaling it is possible to predict the results of long-term experiments by using the results of short-term experiments performed at higher ratios; for instance, 1 yr of leaching at 14 m^{-1} should give the same result as 51 d at 100 m^{-1}. However, the extension of this relationship into the SA:V expected at Yucca Mountain (up to 1,000 m^{-1}) must be demonstrated. This relationship is largely useful to compare leaching data obtained under different conditions.

When materials other than glass and water are added to a leaching system, they participate both by dissolving to some extent and by providing reactive surfaces. Materials that add silica to the water have been shown to be effective in reducing glass dissolution rates by slowing the removal of silica from the glass. However, even in saturated silica solutions, glass continues to dissolve and reprecipitate into more stable compounds (Grambow, 1984). Any material that aids in the formation of these compounds can accelerate leaching. NNWSI Project glass testing (described in Section 7.4.3.2.2) places a strong emphasis on materials interactions. Tests are routinely done

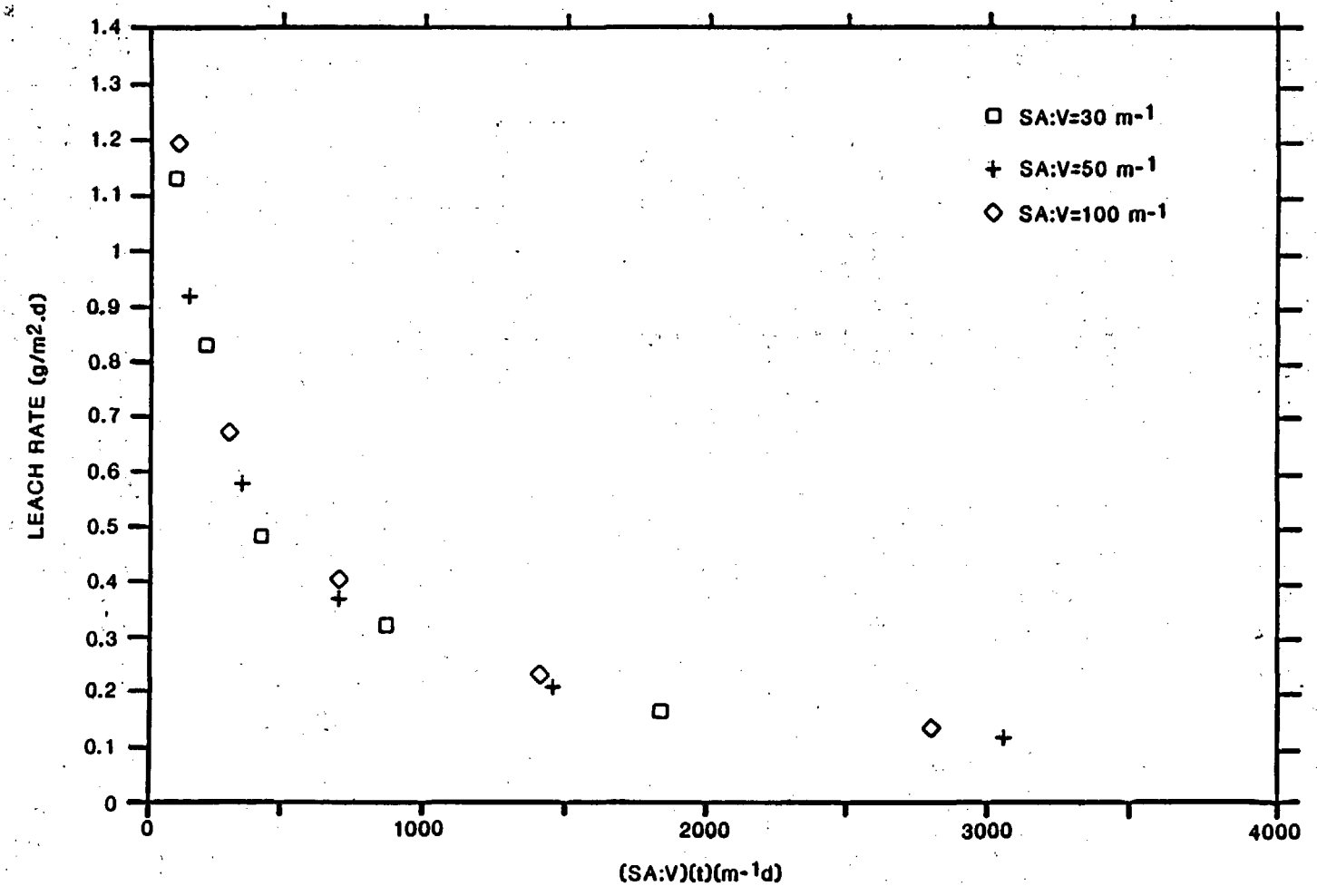

Figure 7-27. Effectiveness of surface area to volume ratios and times (SA:V (t)) scaling demonstrated by leaching of frit 165 glass in deionized water. Modified MCC-1 tests at 90°C from Bazan and Rego (1985). Tests are identical except for SA:V ratio.

using well J-13 water (Section 7.4.1.3). In this water, leach rates are considerably reduced from the rates observed using deionized water (Figure 7-28) a result that is typical for silicate rock ground water (Mendel, 1984). Figure 7-29 shows the effect of adding tuff rock to a static leaching experiment. The addition of a monolith (wafer) has a small effect, but adding rock powder dramatically reduces leaching. This is attributed to the more rapid addition of silica to the water by the rock powder relative to the monolith, which is less reactive. The reduction in leach rate brought about by tuff rock and tuff water is not fortuitous. The rock is somewhat similar in composition to the glass (both are composed largely of silicon, aluminum, alkalis, and alkaline earth oxides), but the rock has a higher silica content and it saturates the solution with silica, slowing glass dissolution. In a repository at Yucca Mountain, vadose water that has passed through heated rock in route to the waste container is expected to contain high levels of dissolved silica (Section 7.4.1.3).

Most other possible repository materials are not close to the waste glass composition, and interactions with them cause increased leach rates. Examples include mild steel and bentonite clay, which were investigated in the defense high-level leaching mechanisms program. The experimenters found that 1020 carbon steel caused the precipitation of iron silicate compounds with a resulting doubling of leaching (Mendel, 1984). Grambow et al. (1987) showed that adsorption of silica on iron or carbon steel surfaces can be responsible for increased leach rates. NNWSI Project testing has found similar results for 1020 steel in the presence of well J-13 water and tuff rock (Figure 7-30). Mendel (1984) found that bentonite increased leach rates, possibly because of adsorption of leached ions or reaction with silica. This effect was later attributed to higher pH values in the presence of the clay, which has a significant cation-exchange potential resulting in replacement of sodium in the clay for hydrogen from solution (Grambow et al., 1985). Grambow et al. (1985) predict that the long-term rate of dissolution in the presence of bentonite will be the same as in water alone, because of the onset of silica saturation in solution. This predicted effect would depend on the water staying in contact with glass and bentonite simultaneously for a long period of time (more than 1 yr).

The 304L SS is being extensively investigated but appears to have substantially no effect on static leach rates (Figure 7-30) (McVay and Robinson, 1984; Bazan and Rego, 1985, 1986). This is in accord with its low reactivity in well J-13 water (Section 7.4.2). The effect on leach rates caused by contact with heat-affected 304L SS is being investigated (Section 8.3.5.10).

Other repository materials that affect the pH of ground water are also expected to affect leach rates. An adverse effect on leach rate would be caused by material that water could contact before contacting waste glass and that causes the pH of the water to rise. Concrete containing unreacted portlandite ($Ca(OH)_2$) in the cement could raise water pH into the rapid dissolution regime. For instance, Atkinson et al. (1985) showed that water in continuous contact with concrete and clay would maintain a pH above 10.5, which is in the rapid dissolution regime, until the concrete is completely decomposed by ground water. In their example, this would take 1 million years. Nitric acid production by gamma radiolysis of air (Section 7.4.3.2.2) could result in acidic ground water during the containment period, but

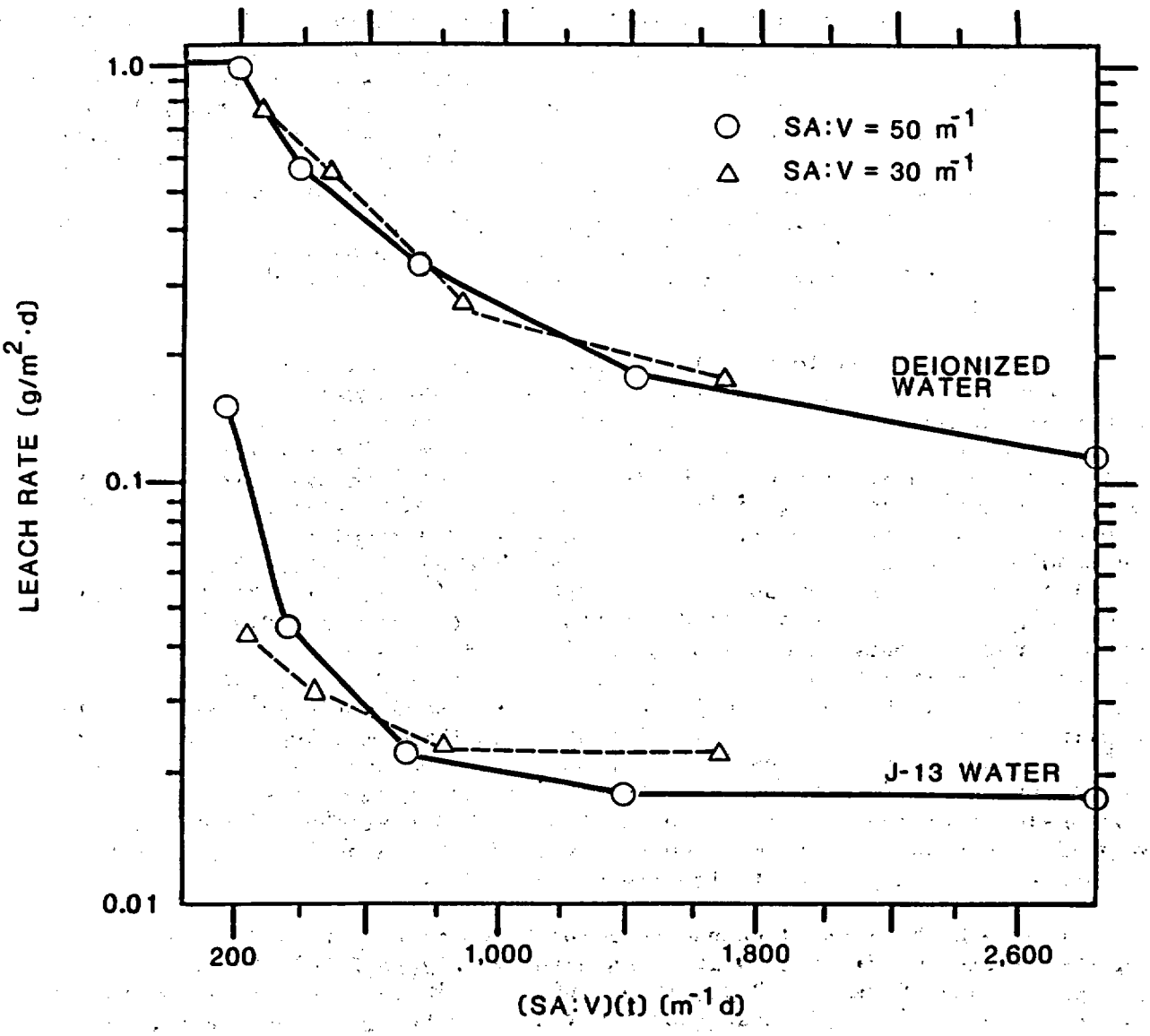

Figure 7-28. Effect of water from well J-13 on leach rates of lithium from frit 165 glass. Modified from Bazan and Rego (1985).

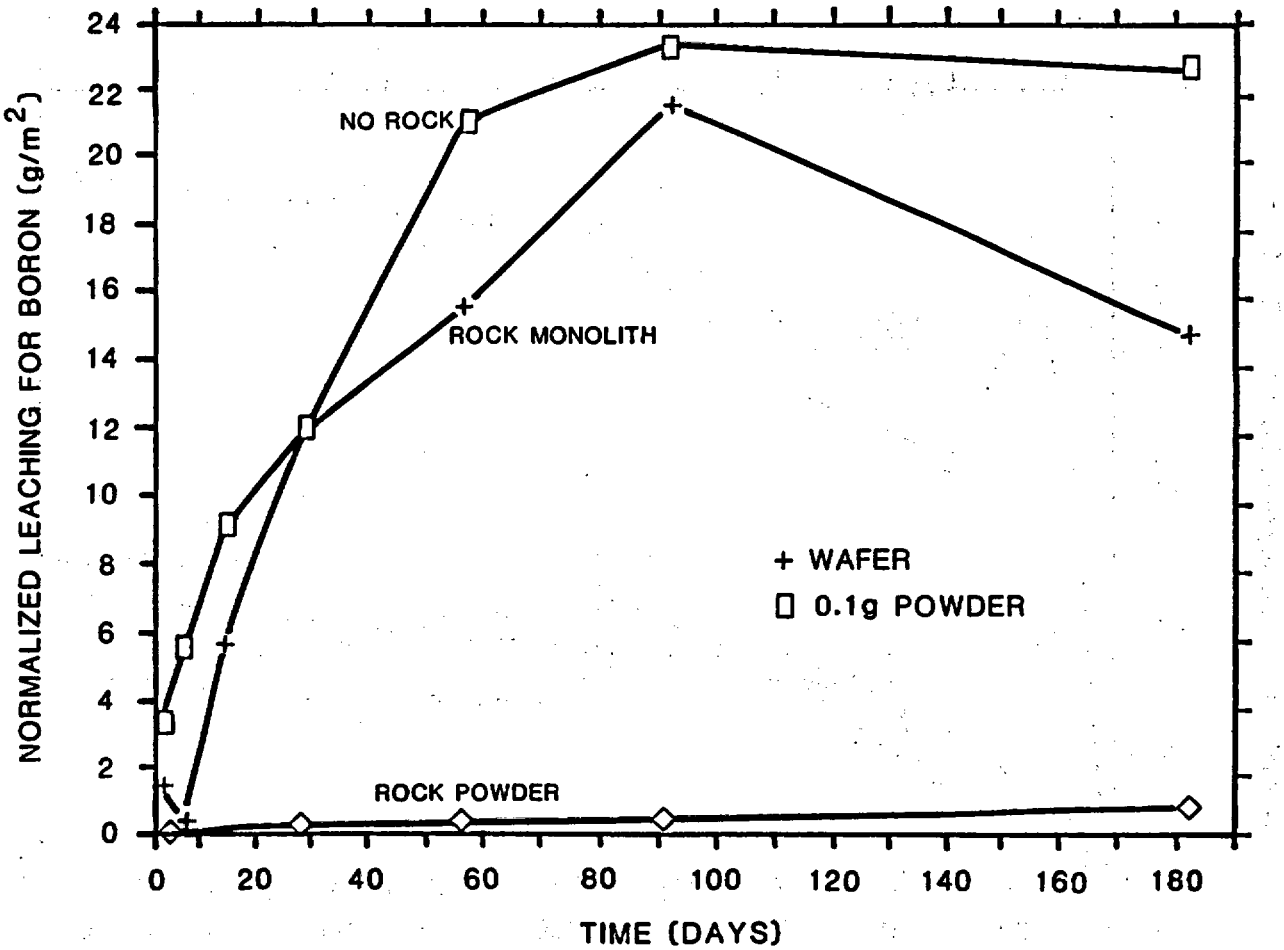

Figure 7-29. Effect of tuff rock being present in the leaching vessel on the leach rate of PNL 76-68 glass. 90°C, ratio of surface area of glass to volume (SA:V) = 10 m^{-1}. Rock monolith has same surface area as glass. Modified from McVay and Robinson (1984).

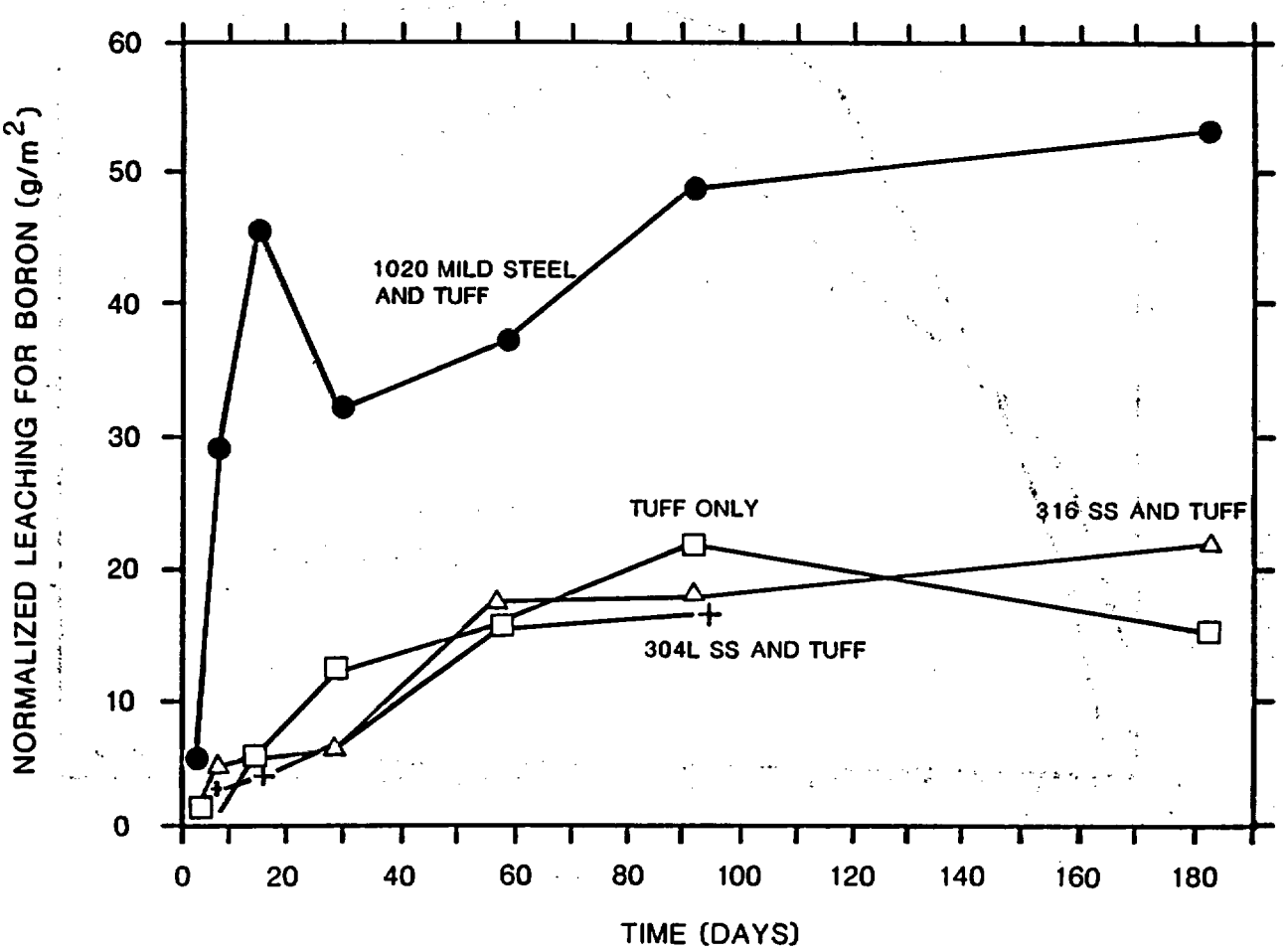

Figure 7-30. Effect of repository components on leaching of PNL 76-68 glass. All experiments included tuff monolith with same surface area as glass. Metals had same surface area (SA). Ratio of surface area to volume (SA:V) = 10 m^{-1}. The data for 304L stainless steel for 180 days were lost. Modified from McVay and Robinson (1984).

radiation fluxes will be sufficiently reduced in the isolation period that this effect is not expected to be significant (Section 7.4.3.2.2).

The results of studies on the effect of possible backfill and packing materials like bentonite have shown that increasing the complexity of the system may slow the movement of some radionuclides but that one likely result is also increased radionuclide leaching from the glass. Only materials that increase the local silica concentration or buffer the pH near the neutral point seem to effectively reduce total glass dissolution rates.

7.4.3.2.2 Results of recent NNWSI Project glass waste form testing

Research up to this point has involved parametric tests evaluating the effects of repository materials (glass, tuff, equilibrated water, and canister metals) on leach rates and developing tests designed to evaluate the effects of intermittent water contact in a water-unsaturated environment. In this section, materials used in NNWSI Project tests and their similarity to anticipated repository materials are discussed. This discussion is followed by descriptions and results of these tests.

Although different borosilicate waste glasses behave in generally similar fashions, small changes in composition can cause changes of several orders of magnitude in release rates under static conditions (Mendel, 1984). The behavior of radionuclides can be inferred from simulated waste glasses but must ultimately be measured in tests using glass containing radionuclides. The variability in composition of sludge waste streams means that waste glasses will have some variability in composition. These factors make the glass compositions used for testing important. The NNWSI Project is currently using actual sludge glasses, simulated glasses, and glasses doped with specific elements of interest in its testing program.

Table 7-25 gives the compositions of four SRL glasses used by the NNWSI Project and SRL. It also contains the composition of the reference DWPF glass used by the defense high-level waste leaching mechanisms program. The four simulated glasses in the table are very similar in composition. The actual-waste glass has a slightly lower iron content and higher alumina content. This type of variation must be expected (and its effect evaluated) due to the inhomogeneity of SRP sludge. The NNWSI Project is also using selectively doped PNL 76-68 glass in parametric tests (Table 7-19).

An important aspect of evaluating release rates is the homogeneity and quality of the waste glass. Phase separation of radionuclides, such as the technetium globules made by Bradley et al. (1979), results in erratic and nonreproducible results. The only separate phases currently expected in DWPF waste glasses are spinel, which precipitates at the canister wall, and spinel and acmite, which can precipitate near the canister centerline (Bickford and Jantzen, 1984). Spinel formation appears to have little effect on leach rates, but acmite formation may increase leach rates. No assessment of the devitrification characteristics of West Valley glass is yet available, but similar products may be expected due to the similar chemistries of the glasses. Possible precipitation of thorium-containing phases will be examined in West Valley glass when it is available (Section 8.3.5.10). Glasses

Table 7-25. Frit 165 based glasses

Oxides	Radioactive sludge tank 42 slurry fed melter (Bibler, 1986)		Simulated slurry fed melter (Bibler et al., 1984)		Simulated slurry fed melter (Basan and Rego, 1985)		Simulated "Black Frit" (Bates and Gerding, 1985)		Simulated defense waste reference glass (Mendel, 1984)	
	Wt%[a]	Mole%[b]	Wt%	Mole%	Wt%	Mole%	Wt%	Mole%	Wt%	Mole%
SiO_2	55.40	42.17	56.20	43.44	54.90	42.44	54.10	43.22	51.60	43.33
Na_2O	11.00	16.35	10.90	16.34	11.40	17.09	10.30	15.96	7.70	12.54
Fe_2O_3	6.00	3.46	12.30	7.16	10.60	6.17	12.30	7.40	10.10	6.38
B_2O_3	8.40	11.12	7.00	9.34	7.20	9.60	6.80	9.38	7.30	10.58
Al_2O_3	9.80	8.86	4.90	4.47	5.13	4.67	4.10	3.86	5.50	5.44
Li_2O	4.90	15.11	4.70	14.61	5.04	15.67	4.70	15.10	4.10	13.85
UO_2							1.12	0.20	2.70	0.50
MnO_2	1.90	1.01	2.80	1.50	2.72	1.45	3.56	1.97	3.40	1.97
NiO	0.90	0.56	0.96	0.60	0.84	0.52	0.90	0.58	2.10	1.42
CaO	0.24	0.20	2.00	1.66	1.51	1.25	1.50	1.28	1.90	1.71
Cs_2O					.00	.00	0.11	0.04	0.40	0.14
K_2O					0.14	0.14			0.04	0.04
MgO	1.00	1.14	0.78	0.90	0.72	0.83	0.80	0.95	0.80	1.00
SrO					0.10	0.04	0.15	0.07	0.50	0.24
CeO_2					0.42	0.11			0.04	0.01
Other[c]									1.67	0.85
Total	99.2	100.0	102.54	100.00	100.72	100.00	100.44	100.00	99.85	100.00
Sum of Si and B		53.29		52.78		52.04		52.60		53.90

[a] From published analyses or nominal values from Savannah River.
[b] Mole % cation in glass (total constrained to be 100%).
[c] Defense waste reference glass also contains Cr_2O_3 0.3%, ZrO_2 1.0%, P_2O_5 0.2%, and traces of Cu, Co, Ti, Zn, and Nd.

produced in the full-size melters at DWPF and West Valley are not yet available to the NNWSI Project for testing. The quality and homogeneity of samples will have to be evaluated before placing full confidence in results from laboratory-produced glasses. Preliminary results of laboratory-scale leach testing of glasses produced by a full-scale melter and poured into DWPF reference canisters have recently become available (Savannah River Plant and Laboratory, 1984). No difference in leach rate was observed between laboratory and full-scale 165-frit glasses. When full-sized slices from the canisters were leach-tested, release increased by less than a factor of three due to cracking (Bickford and Pellarin, 1986).

Materials that are likely to be present in a repository at Yucca Mountain are used in NNWSI Project testing. The reference container and pour canister material, 304L SS, is currently being used in parametric testing and for test-vessel construction. Well J-13 water is used for testing. When used for elevated temperature testing (e.g., 90°C), well J-13 water should be re-equilibrated with tuff at that temperature. Tuff representative of that from the potential repository horizon is currently available from surface samples, conventional drill cores, and air-drilled core samples (Section 7.4.1). The core samples are expected to be representative of the rock that will be found in the repository and are in limited supply due to the expense of drilling. Surface samples suffer from contamination by caliche and soluble salt deposits (Knauss, 1984). This material is common in the arid regions of the southwestern United States (Conca, 1985) and is caused by deposition of airborne salts and surface evaporation of moisture. It is confined to the exposed area of the rock and is frequently only detectable by analysis of water that has equilibrated with a tuff sample; use of samples containing these soluble salt deposits causes elevated anion, calcium, sodium, potassium, and boron concentrations in the water (Oversby, 1984a). Boron in these surface deposits is particularly troublesome because it obscures boron release from the glass when testing is done in the presence of tuff rock. The deposits may be substantially removed from tuff samples by pre-equilibration with well J-13 water. However, the presence of this material has complicated the analysis of some of the initial NNWSI Project tests.

The NNWSI Project has completed parametric tests examining the effects of repository materials on the leaching of SRL 165 frit-simulated glass (Bazan and Rego, 1985), PNL 76-68 U-doped glass (McVay and Robinson, 1984), and PNL 76-68 actinide-doped glass (Bazan and Rego, 1986). Figure 7-31 shows nonmalized leaching (NL) values for lithium at an SA:V of 30 m^{-1} from the 165-frit study. This study showed that 304L stainless steel has no substantial effect on leaching and that the presence of tuff slightly decreases leaching rates. These results were also found in the PNL 76-68 glass study (McVay and Robinson, 1984). However, the presence of ductile iron is known to increase leach rates in static tests (Mendel, 1984). The NNWSI Project is therefore currently examining the effects of heat-affected 304L SS, which may also be more reactive. Heat-affected 304L steel will be present in the glass pour canisters. Preliminary results (Bates et al., 1986b) indicate increased glass reaction in the presence of weld-affected steel, as evidenced by the formation of nickel and chrome silicates. This effect is being examined (Section 8.3.5.10).

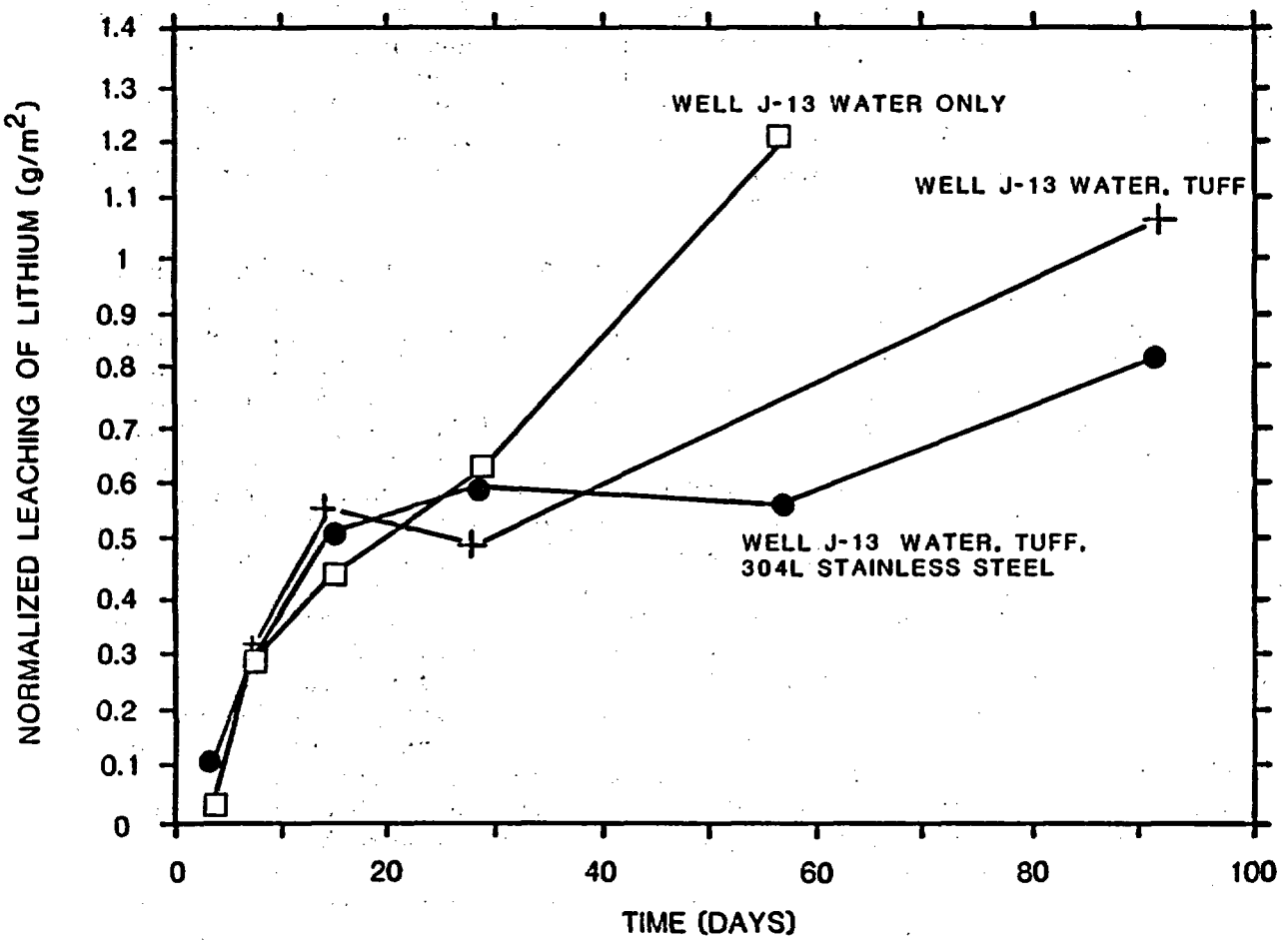

Figure 7-31. Effect of repository components on the leaching of 165-frit glass. MCC-1 tests at 30 m^{-1}, 90°C, 1 g of tuff per 20 ml well J-13 water. Note that these experiments only extend to 90 days. Data from Bazan and Rego (1985) were corrected for leachate loss.

In parametric studies, the analysis of glass release is complicated by the presence of elements occurring in both the tuff and the glass. Elements such as silicon cannot be used to measure glass release when tuff is present. Boron and, for 165 frit glass, boron and lithium can give results with minimum interference. In many instances with 165-frit glass, the glass releases so little of an element that analysis is difficult even without interferences.

The effects of gamma radiation on leaching rates of SRL 165 and PNL 76-68 glass have been investigated in a series of experiments (Bates and Oversby, 1984; Abrajano et al., 1986; Bates et al., 1986a,b; Ebert et al., 1986). Both nonradioactive and actinide-doped glasses have been leached in cobalt-60 gamma fields with dose rates of 2×10^5, 1×10^4, 1×10^3, and 0 rads/h. The primary effect of this radiation was expected to be the production of nitric acid from air in the test vessels (Burns et al., 1982). This was observed. The pH for the 165 frit glass leaching solution (well J-13 water) was 6.5 after 56 days in the 2×10^5 rads/h field (Figure 7-32). Bazan and Rego (1985) obtained a pH of 9.5 to 9.7 under similar conditions but with no irradiation. Blanks (no glass present) run by Bates et al. (1986b) yielded results of 11 ppm nitrate production, which is in excellent agreement with the predicted value of 10 ppm obtained by using the equation from Burns et al. (1982).

NL values from the gamma irradiation work at 2×10^5 rads/h are shown in Figure 7-33 for SRL 165 frit glass. Notable are the NL values for plutonium, uranium, and americium; all are below those of the most leachable elements (lithium and sodium). For PNL glass, the pH first increased, then decreased after 14 d. This was reflected in the actinide data for that glass, which show a decrease in actinide concentration in solution at the end of the 56-day period (Bates and Oversby, 1984).

Results for SRL glass at 1×10^4 rads/h (Abrajano et al., 1986) are similar to those at 2×10^5 rads/h, (Bates et al., 1986a) but show slightly increased releases at corresponding times (e.g., normalized loss of lithium at 56 d was 3.4 g/m^2 compared with 2.3 g/m^2 in Figure 7-33). The solution pH values with glass present were also slightly higher, and less nitrogen was fixed by the radiation. The increased glass reaction was interpreted as due to the increased pH, with glass dissolution (which drives the pH upward) now balancing more of the acid production by radiolysis. However, the differences between reaction rates in the irradiated samples are small compared with the difference between them and the nonirradiated samples, leading to the interpretation that glass reaction rate is fairly unresponsive to irradiation flux above 1×10^3 rads/h (Ebert et al., 1986). This is an example of the buffering effects of the solution products of glass dissolution and radiolysis; the glass reaction remains approximately constant as long as buffering species from both processes are present and is not sensitive to the quantity of the buffers (i.e., radiation flux). Experiments are under way (Section 8.3.5.10) to discover how much radiation is required to maintain the radiolysis buffer.

Actinide releases in the gamma-irradiation experiments are very sensitive to solution pH. In the experiments at 1×10^4 rads/h run for 182 d in well J-13 water only (Abrajano et al., 1986), the pH rose slightly (from 6.8 to 6.9) from the 91-day value after a continuous decrease up to that point

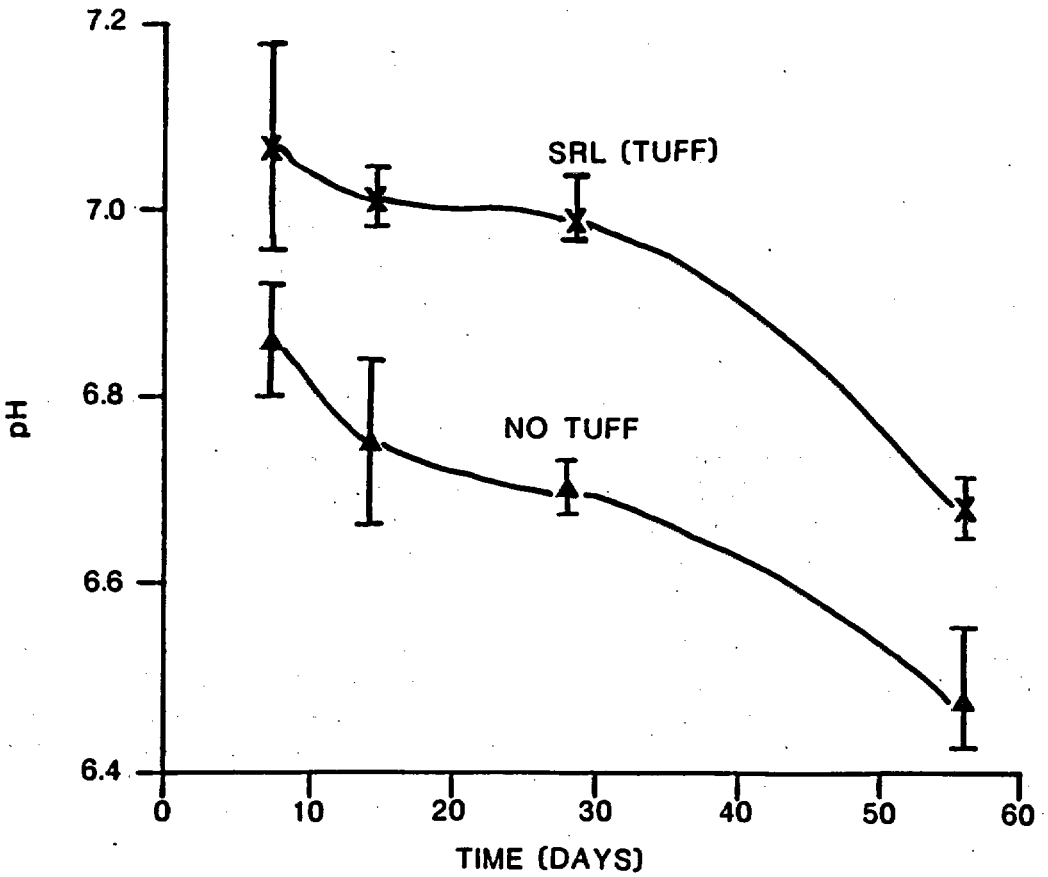

Figure 7-32. The solution pH from leaching experiments with a uranium-doped defense waste processing facility glass, from Savannah River Laboratory (SRL) in the presence of 2×10^5 rads/h gamma irradiation. Modified from Bates et al. (1986a).

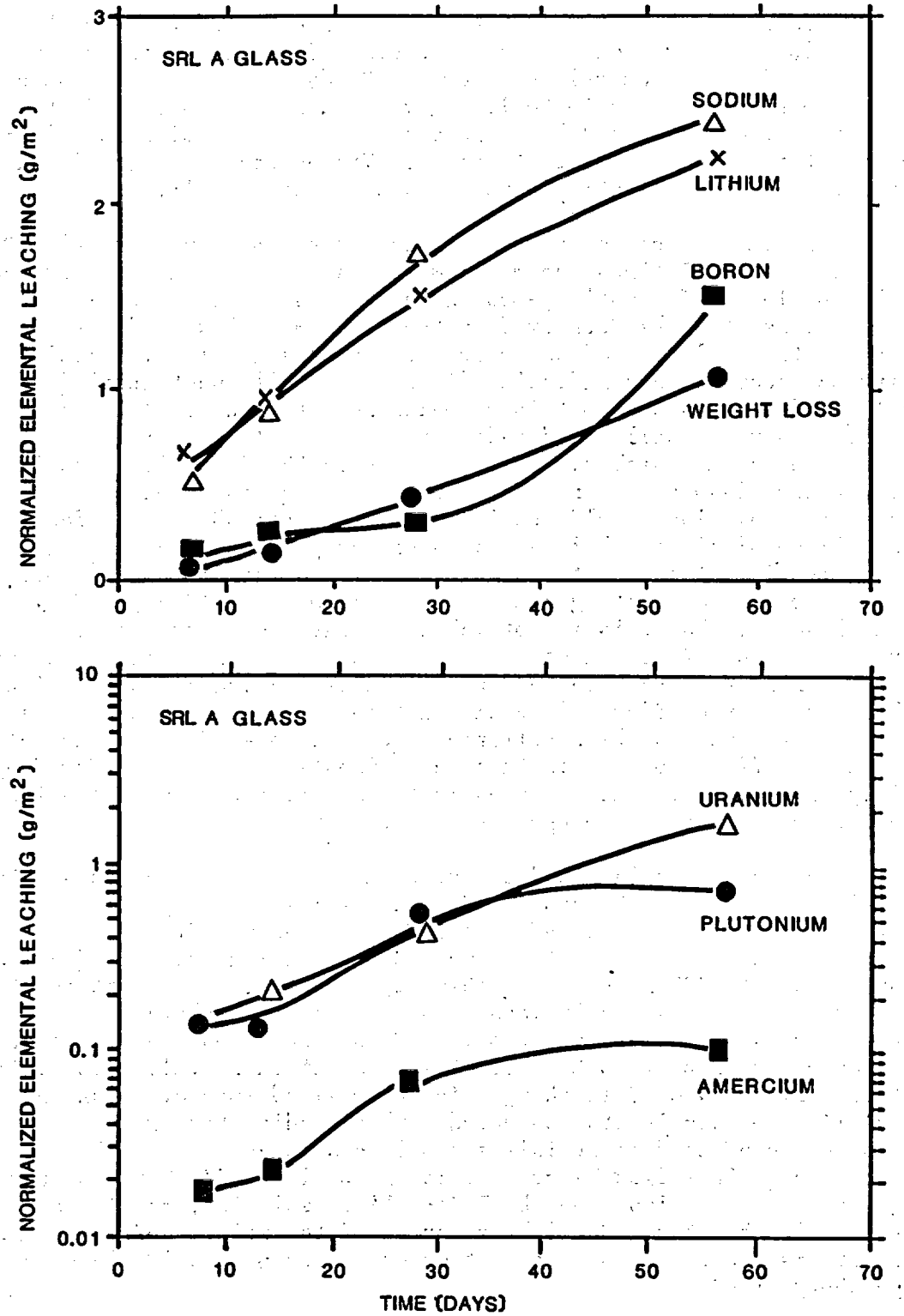

Figure 7-33. Release of actinides and frit elements from actinide-doped SRL-165 glass in the presence of 2 x 10^5 rads/h gamma irradiation in water from well J-13, MCC-1 type tests ratio of surface area to solution volume (SA:V) = 30 m^{-1}, temperature 90°C. Modified from Bates et al. (1986a).

(similar to Figure 7-32). Abrajano et al. interpreted this as the result of a slight loss of gas from the test vessels. It resulted in decreases in plutonium and neptunium release over the 91-day values; plutonium normalized release decreased from 2.15 to 1.67 g/m^2, and neptunium from 4.15 to 2.66 g/m^2. The normalized loss includes the concentration in solution and the amount adsorbed on the test vessel. The decrease in normalized loss must then represent precipitation onto the waste glass itself.

The gamma dose rates in these experiments were approximately 30 times, 1.5 times, and 0.15 times the maximum that would occur at the surface of fresh SRL glass. The anticipated pH change that could occur in repository water is less than that observed in the experimental work due to radioactive decay and the exclusion of water from the package vicinity immediately following emplacement when radiation fluxes are still substantial (Section 7.4.1). If a premature container breach were to occur, glass could come in contact with water while acid radiolysis was still occurring. However, because the gamma radiolysis drives the pH in the direction opposite to that of the glass dissolution, no increase in glass dissolution rate is expected because the solutions would remain at near-neutral pH. The effect of long-term buildup of nitrate before container and pour canister breach is not known. Testing at dose rates higher than those anticipated was originally intended as an accelerating mechanism (Bates et al., 1986b). They have shown, however, that this is not valid because the glass reaction changes dramatically as a function of dose rate and the accompanying pH changes. These experiments have been very useful in evaluating glass reaction mechanisms and the effect of pH on reaction rates and actinide release. Unlike experiments in which buffering chemicals are added to the solution to examine the effects of pH, in these experiments the pH is buffered by radiolysis with very minor changes in the solution chemistry (an increase of about 10 ppm nitrate and 5 ppm nitrite at most).

The effect of radiation from fresh-waste glass was tested at SRL using a 165-frit glass made with actual SRP sludge (Bibler, 1986) and with a SA:V of 100 m^{-1}. This glass contained high levels of cesium-137 and strontium-90, resulting in a dose rate to the surrounding leaching solution (well J-13 water) of about 1400 rads/h. In this experiment, the leachant solution absorbed most of the beta emissions, and there was no substantial dose to air in the vessels. However, the results of the experiment were similar to those just described (Bibler et al., 1984) with solution pH values remaining near neutral during 134 d of leaching. The normalized loss of boron and lithium was similar to experiments conducted with nonradioactive glass. These experiments were conducted in stainless steel vessels and showed that previous work conducted in Teflon™ vessels (Bibler et al., 1984) were compromised by large releases of F^- ion from the Teflon™ into solution, resulting in greatly increased leach rates. One likely source of the acidic buffer in these experiments is the radiolytic production of hydrogen peroxide in solution (Van Konynenberg, 1986).

In an effort to simulate the dissolution of glass in a tuff-dominated environment, the NNWSI Project and SRL have conducted leaching experiments similar to the MCC-1 static leach test but in which the glass sample is held inside a closed cup made of tuff. The glass in the SRL work was 165 frit glass, cast into 304L stainless steel tubes and then cut into wafers for

testing. Both simulated and actual-sludge glasses were used (Table 7-25). A similar test was done by Bazan and Rego (1986) using ATM-8, a PNL 76-68 based glass doped with low levels of technetium, neptunium, uranium, and plutonium (Wald, 1985). Results of the SRL experiment are shown in Figures 7-34a and b, (Bibler et al., 1984). In both the SRL and NNWSI Project work, a significant result of the presence of the tuff cups was the control of solution pH by the tuff. The pH remained in the vicinity of 8.3 to 8.7, which is the same as that found when well J-13 water alone is equilibrated with tuff. Glass reaction rates in the presence of rock were reduced relative to those without tuff (Figures 7-34a and b). This may be due to a combination of the lowered pH (≈8.5 with tuff vs. 9.3 without) and the addition of silica to solution by the tuff rock.

The results for plutonium-238, cesium-137, and strontium-90 release from 165-frit glass in the absence of tuff show increases followed by decreases, brought on possibly by the precipitation of colloids. This is typical behavior for these elements in leach testing (Mendel 1984). The NL values for radioactive glass with tuff absent were redetermined by Bibler (1986) using 304L stainless steel vessels, which are unaffected by radiation from the glass that caused fluorine release from the original Teflon™ vessels. Overall degradation of radioactive glass measured by boron and lithium release in the stainless steel vessels was identical within error to the results for nonradioactive glass (Figure 7-34a). In radioactive glass, the results for cesium-137 and strontium-90 were the same within error in the stainless steel and Teflon™ vessels (Figure 7-34b), indicating that they are solubility controlled. Plutonium-238 results were slightly larger in stainless steel (up to NL = 0.69 g/m^2 at 91 d).

Where tuff is present, the solution concentrations may be lowered because of adsorption by the rock. NL values reported for the tuff reaction vessel experiments (Bibler et al., 1984; Bazan and Rego, 1986) do not include amounts that were removed from the glass and then adsorbed onto the tuff. Plutonium, neptunium, uranium, and technetium release from PNL 76-68 based glass were measured in the Bazan and Rego study (1986). Similar results to Figure 7-34a were found, with very low releases of the actinides but no decrease in release rate at long times. Technetium was released at approximately the same rate as the other soluble components of the glass frit (molybdenum and boron). The actinides did not migrate through the tuff vessel in this experiment, but technetium did.

The tuff reaction vessel experiments show that, in the presence of the anticipated repository materials including tuff, tuff-equilibrated well J-13 water, and 304L stainless steel, glass degradation rates and radionuclide release rates are decreased relative to experiments done with either well J-13 water alone or deionized water. The effect is due to pH buffering and silica addition to solution by the tuff. It is not anticipated that glass will contact water under these tuff-dominated conditions in the repository since the pour canister and container will be present and will prevent extensive direct contact of the glass with tuff. However, should these conditions occur, glass degradation would be decreased relative to the expected condition.

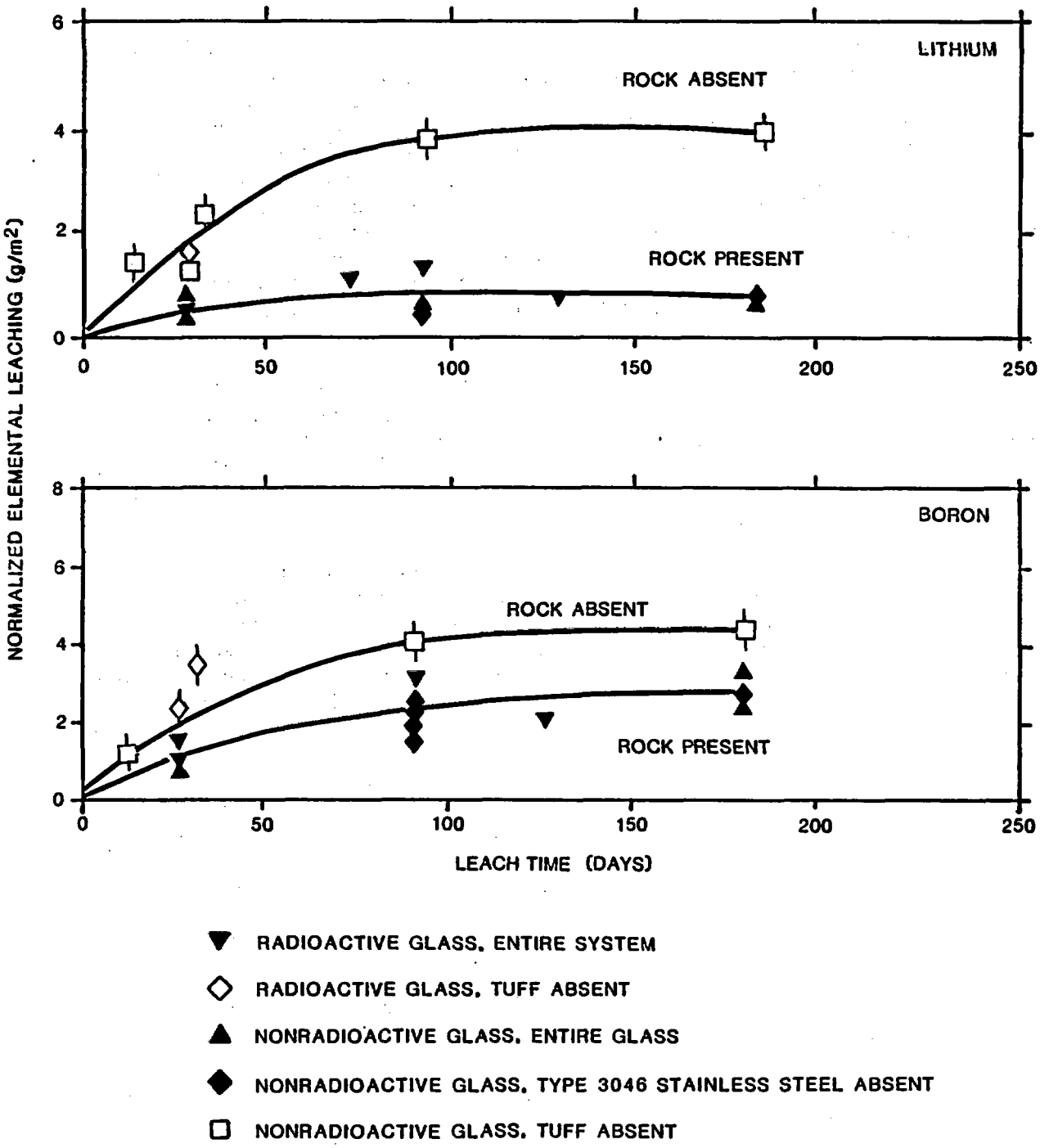

Figure 7-34a. Normalized mass losses (NL) based on lithium and boron for actual and simulated Savannah River Plant waste glass in presence (solid symbols) and absence (open symbols) of tuff leach vessels (Bibler et al., 1984). T = 90°C. SA:V = 100 m^{-1}. The lithium data shown here have been corrected from the original reference according to the new analysis given in Bibler (1986).

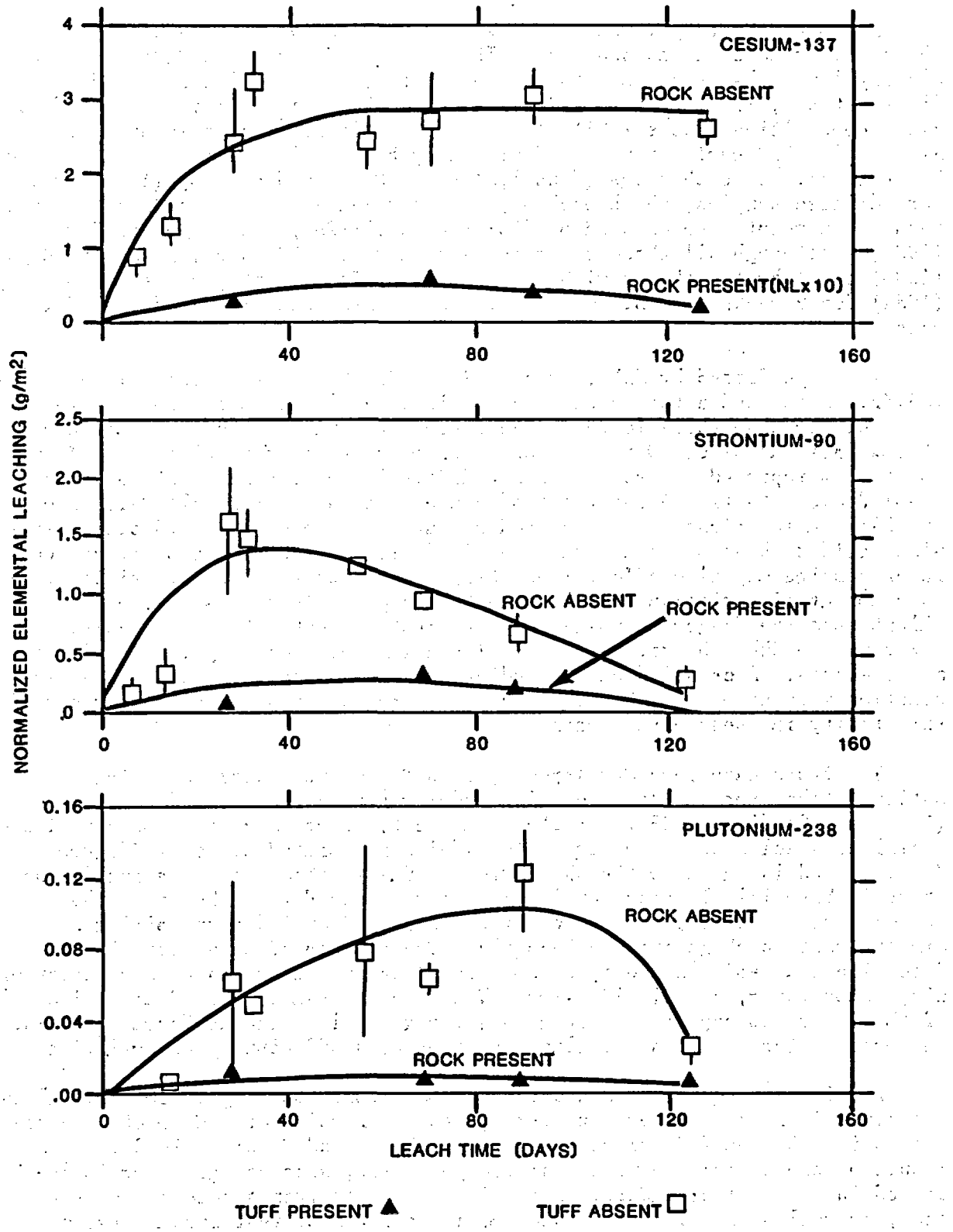

Figure 7-34b. Decrease in normalized mass losses for cesium-137, strontium-90, and plutonium-238 to tuff T = 90°C, SA:V = 100 m^{-1}.

Bates and Oversby (1984) compare the quantitative results of three of the static studies discussed here. The results of Bazan and Rego (1985) are clearly lower than those of other experiments (Bates and Oversby, 1984; Bibler et al., 1984). This difference cannot be individually attributed to glass composition (Table 7-25), leaching conditions, or experimental method. All samples had surfaces prepared similarly but not identically, and this is known to affect leach rates (Mendel, 1984). Bates and Oversby (1984) used core-drilled samples, which probably have a slightly rougher average surface than the saw-cut samples used by Bibler et al. (1984) and Bazan and Rego (1985). Although all three experiments used well J-13 water, Bazan and Rego (1985) equilibrated theirs with tuff (at 90°C) for 1 month, Bates and Oversby (1984) for 2 weeks, and Bibler et al. (1984) used unequilibrated well J-13 water.

Tests performed by SRL (Savannah River Plant and Laboratory, 1984) using 165-frit glass and a tuff ground water yielded release rates two to three times higher than those found in NNWSI Project studies. These tests were run at low SA:V ratios of 10 m^{-1} and only for short periods of time. The final pH was not reported. These tests are difficult to compare quantitatively to NNWSI Project tests. A later set of SRL experiments using well J-13 water and SA:V ratios closer to those used by Bazan and Rego (1985) (Bibler, 1986) also yielded about twice as much reaction. It is possible that differences in processing may also affect leachability, despite similar compositions. This amount of variation must be accepted in glass leach testing, and it illustrates the danger in using only one test or test method. Notably, however, the SRL 165 frit glass in all studies released very low levels of all elements. A detailed understanding of solution compositions and glass reaction mechanisms will be required to understand completely the sources of variability in these experiments.

Two tests have been developed by John Bates and coworkers at Argonne National Laboratory to test leaching under water-undersaturated conditions (Bates and Gerding, 1985). In the first test, water is dripped onto a glass-stainless steel assembly designed to model a perforated canister (Figure 7-35(a)) and is known as the NNWSI Project Unsaturated Test (previously the Phase II Materials Interaction Test). In the second test, known as the analog test, water vapor is forced through a tuff cylinder containing a similar waste package (Figure 7-35(b)). The purpose of both tests is to determine what effects are important when leaching occurs in a combination of air, water vapor, and liquid water. These tests examine the effects of one of the important expected environments for glass leaching at Yucca Mountain: one where water contacts the glass and then runs off without accumulating.

Preliminary results for unsaturated and analog testing on 165 frit glass are given in Bates and Gerding (1985), and the results of a complete one year test using SRL-165 frit glass are given in Bates and Gerding (1986). As a result of the experience with that one-year test, some changes were implemented in the test procedure. Preliminary results from a second one year test, as well as parametric studies on the effects of test parameters, are available in Bates et al. (1986a,b). These tests will help determine whether periodic wetting of glass can result in higher release rates than those determined in static tests.

The most important purpose of these tests is to examine interactions between materials. One notable interaction occurs between the perforated 304L stainless steel and the glass it contacts (Figure 7-35). Particularly at welded regions, discoloration of the stainless steel is observed, and rust flakes have been found in the solution (Bates and Gerding, 1986). This interaction has not been found in experiments involving static solutions.

The effect of using deliberately sensitized 304L stainless steel is being investigated currently (Bates et al. 1986b; Bates and Gerding, 1986). This examines the possible importance of the pour (inner) canister in affecting glass release rates. In some instances, the use of sensitized stainless steel has lead to considerable interaction between the glass and the steel (Bates et al., 1986b). In the first year-long unsaturated test (Bates and Gerding, 1986), the assemblies that showed the greatest release from the glass showed extensive discoloration of the stainless steel in contact with the glass. The 26-week test released three times as much boron as the 52-week test, a result that correlates with the observed greater interaction between the glass and the steel in the 26-week test.

Release rates are very low in unsaturated testing, even in the presence of glass-steel interactions. The greatest NL value observed for boron in the first year of testing was 0.8 g/m^2. Some elements (for instance, calcium and silicon) are actually added to the waste form (lost from the well J-13 water) as a result of precipitation reactions on the glass and stainless steel. These tests use the maximum water flow expected in the repository, scaled to glass surface area, and are run at 90°C. Parametric testing has been done to examine the effect of varying the water-to-glass ratio (Bates et al., 1986b). The release of glass components was found to be insensitive to this ratio; as long as there is water on the glass that never dries out completely, the release is approximately constant (within a factor of two). Most of the glass reaction occurs on the bottom of the waste package assembly (Figure 7-35) where water is observed to accumulate before dripping off.

Unsaturated tests are sampled in two ways; some are run to completion, the apparatus is dismantled, and all parts are analyzed. In others, the solutions that have dripped off the waste package are analyzed at 6.5-week intervals, and the waste package is reinserted into a new vessel for further testing. Preliminary comparisons show that similar results are found for each method.

The analog test is intended as a second method of measuring materials interactions and unsaturated leaching. In this test, a waste package similar to that in the unsaturated test is used, but the water contacts it as a result of vapor and unsaturated flow through the tuff rather than dripping onto the waste package from a tube as in the unsaturated test. NL values after 13 weeks of testing (Bates and Gerding, 1986) for radionuclides in the glass were NL (europium-152) = 0.2 g/m^2, NL (barium-133) = 0.2 g/m^2, NL (cesium-137) = 0.3 g/m^2. These are in reasonable agreement with unsaturated test results. The glass in the analog test showed marks indicative of water drying on the surface, and the bottom surface was wet when removed. Some glass-stainless steel interaction was indicated by slight discoloration of the stainless steel. The appearance of the waste package was very similar to waste packages in the unsaturated tests, indicating that the water contact and reaction mechanisms in the unsaturated test are not unique, and the

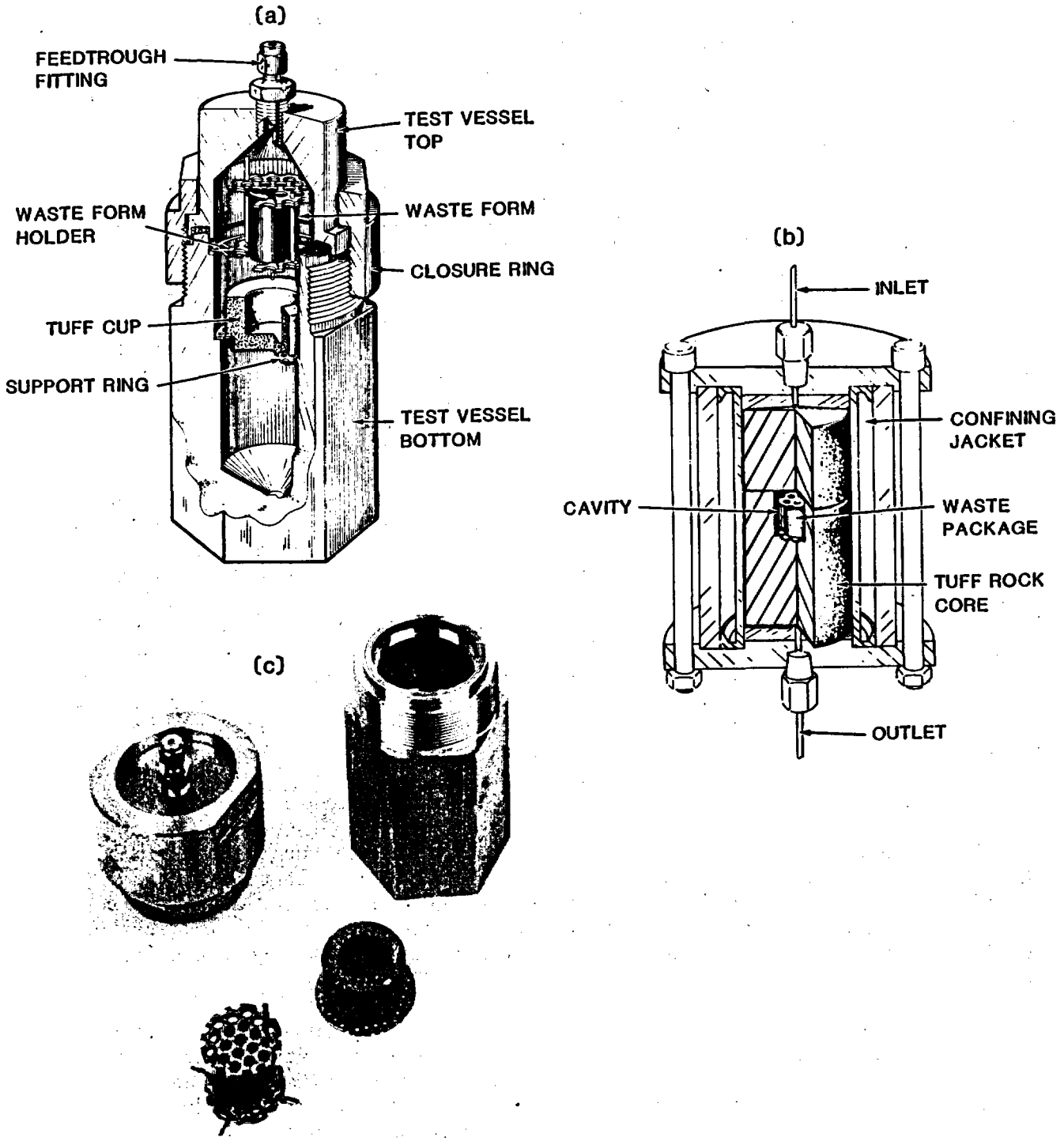

Figure 7-35. Equipment for two tests of leaching under water-unsaturated conditions. Panel (a) shows the unsaturated test vessel, (previously, Phase II materials interaction test) from Bates and Gerding (1985). Vessel is made of 304L stainless steel. Tuff cup is included in some experiments. Water drips from feed-through pipe onto waste package and is then collected from tuff or vessel bottom. Panel (b) shows the analog test apparatus. Water vapor under pressure is forced through the tuff core and collected from bottom. The contact of water with the waste package is uncontrolled. Panel (c) depicts selected parts.

results and interactions observed are applicable to a range of water contact mechanisms.

7.4.3.2.3 Release model for determining the source term for glass waste forms

The results the NNWSI Project and SRL tests cited in Section 7.4.3.2.2 confirm the previously established result that radionuclides are released at (normalized) levels equal to or below that of the soluble matrix elements of the glass (Mendel, 1984). The elements of interest are not left behind in the glass, however. They are reprecipitated onto the surface of the glass or test vessel in amorphous layers or crystalline deposits, or they are found in colloids in the solution that can settle out, attach to test components, or be trapped by filtering before the solution is analyzed. The decrease in plutonium concentration in Figure 7-34 in the absence of tuff was probably the result of colloid formation.

The amorphous layers and crystalline products have been studied by a number of workers, including Bates (Bates et al., 1982); investigators in the defense high-level leaching mechanisms program (Mendel, 1984); and Strachan et al. (1984). These new compounds are more stable forms of the components of the glass, and there are forms even more stable that can be expected to form over longer periods of time. The solubility and solution kinetics of both stable and metastable compounds will control the release of the radionuclides they contain. Only in the event of the fracturing of a glass waste form or of the separation of a surface layer will fresh glass be exposed. Mendel (1984) showed that even in that instance, reformation of a surface layer occurs quickly on a repository time scale. The nature and composition of surface layers can be strongly affected by minor components of the glass.

Prediction of the long-term behavior of waste glasses will require a better understanding of these secondary products. Current evidence (Mendel, 1984) indicates that the secondary products substantially reduce initial leach rates, but in the long-term, the presence of the crystalline products can provide the thermodynamic driving force for glass dissolution to continue even in relatively concentrated solutions (Grambow et al., 1985). The effects of the presence of crystalline materials need to be quantified, and the fate of colloids and flocculent precipitates in the solution needs to be determined, particularly of the hydroxide compounds whose solubilities are very sensitive to pH. The current knowledge of these compounds is not sufficient to rely upon them solely as a control of radionuclide release although, for specific radionuclides, some prediction of solubility behavior and its effect on leaching can now be made. A conservative approach for the present is to assume that some radionuclides will be released at the same rate as are the soluble frit elements and that overall glass degradation rates must be controlled so that these releases meet the regulatory requirements. The existence of the secondary compounds is the primary reason no glass source term can be accurately determined without considering all repository interactions; the glass-canister-container-water-rock system is synergistic, and the behaviors of the individual parts are impossible to separate.

Release limits based on congruent release are straightforward to calculate. The reference DWPF canister weight, 1710 kg (Baxter, 1983), yields a 1-part-in-100,000 release of 16.6 g/yr. Therefore, when scaled for surface area, normalized releases per canister must be less than that value. If the entire surface area of glass in a DWPF canister were exposed, it would have a geometric surface area of 5.0 m^2, yielding an allowed NL (normalized loss for each radionuclide) of 3.3 g/m^2 per year. Because of the expected persistence of container and canister material throughout the isolation period (discussed in Section 7.4.2.), it is unlikely that standing water will be able to react with the entire surface area of the glass. Two more likely scenarios are that the headspace of the canister could fill with water or that water will drip onto and off the waste form. The surface area in the first instance would be that of the top of the glass, which is about 0.275 m^2, yielding normalized loss units of allowed release (NL) of 60 g/m^2 per year. The factor of up to three increase in leach rate due to cracking observed in full-scale tests by Bickford and Pellarin (1986) would make the effective value 30 g/m^2 per year for comparison with laboratory experiments on uncracked glass. Allowed releases for the case where water drips onto and off the waste may be calculated similarly for various contact scenarios.

Current water availability estimates per canister of DWPF waste in the Yucca Mountain repository range from 0.25 L/yr to zero. The value of 0.25 L/yr is calculated using the maximum downward flux of 0.5 mm/yr (Section 7.4.1) and assuming that amount enters a vertical borehole with a diameter of 76 cm. Since there is no mechanism to concentrate water onto the waste packages, this is a reasonable upper estimate of the water flux per container. The unfilled head space of a DWPF canister is about 108 L. If cracks were to occur in the container and pour canister near the top (as emplaced), this space could conceivably fill with water in about 400 yr. The resultant glass surface-area-to-solution-volume ratio (SA:V) would be about 2.5 m^{-1}. The anticipated SA:V for glass in the repository range upward from this value depending on canister perforations, water contact, and cracking of glass.

Aines (1986) presented a calculation of the long-term release rate from glass under the conditions where the head-space fills with water. Larger water fluxes were used in that calculation than are now anticipated (1 mm/yr versus 0.5 mm/yr, respectively), but the calculated releases were well below 1 part in 100,000/yr (1.3 g/yr or 0.08 part in 100,000). These calculations involved extrapolation of the boron and lithium normalized loss rates to long times, using the change in silica concentration as glass dissolves. Because of the controlling effects of silica concentration, the reaction was assumed to reach a steady-state rate when the silica added to water in the headspace was equal to the silica lost by overflow of water.

This type of calculation yields larger releases than those assuming that glass breakdown will follow the same square root of time $(t)^{1/2}$ relationship observed in the laboratory at short times, which predicts that glass degradation effectively stops after several years. However, because of the long times involved in reaching steady state (400 yr just to fill the headspace), it is still difficult to calculate release with high precision. One approach to this problem that is currently being investigated is to use explicit geochemical modeling of aqueous species and glass dissolution kinetics to examine the sensitivity of the analysis to changes in various parameters

(Section 8.3.5.10). Geochemical modeling can also be used to examine whether additional interactions not observed in laboratory experiments may occur at long times and to calculate the composition of fluids that are in thermodynamic equilibrium with the phases precipitated on waste glass and with other repository phases.

Much information regarding conservative estimates of release can be obtained from the solubilities of radionuclides by assuming that the water can, at most, remove from the engineered barrier system an amount equivalent to a saturated solution. This is a conservative approach and is very useful for nuclides whose solubilities are well known under tuff rock conditions. It is not as conservative an approach, however, as using the normalized leach rate (LR_i) for a highly soluble, matrix-forming element such as boron or lithium.[1] Regardless of the fate of a radionuclide after release from the glass (i.e., precipitation, formation of a colloid, adsorption, or removal by remaining in solution), the normalized leach rate will not exceed that of boron or lithium; this is the maximum amount of a radionuclide that could be released from the waste form. However, the amount that can be removed by remaining in solution is limited by the solubility of the element in the form it assumes under the pH and redox conditions of the environment. These effects are being investigated (Section 8.3.5.10), and the coupling of solubility effects (limiting release) with kinetically limited breakdown of the glass matrix (providing maximum release rates) will provide accurate bounds on the release of radionuclides from glass. The performance of glass in the repository will be determined from a combination of these release calculations with water influx and container perforation calculations. These will provide estimates of the number of containers likely to contain standing water and the amount and overflow rate of that water, and the number of canisters subject to water dripping onto and off the glass waste. A description of the research and testing program of the glass degradation and radionuclide release process is given in Section 8.3.5.10 under Issue 1.5.

7.4.4 GEOCHEMICAL MODELING CODES: EQ3/6

Chemical interactions among nuclear waste, waste packaging, ground water, gases, and host rock are critical factors in determining the consequences of geologic waste disposal. The removal of radionuclides from the waste forms and their transport through the geologic environment is controlled by chemical processes. Numerical simulation of the various processes will play an important role in the prediction of long-term performance because of the complexity of these interactions, the physical scale, and the 10,000-yr period being considered for the release limit (Coffman et al., 1984). Two of the four performance objectives detailed by the NRC (10 CFR Part 60) are concerned with the engineered barrier system (EBS). Geochemical modeling is needed to carry out the performance assessment to determine whether these objectives will be met.

The first performance objective for the EBS concerns the 300- to 1,000-yr containment period for the waste package during which there will be a thermal pulse from radioactive decay of high-level waste that will cause an increase of temperature of the surrounding rock, water, and gas in the unsaturated zone. This temperature increase will cause the fluid and rock to

react with one another to regain equilibrium, resulting in changes in fluid composition and rock mineralogy. Geochemical modeling will be used to characterize the fluid that may interact with and potentially cause a breach in the waste package. The composition of the water, if present, is important because chemical processes (such as corrosion of the container) depend on the composition of the fluid. Geochemical simulation of the heating of the rock-fluid system will characterize the evolving composition of the fluid as it reacts with the rock.

The second performance objective for the EBS encompasses the radionuclide release rate. Geochemical modeling will be used to predict the release of radionuclides from the EBS following a breach of the container and subsequent interactions involving the waste package, aqueous fluids, gases, and surrounding rock. Furthermore, it will permit evaluation of the potential for migration of radionuclides to an aquifer and the accessible environment.

The geochemical modeling codes that are the most general and have the widest application (Nordstrom and Ball, 1984) are in the EQ3/6 package developed by Wolery (1978) and later improved (Wolery, 1983; Delany and Wolery, 1984; Wolery et al., 1984; Jackson and Wolery, 1985; and Delany et al., 1986). Additional development for both codes and the supporting thermochemical data base is essential to account for all important geochemical processes that potentially could affect the performance of the repository (Jacobs and Whatley, 1985).

EQ3/6 was initially developed by Wolery (1978) to model interactions between sea water and basalt in hydrothermal systems at midocean ridges. It is based on principles elucidated by Helgeson (1968) and Helgeson et al. (1970) who pioneered computerized geochemical modeling. Wolery introduced improved numerical methods for solving the requisite equations, which eliminated computational problems in Helgeson's (1968) code, and reduced computer time for a modeling run by several orders of magnitude. This was an important step because of the large amount of computer time required to run simulation studies for geochemical processes involving complex systems such as for the proposed repository.

Improvements in EQ3/6 since then included adding dissolution kinetics capability and expanding the thermodynamic data base. Simulations with EQ3/6 included modeling of the dissolution of uranium(IV) oxide in granitic ground water (Wolery, 1980). Most of the funding to support EQ3/6 at Lawrence Livermore National Laboratories since 1982 has come from the NNWSI Project, with additional funding from the Salt Repository Project and the Basalt Waste Isolation Project. Recent developments during this later time period are described in the following sections. Plans for future development can be found in Section 8.3.5.10.

7.4.4.1 EQ3NR, a computer program for speciation-solubility calculations

EQ3NR (Wolery, 1983) calculates the thermodynamic state of an aqueous solution, which involves the determination of the distribution of activities of aqueous species. The degree of formation of ion pairs, concentrations of

complex aqueous species, ionic strength, Eh, pH, and essentially all the variables needed to fully characterize the solution are evaluated. This allows calculation of a quantitative measure of the thermodynamic state of the solution with respect to solid phases (undersaturated, in equilibrium, or supersaturated). This speciation-solubility calculation is useful as a method to test if a solution is in equilibrium with a particular solid phase. EQ3NR is widely used by experimentalists both as a tool for optimizing experimental conditions and as a method for extracting thermodynamic and kinetic information from experimental results. EQ3NR also initializes the solution composition used as input to reaction-path calculations made by the EQ6 code.

7.4.4.2 EQ6, a computer program for reaction-path modeling

EQ6 (Wolery, 1979) calculates reaction paths and mass transfer in dynamically reacting fluid-rock systems by considering consecutive stages of partial equilibrium as equilibrium is approached and then attained. For example, when a mineral reacts with a fluid with which it is not in equilibrium, a series of solid phases usually precipitate and dissolve before saturation with the initial reactant mineral is reached. EQ6 tracks the changes in mineralogy and corresponding changes in fluid composition as the fluid and the rock react. Changes in pH, oxidation-reduction potential, and other parameters are also output by the code. To calculate precipitation and dissolution events, small amounts of the reactant mineral are dissolved into the solution and the solution is tested for equilibrium. Product phases will precipitate in the case of supersaturation and dissolve in the case of undersaturation. When the solution is in equilibrium with all product solid phases, more of the reactant mineral is allowed to dissolve. The rate at which the reactant mineral dissolves can either be specified arbitrarily by the user or calculated according to one of several kinetic rate laws programmed into EQ6. The reaction path terminates when the solution becomes saturated with respect to the initial reactant mineral, or when the reactant mineral is totally consumed.

7.4.4.3 Thermodynamic data base

The thermodynamic data base is a summary of the available thermochemical data for aqueous species, solids, and gases in tabular form that are necessary to serve as input to the geochemical modeling codes EQ3NR and EQ6. These values have been gathered from the available literature and inserted into the data base format as part of an ongoing effort. Data are made compatible with Committee on Data for Science and Technology (CODATA) task-group-recommended key values and with Nuclear Energy Agency (NEA) data values that are released after peer reviews. The portion of the data file that represents rock-forming minerals is taken from SUPCRT (Helgeson et al., 1978), a data base maintained at the University of California, Berkeley.

Thermodynamic data are processed through a code, MCRT, that checks for thermodynamic consistency, extrapolates heat capacity functions with temperature, and generates data blocks for insertion into the master EQ3/6

thermodynamic data file DATA0. MCRT contains an internal data base of free energies and enthalpies of formation, third law entropies, and heat capacities of specified reactions that are commonly used in geochemical calculations. Thermodynamic data in DATA0 are processed through an additional code, EQTL, that checks for mass and charge balance, fits all data to a predetermined temperature grid, and writes the data files that are read directly by the EQ3NR and EQ6 codes.

7.4.4.4 Theory and code development

EQ3/6 simulations of experimental results have revealed chemical processes that should be accounted for in the code to ensure better matches between simulation results and experimental measurements. Credible predictions of geochemical interactions on a scale of up to 10,000 yr require continual updates of EQ3/6 to account for these complex processes. Recent progress in this regard has been made in the ability of the codes to account for solid solutions, precipitation kinetics, and fixed fugacities for gases. Future theory and code development activities will be focused on incorporating a geochemical flow model, studying the effects of nucleation and substances inhibiting precipitation on kinetics, including an option for variable fugacity, extending the solid solutions model to include an option for site mixing, and adding an equilibrium sorption model (Section 8.3.5.10).

The treatment of solid solutions in EQ3/6 has been improved by incorporating a new algorithm for molecular mixing models (Bourcier, 1985). This model is mathematically equivalent to a single-site mixing model. The data base has also been expanded to include calcite-structured solid solutions based on the model of Sverjensky (1984). Solid solutions are common in nature and occur both as primary and secondary phases. At Yucca Mountain, the principal primary minerals present as solid solutions are the feldspars and biotite. Secondary solid solution phases, which result from water-rock interactions, include the clays and zeolites. To compute chemical equilibrium and simulate reaction path models of these interactions, it is necessary to incorporate solid solution models to account for phases with variable composition.

A precipitation-kinetics option has been added to EQ6 that complements a preexisting capability to model dissolution kinetics (Delany et al., 1986). Several precipitation rate laws have been programmed into EQ6 as well as options for activity-term expressions and transition state theory. Transition state theory was reexamined, resulting in new theoretical insights that will provide the foundation for further improvements necessary to model chemical kinetics (Wolery, 1986). Rates of reactions must be taken into account in cases where simulations are made of laboratory experiments in which reaction kinetics are sluggish and equilibrium is not attained. For example, in the hydrothermal tests discussed in Section 7.4.1.8 involving the Topopah Spring tuff and well J-13 water, it is observed that the phase controlling the solubility of silica is cristobalite. However, cristobalite is thermodynamically metastable under the test conditions because quartz is a thermodynamically more stable (less soluble) form of silica. Cristobalite solubility is maintained in the short term only by the slow growth kinetics of quartz, which is present in the tuff. It is also important to be able to

model laboratory experiments in real time in order to understand the factors that affect extrapolation to longer time periods. Without geochemical modeling to allow this extrapolation, one would have to assume that short-term conditions observed in experiments apply to the long term. Modeling calculations, on the other hand, allow an evaluation of whether laboratory results do or do not represent thermodynamic equilibrium or may be kinetically controlled.

A fixed-fugacity option has been added to the EQ6 geochemical reaction path code (Delany and Wolery, 1984). Ground-water systems that are either open or closed to the atmosphere as well as buffered laboratory experiments can now be modeled. Permitting the fugacity of any gas to be set at a fixed value allows simulation of the effect of rapid chemical exchange with a large external gas reservoir such as the unsaturated zone at Yucca Mountain, which is open to the atmosphere. In addition, quantities of various gases (e.g., carbon dioxide, methane, and hydrogen sulfide) may be produced by chemical reactions in the repository site. It is therefore imperative that geochemical models have the capability to include gases in the systems under consideration. For example, if a species has a greater proportion of its mass in the gas phase than the aqueous phase, the fugacity of the gas phase can be assumed to control the fugacity of the aqueous phase. The paths and rates of chemical reactions in the aqueous phase can be predicted when so constrained.

7.4.4.5 Thermodynamic data base development

Expansion and refinement of the data base (Section 8.3.5.10) is required to model the complex chemical systems involved in radioactive waste disposal. Sensitivity analysis will be reconducted to (1) identify reactions that can be neglected and (2) recommend additional experiments for improving and obtaining important thermodynamic data. A plan for experimental and theoretical work has been developed to obtain needed thermodynamic data and to resolve inconsistencies in existing data. This plan resulted from a review of the thermodynamic data for the actinides, which uncovered the need to conduct laboratory experiments and to obtain thermochemical data for solubility-limiting solid phases and solution species. An example of how the correspondence, or lack of it, between experimental results and EQ3/6 predictions is being used to identify phases for further thermodynamic study is given below.

The concentration of uranium in solution following spent fuel tests (Oversby and Wilson, 1985) reacting with well J-13 water at 25°C during the first few days is about 5 ppm. The concentration decreases to about 1 ppm after 240 days as equilibrium solubility is approached. If the solubility is controlled by an oxide, shoepite, EQ3NR predicts that 65 ppm uranium should be in solution at equilibrium. On the other hand, if a silicate, soddyite, controls uranium solubility, EQ3NR predicts an equilibrium concentration of 0.2 ppm uranium using provisional thermodynamic data. Clearly, soddyite is a candidate among others (e.g., boltwoodite) for further thermodynamic study.

To adequately model the requisite geochemical processes that are critical in the evaluation of performance objectives, it will be necessary to generate a resource body of data on possible solubility-controlling solid

phases and to determine the free energies of solubility reactions needed by EQ3/6. Some redetermination of existing data may be necessary because the solid phases were not adequately characterized with regard to structure and composition. A library of infrared spectra is currently being generated and will be used to identify spectra of unknown solids from spent fuel and waste form dissolution experiments. In addition, this spectroscopic data will be used together with bulk and acoustic properties and structural data to predict thermodynamic functions using an averaging model developed by Kieffer (1985). This model is based on the theory of lattice vibrational properties of minerals and on observed trends in the high-temperature thermodynamic properties of silicates. The code for this model is presently available at Lawrence Livermore National Laboratory. Model values of heat capacities and third-law entropies have been shown to be in good agreement with experimental values to 1,000°C for more than 30 minerals. Heat capacities and third-law entropies are needed to make thermodynamic calculations of free energies of formation of the minerals for which spectra have been collected.

Solubility product constants are not usually sufficient to predict accurate solution concentrations. Hydrolysis products and other complexes can increase solubilities above predicted values based on solubility product alone. Therefore, reliable formation constants for the major solution species that are likely to form under site-specific ground-water conditions are needed to make accurate EQ3/6 calculations. However, gaps and inconsistencies exist in the present thermodynamic data base. One reason is that the indirect methods (e.g., nuclear counting methods) used to determine the amount of the radionuclide in solution do not provide information, critical to geochemical modeling, on the nature of the solution species. Another reason is that some specie's concentrations are at such low levels that conventional spectroscopic techniques (ultraviolet, visible, near infrared) do not have sufficient sensitivity. Attempts are presently under way to apply more sensitive laser techniques to these measurements. The favored approach is to measure directly the deposited energy resulting from the adsorption process rather than the more conventional method of measuring the attenuation in a light beam. This technique, called pulsed photoacoustic spectroscopy, has been shown to be several orders of magnitude more sensitive than the conventional approach. A West German group has demonstrated that this technique can be applied to measurements of actinide speciation at submicromolar concentrations (Stumpe et al., 1984).

A pulsed photoacoustic system is presently being developed using an existing Nd-YAG (neodymium-yttrium/argon gas) pumped dye laser and associated computer-control instrumentation. The capabilities and sensitivity limitations of this system for characterizing waste radionuclide species in aqueous solutions is being evaluated.

7.4.4.6 Applications: water-rock interactions

Although additional geochemical model development is planned (Section 8.3.5.10), several applied results have clearly demonstrated the utility of the approach. These preliminary calculations indicate a good agreement between predicted phase relations and solution composition and those observed in laboratory experiments. It is not possible to conduct all the laboratory

tests necessary to cover all possible repository conditions (e.g., varying temperature, solution composition, and rock:water ratios). The size of such a test matrix is prohibitively large with respect to available resources. The close match between geochemical modeling calculations and laboratory tests demonstrates that the code has the capability to quickly and relatively inexpensively provide credible predictions of the results of fluid rock interactions. Simulation predictions are necessary to carry out performance assessments for containment and release rates over time periods of 10,000 yr, which are not attainable in the laboratory.

Experimental results of reacting Topopah Spring tuff with well J-13 water at room and at elevated temperatures were compared with simulation results modeled using EQ3/6 (Knauss et al., 1984; Delany, 1985). The details of this comparison are in Section 7.4.1.8. There was good agreement between the measured and the calculated solution composition. As more complete data on phase composition, dissolution kinetics, and thermodynamic properties become available for primary and secondary phases, it is to be expected that an even closer match between EQ3/6 geochemical modeling results and the observations from laboratory tests will result. This will provide a critical component for making the predictions needed for performance assessment.

In addition to simulating laboratory experiments involving water-rock reactions, EQ3/6 can be used in parametric analyses to determine which factors must be controlled during experimentation and the relative magnitudes of the effects of these factors. The EQ6 code was used to simulate the dissolution of pure albite in distilled water at 25°C for various carbon dioxide pressures (Delany and Wolery, 1984). This was done to investigate the influence of constant fugacities on reacting aqueous geochemical systems. At higher carbon dioxide fugacities, more albite must dissolve to reach saturation. This is expected because, as carbon dioxide is added to maintain the higher fugacities, more acid is created, which in turn hydrolyzes more albite. At lower fugacities of carbon dioxide, the sequence of secondary mineral formation is gibbsite, quartz, and paragonite. With increasing fugacity of carbon dioxide, gibbsite does not appear, and the product assemblage is dominated by quartz and kaolinite. More of the secondary reaction products are formed at higher carbon dioxide fugacities, which is expected because more of the albite dissolves. The secondary phases that formed in these calculations were those that are thermodynamically most stable according to the data base. However, this does not always result in the most realistic model because thermodynamic data is lacking or kinetic effects have not been accounted for. For example, a clay of roughly the composition of sodium montmorillonite, for which thermodynamic data is not available, is a more likely product than paragonite. And a solution may become supersaturated with respect to a phase, such as quartz, rather than precipitating the phase upon reaching saturation. There is a clear need for better kinetic models of mineral precipitation that can describe these phenomena.

7.4.5 WASTE PACKAGE POSTCLOSURE PERFORMANCE ASSESSMENT

7.4.5.1 Introduction

The long-term performance of nuclear waste packages must be assessed to qualify the waste package designs with respect to postclosure performance requirements. The performance requirements are presented in Section 7.2. The processes affecting long-term performance are identified in earlier parts of Section 7.4; knowledge to date, information needs, and investigations planned to satisfy the information needs are presented in Sections 7.4, 7.5, and 8.3. Performance assessment as an activity takes information from the other waste package investigations, constructs coupled models, validates these models, and assesses waste package designs in terms of the performance requirements. The outputs address both performance of an ensemble of waste packages and reliability in the waste packages' performance.

The generic postclosure functional requirements of the waste package were listed in Section 7.2.1.2. The plan for determining the final performance allocation is described in Section 8.3.5.2. Performance criteria addressing the NRC 10 CFR 60.113 are terms of (1) time to loss of substantially complete containment and (2) release rates of radionuclides of concern from the engineered barrier system. The parameters to be calculated in the assessment are as follows: (1) time to failure of individual containers; (2) time to initiation of release for each radionuclide; and (3) release rates and quantities from the waste package of all radionuclides of concern, as a function of time. These parameters will be determined for an ensemble of waste packages. To document regulatory compliance, the aggregate of these measures will be compared with the postclosure performance criteria given in Section 7.2.3.2. Reliability results to be assessed are discussed later in this introduction.

The NRC design criteria in 10 CFR 60.135(a)(1) concerns waste package interactions with its emplacement environment. The waste package performance assessment evaluates impacts of the waste package on its environment through heat, mechanical, radiation, and chemical effects. The effects of the environment on waste package performance are included in the assessment. The magnitudes of heat, mechanical, radiation, and chemical impacts will be available for repository-scale evaluation of the effects of these impacts on repository performance.

Performance assessment as an activity within the waste package investigations creates information needs only with respect to the methodology used for assessment. Basic scientific and engineering studies necessary to predict performance of waste package components and to validate component performance are periodically described earlier in this chapter and in Section 8.3. These studies will satisfy information needs through investigations during site characterization. The information needs of performance assessment are served by those investigations and, therefore, place requirements on those investigations with regard to data type and sensitivity. To understand these data requirements, a brief discussion of performance assessment methodology is useful.

Given the long periods discussed in the criteria and given the general complexity of the problem, long-term assessments will use computational

models. It is the task of performance assessment to construct and validate these computational models and then to analyze waste package designs to demonstrate that selected designs perform as required. These analyses will also guide the design process by allowing comparison of alternative waste package designs. Such models can help determine the sensitivity of performance to environmental and design parameters. Further, the integrated performance calculations will aid in determining the adequacy of the current envelope of environmental conditions used in the individual waste package process tests, as determined by one- or two-process detailed models.

Stephens et al. (1986) describes attributes that waste package performance assessment methodologies must have in addition to those previously described. In particular, since the environment and processes affecting performance in a mined repository are subject to uncertainties, computational models that integrate the effects of these processes must also reflect those uncertainties. To allow for these uncertainties in the licensing processes, the NRC intends to use a reasonable assurance standard for determining that regulatory criteria are met (NRC, 1986). The NRC has identified probabilistic reliability analysis as a means to supply reasonable assurance. To date no integrated performance assessments have been performed on NNWSI Project conceptual waste package designs. Calculations of thermal effects and mechanical effects on packages have been made (Hockman and O'Neal, 1984; O'Neal et al., 1984), and the results of those calculations have been considered as part of the conceptual designs that appear in this document. Therefore, the waste package performance assessment methodology intends to include a probabilistic reliability analysis method. This approach will allow waste package performance assessment calculations to provide predictions of time-to-loss-of-containment and release rate as a function of time, as well as the probability distributions of these predicted performance measures. In addition, models must allow consideration of anticipated and unanticipated events. This attribute allows the analysis of performance resulting from extreme event scenarios for use as input to the total repository performance assessment. Finally, these calculations must also incorporate those needed to assess performance with respect to preclosure design criteria.

As stated earlier, methods used for performance assessment will incorporate the results of the studies of physical and chemical processes discussed elsewhere in this chapter. These results, in the form of data or submodels, must be integrated into a single model to represent the interaction or coupling that would exist among processes in a repository setting. The current approach to waste package performance assessment calculations relies on coupling of processes at the systems level; that is, process submodels are joined through an explicit set of data transfers. The data transfers and their timing and logic are represented in a driver model.

The use of parametric submodels for physical and chemical processes adds requirements to the data developed during the previously discussed investigations. First, the detailed studies to be performed on waste package processes must be analyzed for sensitivity of parameters; and second, once the sensitive parameters are identified, descriptive parametric relationships for those processes must be developed. Those relationships may take several forms (e.g., data tables, regressions, and simplified mechanistic models);

however, they must be valid and computationally efficient. Therefore, a third requirement is that submodels that describe processes be validated.

Some indication of the probability of parameter values must also be supplied to perform the probabilistic analysis required for NRC review (NRC, 1983, 1986). At a minimum, sufficient information will be required to perform bounding value calculations of performance so that conservative estimates of performance can be made. Finally, integrated tests of the interaction of several processes will be needed to provide a means for partial validation of the system model.

Clearly, the waste package functions within the larger setting of the total repository. Total system performance assessment is discussed in Chapter 8. Scenarios for anticipated and unanticipated events must be supplied by the total system performance assessment. Although these scenarios are data needs for the waste package performance assessment, they do not generate information needs to be satisfied within waste package activities. This information will be developed in the total system performance activities and will not be discussed in detail in this section. It should be recognized that bounding estimates of performance will often depend on the scenarios for these events.

In summary, the information needs of performance assessment are basically satisfied by the needs of the studies supporting the assessments. The work done to address these needs is discussed in greater detail earlier in this chapter; the plans for collecting additional information is described in Chapter 8. Performance assessment requires that those investigations assess the relative sensitivity of the parameters affecting the individual processes and formulate predictive relationships from these parameters. Further, for those parameters used by the submodels, information describing the probability assigned to given parameter values is also necessary. Finally, data for verification and validation of the predictive methods used must be supplied.

Our approach to developing models for the system performance assessment has several stages. First, a model is being developed that integrates the processes affecting the postclosure performance of a nuclear waste package, with deterministic outcome under a given set of conditions and design parameters. Second, recognition will be given to the distribution of waste heat loadings, emplacement times, and fabricational and environmental parameters in the ensemble of waste packages. Repeated calculations with the model of a single waste package can assess the postclosure performance of the ensemble of waste packages. Third, a probabilistic reliability analysis methodology will be selected and implemented to assess reliability in the waste packages' performance. This methodology will include tools of failure modes and effects analysis, anticipated and unanticipated events scenario analysis, and propagation of input parameter uncertainty, as appropriate. The reliability topics are of two related types: (1) what is the reliability with which the waste package performance values will meet or surpass the postclosure requirements and (2) what is the estimated distribution of the waste package performance values. The products of each of the three stages may be used in sensitivity analysis to quantify the sensitivity of the results of the integrated process to input parameters and to subprocesses.

The deterministic system model of a nuclear waste package performance is being developed in three cycles, to track phases in waste package design, (i.e., conceptual design, advanced conceptual design, and license application design). The purposes of the first-cycle model are to get some informative results from incorporating important processes in the model, to explore for effects of coupling that were not apparent from models of individual processes, and to explore for any information needs not already recognized by the other waste package investigations (Sections 7.5 and 8.3). The conceptual model is described in the following paragraphs to provide the performance modeling perspective for data requirements. Data from site characterization are required for model synthesis, verification, validation, final waste package performance assessment, and final reliability assessment. At each design stage, assessments of waste package performance will serve as a design input.

The following parts of Section 7.4.5 describe the conceptual model development of the first cycle of the deterministic system model. The conceptual model development (O'Connell and Drach, 1986) was based on information in drafts of the SCP, Chapter 7, and on internal reviews by experienced personnel within the NNWSI Project. Section 7.4.5.2 briefly discusses the principal processes that affect waste package performance. This identification is already a modeling step in that it involves selection of the processes to include in the first system model and corresponding computer code. Section 7.4.5.3 is a brief aside to explain that the site-specific processes at the Yucca Mountain unsaturated tuff site are sufficiently different form those included in previous waste package models to require development of a new model. Section 7.4.5.4 describes the conceptual model for the first cycle of the NNWSI deterministic system model.

Included in this background material are summarized results of preliminary performance assessment calculations for some individual physical and chemical processes. Note, however, that these calculations do not represent integrated performance assessment results. The results presented are first estimates of bounding calculations for individual processes, often under different assumed conditions. However, they provide some initial insight into the expected performance of individual waste package components based on work to date. Section 7.4.5.5 identifies some possible techniques for use in probabilistic reliability analysis.

7.4.5.2 Processes affecting waste package performance

This subsection summarizes the important processes affecting the waste package performance. More detail, process information status, and modeling status are provided in later subsections. The summary is based principally on the detailed presentations in Section 7.4.2 on metal barriers and in Section 7.4.3 on waste form performance research and testing. The processes described are assumed to be acting on a waste package. Prospective waste package designs are described in Section 7.3.

The current waste package design provides a sealed metal container barrier. For a single container, a containment failure is assumed to occur when the barrier integrity is lost. This integrity loss can develop by

either mechanical means (e.g., rupture due to stress) or chemical means (e.g., uniform corrosion, stress corrosion cracking, or pitting corrosion). Processes leading to containment failure are also influenced by the nearby external environment (e.g., rock failures that can cause localized stress on the waste package, ground-water hydrology, and ground-water chemistry). The processes leading to containment failure are also influenced by the interaction between the internal and external environments. Examples include (1) the heat generated by the radioactive waste and transferred to the external rock, thus establishing a temperature field, and (2) gamma radiation generated by the waste and attenuated by the waste and metal barriers producing a net gamma ray flux at the surfaces of the metal barriers. The gamma ray flux can cause radiolysis in the water and perhaps can increase the corrosion rate. Loss of containment for the ensemble of containers occurs when enough individual containers have experienced failure so that the consequential release of radionuclides exceeds some threshold value.

For spent fuel, the Zircaloy cladding may provide an additional barrier to release of materials from the fuel pellets and, even when partially breached, may help limit the rate of release from the waste. A small part of the spent fuel radioactive waste consists of activated elements in the Zircaloy itself and in the stainless steel framework of the fuel assemblies; for these waste components, the cladding or metal components degradation rate determines the release rate of radionuclides.

Processes influencing or leading to the loss of waste package containment can be listed as follows:

1. Radiation.
    a. Gamma ray source.
    b. Gamma ray attenuation.
2. Thermal.
    a. Heat source from radioactive decay.
    b. Heat transfer, temperature field effects.
3. Mechanical loads.
    a. External (pressure, general, or localized).
    b. Internal (pressure).
    c. Thermal expansion.
4. Yielding.
    a. Ductile rupture.
    b. Crack extension.
    c. Brittle rupture from a crack.
5. Ground-water movement and chemistry.
    a. Flow surrounding engineered barrier system.
    b. Flow mechanisms for water contacting the waste package.

c. Transport in nearby host rock.
d. Water volume available for contact with waste package.

6. Corrosion.

a. Uniform corrosion.
b. Stress corrosion cracking.
c. Pitting and crevice corrosion.
d. Galvanic corrosion.
e. Other corrosion modes.

Some of these processes are continually in a quasi-steady state. For example, with some time lag during the first few years after emplacement, the temperature distribution is essentially in equilibrium with the heat generation, which changes very slowly. The stress distribution forms a static equilibrium with the internal and external forces. Other processes cause gradual changes (e.g., uniform corrosion that reduces barrier thickness). Some processes cause abrupt and discrete changes (e.g., perforation of a barrier due to mechanical rupture or due to corrosion penetration reaching the full thickness of the barrier).

The existence and rate of waste release from the waste package are dependent on three processes:

1. Existence of a penetration of the metal container, opening a potential path between the waste form and the external environment.

2. Alteration of the waste form, converting some part of the waste into mobile form.

3. Transport of the mobile form of the waste from the waste form to the external medium (the rock around the borehole).

The major part of the waste is in the spent fuel's uranium-oxide-matrix fuel pellets or in the glass matrix for reprocessed waste. The mobilization of this waste in ground water is assumed to be governed by its solubility in the local ground water. Transport from the engineered barrier system (EBS) is through or with ground water. For the spent fuel, there are a few exceptions: (1) some radioactive elements due to activation of structural materials are in the Zircaloy cladding and in the metal framework of spent fuel assemblies; (2) some elements may be released in gaseous form, principally carbon-14 in the oxidized form of carbon dioxide; and (3) a gap-grain-boundary inventory of the waste is available in a form that can be released rapidly into water after the Zircaloy is breached (Oversby and Wilson, 1985).

The rate of waste form alteration depends on the amount and duration of ground-water contact with the waste form (Section 7.4.3). This contact, in turn, depends on the ground-water flow and on the waste container conditions (e.g., one small breach, several small breaches, many breaches, or essentially dismantled). The rate of waste form alteration may also depend on the temperature, water chemistry, gamma ray flux at the waste form-water interface, and waste form material damage accumulated due to alpha decays and

spontaneous fissions within the waste form. The rate of waste form alteration will also depend on the rate of mobile waste transport away from the waste form-water interface.

The mobilized waste may increase the gamma radiation flux near the barrier surface and hence may increase the rate of corrosion of the breached barriers. This is not expected to be an important factor, however, because (1) the radiation source strength will be low by the time the barriers become breached (Croff and Alexander, 1980) and (2) only a small fraction of the waste will be in mobile form in the waste package volume (Oversby and Wilson, 1985).

In summary, the processes affecting the rates of waste form degradation and release from the waste package include most of those listed for barrier failure, plus the following:

1. Radiation.
    a. Alpha radiation (and spontaneous fission) source.
    b. Alpha (and fission) integrated quantities.
2. Waste form alteration.
3. Transport of mobile waste.

The parameters affecting each process and the interactions between processes are described in Section 7.4.5.4.

7.4.5.3 Earlier models of similar scope

Earlier deterministic models of waste package performance are BARIER (Stula et al., 1980) and WAPPA (INTERA, 1983). These waste package system models have relatively simple submodels of each process and treat the interactions of the processes over time, as does our approach.

WAPPA was examined and tested for possible application to the NNWSI Project waste package. That WAPPA provided a good starting list of phenomena and concerns that should be addressed. However, specific aspects of the NNWSI Project candidate repository indicated that additional submodels were needed for waste package design and site-specific conditions. For example, the NNWSI Project waste forms include spent fuel in several geometric arrangements. The heat transfer problem is thus somewhat different. A gamma ray dose attenuation model adequate for sensitivity analysis was needed. WAPPA assumes a location below the water table. The NNWSI Project repository location is above the water table in the unsaturated zone. Hence, the mechanisms of ground-water flow, water contact with the waste package, waste form alteration, and mobilized waste transport differ substantially from those assumed in the WAPPA formulation. Therefore, it was decided to develop a new waste package performance program specific to the NNWSI Project site conditions and design parameters.

7.4.5.4 Nevada Nuclear Waste Storage Investigations Project waste package system model description

This section briefly describes the system model for waste package performance currently under development (O'Connell and Drach, 1986). The system model must treat the waste packages and processes described earlier. The system modeling approach is to model the processes separately as far as possible and then couple these models through an explicit set of data transfers. The process models are simplified ones, combining parametric models and sets of data tables. Detailed models of one or two processes are available or are being developed. These detailed models calibrate the degree of accuracy of the simpler models or provide the data tables. The system model geometry has one dimension of variation, the radial direction in a cylindrical geometry. End effects will be examined in future work. Currently only the more detailed supporting models can treat end effects.

The process models include the following seven models:

1. Radiation model.
2. Thermal model.
3. Mechanical model.
4. Waste package environment model.
5. Corrosion model.
6. Waste form alteration model.
7. Waste transport model (covering transport within the waste package system).

Each model may consist of several interacting or related submodels with diverse time characteristics as noted in Section 7.4.5.2. Functions of the individual models are described and then data interactions and the sequencing of these interactions will be described. The data interactions lead to a grouping of submodels by time characteristics rather than solely by model topic.

7.4.5.4.1 Waste package geometry

The waste package model describes the initial geometry and properties and tracks the current conditions of the waste package in time. A cylindrical geometry is assumed with variability only in the radial direction. Because of the large length-to-radius ratio of the waste packages, an assumption of no axial variation seems suitable over most of the length of the waste package. An examination of processes active in directions other than the radial directions will be conducted to substantiate this assumption. If axial variations are found important, the model will be modified as required. Different conditions at the ends of the waste package will require evaluation in future work. Cylindrical symmetry seems suitable in most

instances but its use for some types of spent fuel assemblies (Figure 7-2) will represent a coarser degree of approximation and will require comparison with two-dimensional calculations.

The Zircaloy cladding may serve as an additional release barrier protecting the spent fuel waste form. This barrier does not have the common radial center of the outer barrier(s) but does have the logical relation of one barrier within another. Such barriers, as well as the waste forms, will be tabulated with their logical contained-within-barrier relations and the larger-scale annulus within which they are located.

7.4.5.4.2 Radiation model

The radiation model treats radiation sources and radiation doses in the waste package. The source submodel calculates the heat generation rate, the radiation generation rates, and the radionuclide inventory. The gamma ray dose submodel calculates the gamma ray absorbed dose rate in water at locations in the waste package where corrosion or waste form alteration may take place. The waste form dose model calculates the dose, in terms of atomic displacements per unit volume, due to alpha particles and spontaneous fission. The effects of these dose rates and doses will be considered in the corrosion and waste form alteration models, respectively.

The source submodel interpolates data from tables generated by the ORIGEN2 code (Croff, 1980). ORIGEN2 calculates the burnup of nuclear fuel and the buildup and decay of fission products, activation products, and decay products during reactor operation and after the fuel has been removed from the reactor. ORIGEN2 also accounts for the partitioning of elements if reprocessing is done. The ORIGEN2 tables provide data, as a function of time since removal from the reactor, for a unit quantity of waste derived from nuclear fuel of a specified type and burnup. The unit quantity is the amount of derived waste (or spent fuel) per metric ton of heavy metal (MTHM) originally in the fuel. The source model scales from the tabulated unit quantity to the quantity of waste in the waste package.

The waste form is both a source and an attenuator of gamma rays. The metal barriers are attenuators of gamma rays. If and when water is present at the surface of a barrier or of a waste form, the gamma ray absorbed dose rate in water is significant because of the resulting radiolysis of either liquid or gaseous water. This radiolysis may cause enhanced corrosion or enhanced alteration of the surface of the barrier or waste form.

The attenuation and absorbed dose rate from gamma rays are complex processes. A simplified model cannot be expected to calculate the results from first principals. Rather, reference data from measurements or from detailed calculations is needed. For reference data, the detailed code MORSE-L (Wilcox, 1972), which calculates radiation transport using a Monte Carlo method, will be used. This code has a history of extensive use. Calculations for a spent fuel canister emplacement (Wilcox and Van Konynenburg, 1981) have been validated by measurements (Van Konynenburg, 1984) taken in a granite repository.

The gamma ray dose submodel within the system model will scale or adapt results from a MORSE-L reference calculation to a range of similar waste forms and waste package designs. Two scalings will be performed: the first scales the absorbed dose rate at the waste form surface, and the second scales the attenuation factors between the waste form surface and the barrier surfaces. The waste forms are self-shielding sources, with radii considerably greater than their gamma ray energy absorbtion lengths. This allows a simplified scaling of results for dose rate at the surface. The absorbed dose rate at the waste form surface is scaled linearly with gamma ray source strength in (average MeV x number)/(sec x m^3), and inversely with source mass density. There is to first order no effect from the radius of the waste form, and within a limited range of waste form materials, only a small adjustment for the percentages of atomic composition of the waste form. The absorbed dose rate at the waste form surface times this attenuation factor gives the absorbed dose rate at a barrier surface.

The attenuation factor for absorbed dose rate depends primarily on the mass thickness in kg/m^2 between the waste form surface and the point of observation, with only a small adjustment for the percentages of atomic composition of this intervening material; and it depends on a geometrical factor of one per radius due to the cylindrical geometry. Thus a scaling from a reference calculation can be done between points with the same mass thickness between the waste form surface and the point of observation.

The accuracy of this scaling approach will need to be validated by comparison with a series of MORSE-L calculations, which will determine whether a few or many reference calculations are needed to provide a basis for scaling to a range of waste package designs.

The waste form dose model for atomic displacements per unit volume is simple. Alpha particles and fission fragments have short ranges but cause atomic displacements as a side effect of their slowing-down process. These displacements do not fully anneal at the temperatures encountered in high-level waste disposal. Experimental factors are used for the number of atomic displacements per alpha particle and per spontaneous fission. The model accumulates these displacements over time generated by the respective radiation source rates. For spent fuel, the displacements caused by these processes during emplacement are not expected to be a significant factor with respect to waste package performance since most displacement will have occurred in the reactor environment (Woodley, 1983).

7.4.5.4.3 Thermal model

The thermal model calculates temperature as a function of radial position in the waste package. As input, the model requires (as functions of time) the heat generation rate of the waste form and the boundary temperature at the waste package-borehole wall interface. This boundary temperature will be calculated by a more detailed model that handles dynamic conditions and three-dimensional geometry of the waste containers and repository configurations. The thermal submodel assumes a steady-state condition inside the waste package. The temperature gradient across each component of the waste package is that needed to transport the power generated in the waste form.

The thermal model results will be used as inputs to the mechanical, corrosion, package environment, release, and waste transport models.

A detailed model, TAC02D, a code developed by Burns (1982), has three-dimensional and transient capabilities. The model has been extensively used. The three-dimensional geometry of the waste package and emplacement can be reduced to the two-dimensional calculation in TAC02D by using axisymmetric or plane symmetry and the regular repetition of waste package emplacement locations (Stein et al. 1984). TAC02D handles dynamic conditions, a necessary capability when the repository rock mass is included in the heat transfer calculation. TAC02D does not include hydrothermal effects. WAFE (Travis, 1984), a hydrothermal model currently under testing and development, has the geometric and dynamic capabilities of TAC02D and also considers the heat-transfer effects of vaporizing and recondensing the pore water in an unsaturated medium. This model is also currently being used to characterize the hydrothermal environment surrounding the waste package. TOUGH (Pruess and Wang, 1984) is another hydrothermal model currently under testing.

The steady-state assumption inside the waste package neglects the heat capacity of the waste package. This leads to only a small overestimate of waste form peak temperature.

The steady-state one-dimensional thermal model to be used in the system model is nearly the same as that of WAPPA (INTERA, 1983). Its results agree with those of TAC02D, which was used to calculate thermal histories of reference waste packages (Hockman and O'Neal, 1984) to within 7 percent. The disagreement occurs only at early times near the time of peak temperature, based on rise above ambient temperature.

7.4.5.4.4 Mechanical model

The mechanical model calculates the stress at various locations in the waste package. Contributions will come from external loads, thermal expansion and thermal gradient stresses, volume expansion of corrosion products, and residual stresses from waste package fabrication. The mechanical model will check for mechanical failure modes such as yielding and unstable propagation of a crack (i.e., rupture). Stable crack extension that could result in a physically larger breach in the container will be considered for a future model version.

The surface stress from the mechanical model will be used as input to the corrosion model. The waste form mechanical integrity condition will be used as input to the waste form release model. Changes in barrier integrity may also affect the thermal behavior and thus will be used as input for the thermal model as well.

The NIKE2D code (Hallquist, 1983) has been selected as a detailed model for mechanical stress analysis of the waste package. To further check the mechanical model, the approximate formulas for thin-walled pipes given in the ASME Boiler and Pressure Vessel Code (ASME, 1983) will be used. These formulas may be compared with the mechanical model results when thin-walled metallic barriers in the waste package are modeled.

7.4.5.4.5 Waste package environment model

The waste package environment model will evaluate the flow of water, steam, and air that can affect the waste package barriers and the waste form and assist in waste transport. This model will ultimately include fluid flow rates, paths, and chemical contents for flows to, within, and from the waste package. The waste package environment model should describe the process of water contact with the waste package or waste form. Mechanisms of contact might include unsaturated porous flow, localized dripping, and standing water in a partially degraded waste package.

The mechanisms and quantity of water flow may limit the amounts of corrosion and of waste form alteration. A description of detailed hydrothermal modeling of fluid flow in the host rock surrounding the waste package fluid flow is a future information need (Sections 7.4.1 and 8.3.5.10). For the present system model, a simplified bounding model of the fluid flow is being used. The water flow rate is bounded as described below. The water chemical content is effectively bounded by using experimental corrosion and alteration rates determined with appropriate water samples.

As input, the simplified bounding model takes the time of reestablishment of the liquid water continuum, at the rock boundary of the waste package emplacement borehole, from a more detailed model or evaluation. It also uses the regional ground-water flux value, or a bounding value on that flux. The simplified model assumes that, starting with the time of rewetting, all the regional downward water flux that intersects rock disturbed by repository construction comes into contact with the waste packages. Each package is assigned a catchment area that encompasses an area halfway to neighboring waste packages in each direction.

This modeled water flux is assumed to be an upper bound on the average water flux per waste package. Oversby and Wilson (1985) have calculated the bounding flux to be 40 L/package-yr for spent fuel packages assuming a recharge flux of 1 mm/yr. If no diversion of water toward waste packages were to occur, the flux per package would be approximately 0.5 L per year for a recharge flux of 1 mm/yr passing through a 76-cm diameter vertical borehole.

7.4.5.4.6 Corrosion model

The current corrosion model calculates the corrosion rate and the cumulative thickness of barrier metal altered under two environmental conditions: moist air and water. Each rate may be a function of temperature and gamma ray dose rate; dependence on water chemistry may be added when the water chemistry data become available from the waste form environmental model. The data on corrosion rate in water are input by the program user; they may represent uniform corrosion or uniform and pitting corrosion. The waste package will most likely not be wetted uniformly; the intent is to calculate the corrosion rate at the most critical location.

A future corrosion model will incorporate checks for sensitization history and for environmental conditions that would allow other local modes

of corrosion such as intergranular stress corrosion cracking, pitting, and crevice corrosion. Threshold conditions for these modes, or envelopes on such thresholds, and corrosion rates will be established for use in the model. Determination of these conditions will require an assessment of the considerable uncertainties that accompany corrosion models. These uncertainties are an important component of the metal degradation investigations and will be incorporated in the performance assessment model.

Corrosion-induced changes in material thickness will affect the thermal and mechanical behavior of the container. Ultimately, these changes will also affect fluid flow and waste form release behavior. Corrosion model output will be used as input to the corresponding models. The corrosion rate may depend on data from the thermal and gamma ray dose rate models, or a bounding rate may be used.

The corrosion model will find the following in data tables that will be supplied by the metal barriers subtask:

1. Rate of corrosion of the metal (micrometers per year).

2. Percentage of the corrosion product that remains on the surface as a solid layer.

3. Rate of removal of an existing corrosion product layer by water.

Another data item required for transfer to the mechanical model is the change in specific volume between a unit of metal and the corresponding amount of solid corrosion product.

Sections 7.4.2.8 and 7.5.4.6 summarize investigations and data to date on corrosion of the austenitic barrier materials. In water, general corrosion is the most likely corrosion mode, and pitting corrosion may be expected in some locations on the barrier; but the rates are low enough that these degradation modes are not likely failure modes. One corrosion mode that may be a likely failure mode is intergranular stress corrosion cracking. This mode depends on sensitization (Section 7.4.2.5) versus temperature history (see Section 7.4.1.2 and the systems model's thermal model) and on stress (see the system model's mechanical model).

Tests to quantify sensitization and stress corrosion cracking will be conducted during characterization (Section 8.3.5.9, Issue 1.4). When results are available, the process will be added to the corrosion model.

7.4.5.4.7 Waste form alteration model

The waste form alteration model will calculate the annual quantity of each radionuclide converted into mobile forms. The mobile forms are assumed to be solutes in water, carbon-14 in the form of carbon dioxide, and noble gas radioisotopes. The processes and the input values to be developed for both spent fuel and glass waste forms are discussed in Section 7.4.3.

The radionuclide mobilization rate of spent fuel is limited by properties of the waste form (such as the solid matrix form of spent fuel, Zircaloy and steel framework components) and the initially intact cladding of many of the fuel rods.

The radionuclide mobilization term for spent fuel includes five components:

1. Elements whose release is controlled by the spent fuel matrix dissolution rate.

2. Elements present in part in the pellet-cladding gap and available for rapid release when the cladding is breached.

3. Elements contained in stainless steel or Inconel support components.

4. Elements contained in the Zircaloy or stainless steel fuel cladding.

5. Elements present in part in the oxidized layer present on the outer surface of the Zircaloy and available for rapid release when the container is breached (i.e., Carbon-14).

Initially, the model for each component is essentially a table look-up based on data to be determined under relevant conditions of water flow and environment.

Cladding degradation has two functional effects. Cladding corrosion exposes activation products contained in the cladding material for mobilization. Localized degradation leading to cladding breach initiates the exposure of the spent fuel within the fuel rod. The rates for each of these processes will be inputs to the model (Section 7.4.3.1.3). The current model treats a percentage of initially failed fuel rods and degradation of only a single leading fuel rod as representing all intact fuel rods within the package; a future model will treat the ensemble of intact fuel rods within a waste package.

The rapid release fraction for a spent fuel rod will all be assigned to the first year after breaching of the fuel rod. Future model development will account for distribution over time of the time-to-breach for waste containers and time-to-breach for cladding of fuel rods, given a container breach.

The degradation rate of spent fuel depends on the water flux, on the mechanism of water flow in the waste package and on the solubility of uranium. If the barrier container has several perforations and the ground water trickles through, then the matrix dissolution rate will be that determined from measurements under similar conditions, as a function of water flow rate. If the barrier container has one perforation placed so that water can fill the container, then the spent fuel will eventually be exposed continuously to a nearly fixed mass of water. A small rate of inflow of new water will be assumed to displace an equal amount from the standing water. In this instance, the matrix dissolution rate is determined by the matrix dissolution together with the recharge water flow rate. The matrix dissolution rate will depend on uranium solubility.

The approach to waste form alteration modeling for spent fuel is consistent with the methodology presented in Section 7.4.3.1.4. The definitive data for the model are an information need (Sections 7.4.5.7 and 8.3.5.10).

For a glass waste form, the waste form alteration model assumes that release of all elements is controlled by the matrix alteration rate. Similar to the spent fuel case, this rate will be input as determined for two water flow scenarios: the trickle-through scenario and the standing-water scenario. Under very conservative conditions, which differ from those for spent fuel, Aines (1986) estimates that release rates from glass waste forms are approximately 0.08 part in 100,000 per year.

More precise results taking conditions into account are an information need (Sections 7.4.3.2.3, 7.5.4.8, and 8.3.5.10).

Some radioactive elements may be mobilized more slowly than indicated by their congruent release with the spent fuel matrix because of their low solubility. For glass waste forms, surface layers formed with secondary products and additional interactions of the glass-canister-water-rock system may slow down the mobilization of waste elements (Section 7.4.3.2.3). These features are neglected in the first-generation model, but they will be included in later versions.

7.4.5.4.8 Waste transport model

A hydrothermal flow and waste transport model will calculate the flux of each radionuclide at the waste package-repository host-rock interface. The interface is at the borehole wall. Ultimately, this prediction will be a function of the flow, transport, and chemical processes active in the host rock immediately adjacent to the emplacement hole. A waste package near-field environment model will be incorporated to provide a link to near-field processes since package performance both depends on and affects this environment (e.g., the heat flux from the package affects hydrology and geochemistry). This near-field environment model will combine effects from the supporting models for the radiation, thermal, hydrothermal, and fluid chemistry models (see previous subsections of Section 7.4.5.4).

The submodel in the first system model revision will be simplistic and conservative. For water soluble elements, the model considers advection with the water flux. The first-generation model assumes that the water flux out equals the water flux in after any storage volume within the breached container is filled and that any elements mobilized in the water filling the canister are transported out of the waste package volume proportionally with the existing water flux.

Gas phase transport is by diffusion into the host rock. Any gases mobilized are assumed available immediately for transport beyond the boundary of the waste package.

The flux of transported radionuclides will be in units of a fraction per year of the current inventory of a whole waste package. The flux will also

be reported in units of grams per year and in units of the fraction per year of the activity of a whole waste package at 1,000 yr after repository closure. The model will require, as inputs, the fluid flow results and the waste mobilization rate within the waste package volume.

7.4.5.4.9 Driver model

The driver model couples all the process models, calculates the time history of the waste package's condition and processes, and from this time history extracts the performance measures.

The specific solution is essentially determined by the initial conditions and the boundary conditions over time. Figure 7-36 shows the overall structure of operations establishing the initial and boundary conditions and calculating the waste package performance. Gane and Sarson's (1979) notation is used for data flow diagrams (Figure 7-37).

Data delivered to the process models must have the current-time values. Data flow diagrams show the logical dependencies of data needs but abstain from specifying program sequence or control. Data flow diagrams are a good starting point for the specification of the necessary properties of the linkages among the process models.

The construction of the data flow diagrams for the driver model is presented in a sequence to express some of the time properties of the data and to clarify parts of the process being modeled. Some data adjust to the boundary conditions with essentially no time delay (e.g., radiation, temperature, and stress). Some data change slowly with time (e.g., intact barrier thickness as reduced by corrosion). Some data have discrete values and change infrequently (e.g., barrier surface environment (dry/wet)).

Table 7-26 identifies the data elements in the data flows that follow. Figure 7-38 shows some data that adjust immediately to the boundary conditions and also shows the associated processes. The radiation model's heat source rate, radiation source rate, and attenuated gamma ray dose rate are immediately dependent on the input value from the radiation source time history. The temperatures adjust to the heat source rate and the input value from the boundary temperature time history. The mechanical stresses immediately find a static equilibrium dependent on the temperatures and the input value from the boundary pressure time history.

The environmental condition and the corrosion rates also depend on the current-time boundary conditions and on the data shown in Figure 7-38 (refer to Figure 7-39). Note that an additional output from the environmental model has a time delay.

Some waste package data change slowly over time. For example, the geometry (intact container wall thicknesses) changes slowly due to general corrosion (Figure 7-40).

Now the sequence of diagramming has reached a closed feedback loop. The processes in the loop are shown in Figure 7-41. (The external data stores of

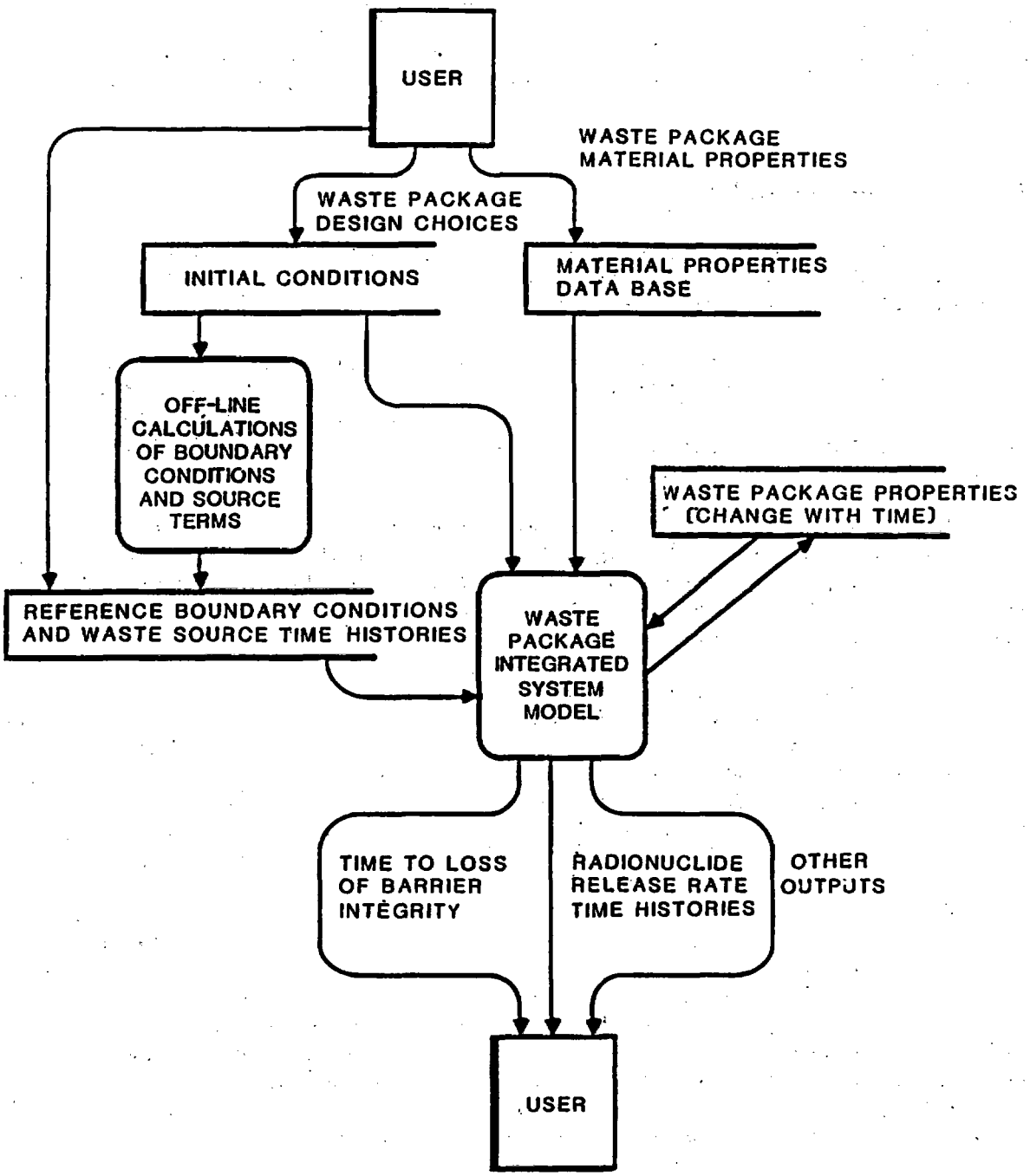

Figure 7-36. The data flows, data stores, and grouped inputs and outputs for the waste package system performance problem. (See Figure 7-37 for notation used in data flow diagrams.)

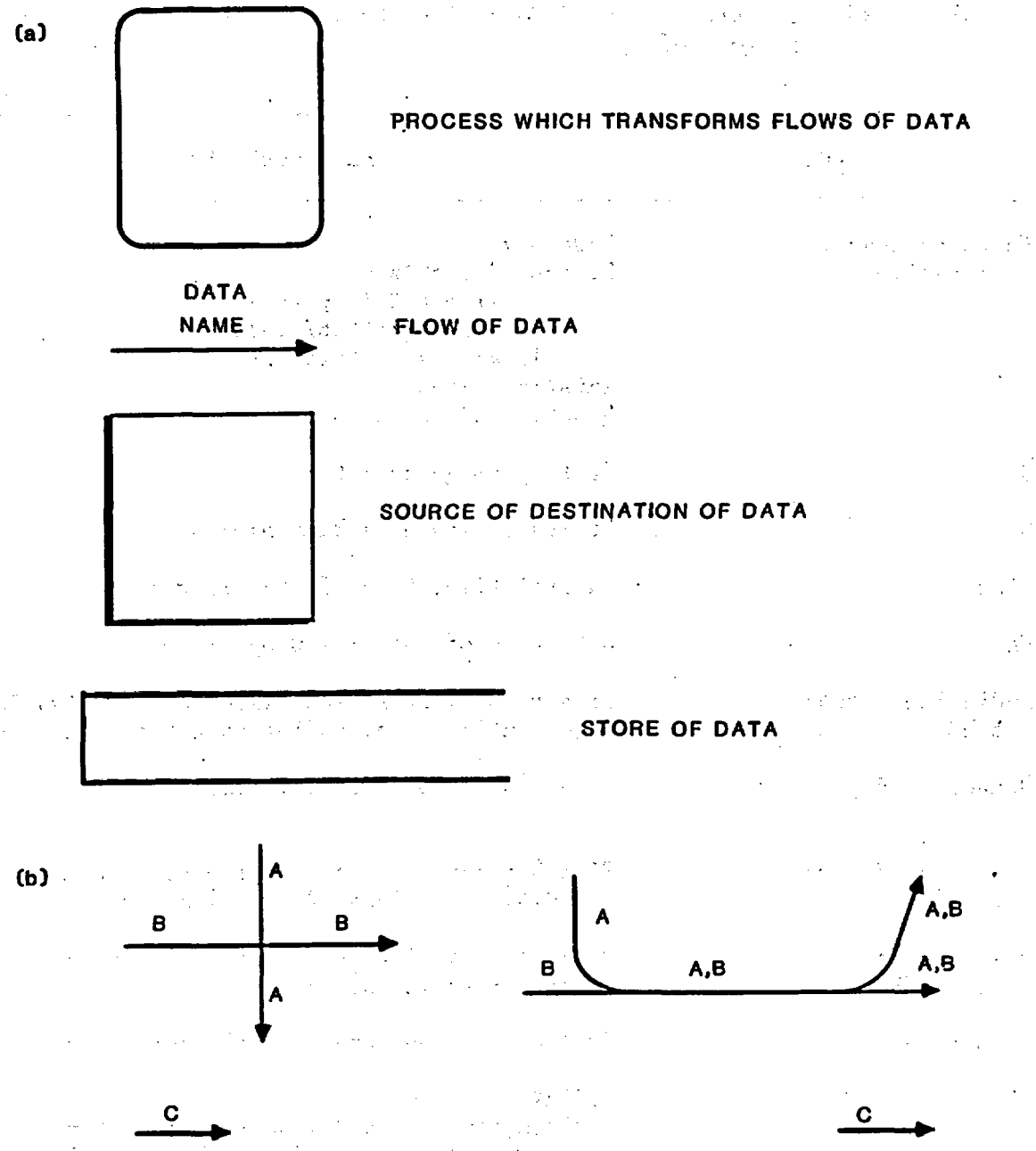

Figure 7-37. *Data flow symbols and conventions: (a) shows data flow symbols and (b) conventions.* Crossed data flow lines do not join, merging lines do join. To avoid "spaghetti diagrams," connectivity may be indicated by labeling with the data group name, or an entity such as a data store may be drawn in duplicate positions. A data flow indicates data needs and sources; it does not indicate sequence or control.

Table 7-26. Identification of data elements in the data flow diagrams (page 1 of 2)

Label	Data contents
Waste package properties	Geometry Status of elements Environment (dry/wet) Strength (intact/yielded) Integrity (intact/breached) Material types Quantity of waste form
G	Waste package geometry
S	Status of waste package elements
Time	Current time, time of next time step
DB	Data base of material properties
Radiation source t/h[a]	Time history of radionuclide inventories, heat generation rate, radiation generation rate
Boundary temp t/h	Time history of boundary temperature
Boundary pressure t/h	Time history of external pressures in axial and radial directions of waste package
Boundary fluid flow t/h	Time history of rate of water flow into the waste package volume
Heat rate	Heat generation rate of each waste form
R1	Radiation data: Gamma ray absorbed dose rate in water at waste form surface of each barrier element
R2	Radiation data: Alpha particle dose (integrated up to current time) in waste form and alpha particle dose rate in water at waste form surface
R3	Radiation data: Inventory of each radionuclide per unit of waste form

Table 7-26. Identification of data elements in the data flow diagrams (page 2 of 2)

Label	Data contents
Temp	Temperature at inner and outer surfaces of each element of the waste package
Stress	Stress components at surfaces of each barrier element and at surface and interior of waste form
Corrosion rate	General corrosion rate for each barrier
Wet (Y/N)[b]	Environmental status of boundary of waste package
Water flow rate	Water flow rate into the waste package volume
New thickness	New thickness of intact container and of corrosion layers
New barrier status, new dimensions, or no change	Any changes to waste package geometry or status
Time to loss of container integrity	Time of breach of containment function due to loss of container integrity
Standing quantity of water	Quantity of standing water in a partially degraded waste package
Waste mobilization rate, increment	Waste mobilization rate and increment of waste released from the waste form to the waste package volume during a time interval
Waste release rate, increment	Waste release rate and increment of waste released from the waste package to its exterior during a time interval
Mobilized waste quantity in waste package volume	Quantity of waste radionuclides and matrix in mobile form and within the waste package geometric volume
Waste form quantity	Quantity of waste remaining in the unmobilized waste forms

[a]Temperature per hour.
[b](Yes/No).

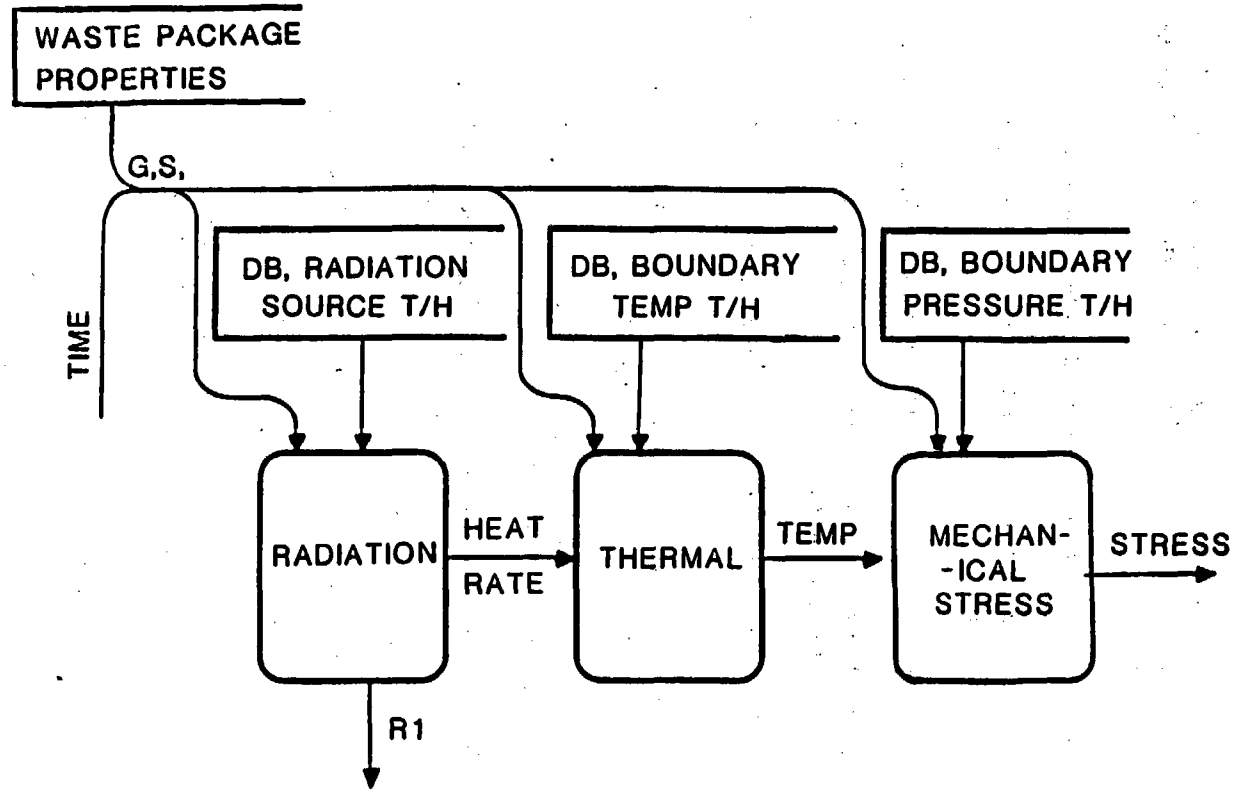

Figure 7-38. Data flows for the radiation, thermal, and mechanical stress processes. The process outputs shown heat rate, temperature, and stress adjust without time delay to the input boundary conditions. (See Figure 7-37 for an explanation of data flow symbols and Table 7-26 for an identification of data elements used in data flow diagrams.)

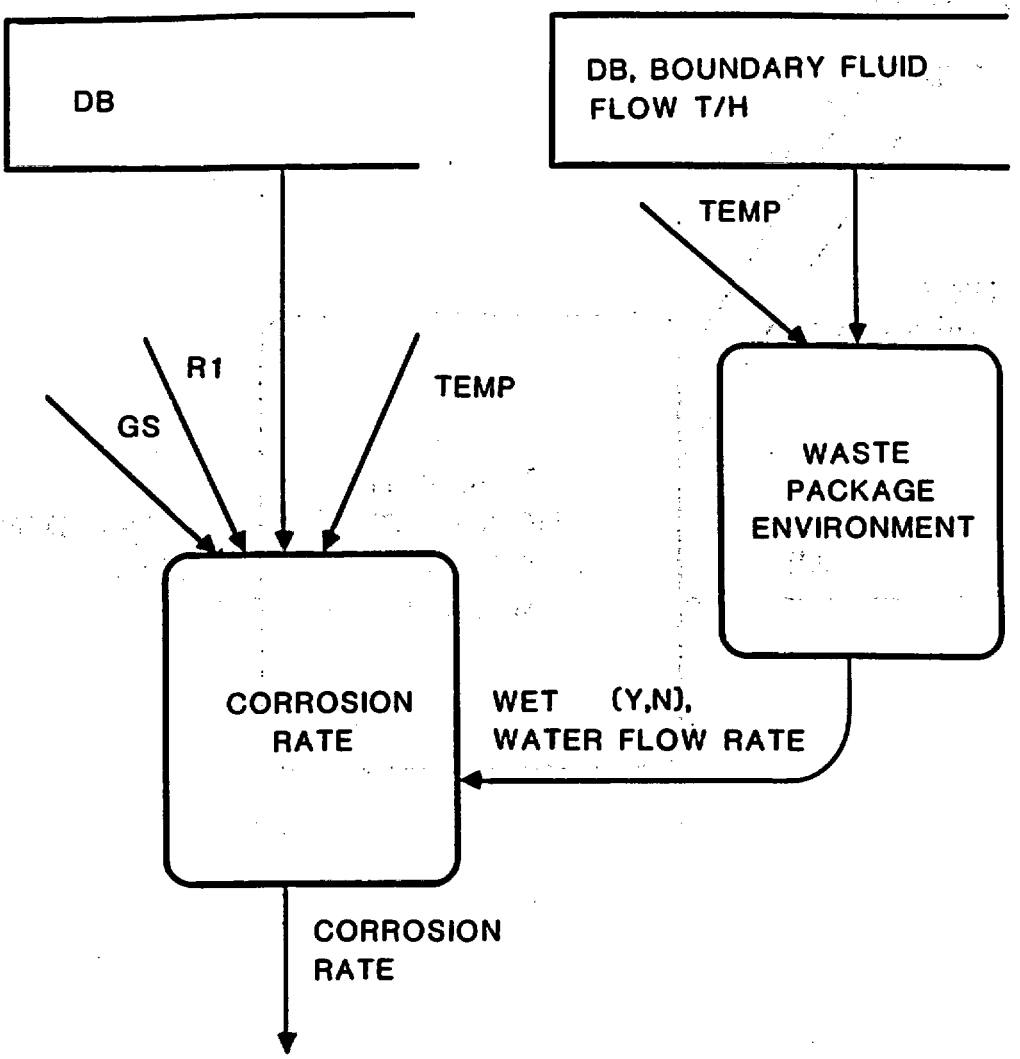

Figure 7-39. Data flows for the waste package environment and corrosion rate processes. The process outputs shown adjust without time delay to the input conditions. (See Figure 7-37 for an explanation of data flow symbols and Table 7-26 for an identification of data elements used in data flow diagrams.)

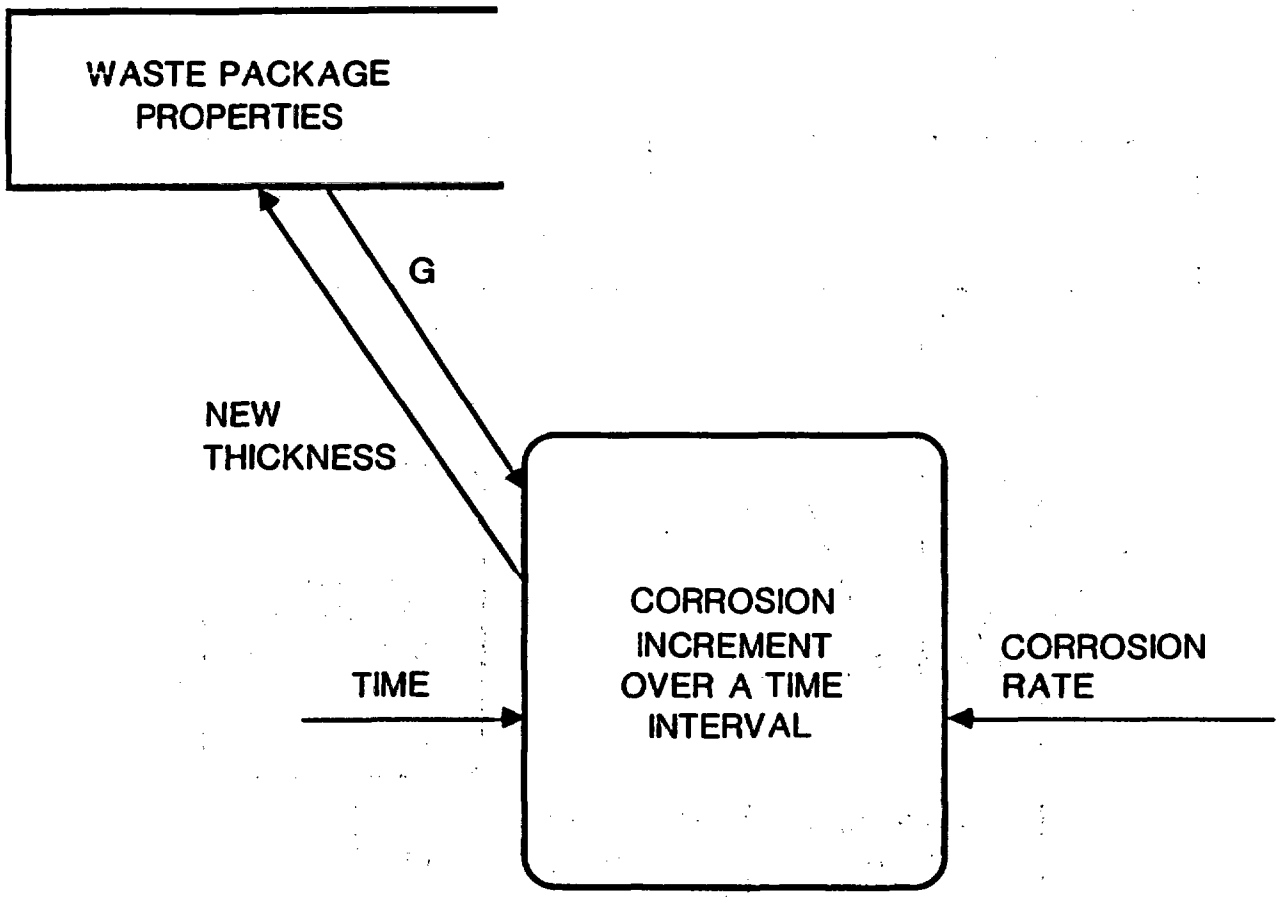

Figure 7-40. Data flows for the corrosion increment process. The output (new thickness) changes slowly: its value depends on past history as well as on current conditions. (See Figure 7-37 for an explanation of data flow symbols and Table 7-26 for an identification of data elements used in data flow diagrams.)

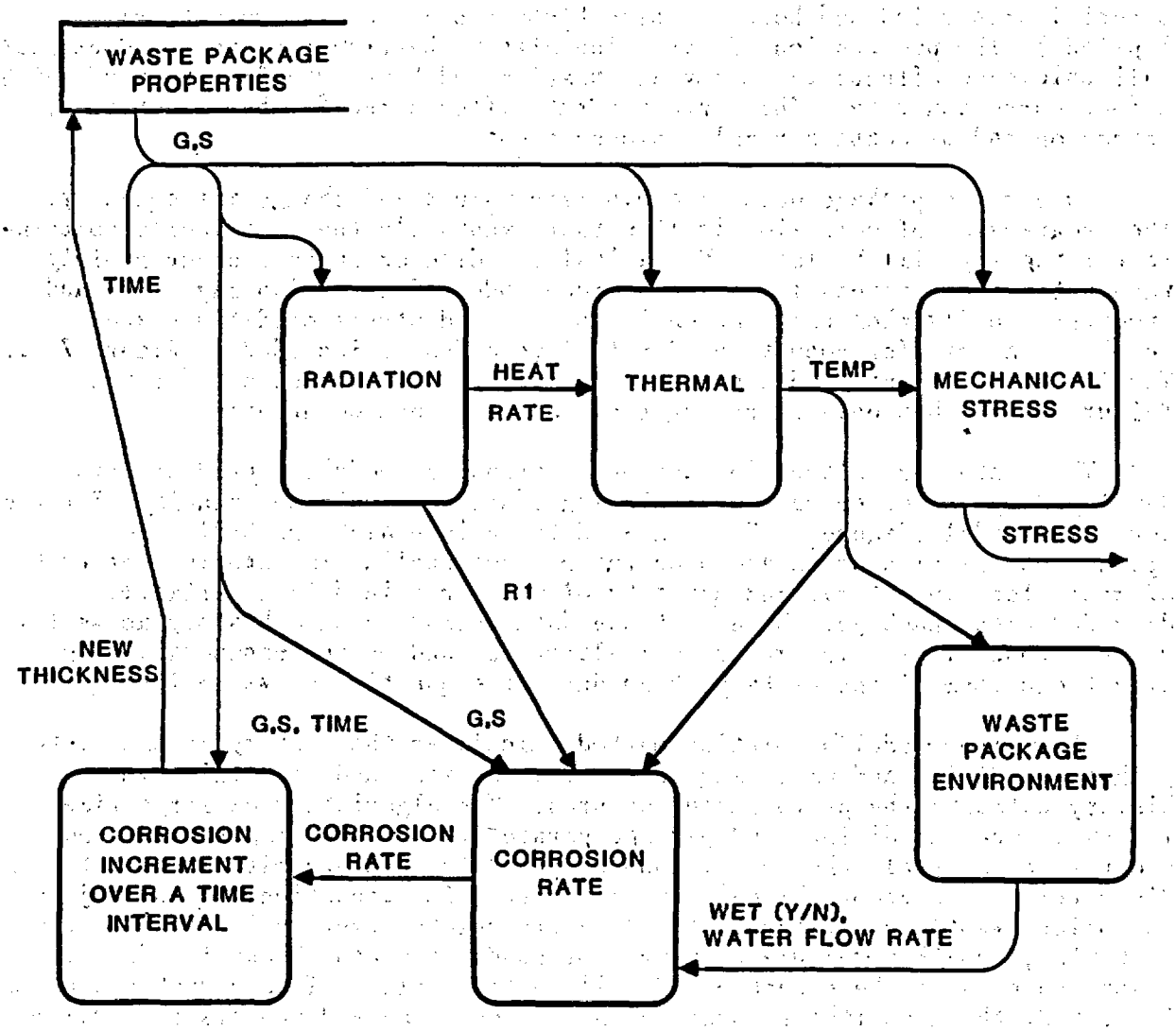

Figure 7-41. Data flow diagram combining the processes shown in Figures 7-38 through 7-40. Some of these processes are coupled in a continuous (over time) feedback loop. (See Figure 7-37 for an explanation of data flow symbols and Table 7-26 for an identification of data elements used in data flow diagrams.)

material properties and boundary time histories are not drawn but are implied.) The progression of corrosion affects barrier thickness. Container wall thickness affects gamma ray attenuation and heat transfer, both of which affect corrosion rate. The corrosion rate affects the further progress of corrosion and of container wall thickness change.

Some waste package data have discrete values and change infrequently. The progression of corrosion implies that eventually the container's containment integrity will be lost. Mechanical yielding or rupture occur rapidly when a threshold stress is reached. Some modes of corrosion may occur and progress rapidly when enabling environmental and stress conditions are reached. A test for conditions for failure modes is included in Figure 7-42. The increment failure modes process requires the time value not for the failure checks but only to report the time of breach occurrence.

The waste form alteration and waste transport models depend on data developed by the other models, including additional data not required for the corrosion model (Figure 7-43). These data include alpha particle and spontaneous fission doses and dose rates, radionuclide inventories per unit of waste form inventory, and quantity of water retained in a partially degraded waste package. Some of these data depend on past history as well as current conditions. The waste form alteration and waste transport models affect one item of the waste package data, the quantity of waste form.

The driver model's solution method calculates the history of the waste package condition and processes in the time domain, and from this time history extracts the performance measures. The algorithm uses large time intervals when conditions and package parameters are changing slowly, and short time intervals when conditions or parameters change with large rates or discretely. The algorithm calculates current-time conditions, then projects corrosion, waste form alteration, and waste release over an interval to the next time, and then calculates next-time conditions and checks for discrete status changes or the exceeding of failure thresholds. If any such change is indicated, the algorithm returns to the current-time and repeats the projection with a smaller time step. If a discrete change occurs during a minimum time interval (specified by the user, down to a minimum of 1 yr), then the waste package status is updated with the change at the current time. If no discrete change occurs during a time interval, then the continuous process results are updated and the next-time becomes the current-time for the start of the next step.

This algorithm models both discrete and continuous changes in waste package condition, identifies the time of breach of containment to within a desired tolerance, and provides radionuclide release rates and release quantities over a time interval. More details of implementation will be developed during the program design stage, but the final algorithm will perform functionally as described in the conceptual model.

7.4.5.5 Reliability analysis

The goal of the reliability analysis is to provide reasonable assurance that the waste packages will meet the postclosure performance criteria. The

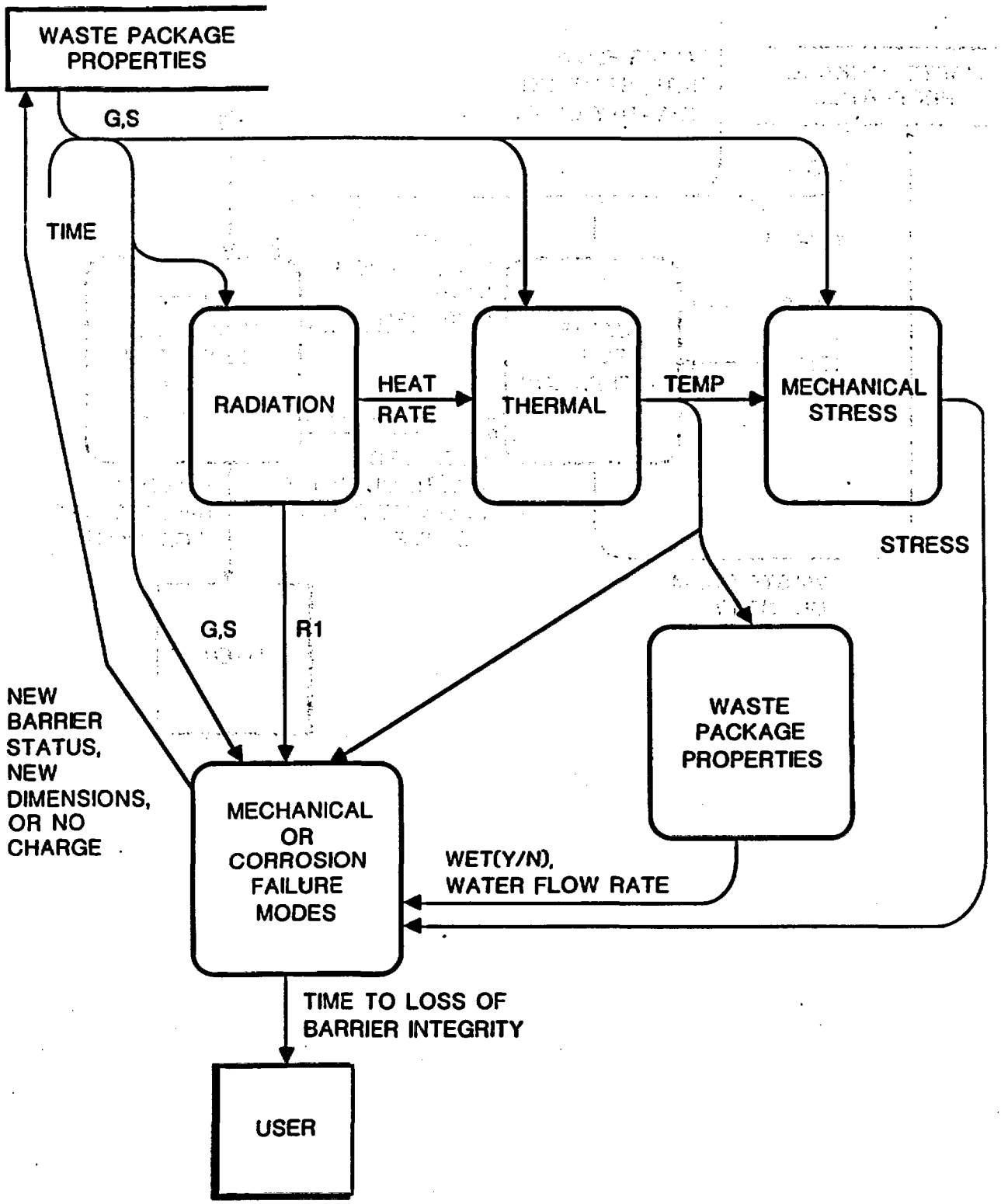

Figure 7-42. Data flow diagram showing the mechanical or corrosion failure modes process and the processes it depends upon for input data. There is a feedback loop present, but the feedback occurs only occasionally and by discrete amounts. (See Figure 7-37 for an explanation of data flow symbols and Table 7-26 for an identification of data elements used in data flow diagrams.)

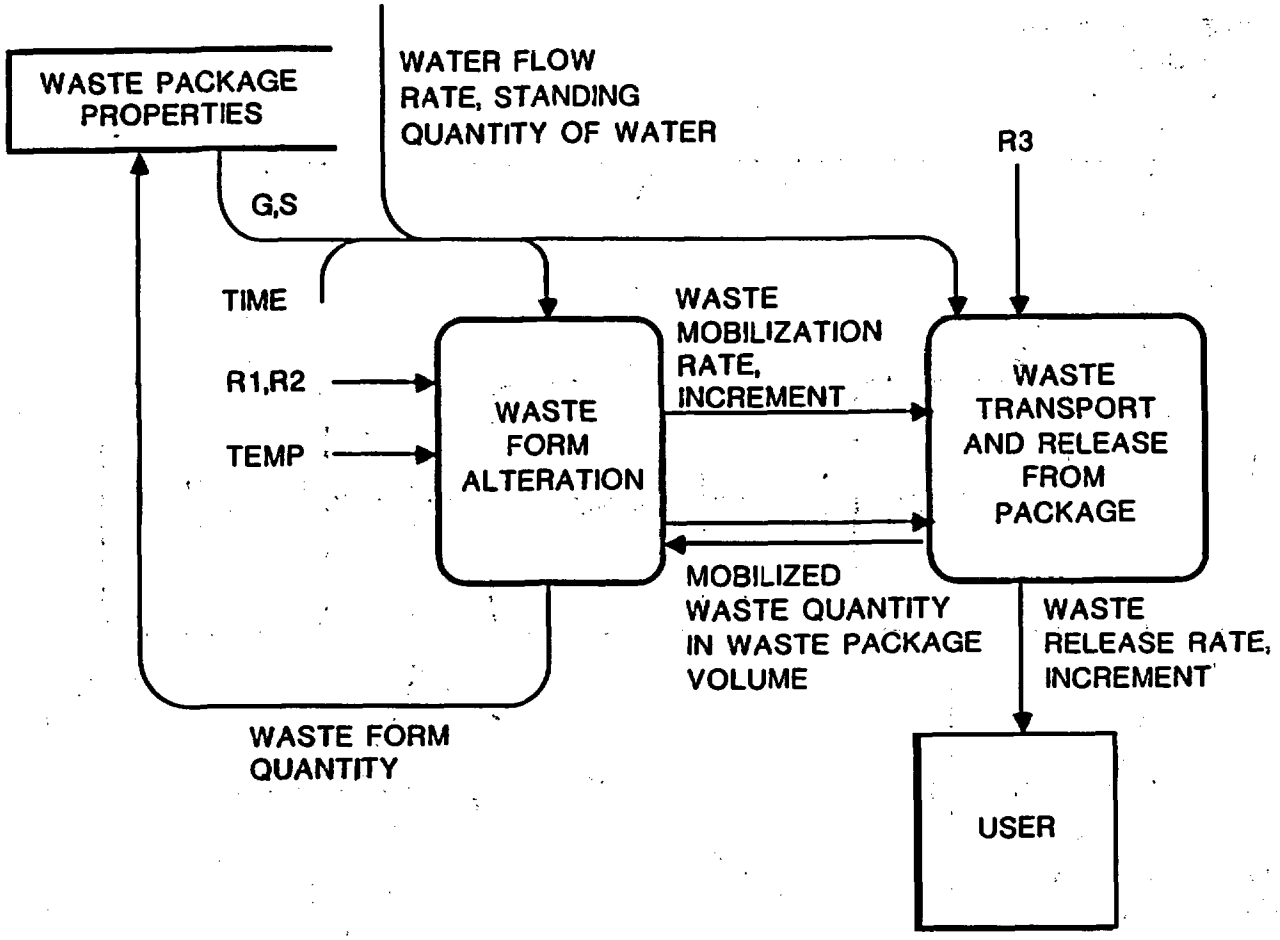

Figure 7-43. Data flow diagram for the waste form alteration and waste transport processes. Inputs from other processes are shown by the data flow names. The outputs and some of the inputs change gradually and depend on past history as well as on current conditions. (See Figure 7-37 for an explanation of data flow symbols and Table 7-26 for an identification of data elements used in data flow diagrams.)

proximate goals of the reliability analysis are (1) to identify the contributing failure modes of the waste packages, (2) to ensure that there are no common mode failures that would lead to an excessive early failure rate, (3) to estimate the reliability with which the waste package times of containment failure and rates of release will be better than values adequate to meet the performance criteria, and (4) to estimate the frequency distribution of the waste package performance values.

A probabilistic reliability analysis methodology will be selected and implemented to assess reliability in the waste package performance. This methodology will include tools of failure modes and effects analysis, anticipated and unanticipated events scenario analysis, and propagation of input parameter uncertainty, as appropriate.

Propagation of input uncertainties will estimate the frequency distributions of probability distributions (cumulative distribution functions (CDF)) of the waste package performance values. A point somewhere on the lower tail of the CDF will correspond to a performance threshold value and the reliability with which the waste packages will exceed this performance threshold.

Propagation of input uncertainties can be evaluated by several methods. One group of methods involves sampling from the probability distribution of the input variables and doing repeated deterministic calculations of the performance using these samples of inputs (NRC, 1986). The deterministic calculations are done using the model for a single waste package. In this way, a sample of output performance values is accumulated, that approximates the CDF of the output. The input sampling may be purely random sampling, stratified sampling such as Latin hypercube sampling (McKay et al., 1979), or stratified selection.

To estimate a point on the lower tail of the CDF to reasonable accuracy with reasonable sample size may require weighted biased sampling emphasizing the region of input corresponding to the threshold output value. Another approach is to determine the threshold surface in the input space and integrate the probability density of the input space below this threshold.

The data requirements are estimates of the variability of package and local environment parameters among the population of waste packages. This variability may be expressed as a probability distribution or a frequency distribution. Since major interest is centered on providing reasonable assurance that most of the performance values are above the threshold criteria, the corresponding interest is on that part of the input space corresponding to or near the output threshold. Bounding values of inputs and statements of the probability that the input values are below or above this boundary may be sufficient for this purpose. Estimates of means and variances of inputs may be needed to estimate the means and variances of the output CDF, but more approximate estimates may suffice as long as the threshold points are separately specified.

To date the project has identified the principles explained above that give some guidance on the types of data required. Selection and implementation of specific methods and acquisition of data are information needs; they are discussed in Sections 8.3.5.9 and 8.3.5.10.

7.4.5.6 Summary

This section emphasizes the waste package system model in order to discuss performance assessment. This model is central to the prediction of long-term performance since it integrates the results of studies described elsewhere in this chapter to make those predictions. The current status of this modeling activity has been described, and its link to the probabilistic analysis needed to satisfy the NRC regulations has been discussed. It has been shown that the information needs of performance assessment that will be satisfied during site characterization will be derived from data to be gathered by the waste package processes investigations. The unique requirements of performance assessment are that those investigations establish the important parameters describing each process, determine predictive relationships for the processes that incorporate those parameters, and provide statements of probability for the occurrence of parameter sets. Therefore, though not directly specifying data needs to be obtained during site characterization, performance assessment does specify data types and analyses that must be performed by the process investigations. Plans for further development of the waste package system model are discussed in Section 8.3.5.10.

7.5 SUMMARY

The summary of Chapter 7 is broken down into the same overall subsections as the chapter itself to facilitate referencing the more detailed discussions.

7.5.1 EMPLACEMENT ENVIRONMENT

Sections 7.1 and 7.4.1 discusses the emplacement environment. One of the candidate sites for disposal of HLW is in the Topopah Spring Member of the Paintbrush Tuff. This member is welded and devitrified and, in the candidate site, is unsaturated. Humid conditions are expected since the degree of saturation averages 65 ± 19 percent.

For the purpose of waste package performance assessment and design it has been assumed that the thermal loading will result in borehole rock temperatures that will reach a maximum of 230°C a few years after emplacement and gradually decrease to about 190°C 10 to 20 years after emplacement. With an expected boiling point of water of 97°C, the elevated rock temperatures will result in a dried-out zone that will extend more than 1 m from the borehole into the rock. This dried-out zone is predicted to remain dry for at least 300 yr. The container design, which is discussed later, takes advantage of the lack of liquid water in the borehole as a result of the drying out. Information that is needed regarding the dried out zone includes a better understanding of the potential heat pipe effect and fracture influence on the drying mechanism. The plans to obtain this information are discussed in Section 8.3.4.2.

Water chemistry has a direct impact on waste package performance. The expected chemistry of the water, as discussed in Section 7.4.1.3, is similar

to that obtained from well J-13, which is located in the Topopah Springs welded tuff in an area where the tuff is saturated. Well J-13 water chemistry has been used in the materials testing activities for the waste package. A need to obtain actual samples of the water from the repository area is discussed in Section 8.3.4.2.

7.5.2 DESIGN BASIS

The bases for waste package design are the various regulatory requirements (both direct and indirect waste package requirements) that are placed on the waste package. These are categorized into preclosure and postclosure requirements. The preclosure requirements include consideration of handling, criticality control, identification, and overall repository performance. The postclosure requirements include considerations for substantially complete containment and performance after closure to control release rates of radionuclides. In addition to these requirements, there are general requirements that include consideration of retrieval, the types of waste that will be included (waste forms), the material interactions among components of the waste package, and the limitations on waste form temperature.

In addition, design criteria require that (1) the production and emplacement of the waste package can be demonstrated to be technically feasible using reasonably available technology, (2) the waste package designs shall not make application of reasonably available technology impractical for other portions of the repository system or operations, and (3) the cost effectiveness be considered.

General design requirements for the preclosure period include constraints on explosive, pyrophoric, and chemically reactive materials, and exclusion of free liquids in amounts that could impact long-term performance. For the postclosure period, the waste package design will consider material specification to provide substantially complete containment and to ensure that interactions between the waste package and the environment do not compromise the long-term waste package performance, as discussed in Section 7.4 and Sections 8.3.4 and 8.3.5.

How the performance is allocated (to which system components, etc.) has a direct impact on the waste package design. For preclosure performance, the waste package is designed so that the container will provide containment of the waste forms under normal handling loads. The waste form geometry and internal container environment provide criticality control under anticipated conditions. The identification and exclusion of reactive materials and free liquids is allocated entirely to the waste package. To meet these requirements, additional information will be required regarding the waste forms, as discussed in Sections 8.3.5.10 and 8.3.4.3, respectively.

The allocation of postclosure performance to components of the waste package and the engineered barrier system was not completed at the time that the conceptual designs described in this chapter were developed. The information that will be needed regarding performance assessment of the waste package is discussed in Sections 8.3.5.9 and 8.3.5.10.

7.5.3 WASTE PACKAGE DESIGN DESCRIPTIONS

7.5.3.1 Reference design

The reference design of the waste package specifies a 304L stainless steel metal container and a waste form (either spent fuel or reprocessed waste in a glass poured into a stainless steel canister). Reference designs for spent fuel are shown in Figure 7-2 (Section 7.3.1.3). The container for spent fuel is 66 cm in diameter with 1-cm-thick walls and varies from 3.1 to 4.7m long depending on the waste form dimensions. Container designs have been developed for disposal of repository-consolidated and intact assemblies. There are different designs for pressurized water reactor assemblies and boiling water reactor assemblies. The design provides for different forms of spent fuel with different burnups. The reference design is based on consolidated fuel assemblies. The concept includes the option of disposal of intact assemblies to provide for damaged or failed assemblies that cannot be consolidated as well as to provide for unconsolidated very high burnup and short cooling time fuel disposal. This option is necessary to meet the temperature limitations on the waste form. Thus, there are different designs because of the variety of fuel rod and fuel assembly dimensions and because of the different waste forms. The reference design for reprocessed waste is shown in Figure 7-3, Section 7.3.1.3. The reference design is a container similar to that for spent fuel with a diameter of 66 cm (the 61-cm pour canister is inserted into the 66-cm container) and with a length to accommodate either the West Valley or defense waste processing facility wastes.

Rolled and welded pipe manufacturing processes are representative of the conventional type of fabrication that may be involved in manufacturing the waste containers. Many more advanced techniques are under consideration. The fabrication and closure processes have not been selected at this time. This selection will depend upon the details of design that evolve during advanced conceptual and license application design phases. Plans for evaluation, selection, and development of fabrication, closure, and inspection processes are described in Section 8.3.4.4.1. Welding and nondestructive evaluation of the final closure of the container will be done remotely.

7.5.3.2 Alternative designs

Alternative designs include a conceptual design allowing for disposal of intact PWR and BWR assemblies. The design concept is a modification of the reference design diameter (to 71 cm) and internal spacing geometry to allow packing efficiency of the assemblies and disposing of four PWR and three BWR assemblies(Figure 7-4). Considering the expected mix of PWR and BWR assemblies (40 percent PWR and 60 percent BWR), a hybrid package allowing three PWR and BWR assemblies to be disposed of in the same package leads to a surplus of BWR assemblies. This imbalance is corrected by providing that 7 percent of the packages contain only BWR assemblies in an arrangement with 10 BWR assemblies in a container. Alternative designs also include containers fabricated from a copper or copper-based alloy. The designs for copper containers are similar to the reference designs except a thicker wall may be required to compensate for lower strength of copper, especially at elevated temperatures.

7.5.3.3 Other emplacement hole components

In addition to the waste packages, other components will be present in the reference vertical or alternative horizontal emplacement holes. Because of their proximity to the waste emplacement packages, they have the potential for altering the package environment and impacting the package performance. The materials for these components, borehole liners, emplacement hole shielding plugs, and emplacement dollies will be selected to avoid adverse impact on long-term performance of the waste package.

7.5.4 WASTE PACKAGE RESEARCH AND DEVELOPMENT

7.5.4.1 Radiation field effects

Considerations of the dominant radiation effects indicate that radiolysis products from the interaction of gamma radiation with water, steam, or air are the only effects of significance. More than 99 percent of the gamma radiation will be restricted to the first meter of rock immediately around the emplacement borehole. The radiolysis products will vary with time as the thermal conditions change. During the first 300 yr, the rock in this first meter will essentially be dried out. Therefore, the radiolysis products will be those resulting from gamma radiation in moist air. At some time after 300 yr, when liquid water returns to this portion of the rock, the gamma radiation flux will have decayed by three orders of magnitude. Therefore, the radiolysis of liquid water is not of concern. Additional studies of moist air radiolysis are discussed in Section 8.3.4.2.

7.5.4.2 Water flow

Water transport under ambient conditions is through a combination of vapor transport, water migration through the matrix, and water transport through fracture flow. The influence of the thermal loading on flow under unsaturated conditions is not well understood. Studies of dehydration and rehydration under fully saturated conditions are discussed in Section 7.4.1.5. These studies revealed a basic difference in the response of fractured and intact rock. For intact rock, the permeability was independent of temperature and thermal history. However, there was a significant decrease in permeability of the fractured rock upon successive cycles of dehydration-rehydration. This decrease appears to have been the result of deposition of silica on the fracture walls. The mechanism for the change in hydrologic properties of fractured rock remains to be fully characterized and has not been thoroughly evaluated for unsaturated conditions. Additional work on near-field water flow mechanisms is discussed in Section 8.3.4.2.

7.5.4.3 Numerical modeling

Numerical modeling of water flow under hydrothermal conditions will require an understanding of the fundamental properties of multiphase fluid

flow under thermal loading conditions. Some of the properties that will need to be better understood include the characterization of the fractures, characteristic curves for multiphase flow in unsaturated conditions, and actual degree of saturation in the rock immediately adjacent to the containers. These properties will be obtained through studies that are described in Section 8.3. In addition, appropriate models will require better understanding of the fundamental mechanisms governing the hydrology and flow. This will require evaluation of the use of equivalent continuum models, development of means of evaluating gas flow in fractured media where fracture flow can dominate depending on the fracture system, and development of means of evaluating whether water condensing outside of the dried-out zone will allow sufficient saturation to allow water flow through fractures. All these information needs are discussed in Section 8.3.4.2.

7.5.4.4 Rock-water interaction

The corrosion of the waste container and the dissolution and transport of radionuclides are influenced by the chemical composition of the ground water. This in turn is influenced by the mineralogy, temperature, duration of water contact with the rock and ratio of the rock to water volume. Ongoing experiments that have used well J-13 water indicate that there will be a decrease in calcium, magnesium, and carbon dioxide and that there will be early peaks in potassium and aluminum followed by a gradual and moderate decrease. The pH of the solution will decrease from approximately 7.5 to 6.8 in response to precipitation of carbonate from solution. Preliminary conclusions are (1) the fluid in a saturated environment will evolve toward cristobalite and carbonate saturation, (2) the secondary phases resulting from hydrothermal interaction will include sorptive clays and zeolites, and (3) the composition of the fluid phase will remain benign at all temperatures.

It has not been established whether the results from vitric and vitrophyre-rich units are similar to those observed for the devitrified welded tuff. Studies of material from the exploratory shaft to address this question are discussed in Section 8.3.4.2.

7.5.4.5 Modeling rock-water interactions

The EQ3/6 geochemical code has been used to model the results of dissolution studies. The code is not able to assess precipitation as a function of time. Revisions to the code to allow this assessment as well as to address thermodynamics and reaction path are required. Plans for these activities are discussed in Section 8.3.5.10. In addition to model refinements, data will be needed on phase compositions, dissolution kinetics, and thermodynamic properties. This information will be addressed in Section 8.3.5.10.

7.5.4.6 Metal barriers

Six candidate materials from two alloy families (austenitic and copper base) have been evaluated by the Nevada NNWSI Project for use in the waste package container. AISI 304L stainless steel has been selected as the reference material for the NNWSI Project waste package on the basis of its predicted performance in the unsaturated tuff environment at Yucca Mountain. Therefore, the evaluation of performance focused on this alloy. The reference material is a benchmark upon which the performance of the other austenitic materials is compared. The other austenitic materials are AISI 316L and Alloy 825.

Corrosion and oxidation attack of austenitic materials are the most likely degradation modes although the processes of fabrication and closure, as well as stresses, can affect the degradation modes. The most important determinant for which degradation modes are operable is the postclosure anticipated environment.

The expected degradation mode(s) depends on the time frame. During the first 300 yr (substantially complete containment) when the boreholes are anticipated to remain dry, oxidation is the only mode expected to be significant. During the postclosure period from 300 to 1,000 yr, general aqueous corrosion may be possible depending on the time for hydration of the rock around the emplacement boreholes. The rates of general corrosion are sufficiently low (0.07 to 0.15 micrometer per year for dry steam and water immersion, respectively) that the limiting case is rarely general corrosion, but rather the more rapid penetration of localized or stress-assisted corrosion. The NNWSI Project metals testing activities have focused on determining the extent to which the various forms of corrosion would occur during the periods of time outlined above.

The general corrosion rates of the candidate austenitic materials exposed to water of expected chemical makeup are quite small and, thus far, do not seem to be significantly affected by (1) alloy composition, (2) temperature (28 to 150°C), (3) exposure time (up to 11,000 h), (4) irradiation (to more than 10^5 rads/h), or (5) aqueous or steam environment. A rate of approximately 0.2 micrometers per year has been determined, which for the 1-cm-thick reference container would not result in complete container corrosion for well over 10,000 yr. A model is being developed to quantify general corrosion and to allow for extrapolation of the data to long time periods. This development work is discussed in Section 8.3.5.9.

Localized or stress-assisted forms of corrosion, particularly intergranular corrosion (IGA) and intergranular stress corrosion cracking (IGSCC) are potential degradation modes if a sensitized microstructure develops. Difficulties have been encountered in applying American Society for Testing and Materials (ASTM) tests to predict sensitization. Electrochemical potential reactivation (EPR) tests are helpful in screening materials and conditions that could lead to IGA and IGSCC. A series of tests have been undertaken to consider the effects of loading-stresses, low temperature sensitization, environmental factors, residual stresses from fabrication, and alloying factors on IGSCC susceptibility. Analysis shows that if sensitization will occur, it would be evident in a few years at temperatures in the

range of 200 to 300°C, which are within laboratory ranges. Plans to determine the time to sensitization are discussed in Section 8.3.5.9.

Experiments have not shown IGSCC of L grades of stainless steels even when stressed beyond yield strength and when heat treated. Severe exposure conditions have also been evaluated. Results indicate that low temperature sensitization could occur in containers that were heavily cold-worked if the temperatures were higher than the reference case. Use of AISI 316 stainless steel or Alloy 825 material would minimize this sensitization. Reduction of the peak surface temperature and reducing the residual stresses in the container would also alleviate intergranular stress corrosion susceptibility. Future testing of these materials is planned as discussed in Section 8.3.5.9.

A model to predict sensitization in austenitic stainless steels and extension of this model to higher nickel content materials is being developed. This model considers temperature, strain, and compositional effects in materials. Plans for further development of this model are discussed in Section 8.3.5.9.

Pitting corrosion, crevice corrosion, and transgranular stress corrosion cracking (TGSCC) are governed principally by the composition of the aqueous environment (ionic species concentration). Both the attack and the causative environment may be localized. In the majority of cases, these degradation modes are dependent on chloride ion concentration in the environment. The candidate austenitic materials appear to be sufficiently resistant to pitting, crevice attack, and TGSCC in unmodified well J-13 water or steam generated from that water to meet the performance objectives. Even if the highest measured localized corrosion rate is added to the general corrosion rate, container service life far exceeds the maximum containment requirement. It is also necessary to consider whether biological degradation is possible, which could enhance the factors leading to pitting or crevice attack. Studies to address these considerations are discussed in Section 8.3.5.9.

Other considerations are related to phase stability of austenite over long periods of time. Phase transformations, particularly in weld and heat-affected zones, might adversely affect long-term fracture toughness and result in a more brittle, possibly less corrosion-resistant container. Some materials, such as 316 stainless steel, will improve the resistance to localized corrosion but will have a greater tendency to form brittle phases over long periods of time. This needs to be addressed in future work as discussed in Section 8.3.5.9.

Hydrogen embrittlement might be of concern after the 300-yr time since the waste package walls would be below a critical temperature (85°C for AISI 304Lss) and water could come in contact with the waste package. Hydrogen could enter the container material from radiolytic decomposition of the water vapor; however, the relatively high temperatures would tend to mitigate against trapping of the hydrogen. Also, the oxidizing nature of the environment will tend to combine oxidizing radicals with atomic hydrogen as it is produced. These effects need to be investigated to determine whether hydrogen is produced and, if so, how much can permeate the metal barrier. Studies to address this question are discussed in Section 8.3.5.9.

Nonuniform corrosion caused by sensitized microstructure during the containment period with subsequent wetting of the affected area that induces IGSCC is one mode of corrosion that might place limitations on containment life. A question remains as to whether lower carbon content in the L grades can confer immunity or at least a high resistance to the phenomenon. Control of the processing of the container can confine this phenomenon to the area around the final closure weld; selection of the alloy can further reduce the susceptibility to allow for substantially complete containment.

Alloy 825 is considered the most resistant of the candidate materials to virtually every form of corrosion that might occur in a geologic repository in tuff. However, some developmental work would be needed to ensure it can be fabricated should this material be selected for the advanced designs. Development work on weld and fabrication technologies is discussed in Section 8.3.4.4.

Although the austenitic materials have thus far exhibited behavior indicative of material that will withstand the long-term environmental conditions in a repository at Yucca Mountain, the possibility exists that further testing may disclose serious degradation process(es) that affect all three alloys. For this reason, copper-base materials are being considered as an alternative alloy system. Three copper-based materials being considered are CDA 102, CDA 613, and CDA 715.

The types of corrosion that may occur for copper-base materials in a tuff repository are uniform corrosion; pitting, crevice, and intergranular corrosion; selective leaching; and stress corrosion cracking. Uniform corrosion is considered the most likely mode; but pitting corrosion may also be likely, especially because of the irradiated environment.

The NNWSI Project has completed a 2-yr feasibility study on the three copper-base materials. At this time, these materials appear feasible alternatives should the austenitic materials be found unacceptable. It is expected that these materials will be tested further as is discussed in Section 8.3.5.9.

7.5.4.7 Spent fuel waste form performance

7.5.4.7.1 Spent fuel dissolution and radionuclide release

Based on a review of the available data, a three-part testing program has been initiated to establish the characteristics of the spent fuel waste form. The first part is devoted to the study of the dissolution and radionuclide release from irradiated UO_2 (Section 7.4.3.1.1), the second part is intended to establish the oxidation rate of spent UO_2 fuel (Section 7.4.3.1.2), and the third part is intended to establish the mechanisms and rate of corrosion of Zircaloy cladding (Section 7.4.3.1.3).

Water contact with the waste itself is the most credible mechanism for removing most radionuclides from the waste package. The contact with the waste is a function of the orientation and type of the waste form as well as the emplacement configuration and failure mechanisms of the container.

Assuming that water can contact spent fuel, americium and plutonium are the most significant elements subject to dissolution. Semistatic leach tests have been conducted on spent pressurized water reactor fuel using well J-13 water. These tests used both bare fuel and rod segments with undefected and intentionally defected cladding. Results are discussed in Section 7.4.3.1.1. Uranium concentrations in solutions over bare fuel peaked within a few tens of days at around 4.5 to 4.9 micrograms per milliliter and then decreased to between 1.2 to 4 micrograms per milliliter. Because of the hydrogen-bicarbonate (HCO_3) ion in well J-13 water, most of the uranium was in true solution. The fractional release of uranium to solution was consistently higher than that of other actinides. Thus, uranium has the potential to be transported preferentially to other actinides.

Several fission products (cesium, iodine, technetium) are not fully dissolved in the UO_2 matrix, but fractions have migrated either to grain boundaries or to the fuel-cladding gap during irradiation. These elements show an initial rapid release upon contact of the fuel with water. Defected cladding did not provide an effective barrier to the early release of these elements. Unlike the other radionuclides of interest, carbon-14 may be released as carbon dioxide gas under oxidizing conditions without the presence of liquid water. Work to evaluate carbon-14 distributions has shown that approximately half of the inventory is associated with the Zircaloy cladding and the other nonfuel assembly parts.

Studies in the literature indicate that the dissolution of UO_2 is a complex, multistage process, the exact nature of which depends strongly on solution chemistry. In all instances however, it appears that the release of uranium occurs from an oxidized surface layer. Further work on radionuclide release is planned and is discussed in Section 8.3.5.10.

7.5.4.7.2 Spent fuel oxidation

Because of the large positive volume change upon oxidation of UO_2 to U_3O_8, an evaluation was made of the potential for cladding rupture by this mechanism. In addition, the dissolution rate of oxidized fuel may differ from that of unoxidized fuel. Differences between the oxidation rates of nonirradiated fuel and irradiated fuel have been reported in the literature; thus, the NNWSI Project work on the oxidation of UO_2 uses spent fuel. Two complementary techniques used to measure the oxidation rate at temperatures relevant to repository conditions are thermogravimetric analysis (TGA) and conventional oven oxidation.

The TGA data obtained to date suggest a two-stage oxidation mechanism: grain boundary diffusion of oxygen and oxidation of the grain surfaces followed by bulk diffusion and oxidation of grain interiors. At high temperature, the first stage is relatively rapid and bulk diffusion is the rate determining step. At lower temperatures, the rate of the first step has a significant effect on the overall oxidation rate on the time scale of the experiments conducted. The activation energy obtained from the bulk diffusion portion of the tests is approximately 107 kJ/mole. This value is within the range of values given in the literature.

In studies conducted by others on the dry storage of spent fuel assemblies, no cladding splits were noted for both undefected and defected nonirradiated fuel stored in an inert atmosphere at temperatures as high as 230°C. Fuel in rods with defected cladding stored in an oxygen atmosphere oxidized causing deformation and rupture of the cladding. Based on these results, a recommendation to use inert atmosphere has been adopted for the atmosphere in disposal containers to help preserve the integrity of the cladding during the early high temperature phase in the repository. Work is continuing on the oxidation rate and mechanism of spent UO_2 fuel and is discussed in Sections 7.4.3.1.2 and in Section 8.3.5.10.

7.5.4.7.3 Zircaloy corrosion

Zircaloy cladding, if it maintains its integrity for long time periods and if the cladding failures that occur are spread out over time, may provide a partial control on the release of the rapidly released, gap and grain boundary inventory of radionuclides. Stress rupture, hydride cracking, and stress corrosion cracking have been investigated as failure mechanisms of the Zircaloy cladding. Stress rupture was concluded not to be a significant failure mode for fuel rods under the NNWSI Project tuff repository disposal conditions at Yucca Mountain. While most data do not support the concept of hydride cracking, there is some concern that hydrides might reorient under storage conditions. Initial studies of Zircaloy-4 together with other components of the waste package in well J-13 water at 90°C did not detect any corrosion after 12 mo at a detection sensitivity of 1 to 2 micrometers per year. General corrosion data in water representative of the repository area is needed. Future studies on Zircaloy corrosion and cladding failure are discussed in Section 8.3.5.10.

7.5.4.8 Glass waste forms

Studies performed for glass waste forms indicate that, at long times, glass may be considered to dissolve congruently with less soluble elements, immediately reprecipitating onto the glass. A very conservative estimate of the leaching rate of any radionuclide is that the maximum rate will not exceed that of very soluble major elements in the glass. Only one possible exception to this was found during the NNWSI Project testing. To confidently predict the long-term behavior of the waste in glass form will require a thorough understanding of the glass leaching mechanisms.

One of the critical factors that influences leach rates is temperature. There is an expected leach rate difference of about two orders of magnitude between glass at temperatures of 40 and 95°C. The NNWSI Project tests for leaching are routinely performed at temperatures of 90°C, which exceeds the anticipated temperature at which leaching would occur in the repository.

An additional important factor is the pH of the leaching solution, which can be controlled to some extent by the overall repository design. When the pH is between 5 and 9, leaching is at a minimum. Since the pH is initially buffered at Yucca Mountain by the presence of dissolved CO_2 and silica as

well as by the dissolved glass components, this factor can be controlled. Large excursions in pH, which are feasible, would be more than the buffering capacity of the ground water at Yucca Mountain. Therefore, glass composition must be carefully controlled, which is beyond the NNWSI Project control except for rigid enforcement of acceptance standards or specifications. The use of acceptance standards is discussed in Sections 8.3.5.10 and 8.3.4.3 under Issues 1.5 and 2.6.

Studies of leach rates as a function of the volume of water indicate that volume is an important consideration. Scaling experiments indicate that about a sixfold shortening of experimental time is possible by increasing the surface area to volume by approximately the same factor. However, it is not clear whether the scaling can be applied to predict the result of much larger surface-area-to-volume ratios expected for Yucca Mountain. This, plus the effect of large concentrations of silica in the solution, will be considered in studies discussed in Section 8.3.5.10 under Issue 1.5 and Information Need 2.6.3.

Studies to look at the leach rates given the reference design for the waste packages, the Topopah Springs tuff, and well J-13 water indicate that 304L stainless steel has no substantial effect on leaching and that the presence of tuff slightly decreases the leaching rates. The presence of ductile iron is known to increase leach rates in static tests. Therefore, tests are to be conducted on heat-affected 304L stainless steel, which may be more reactive. This work is discussed in Sections 8.3.5.10 and 8.3.4.3.

Radiolysis studies indicate that, after an early decrease in pH due to radiation exposure (nitric acid generation), increased glass leaching occurred, which in turn buffered the acid production from radiolysis. Thus, for irradiation fluxes above 1 x 10^5 rads/h, the glass reaction rate becomes insensitive to the flux. Experiments to determine how much radiation is required to maintain the radiolysis buffer are discussed in Section 8.3.5.10. Actinide releases in gamma-irradiation are sensitive to the pH. However, anticipated pH changes that would occur at Yucca Mountain are expected to be small since the rock will be essentially dried out during the period of high gamma radiation flux.

Prediction of the long-term behavior of waste glasses will require a better understanding of secondary products that appear to substantially reduce initial leach rates but, in the long term, these crystalline products may provide the thermodynamic driving force for glass dissolution. The current knowledge of these compounds is not sufficient to rely upon solely as a control of radionuclide release. An approach under development is to use explicit geochemical modeling of aqueous species and glass dissolution kinetics to improve the understanding of this system. This work is discussed in Section 8.3.5.10.

7.5.4.9 EQ3/6 model development

The EQ3/6 geochemical modeling code will supplement field and experimental programs in the NNWSI Project. EQ3/6 will simulate waste package performance over tens of thousands of years and will extrapolate short-term

laboratory experiments to much longer time scales. Simulation of laboratory experiments will aid in validating the code. The EQ3/6 package lends itself to modeling the controlled conditions of laboratory experiments. EQ3/6 can then be used to investigate the consequences of variations in the environment on waste package performance.

The EQ3/6 geochemical modeling program focuses on determining

1. The potential degradation of the waste container resulting from interactions between ground water, host rock, and gases in the unsaturated zone during and following the thermal pulse from radioactive decay of high-level waste.

2. The extent and degree of transport of radionuclides into the environment after container breaching and resulting ground-water-host rock interactions.

A three-phase approach is being carried out to address these issues:

1. The EQ3/6 code is being expanded and refined to provide for chemical processes that will control fluid-rock interaction and radionuclide transport in the short and long term.

2. Thermodynamic data are being acquired to describe solid substances and aqueous species.

3. Applications work is under way to

   a. Simulate laboratory results to evaluate code capabilities and interpret laboratory results.

   b. Complement the experimental program by simulating laboratory experiments under a wider variety of conditions than can be carried out in the laboratory.

   c. Extrapolate laboratory results to the long-time periods involved in waste disposal effects.

This work is further discussed in Section 8.3.5.10.

7.5.4.10 Waste package performance assessment

Information needs relative to performance assessment relate to the methodology used for the assessment. Most of the information used in this assessment will be collected outside of the performance assessment itself and is discussed in other portions of Chapter 7 and in Chapter 8. It is the task of performance assessment to construct and validate the computational models necessary and then to analyze waste package designs to demonstrate that they will perform as intended.

The overall approach that will be used is to develop a deterministic model to describe waste package performance under a given set of conditions

and design parameters. The most likely approach to uncertainty or reliability analysis will be to use this deterministic model to calculate performance parameters based on input variables selected by a statistically valid method. Using a sufficient number of the calculations, distributions of time to loss of containment and engineering barrier system release rates will be constructed. Site characterization and materials performance data will be required to verify and validate the model and then to make the final waste package performance assessment. How this data will be obtained is discussed in Sections 8.3.4.2, 8.3.5.9, and 8.3.5.10.

A system model for waste package performance that is specific to the NNWSI Project site conditions and design parameters is under development. This model is a compilation of submodels that includes radiation, thermal, mechanical, environment, corrosion, waste form alteration, and waste transport models. Each of these models may consist of several interacting or related submodels. These models are discussed in Section 7.4.5.4, and additional work to further develop and refine the models is discussed in Section 8.3.5.10.

7.5.5 UNCERTAINTIES IN WASTE PACKAGE DEVELOPMENT

Throughout this chapter, references have been made to tests and investigations that are needed to gain additional information. The primary motivation for identification of these activities is reduction of significant uncertainties that are inherent in the project. These will require quantification by expert judgment and bounding calculation or assumptions explicitly stated in the bases for design and assessments of performance.

The following sections briefly discuss the principal sources of uncertainty in the major elements of the waste package development activities and make a preliminary judgment of those factors that are amenable to reduction by additional testing. Those factors that will require quantification by other means are also identified.

7.5.5.1 Waste package design

The waste package design development process provides the mechanism for accommodating the uncertainties in the service environment, the waste forms, and other package components that are discussed in the sections that follow. The design development process is structured to be an iterative, phased approach. The design bases for each phase of the design development will be reevaluated prior to initiation of the design phase to include revisions as appropriate that reflect the current information from the site investigations and other data, such as projections of the characteristics of the waste to be packaged and disposed in the repository. The resulting designs will then be evaluated by comparison of the predicted performance relative to the performance goals and revised as necessary.

Although the design development process introduces few uncertainties, it is structured to assess the effect of uncertainties in the design bases and to accommodate the residual uncertainties in the design itself.

7.5.5.2 Waste package environment

The major uncertainties in the waste package environment arise from inadequate characterization of the repository host rock mass and its response to the loads imposed by the construction of the facility and emplacement of the waste. The level of uncertainty is expected to be substantially reduced by the performance of the site characterization investigations described in Section 8.3. Some residual uncertainty will remain after that work is completed, simply because the natural variability of the host rock will not be completely explored and the response of the coupled geochemical-geohydrologic system for the long time span of required performance cannot be completely tested.

Two major technical uncertainties exist with respect to the near-field environment adjacent to waste packages. The first concerns the composition and form of the chemical products resulting from a system that contains unsaturated tuff, an aqueous fluid (liquid or vapor), and air at elevated temperatures and ionizing radiation levels that vary as a function of time. The second involves the processes that control the flow of vadose water in both liquid and vapor phases under the influence of elevated temperatures, especially those that exceed the unconfined boiling point, in a fractured medium. Both of these uncertainties will be addressed in the laboratory and field tests that are planned during site characterization. Residual uncertainties will remain because the techniques that may be required to investigate some aspects of these processes involve imposing loads and flow rates that questions remaining on scale effects.

The investigations specifically planned to address these uncertainties, including the development of models for predicting the processes into the far future are described in Section 8.3.4.

7.5.5.3 Metallic containers

The major uncertainties in the metallic components of the waste package are related to the indentification of the degradation modes that will limit the service life and prediction of the rates or frequencies of occurrence of these models. These factors are directly related to the composition of the material and the microstructure and residual stresses resulting from the forming and joining processes used in fabrication. The metal alloy to be used has not been selected, nor have the fabrication processes been determined. Both of these activities have been planned and are described in Sections 8.3.4 and 8.3.5.9. Plans for the development of models to predict the degradation rates and relatively short (few year) duration tests to assist in the validation of these models are also discussed.

The uncertainties in the waste package environment (Section 7.5.5.2) also influence the predictions of the performance of the container. These factors will affect the quantities, speciation and concentration of species in both the vapor and liquid phases present to degrade the container material.

Residual uncertainties will exist due to the lack of relevant experience with currently available metallic materials over the time periods of concern in this project. The service lifetimes are far longer than for any other engineered structures and, therefore, beyond the limits of experience.

7.5.5.4 Waste forms

All the waste forms to be accepted for disposal in a geologic repository are subject to two important factors. First, they are known to possess variable physical and chemical properties at a scale such that detailed individual characterization is not feasible. This implies that the waste forms can only be sampled on a limited basis and the ranges of significant characteristics will require estimation based on the samples. The prediction of the long-term behavior of both waste forms depends upon developing suitably comprehensive models of waste form degradation and geochemical interactions. Uncertainties in this area involve the ability to identify and quantify the most important factors and to obtain an understanding of less important factors sufficient to provide confidence that the long-term models will be accurate to within a known statistical uncertainty.

The second important aspect is that a large fraction of the waste forms to be disposed in the repository do not exist now and will not exist prior to the application for a license for the disposal system. Thus, it will be necessary to develop projections of the important characteristics in a situation where DOE-OCRWM does not have control over the design and operation of the waste generation sources. The importance of these two inherent sources of uncertainty remains to be determined. In addition, there is some uncertainty introduced by regulatory proceedings to revise the definition of high level radioactive waste. The impact of this proposed rulemaking has not been assessed in this document.

7.5.5.4.1 Spent fuel waste forms

Uncertainties in the characteristics of the spent fuel to be received at the repository fall into two broad categories. The first involves the external physical characteristics that affect the design of the waste package and the repository, such as dimensions, configurations, quantities, thermal and radiation outputs. These characteristics, as indicated in Section 7.5.5.4, will remain uncertain to the extent that the waste receipt schedule reflects a projection into the future.

The second category of uncertainty involves those internal characteristics of the spent fuel that may significantly affect the rate of release of radionuclides from the waste packages following the containment period.

Limited testing of irradiated fuel so far has indicated that the release rates may be affected by a number of factors such as oxidation state of the uranium; inventory of nuclides occurring in the fuel-cladding gap and on fuel grain boundaries; magnitude and number of cladding defects; the inventory of nuclides, e.g., carbon-14, that may be released as gases and the sensitivity of this release to environmental conditions such as temperature; and the effect of the composition and quantity of water contacting the waste.

The planned activities described in Section 8.3.5.10 have been designed to address these uncertainties to the extent feasible in the time available for this phase of the project, including the testing of several spent fuels, and development of release models for the time periods of concern.

7.5.5.4.2 Glass waste forms

The high level glass waste forms have less variability in form, dimension, and external characteristics than spent fuel, but share the uncertainty arising from projecting the production of the waste form into the future because none of the vitrification facilities are yet in full scale operation.

The major sources of uncertainty for glass waste forms concern the physical characteristics that may significantly affect the release rate of radionuclides. Testing of the glass waste forms has been limited to surrogate materials compounded to approximate the reference composition of the production glass. Most of the test materials have been produced in very small melters, thus introducing some uncertainty with regard to scale effects. The nature of the wastes and vitrification processes implies that there will be batch compositional variation that will affect release rates. In general, the testing has been performed on glass that is a representative of the average material in a canister. However, the waste most readily available for initial release may be contained in inhomogeneous material at the top of the glass monolith, or splatter or condensate adhering to the canister in the empty space above the glass. Tests have not been performed yet on these types of material, or to determine the relative importance of these factors and glass cracking and canister-glass interactions.

The planned activities described in Section 8.3.5.10 have been designed to address these uncertainties to the extent feasible in the time available for this phase of the project, including the development of release models for the time periods of concern.

7.5.5.5 Waste package performance assessment

The principal uncertainties in the performance assessments arise from the need to propagate all of the uncertainties in the models that represent the process acting on the waste package components and the boundary conditions of the package environment through a coupled deterministic model of the system. This system model will necessarily involve simplifications of the coupled interactions and of the processes themselves to be manageable.

It is also inherently not possible to fully validate the system model over the time periods of concern. Therefore, an additional level of uncertainty will be introduced as to the efficiency of the simplifications to the process models and their interactions.

The methodology for probablistically analyzing the residual uncertainties in the waste package performance has not been selected. This selection will be based on the criterion that it provide a realistic analysis of the uncertainties and, to the extent possible, avoid introducing additional sources of uncertainty.

The plans for phased development of the waste package performance assessment system models are described in Section 8.3.5.10. The planned applications of these models to assess containment and controlled release performance of the waste packages and provide release predictions for the total system assessments are described in Sections 8.3.5.9 and 8.3.5.10.

DOE/RW-0160

Nuclear Waste Policy Act
(Section 113)

Consultation Draft

Site Characterization Plan

Yucca Mountain Site, Nevada Research and Development Area, Nevada

Volume III

January 1988

U.S. Department of Energy
Office of Civilian Radioactive Waste Management
Washington, DC 20585

REFERENCES FOR CHAPTER 7

ASME (America Society of Mechanical Engineers), 1983. "Analysis of Piping Products," ASME Boiler and Pressure Vessel Code, Rules for Construction of Nuclear Power Plant Components, ANS Section III, Section NB-3650, New York.

ASTM (American Society for Testing and Materials), 1986. "Detecting Susceptibility to Intergranular Attack in Austenitic Stainless Steel," Annual Book of ASTM Standards, A 262-81, Part 10, Philadelphia, Penn., pp. 1-29.

Aagaard, P., and H. C. Helgeson, 1982. "Thermodynamic and Kinetic Constraints on Reaction Rates Among Minerals and Aqueous Solutions. I. Theoretical Considerations," American Journal of Science, Vol. 282, pp. 237-285.

Abe, S., T. Ogawa, S. Iwasaki, K. Hattori, M. Akashi, and R. Kume, 1982. "Development of SCC Resistant 347LP," Predictive Methods for Assessing Corrosion Damage to BWR Piping and PWR Steam Generators, H. Okada and R. Staehle (eds.), National Association of Corrosion Engineers, Houston, Tex., pp. 179-186.

Abrajano, T., J. Bates, W. Ebert, and T. Gerding, 1986. The Effect of Gamma Radiation on Groundwater Chemistry and Glass Leaching as Related to the NNWSI Repository Site, UCRL-15825, Lawrence Livermore National Laboratory, Livermore, Calif.

Acton, C. F., and R. D. McCright, 1986. Feasibility Assessment of Copper-Base Waste Package Container Materials in a Tuff Repository, UCID-20847, Lawrence Livermore National Laboratory, Livermore, Calif.

Aines, R. D., 1986. Estimates of Radionuclide Release from Glass Waste Forms in a Tuff Repository and the Effects on Regulatory Compliance, UCRL-93735, Lawrence Livermore National Laboratory, Livermore, Calif.

Alexander, C. W., C. W. Kee, A. G. Croff, and J. O. Blomeke, 1977. Projections of Spent Fuel to be Discharged by the U.S. Nuclear Power Industry, ORNL/TM-6008, Oak Ridge National Laboratory, Oak Ridge, Tenn.

Apted, M. J., and R. Adiga, 1985. "The Effect of Groundwater on Release Rate Behavior of Borosilicate Glass," Scientific Basis for Nuclear Waste Management VIII, Materials Research Society Symposia Proceedings, Boston, Massachusetts, November 26-29, 1984, C. M. Jantzen, J. A. Stone, and R. C. Ewing (eds.), Vol. 44, Materials Research Society, Pittsburgh, Penn., pp. 163-170.

Aronson, S., R. B. Roof, Jr., and J. Belle, 1957. "Kinetic Study of the Oxidation of Uranium Dioxide," The Journal Chemical Physics, Vol. 27, No. 1, pp. 137-144.

Atkinson, A., D. J. Goult, J. A. Hearne, 1985. "An Assessment of the Long-Term Durability of Concrete in Radioactive Waste Repositories," Scientific Basis for Nuclear Waste Management IX, Materials Research Society Symposia Proceedings, Stockholm, Sweden, September 9-11, 1985, L. O. Werme (ed.), Vol. 50, Materials Research Society, Pittsburgh, Penn., pp. 239-246.

Baker, C., 1977. "Fission Gas Bubble Distribution in Uranium Dioxide from High Temperature Irradiated SGHWR Fuel Pins," Journal of Nuclear Material, Vol. 66, pp. 283-291.

Bandy, R., and D. Van Rooyen, 1985. "Properties of Nitrogen-Containing Stainless Alloy Designed for High Resistance to Pitting," Corrosion, Vol. 41, No. 4, National Association of Corrosion Engineers, pp. 228-233.

Barkatt, A., P. B. Macedo, W. Sousanpour, A. Barkatt, M. A. Boroomand, P. Szoke, and V. L. Rogers, 1983. "Correlation Between Dynamic Leach Test Results and Geochemical Observations," Scientific Basis for Nuclear Waste Management VI, Materials Research Society Symposia Proceedings, Boston, Massachusetts, November, 1982, D. G. Brookins (ed.), Vol. 15, North Holland, New York, pp. 227-234.

Barkatt, A., B. C. Gibson, and M. Brandys, 1985. "A Kinetic Model of Nuclear Waste Glass Dissolution in Flowing Water Environments," Scientific Basis for Nuclear Waste Management VIII, Materials Research Society Symposia Proceedings, Boston, Massachusetts, November 26-29, 1984, C. M. Jantzen, J. A. Stone, and R. C. Ewing (eds.), Vol. 44, Materials Research Society, Pittsburgh, Penn., pp. 229-236.

Barnartt, S., 1977. "Electrochemical Nature of Corrosion," Electrochemical Techniques for Corrosion, R. Baboian (ed.), National Association of Corrosion Engineers, Houston, Tex., pp. 1-10.

Barner, J. O., 1984. Characterization of LWR Spent Fuel MCC-Approved Testing Material - ATM-101, PNL-5109, Battelle Pacific Northwest Laboratories, Richland, Wash.

Bates, J. K., and T. J. Gerding, 1985. NNWSI Phase II Materials Interaction Test Procedure and Preliminary Results, ANL-84-81, Argonne National Laboratory, Argonne, Ill.

Bates, J. K., and T. Gerding, 1986. One-Year Results of the NNWSI Unsaturated Test Procedure: SRL 165 Glass Application, ANL-85-41, Argonne National Laboratory, Argonne, Ill.

Bates, J. K., and V. M. Oversby, 1984. The Behavior of Actinide Containing Glasses During Gamma-Irradiation in a Satuated Tuff Environment, UCRL-90818, Lawrence Livermore National Laboratory, Livermore, Calif.

Bates, J. K., L. J. Jardine, and M. J. Steindler, 1982. "Hydration Aging of Nuclear Waste Glass," Science, Vol. 218, pp. 51-53.

Bates, J. K., D. F. Fischer, and T. J. Gerding, 1986a. The Reaction of Glass During Gamma Irradiation in a Saturated Tuff Environment: Part 1, SRL 165 Glass, ANL-85-62, Argonne National Laboratory, Argonne, Ill.

Bates, J. K., T. J. Gerding, T. A. Abrajano, Jr., and W. Ebert, 1986b. NNWSI Waste Form Testing at Argonne National Laboratory: Semiannual Report, July-December, 1985, UCRL-15801, Lawrence Livermore National Laboratory, Livermore, Calif.

Baxter, R. G., 1983. Description of Defense Waste Processing Facility Reference Waste Form and Canister, DP-1606, Rev. 1, E. I. du Pont de Nemours & Co., Savannah River Laboratory, Aiken, S. C.

Bazan, F., and J. Rego, 1985. Parametric Testing of a DWPF Glass, UCRL-53606, Lawrence Livermore National Laboratory, Livermore, Calif.

Bazan, F., and J. H. Rego, 1986. The Tuff Reaction Vessel Experiment, UCRL-53735, Lawrence Livermore National Laboratory, Livermore, Calif.

Beattie, I. R., 1967. "Nitrogen Dioxide and Dionitrogen Tetroxide," Mellor's Comprehensive Treatise on Inorganic and Theoretical Chemistry, Vol. VIII, Suppl. II, J. Wiley and Sons, New York, pp. 247-268.

Benson, L. V., J. H. Robison, R. K. Blankennagel, and A. E. Ogard, 1983. Chemical Composition of Ground Water and the Locations of Permeable Zones in the Yucca Mountain Area, Nevada, USGS-OFR-83-854, Open-File Report, U.S. Geological Survey, Denver, Colo.

Bianchi, G., A. Cerquetti, F. Mazza, and S. Torchio, 1974. "Pitting Corrosion of Austenitic Stainless Steel and Properties of Surface Oxide Films," Localized Corrosion NACE-3, R. W. Staehle, B. Brown, J. Kruger and A. Agrawal (eds.), National Association of Corrosion Engineers, Houston, Tex., pp. 399-409.

Bibler, N. E., 1986. Leaching Fully Radioactive SRP Nuclear Waste Glass in Tuff Groundwater in Stainless Steel Vessels, DP-MS-85-141, E. I. du Pont de Nemours and Co., Savannah River Plant, Aiken, S. C.

Bibler, N. E., G. G. Wicks, and V. M. Oversby, 1984. Leaching Savannah River Plant Nuclear Glass in a Saturated Tuff Environment, UCRL-91258, (preprint), Lawrence Livermore National Laboratory, Livermore, Calif.

Bickford, D. F., and C. M. Jantzen, 1984. "Devitrification Behavior of SRL Defense Waste Glass," Scientific Basis for Nuclear Waste Management VII, Materials Research Society Symposia Proceedings, Boston, Massachusetts, November, 1983, G. L. McVay (ed.), Vol. 26, North-Holland, Elsevier Science Publishing Co., Inc., New York, pp. 557-566.

Bickford, D. F., and D. J. Pellarin, 1986. "Large-Scale Leach Testing of DWPF Canister Sections," DP-MS-86-72, E. I. duPont de Nemours and Co., Savannah River Laboratory, Aiken, S.C.

Bish, D. L., F. A. Caporuscio, J. F. Copp, B. M. Crowe, J. D. Purson, J. R. Smyth, and R. G. Warren, 1981. Preliminary Stratigraphic and Petrologic Characterization of Core Samples from USW-G1, Yucca Mountain, Nevada, A. C. Waters and P. R. Carroll (eds.), LA-8840-MS, Los Alamos National Laboratory, Los Alamos, N. Mex.

Bourcier, W. L., 1985. Improvements in the Solid Solution Modeling Capabilities of the EQ3/6 Geochemical Code, UCID-20587, Lawrence Livermore National Laboratory, Livermore, Calif.

Bradley, D. J., C. O. Harvey, and R. P. Turcotte, 1979. Leaching of Actinides and Technetium from Simulated High-Level Waste Glass, PNL-3152, Pacific Northwest Laboratories, Waste Isolation Safety Assessment Program, Richland, Wash.

Bradley, D. J., D. G. Coles, F. N. Hodges, G. L. McVay, and R. E. Westerman, 1983. Nuclear Waste Package Materials Testing Report: Basaltic and Tuffaceous Environments, PNL-4452, Pacific Northwest Laboratory, Richland, Wash.

Briant, C. L., 1982. Effects of Nitrogen and Cold Work on the Sensitization of Austenitic Stainless Steels, Final Report NP-2457, EPRI Research Project 1574-1, Palo Alto, Calif.

Briant, C. L., R. A. Mulford, and E. L. Hall, 1982. "Sensitization of Austenitic Stainless Steels, I. Controlled Purity Alloys," Corrosion, Vol. 38, No. 9, pp. 468-477.

Bruemmer, S. M., and A. B. Johnson, Jr., 1984. "Effect of Chloride, Thiosulfate, and Fluoride Additions on the IGSCC Resistance of Type 304 Stainless Steel in Low Temperature Water," Proceedings of International Symposim on Environmental Degradation of Materials in Nuclear Power Systems-Water Reactors, August 22-25, 1983, Myrtle Beach, S. Carolina, National Association of Corrosion Engineers, Houston, Tex., pp. 571-582.

Burns, P. J., 1982. TACO2D - A Finite Element Heat Transfer Code, UCID-17980, Rev. 2, Lawrence Livermore National Laboratory, Livermore, Calif.

Burns, W. G., A. E. Hughes, J. A. C. Marples, R. S. Nelson, and A. M. Stoneham, 1982. "Effects of Radiation on the Leach Rates of Vitrified Radioactive Waste," Journal of Nuclear Materials, Vol. 107, North-Holland Publishing Company, pp. 245-270.

CDA (Copper Development Association), 1986. Application Data Sheet, Standard Designations for Copper and Copper Alloys, Greenwich, Conn.

Carlos, B. A., 1985. Minerals in Fractures of the Unsaturated Zone from Drill Core USW G-4, Yucca Mountain, Nye County, Nevada, LA-10415-MS, Los Alamos National Laboratory, Los Alamos, N. Mex.

Clarke, W. L., R. L. Cowan, and W. L. Walker, 1978. "Comparative Methods for Measuring Degree of Sensitization in Stainless Steel," Intergranular Corrosion of Stainless Alloys, R. F. Steigerwald (ed.), ASTM STP 656, American Society for Testing and Materials, Philadelphia, Penn., pp. 99-132.

Coffman, W., D. Vogt, and M. Mills, 1984. A Summary of Computer Codes for Waste Package Performance Assessment, NUREG/CR-3699, U.S. Nuclear Regulatory Commission, Washington, D.C.

Conca, J. L., 1985. Differential Weathering Effects and Mechanisms, Ph.D. Dissertation, California Institute of Technology, Pasadena.

Cowan, R. L., II, and G. M. Gordon, 1977. "Intergranular Stress Corrosion Cracking and Grain Boundary Composition of Fe-Ni-Cr Alloys," Stress Corrosion Cracking and Hydrogen Embrittlement of Iron Base Alloys NACE-5, R. W. Staehle, J. Hochmann, R. D. McCright and J. E. Slater (eds.), National Association of Corrosion Engineers, Houston, Tex., pp. 1023-1070.

Croff, A. G., 1980. A User's Manual for the ORIGEN2 Computer Code, ORNL-TM-7175, Oak Ridge National Laboratory, Oak Ridge, Tenn.

Croff, A. G., and C. W. Alexander, 1980. Decay Characteristics of Once-Through LWR and LMFBR Spent Fuels, High-Level Wastes, and Fuel-Assembly Structural Material Waste, ORNL/TM-7431, Oak Ridge National Laboratory, Oak Ridge, Tenn.

DOE (U.S. Department of Energy), 1984. Generic Requirements for a Mined Geologic Disposal System, DOE/NE/44301-1, Washington, D.C.

DaCasa, C., V. B. Nileshwar, and D. A. Melford, 1969. "M23C6 Precipitation in Unstabilized Austenitic Stainless Steel," Journal of the Iron and Steel Institute, pp. 1325-1332.

Daily, W., W. Lin, and T. Buscheck, 1986. Hydrological Properties of Topopah Spring Tuff - Laboratory Measurements, UCRL-94363, Lawrence Livermore National Laboratory, Livermore, Calif.

Danko, J. C., 1984. "Recent Observations of Cracks in Large Diameter BWR Piping: Analysis and Remedial Actions," Proceedings of the International Symposium on Environmental Degradation of Materials in Nuclear Power Systems-Water Reactors, National Association of Corrosion Engineers, Houston, Tex., pp. 209-222.

Davis, R. B., and V. Pasupathi, 1981. Data Summary Report for the Destructive Examination of Rods G7, G9, J8, I9 and H6 from Turkey Point Fuel Assembly B17, HEDL-TME-80-85, Hanford Engineering Development Laboratory, Richland, Wash.

Delany, J. M., 1985. Reaction of Topopah Spring Tuff with J-13 Water: A Geochemical Modeling Approach Using the EQ3/6 Reaction Path Code, UCRL-53631, Lawrence Livermore National Laboratory, Livermore, Calif.

Delany, J. M., and T. J. Wolery, 1984. Fixed-Fugacity Option for the EQ6 Geochemical Reaction Path Code, UCRL-53598, Lawrence Livermore National Laboratory, Livermore, Calif.

Delany, J. M., I. Puigdomenech, and T. J. Wolery, 1986. Precipitation Kinetics Option for the EQ6 Geochemical Reaction Path Code, UCRL-53642, Lawrence Livermore National Laboratory, Livermore, Calif.

DePoorter, G. L., 1986. Letter from G. L. DePoorter (LANL) to M. D. Valentine (DOE/NV), TWS-ES-NP/01-86-28, January 17, 1986; regarding adjustment for correct mole fraction by dividing solute concentration by 55.5.

Duhaj, P., J. Ivan, and F. Makovicky, 1968. "Sigma Phase Precipitation in Austenitic Steels," Journal of the Iron and Steel Institute, pp. 1245-1251.

Durham, W. B., J. M. Beiriger, M. Axelrod, and S. Trettenero, 1985. The Effect of Gamma Irradiation on the Strength and Elasticity of Climax Stock and Westerly Granites, UCRL-92526, preprint, Lawrence Livermore National Laboratory, Livermore, Calif.

Ebert, W. L., J. K. Bates, T. J. Gerding, and R. A. Van Konynenburg, 1986. The Effects of Gamma Radiation on Groundwater Chemistry and Glass Reaction in a Saturated Tuff Environment, UCRL-95884, (preprint), Lawrence Livermore National Laboratory, Livermore, Calif.

Einziger, R. E., 1985. Technical Test Description of Activities to Determine the Potential for Spent Fuel Oxidation in a Tuff Repository, HEDL-7540, Hanford Engineering Development Laboratory, Richland, Wash.

Einziger, R. E., 1986. Test Plan for Long-Term, Low-Temperature Oxidation of Spent Fuel, Series 1, HEDL-7560, Hanford Engineering Development Laboratory, Richland, Wash.

Einziger, R. E., and J. A. Cook, 1984. LWR Spent Fuel Dry Storage Behavior at 229 deg. C, NUREG/CR-3708, U.S. Nuclear Regulatory Commission, Washington, D.C. pp. 90-92.

Einziger, R. E., and R. Kohli, 1984. "Low-Temperature Rupture Behavior of Zircaloy-Clad Pressurized Water Reactor Spent Fuel Rods Under Dry Storage Conditions," Nuclear Technology, Vol. 67, 107 p.

Einziger, R. E., and R. V. Strain, 1984. "Effect of Cladding Defect Size on the Oxidation of Irradiated Spent LWR Fuel Below 360 Degrees C," Proceedings of International Workshop on Irradiated Fuel Storage, Toronto, Canada, October 17-18, 1984, pp. 599-625.

Einziger, R. E., and R. E. Woodley, 1985a. Evaluation of the Potential for Spent Fuel Oxidation Under Tuff Repository Conditions, HEDL-7452, Hanford Engineering Development Laboratory, Richland, Wash.

Einziger, R. E., and R. E. Woodley, 1985b. Low Temperature Spent Fuel Oxidation Under Tuff Repository Conditions, HEDL SA-3271, Hanford Engineering Development Laboratory, Richland, Wash.

Einziger, R. E., and R. E. Woodley, 1986. Test Plan for Series 2 Thermogravimetric Analyses of Spent Fuel Oxidation, HEDL-7556, Hanford Engineering Development Laboratory, Richland, Wash.

Eisenstatt, L. R., 1986. Description of the West Valley Project Reference High-Level Waste Form and Canister, WVDP-056, Rev. 0, West Valley Demonstration Project, West Valley, N.Y.

Eklund, U., and R. Forsyth, 1978. Leaching of Irradiated Uranium Oxide Fuel, KBS Technical Report No. 70, Swedish Nuclear Fuel Supply Co., Karnbranslesakerhet, Stockholm, Sweden.

Fontana, M. G., and N. D. Greene, 1978. Corrosion Engineering, McGraw-Hill Book Company, New York. pp. 125-127.

Forsyth, R. S., K. Svanberg, and L. Werme, 1984. "The Corrosion of Spent UO2-Fuel in Synthetic Groundwater," Proceedings of the Third Spent Fuel Workshop, L. Werme (ed.), SKBF Technical Report 83-76, Swedish Nuclear Fuel Supply Co., Kaernbraenslesaekerhet, Stockholm, Sweden, pp. 1-12.

Forsyth, R. S., L. O. Werme, and J. Bruno, 1985. The Corrosion of Spent UO2 Fuel in Synthetic Groundwater, SKB Technical Report 85-16, Swedish Nuclear Fuel and Waste Management Co., Stockholm, Sweden.

Forsythe, W. R., and W. F. Giauque, 1942. "The Entropies of Nitric Acid and Its Mono-and Tri-hydrates," Journal American Chemical Society, Vol. 64, pp. 48-61.

Fox, M. J., and R. D. McCright, 1983. An Overview of Low Temperature Sensitization, UCRL-15619, Lawrence Livermore National Laboratory, Livermore, Calif.

Freude, E., B. Grambow, W. Lutze, H. Rabe, and R. C. Ewing, 1985. "Long-Term Release from High Level Waste Glass - Part IV: The Effect of Leaching Mechanism," Scientific Basis for Nuclear Waste Management VIII, Materials Research Society Symposia Proceedings, Boston, Massachusetts, November 26-29, 1984, C. M. Jantzen, J. A. Stone, and R. C. Ewing (eds.),

Vol. 44, Materials Research Society, Pittsburgh, Penn., pp. 99-106.

Fujita, N., M. Akiyama, and T. Tamura, 1981. "Stress Corrosion Cracking of Sensitized Type 304 Stainless Steel in High Temperature Water Under Gamma Ray Irridation," Corrosion, Vol. 37, No. 6, National Association of Corrosion Engineers, Houston, Tex., pp. 335-341.

Gane, C., and T. Sarson, 1979. Structured Systems Analysis: Tools and Techniques, Prentice-Hall, Inc., Englewood Cliffs, N.J., pp. 8-24.

Garrels, R. M., and P. Howard, 1957. "Reactions of Feldspar and Mica with Water at Low Temperature and Pressure," Proceeding of the Sixth National Conference on Clays and Clay Minerals, August 19-23, 1957, Berkeley, California, Pergamon Press, New York.

Glass, R. S., G. E. Overturf, R. E. Garrison, and R. D. McCright, 1984. Electrochemical Determination of the Corrosion Behavior of Candidate Alloys Proposed for Containment of High Level Nuclear Waste in Tuff, UCID-20174, Lawrence Livermore National Laboratory, Livermore, Calif.

Glass, R. S., G. E. Overturf III, R. A. Van Konynenburg, and R. D. McCright, 1985. Gamma Radiation Effects on Corrosion: I. Electrochemical Mechanisms for the Aqueous Corrosion Processes of Austenitic Stainless Steels, UCRL-92311, Lawrence Livermore National Laboratory, Livermore, Calif.

Glassley, W. E., 1986. Reference Waste Package Environment Report, UCRL-53726, Lawrence Livermore National Laboratory, Livermore, Calif.

Grambow, B., 1984. "A Physical-Chemical Model for the Mechanism of Glass Corrosion - with Particular Consideration of Simulated Radioactive Waste Glasses," Dissertation, Freien Universitaet, Berlin, Germany, DP-tr-78, Available in translation from NTIS.

Grambow, B., 1985. "A General Rate Equation for Nuclear Waste Glass Corrosion," Scientific Basis for Nuclear Waste Management VIII, Materials Research Society Symposia Proceedings, Boston, Massachusetts, November 26-29, 1984, C. M. Jantzen, J. A. Stone, and R. C. Ewing (eds.), Vol. 44,

Materials Research Society, Pittsburgh, Penn., pp. 15-27.

Grambow, B., H. P. Hermansson, I. K. Bjorner, and L. Werme, 1985. "Glass/Waste Reaction With and Without Bentonite Present - Experiment and Model," Scientific Basis for Nuclear Waste Management IX, Materials Research Society Symposia Proceedings, Stockholm, Sweden, September 9-11, 1985, L. O. Werme (ed.), Vol. 50, Materials Research Society, Pittsburgh, Penn., pp. 187-194.

Grambow, B., H. U. Zwicky, G. Bart, I. K. Bjorner, and L. O. Werme, 1987. "Modeling of the Effect of Iron Corrosion Products on Nuclear Waste Glass Performance," Scientific Basis for Nuclear Waste Management X, Materials Research Society Symposia Proceedings, December 1-4, 1986, Boston, Massachusetts, J. K. Bates and W. B. Seefeldt (eds.), Vol. 84, Materials Research Society, Pittsburgh, Penn., pp. 471-481.

Grasse, D., O. Kocar, J. Peisl, and S. C. Moss, 1982. "Diffuse X-Ray Scattering from Neutron Irradiated Crystalline Quartz," Radiation Effects, Vol. 66, pp. 61-71.

Hallquist, J. O., 1983. NIKE2D - A Vectorized, Implicit, Finite Deformation, Finite Element Code for Analyzing the Static and Dynamic Response of 2-D Solids, UCID-19677, Lawrence Livermore National Laboratory, Livermore, Calif.

Hastings, I. J., and J. Novak, 1984. "Behavior in Air at 175-250 deg. C of UO2 Fuel Fragments Extracted from Irradiated Elements," Proceedings of the U.S. Nuclear Regulatory Commission Workshop on Spent Fuel/Cladding Reaction During Dry Storage, D. W. Reisenweaver (ed.), NUREG/CP-0049, U.S. Nuclear Regulatory Commission, Washington, D.C.

Hastings, I. J., and J. Novak, 1986. Air Oxidation of UO2 Fuel: Chalk River Studies, AECL-9182, Atomic Energy of Canada Limited, Chalk River Nuclear Laboratories, Chalk River, Ontario, Canada.

Helgeson, H. C., 1968. "Evaluation of Irreversible Reactions in Geochemical Processes Involving Minerals and Aqueous Solutions-I. Thermodynamic Relations," Geochimica et Cosmochimica Acta, Vol. 32, pp. 853-857.

Helgeson, H. C., and W. M. Murphy, 1983. "Calculation of Mass Transfer Among Minerals and Aqueous Solutions as a Function of Time and Surface Area in Geochemical Processes. I. Computational Approach," Mathematical Geology, Vol. 15, No. 1, p. 109-130.

Helgeson, H. C., T. H. Brown, A. Nigrini, and T. A. Jones, 1970. "Calculation of Mass Transfer in Geochemical Processes Involving Aqueous Solutions," Geochimica et Cosmochimica Acta, Vol. 34, pp. 569-592.

Helgeson, H. C., J. M. Delany, H. W. Nesbitt, and D. K. Bird, 1978. "Summary and Critique of the Thermodynamic Properties of Rock-Forming Mineral," American Journal of Science, Vol. 278-A, Kline Geology Laboratory, Yale University, New Haven, Conn.

Helgeson, H. C., W. M. Murphy, and P. Aagaard, 1984. "Thermodynamic and Kinetic Constraints on Reaction Rates Among Minerals and Aqueous Solutions. II. Rate Constants, Effective Surface Area, and the Hydrolysis of Feldspars," Gechimica et Cosmochimica Acta, Vol. 48, No. 12, pp. 2405-2432.

Henne, M. S., 1982. "The Dissolution of Rainier Mesa Volcanic Tuffs, and its Application to the Analysis of the Groundwater Environment," Unpublished Thesis, University of Nevada, Reno.

Hockman, J. N., and W. C. O'Neal, 1984. Thermal Modeling of Nuclear Waste Package Designs for Disposal in Tuff, UCRL-89820, Rev. 1, Lawrence Livermore National Laboratory, Livermore, Calif.

INTERA Environmental Consultants, Inc., 1983. WAPPA: A Waste Package Performance Assessment Code, ONWI-452, Office of Nuclear Waste Isolation, Battelle Memorial Institute, Columbus, Ohio.

Iwasaki, S., 1982. "Methods for Preventing and Ameliorating Cracks in BWR Piping," Predictive Methods for Assessing Corrosion Damage to BWR Piping and PWR Steam Generators, H. Okada and R. Staehle (eds.), National Association of Corrosion Engineers, Houston, Tex., pp. 144-152.

Jackson, K. J., and T. J. Wolery, 1985. "Extension of the EQ3/6 Computer Codes to Geochemical Modeling of Brines," Scientific Basis for Nuclear Waste Management VIII, Materials Research Society Symposia Proceedings, November 26-29, 1984, Boston, Massachusetts, C. M. Jantzen, J. A. Stone, and R. C. Ewing (eds.), Vol. 44, pp. 507-513.

Jacobs, G. K., and S. K. Whatley (eds.), 1985. Proceedings of the Conference on the Application of Geochemical Models to High-Level Nuclear Waste Repository Assessment, Oak Ridge, Tenn., October 2-5, 1984, NUREG/CP-0062, Oak Ridge National Laboratory, Oak Ridge, Tenn., 126 pp.

Johnson, A. B., Jr., and E. R. Gilbert, 1984. "Reaction of Fuel Cladding with Cover Gases Under Dry Storage Conditions," Proceedings of the U.S. Nuclear Regulatory Commission Workshop on Spent Fuel/Cladding Reaction During Dry Storage, D. W. Reisenweaver (ed.), NUREG/CP-0049, U.S. Nuclear Regulatory Commission, Washington, D.C. pp. I-1 to I-10.

Johnson, A. B., E. R. Gilbert, D. Stahl, V. Pasupathi, and R. Kohli, 1984. "Exposure of Breached BWR Fuel Rods at 320 deg. C to Air and Argon," Proceedings of the U.S. Nuclear Regulatory Commission Workshop on Spent Fuel/Cladding Reaction During Dry Storage, D. W. Reisenweaver (ed.), NUREG/CP-0049, U.S. Nuclear Regulatory Commission, Washington, D.C. pp. E-2 to E-5.

Johnson, L. H., 1982. The Dissolution of Irradiated UO2 Fuel in Groundwater, AECL-6837, Atomic Energy of Canada Limited, Whiteshell Nuclear Research Establishhment, Pinawa, Manitoba, Canada.

Johnson, L. H., K. I. Burns, H. Joling, and C. J. Moore, 1981. The Dissolution of Irradiated UO2 Fuel Under Hydrothermal Oxidizing Conditions, TR-128, Atomic Energy of Canada Limited, Pinawa, Manitoba, Canada, pp. 6, 10, 18, 23.

Johnson, L. H., D. W. Shoesmith, G. E. Lunansky, M. G. Bailey, and P. R. Tremaine, 1982. "Mechanisms of Leaching and Dissolution of UO2 Fuel," Nuclear Technology, Vol. 56, pp. 238-253.

Johnson, L. H., K. I. Burns, H. H. Joling, and C. J. Moore, 1983a. "Leaching of 137Cs, 134Cs, and 129I from Irradiated UO2 Fuel," Nuclear Technology, Vol. 63, pp. 470-475.

Johnson, L. H., S. Stroes-Gascoyne, D. W. Shoesmith, M. G. Bailey, and D. M. Sellinger, 1983b. "Leaching and Radiolysis Studies on UO2 Fuel," Proceedings of the Third Spent Fuel Workshop, L. Werme (ed.), KBS 83-76, Swedish Nuclear Fuel Supply Co., Kaernbraenslesaekerket, Stockholm, Sweden.

Johnson, L. H., S. Stroes-Gascoyne, J. D. Chen, M. E. Attas, D. M. Sellinger, and H. G. Delaney, 1985. "The Relationship between Fuel Element Power and the Leaching of 137Cs and 129I from Irradiated UO2 Fuel," Proceedings of the ANS Topical Meeting on Fission-Product Behavior and Source Term Research, Snowbird, Utah, July 1984, American Nuclear Society.

Johnstone, J. K., R. R. Peters, and P. F. Gnirk, 1984. Unit Evaluation at Yucca Mountain, Nevada Test Site: Summary Report and Recommendation, SAND83-0372, Sandia National Laboratories, Albuquerque, N. Mex.

Jones, A. R., 1959. "Radiation-Induced Reactions in the N2 - O2 - H2O System," Radiation Research, Vol. 10, pp. 655-663.

Juhas, M. C., R. D. McCright, and R. E. Garrison, 1984. Behavior of Stressed and Unstressed 304L Specimens in Tuff Repository Environmental Conditions, UCRL-91804, Lawrence Livermore National Laboratory, Livermore, Calif.

Katayama, Y. B., D. J. Bradley, and C. O. Harvey, 1980. Status Report on LWR Spent Fuel IAEA Leach Tests, PNL-3173, Battelle Pacific Northwest Laboratories, Richland, Wash.

Kerrisk, J. F., 1984. Solubility Limits on Radionuclide Dissolution at a Yucca Mountain Repository, LA-9995-MS, Los Alamos National Laboratory, Los Alamos, N. Mex.

Kieffer, S. W., 1985. "Heat Capacity and Entropy: Systematic Relations to Lattice Vibrations," Microscopic to Macroscopic, Atomic Environments to Mineral Thermodynamics, S. W. Kieffer and A. Navrotsky (eds.), Vol. 14, Chapter 3, Reviews in Mineralogy, Mineralogical Society of America, Blacksburg, Virginia, pp. 65-126.

Kingston, H. M., D. J. Cronin, and M. S. Epstein, 1984. "Investigation of a Precise Static Leach Test for the Testing of Simulated Nuclear Waste Materials," Nuclear and Chemical Waste Management, Vol. 5, pp. 3-15.

Klavetter, E. A., and R. R. Peters, 1986. Fluid Flow in a Fractured Rock Mass, SAND85-0855, Sandia National Laboratories, Albuquerque, N. Mex.

Knauss, K. G., 1984. Petrologic and Geochemical Characterization of the Topopah Spring Member of the Paintbrush Tuff: Outcrop Samples Used in Waste Package Experiment, UCRL-53558, Lawrence Livermore National Laboratory, Livermore, Calif.

Knauss, K. G., and W. B. Beiriger, 1984. Report on Static Hydrothermal Alteration Studies of Topopah Spring Tuff Wafers in J-13 Water at 150 deg. C, UCRL-53576, Lawrence Livermore National Laboratory, Livermore, Calif.

Knauss, K. G., and T. J. Wolery, 1986. "Dependence of Albite Dissolution Kinetics on pH and Time at 25 degrees C and 70 degrees C," Geochimica et Cosmochimica Acta, Vol. 50, No. 11, Journal of the Geochemical Society and the Meteoritical Society, pp. 2481-2497.

Knauss, K. G., V. M. Oversby, and T. J. Wolery, 1983. Post Emplacement Environment of Waste Packages, UCRL-89475, preprint, Lawrence Livermore National Laboratory, Livermore, Calif.

Knauss, K. G., J. M. Delany, W. B. Beiriger, and D. W. Peifer, 1984. Hydrothermal Interaction of Topopah Spring Tuff with J-13 Water as a Function of Temperature, UCRL-90853, Lawrence Livermore National Laboratory, Livermore, Calif.

Knauss, K. G., W. J. Beiriger, and D. W. Peifer, 1985. Hydrothermal Interaction of Crushed Topopah Spring Tuff and J-13 Water at 90, 150 and 250 deg. C Using Dickson-Type Gold-Bag Rocking Autoclaves, UCRL-53630, Lawrence Livermore National Laboratory, Livermore, Calif.

Knauss, K. G., W. J. Beiriger, and D. W. Peifer, 1987a. Hydrothermal Interaction of Solid Wafers of Topopah Spring Tuff with J-13 Water at 90 and 150 Degrees C Using Dickson-type, Gold-Bag Rocking Autoclaves: Long-Term Experiments, UCRL-53722, Lawrence Livermore National

Laboratory, Livermore, Calif.

Knauss, K. G., W. B. Beiriger, D. W. Peifer, and A. Piwinskii, 1987b. Reaction of Solid Wafers of Topopah Spring Tuff with J-13 and Distilled Water at 90, 150, and 250 deg. C in Dickson-Type Gold-Bag Rocking Autoclaves: 1. Short Term Experiments, UCRL-53845, Lawrence Livermore National Laboratory, Livermore, Calif.

Latanision, R. M., and R. W. Staehle, 1969. "Stress Corrosion Cracking of Iron-Nickel-Chromium Alloys," Proceedings of Conference: Fundamental Aspects of Stress Corrosion Cracking, National Association of Corrosion Engineers, Houston, Tex., pp. 214-307..

Lin, F. -C., and C. V. Clemency, 1981. "Dissolution Kinetics of Phlogopite. I. Closed System," Clays and Clay Minerals, Vol. 29, No. 1, p. 101-106.

Lin, W., and W. Daily, 1984. Transport Properties of Topopah Spring Tuff, UCRL-53602, Lawrence Livermore National Laboratory, Livermore, Calif.

Logan, R. W., 1983. Computer Simulation of Sensitization in Stainless Steels, UCID-20000, Lawrence Livermore National Laboratory, Livermore, Calif.

MCC (Materials Characterization Center), 1983. MCC-1P Static Leach Test Method, Nuclear Waste Materials Handbook Test Methods, MRB-0328.

Majidi, A. P., and M. A. Streicher, 1984. "Potentiodynamic Reactivation Method for Detecting Sensitization in AISI 304 and 304L Stainless Steel," Corrosion, Vol. 40, No. 8, National Association of Corrosion Engineers, Houston, Tex., pp. 393-408.

Manaktula, H. K., 1982. Nuclear Waste Management Technical Support in the Development of Nuclear-Waste-Form Criteria for the NRC Task 3. Waste Inventory Review. NUREG/CR-2333, Vol. 3, U.S. Nuclear Regulatory Commission, Washington, D.C.

Mansfeld, F., 1977. "Polarization Resistance Measurements - Experimental Procedure and Evaluation of Test Data," Electrochemical Techniques for Corrosion, R. Baboian (ed.), National Association of Corrosion Engineers, Houston, Tex.,

pp. 18-26.

McCright, R. D., 1985. FY 1985 Status Report on Feasibility Assessment of Copper-Base Waste Package Container Materials in a Tuff Repository, UCID-20509, Lawrence Livermore National Laboratory, Livermore, Calif.

McCright, R. D., H. Weiss, M. C. Juhas, and R. W. Logan, 1983. Selection of Candidate Canister Materials for High-Level Nuclear Waste Containment in a Tuff Repository, (preprint), UCRL-89988, Lawrence Livermore National Laboratory, Livermore, Calif.

McCright, R. D., W. G. Halsey, and R. A. Van Konynenburg, 1987. Progress Report on the Results of Testing Advanced Conceptual Design Metal Barrier Materials Under Relevant Environmental Conditions for a Tuff Repository, UCID-21044, draft, Lawrence Livermore National Laboratory, Livermore, Calif.

McKay, M. D., R. J. Beckman, and W. J. Conover, 1979. "A Comparison of Three Methods for Selecting Values of Input Variables in the Analysis of Output from a Computer Code," Technometrics, Vol. 21, No. 2, pp. 239-245.

McVay, G. L., and G. R. Robinson, 1984. Effects of Tuff Waste Package Components on Release from 76-68 Simulated Waste Glass, PNL-4897, Pacific Northwest Laboratories, Richland, Wash.

Mendel, J. E. (comp.), 1981. A State-of-the-Art Review of Materials Properties of Nuclear Waste Forms, PNL-3802, Pacific Northwest Laboratory, Matericals Characterization Center, Richland, Wash., 210 p.

Mendel, J. E. (comp.), 1984. Final Report of the Defense High-Level Leaching Mechanisms Program, PNL-5157, Pacific Northwest Laboratories, Richland, Wash.

Miller, A. K., and A. Tasooji, 1984. "Estimating the Limiting Temperature for Dry Storage with Respect to Stress Corrosion Cracking," Proceedings of the U.S. Nuclear Regulatory Commission Workshop on Spent Fuel/Cladding Reaction During Dry Storage, D. W. Reisenweaver (ed.), NUREG/CP-0049, U.S. Nuclear Regulatory Commission, Washington, D.C.

Montan, D. N., 1986. Memorandum from D. N. Montan (LLNL) to L. B. Ballou (LLNL), May 9, 1986; regarding the boiling point of water - theme and variations.

Montazer, P., and W. E. Wilson, 1984. Conceptual Hydrologic Model of Flow in the Unsaturated Zone, Yucca Mountain, Nevada, USGS-WRI-84-4345, Water-Resources Investigations Report, U.S. Geological Survey, Lakewood, Colo.

Montazer, P., E. P. Weeks, F. Thamir, S. N. Yard, and P. B. Hofrichter, 1986. "Monitoring the Vadose Zone in Fractured Tuff, Yucca Mountain, Nevada," Proceedings of the NWWA Conference on Characterization and Monitoring of the Vadose (Unsaturated) Zone, November 19-21, 1985, Denver, Colo., National Water Well Association, Worthington, Ohio, pp. 439-469.

Morales, A., 1985. Technical Correspondence in Support of the Final Environmental Assessment, SAND85-2509, Sandia National Laboratories, Albuquerque, N. Mex.

Morrow, C., D. Lockner, D. Moore, and J. Byerlee, 1981. "Permeability of Granite in a Temperature Gradient," Journal of Geophysical Research, Vol. 86, No. B4, pp. 3002-3008.

Morrow, C. A., D. E. Moore, and J. D. Byerlee, 1985. "Permeability Changes in Crystalline Rocks Due to Temperature: Effects of Mineral Assemblage," Scientific Basis for Nuclear Waste Management VIII, Materials Research Society Symposia Proceedings, Boston, Massachusetts, November 26-29, 1984, C. M. Jantzen, J. A. Stone, and R. C. Ewing (eds.), Vol. 44, Materials Research Society, Pittsburgh, Penn., pp. 467-474.

Mozhi, T. A., W. A. T. Clark, K. Nishimoto, W. B. Johnson, and D. D. MacDonald, 1985. "The Effect of Nitrogen on the Sensitization of AISI 304 Stainless Steel," Corrosion--NACE, Vol. 41, No. 10, National Association of Corrosion Engineers, pp. 555-559.

Mulford, R. A., E. L. Hall, C. L. Briant, 1983. "Sensitization of Austenitic Stainless Steels II. Commercial Purity Alloys," Corrosion, Vol. 39, National Association of Corrosion Engineers, Houston, Tex., pp. 132-143.

NRC (U.S. Nuclear Regulatory Commission), 1983. PRA Procedures Guide: A Guide to the Performance of Probabalistic Risk Assessments for Nuclear Power Plants, NUREG/CR-2300, Washington, D.C.

NRC (U.S. Nuclear Reglatory Commission), 1986. Waste Package Reliability, NUREG/CR-4509, Washington, D.C.

NWPA (Nuclear Waste Policy Act), 1983. "Nuclear Waste Policy Act of 1982," Public Law 97-425, 42 USC 10101-10226, Washington, D.C.

Nordstrom, D. K., and J. W. Ball, 1984. "Chemical Models, Computer Programs and Metal Complexation in Natural Waters," Complexation of Trace Metals in Natural Waters, C. J. M. Kramer and J. C. Duinker (eds.), Martinus Nijhoff/ Dr. W. Junk Publishers, The Hague, pp. 149-164.

Novak, C. J., 1977. "Structure and Constitution of Wrought Austenitic Stainless Steels," Handbook of Stainless Steels, D. Peckner and I. M. Bernstein (eds.), McGraw-Hill Book Co., New York.

Novak, J. and I. J. Hastings, 1983. "Post-irradiation Behavior of Defected UO2 Fuel Elements in Air at 220-250 Degrees C," Proceedings of NRC Workshop on Spent Fuel/Cladding Reaction During Dry Storage, D. Reisenweaver (ed.), NUREG/CP-0049, Gaithersburg, Maryland, pp. 3-25.

Novak, J., I. J. Hastings, E. Mizzan, and R. Chenier, 1983. "Postirradiation Behavior of UO2 Fuel I: Elements at 220 to 250 deg. C in Air," Nuclear Technology, Vol. 63, pp. 254-263.

Nuttall, K., and V. F. Urbanic, 1981. An Assessment of Materials for Nuclear Fuel Immobilization, AECL-6440, Atomic Energy of Canada Limited, Whiteshell Nuclear Research Establishment, Pinawa, Manitoba.

O'Brien, P. D., 1986. OGR Repository-Specific Rod Consolidation Study: Effect on Costs, Schedules, and Operations at Yucca Mountain Repository, SAND86-2357, Draft, Sandia National Laboratories, Albuquerque, N. Mex.

O'Connell, W. J., and R. S. Drach, 1986. Waste Package Performance Assessment: Deterministic System Model -- Program Scope and Specification, UCRL-53761, Lawrence Livermore National Laboratory, Livermore, Calif.

Ogard, A. E., and J. F. Kerrisk, 1984. Groundwater Chemistry Along Flow Paths Between a Proposed Repository Site and the Accessible Environment, LA-10188-MS, Los Alamos National Laboratory, Los Alamos, N. Mex.

Olander, D. R., 1976. Fundamental Aspects of Nuclear Reactor Fuel Elements, TID-26711-P1, Technical Information Center, Oak Ridge, Tenn.

O'Neal, W. C., D. W. Gregg, J. N. Hockman, E. W. Russell, and W. Stein, 1984. Preclosure Analysis of Conceptual Waste Package Designs for a Nuclear Waste Repository in Tuff, UCRL-53595, Lawrence Livermore National Laboratory, Livermore, Calif.

Ortiz, T. S., R. L. Williams, F. B. Nimick, B. C. Whittet, and D. L. South, 1985. A Three-Dimensional Model of Reference Thermal/Mechanical and Hydrological Stratigraphy at Yucca Mountain, Southern Nevada, SAND84-1076, Sandia National Laboratories, Albuquerque, N. Mex.

Ostwald, W., 1887. Lehrbuch Der Allgemeine Chemie, Wilhelm Engelmann, Leipzig.

Oversby, V. M., 1984a. Reaction of the Topopah Spring Tuff with J-13 Well Water at 90 deg. C and 150 deg. C, UCRL-53552, Lawrence Livermore National Laboratory, Livermore, Calif.

Oversby, V. M., 1984b. Reference Waste Forms and Packing Material for the Nevada Nuclear Waste Storage Investigations Project, UCRL-53531, Lawrence Livermore National Laboratory, Livermore, Calif.

Oversby, V. M., 1985. The Reaction of Topopah Spring Tuff with J-13 Water at 150 deg. C- Samples from Drill Cores USW G-1, USW GU-3, USW G-4, and UE-25h 1, UCRL-53629, Lawrence Livermore National Laboratory, Livermore, Calif.

Oversby, V. M., 1986. Important Radionuclides in High Level Nuclear Waste Disposal: Determination Using a Comparison of the EPA and NRC Regulations, UCRL-94222, (preprint), Lawrence Livermore National Laboratory, Livermore, Calif.

Oversby, V. M., and K. G. Knauss, 1983. Reaction of Bullfrog Tuff with J-13 Well Water at 90 deg C and 150 deg C, UCRL-53442, Lawrence Livermore National Laboratory, Livermore, Calif.

Oversby, V. M., and R. D. McCright, 1984. Laboratory Experiments Designed to Provide Limits on the Radionuclide Source Term for the NNWSI Project, UCRL-91257, Lawrence Livermore National Laboratory, Livermore, Calif.

Oversby, V. M., and H. D. Shaw, 1986. Spent Fuel Data: An Analysis of Data Relevant to the NNWSI Project, UCID-20926, Lawrence Livermore National Laboratory, Livermore, Calif.

Oversby, V. M., and C. N. Wilson, 1985. Derivation of a Waste Package Source Term for NNWSI from the Results of Laboratory Experiments, UCRL-92096 (preprint), Lawrence Livermore National Laboratory, Livermore, Calif.

Paul, A., 1977. "Chemical Durability of Glasses; A Thermodynamic Approach," Journal of Materials Science, Vol. 12, pp. 2246-2268.

Pederson, L. R., C. Q. Buckwalter, G. L. McVay, and B. L. Riddle, 1983. "Glass Surface Area to Volume Ratio and Its Implications to Accelerated Leach Testing," Scientific Basis for Nuclear Waste Management VI, Materials Research Society Symposia Proceedings, Boston, Massachusetts, November, 1982, D. G. Brookins (ed.), Vol. 15, North-Holland, Elsevier Science Publishing Co., Inc., New York, pp. 47-54.

Pessall, N., and J. I. Nurminen, 1974. "Development of Ferritic Stainless Steels for Use in Desalination Plants," Corrosion, NACE, Vol. 30, No. 11, pp. 381-392.

Plodinec, M. J., G. G. Wicks, and N. E. Bibler, 1982. An Assessment of Savannah River Borosilicate Glass in the Repository Environment, DP-1629, E.I. du Pont de Nemours and Co., Savannah River Laboratory, Aiken, S.C.

Povich, M. J., 1978. "Low Temperature Sensitization of Welded Type 304 Stainless Steel," Corrosion, Vol. 34, No. 2, National Association of Corrosion Engineers, Houston, Tex., pp. 60-65.

Proebstle, R. A., and G. M. Gordon, 1982. "Overview of Predictive Testing for BWR Piping Corrosion," Predictive Methods for Assessing Corrosion Damage to BWR Piping and PWR Steam Generators, H. Okada and R. Staehle (eds.), National Association of Corrosion Engineers, Houston, Tex., pp. 19-30.

Pruess, K., and J. S. Y. Wang, 1984. "TOUGH--A Numerical Model for Nonisothermal Unsaturated Flow to Study Waste Canister Heating Effects," Scientific Basis for Nuclear Waste Management VII, Materials Research Society Symposia Proceedings, Boston, Massachusetts, November 1983, G. L. McVay (ed.), Vol. 26, North-Holland, Elsevier Science Publishing Co., Inc., New York, pp. 1031-1038.

Pruess, K., Y. W. Tsang, and J. S. Y. Wang, 1984. Numerical Studies of Fluid and Heat Flow Near High-Level Nuclear Waste Packages Emplaced in Partially Saturated Fractured Tuff, LBL-18552, Lawrence Berkeley Laboratory, Berkeley, Calif.

Rimstidt, J. D., and H. L. Barnes, 1980. "The Kinetics of Silica-Water Reactions," Geochimica et Cosmochimica Acta, Vol. 44, pp. 1683-1699.

Roddy, J. W., H. C. Claiborne, R. C. Ashline, P. J. Johnson, and B. T. Rhyne, 1985. Physical and Decay Characteristics of Commercial LWR Spent Fuel, ORNL/TM-9591/V1, Oak Ridge National Laboratory, Oak Ridge, Tenn.

Roseboom, E. H., Jr., 1983. Disposal of High-Level Nuclear Waste Above the Water Table in Arid Regions, U.S. Geological Survey Circular 903, Alexandria, Va. p. 21.

Rothman, A. J., 1984. Potential Corrosion and Degradation Mechanisms of Zircaloy Cladding on Spent Nuclear Fuel in a Tuff Repository, UCID-20172, Lawrence Livermore National Laboratory, Livermore, Calif.

Russell, E. W., R. D. McCright, and W. C. O'Neal, 1983. Containment Barrier Metals for High-Level Waste Packages in a Tuff Repository, UCRL-53449, Lawrence Livermore National Laboratory, Livermore, Calif.

SAE (Society of Automotive Engineers), 1977. Unified Numbering System for Metals and Alloys, SAE HS1086a, Society of Automotive Engineer's, Inc., Warrendale, Penn.

SNL (Sandia National Laboratories), 1987. Site Characterization Plan Conceptual Design Report, SAND84-2641, Sandia National Laboratories, Albuquerque, N. Mex.

Savannah River Plant and Laboratory, 1984. Waste Management Program Technical Progress Report, January-March, 1984, DP-84-125-1, E. I. du Pont de Nemours Co., Aiken, S. Carolina.

Scott, R. B., R. W. Spengler, S. Diehl, A. R. Lappin, and M. P. Chornak, 1983. "Geologic Character of Tuffs in the Unsaturated Zone at Yucca Mountain, Southern Nevada," Role of the Unsaturated Zone in Radioactive and Hazardous Waste Disposal, J. W. Mercer, P. S. C. Rao, and I. W. Marine (eds.), Ann Arbor Science Publishers, Ann Arbor, Mich., pp. 289-335.

Shoesmith, D. W., S. Sunder, M. G. Bailey, and D. G. Owen, 1983. "Anodic Oxidation of UO2 - Part III, Electrochemical Studies in Carbonate Solutions," in Passivity of Metals and Semiconductors, M. Fromont (ed.), Elsevier Science Publishing Co., Amsterdam, pp. 125-130.

Shreir, L. L. (ed.), 1976. "The Atmosphere," Corrosion, Metal/Environment Reactions, Vol. 1, Newnes-Butterworths, London, pp. 2:26-2:37.

Sinnock, S., Y. T. Lin, and J. P. Brannen, 1984. Preliminary Bounds on the Expected Postclosure Performance of the Yucca Mountain Repository Site, Southern Nevada, SAND84-1492, Sandia National Laboratories, Albuquerque, N. Mex.

Smith, H. D., 1984a. Zircaloy Spent Fuel Cladding Electrochemical Corrosion-Scoping Experiment, HEDL-TC-2562, Hanford Engineering Development Laboratory, Richland, Wash.

Smith, H. D., 1984b. Spent Fuel Cladding Characteristics and Choice of Experimental Specimens for Cladding-Corrosion Evaluation Under Tuff Repository Conditions, HEDL-TC-2530, Hanford Engineering Development Laboratory, Richland, Wash.

Smith, H. D., 1985. Zircaloy Cladding Corrosion Degradation in a Tuff Repository: Initial Experimental Plan, HEDL-7455, Rev. 1, Hanford Engineering Development Laboratory, Richland, Wash.

Smith, H. D., 1986a. Zircaloy Spent Fuel Cladding Electrochemical Corrosion Experiment at 170 Degrees C and 120 PSIA H2O, HEDL-7545, Hanford Engineering Development Laboratory, Richland, Wash.

Smith, H. D., 1986b. "C-ring" Stress Corrosion Cracking Scoping Experiment for Zircaloy Spent Fuel Cladding, HEDL-7546, Hanford Engineering Development Laboratory, Richland, Wash.

Smith, H. D., and V. M. Oversby, 1985. Spent Fuel Cladding Corrosion Under Tuff Repository Conditions: Initial Observations, UCID-20499, Lawrence Livermore National Laboratory, Livermore, Calif.

St. John, C. M., 1985. Thermal Analysis of Spent Fuel Disposal in Vertical Emplacement Boreholes in a Welded Tuff Repository, SAND84-7207, Sandia National Laboratories, Albuquerque, N. Mex.

Staehle, R. W., 1971. "Stress Corrosion Cracking of the Fe-Cr-Ni Alloy System," The Theory of Stress Corrosion Cracking in Alloys, J. C. Scully (ed.), National Atlantic Treaty Organization Scientific Affairs Division, Brussels, Belgium.

Stein, W., J. N. Hockman, and W. C. O'Neal, 1984. Thermal Analysis of NNWSI Conceptual Waste Package Designs, UCID-20091, Lawrence Livermore National Laboratory, Livermore, Calif.

Stephens, K., L. Boesch, B. Crone, R. Johnson, R. Molev, S. Smith, and L. Zarenkov, 1986. Methodologies for Assessing Long-Term Performance of High-Level Radioactive Waste Packages, NUREG/CR-4477, Washington, D.C.

Stoecker, J. G., and D. H. Pope, 1986. "Study of Biological Corrosion in High Temperature Demineralized Water," Materials Performance, Vol. 25, No. 6, pp. 51-56.

Strachan, D. M., K. M. Krupka, and B. Grambow, 1984. "Solubility Interpretations of Leach Tests on Nuclear Waste Glass," Nuclear and Chemical Waste Management, Vol. 5, pp. 87-99.

Strachan, D. M., L. R. Pederson, and R. O. Lokken, 1985. "Results from the Long-Term Interaction and Modeling of SRL-131 Glass with Aqueous Solutions," Scientific Basis for Nuclear Waste Management IX, Materials Research Society Symposia Proceedings, Stockholm, Sweden, September 9-11, 1985, L. O. Werme (ed.), Vol. 50, Materials Research Society, Pittsburgh, Penn., pp. 195-202.

Streicher, M. A., 1978. "Theory and Application of Evaluation Tests for Detecting Susceptibility to Intergranular Attack in Stainless Steels and Related Alloys -- Problems and Opportunities," Intergranular Corrosion of Stainless Alloys, R. F. Steigerwald (ed.), ASTM Special Technical Publication 656, American Society for Testing and Materials, Philadelphia, Penn. pp. 3-84.

Stula, R. T., T. E. Albert, B. E. Kirstein, and D. H. Lester, 1980. Systems Study on Engineered Barriers: Barrier Performance Analysis, ONWI-211, Office of Nuclear Waste Isolation, Battelle Memorial Institute, Columbus, Ohio.

Stumpe, R., J. I. Kim, W. Schrepp, and H. Walther, 1984. "Speciation of Actinide Ions in Aqueous Solution by Laser-Induced Pulsed Photoacoustic Spectroscopy," Applied Physics, Vol. B34, pp. 203-206.

Sunder, S., D. W. Shoesmith, M. G. Bailey, F. W. Stanchell, and N. S. McIntyre, 1981. "Anodic Oxidation of UO2: Part I. Electrochemical and X-ray Photoelectron Spectroscopic Studies in Neutral Solutions," Journal Electroanal. Chem., Vol. 130, pp. 163-179.

Sverjensky, D. A., 1984. "Prediction of Gibbs Free Energies of Calcite-Type Carbonates and the Equilibrium Distribution of Trace Elements Between Carbonates and Aqueous Solutions," Geochimica et Cosmochimica Acta, Vol. 48, pp. 1127-1134.

Szklarska-Smialowska, S., 1974. "The Pitting of Iron-Chromium-Nickel Alloys," Localized Corrosion NACE-3, R. W. Staehle, B. F. Brown, J. Kruger and A. Agrawal (eds.), National Association of Corrosion Engineers, Houston, Tex., pp. 312-341.

Theus, G. J., and R. W. Staehle, 1977. "Review of Stress Corrosion Cracking and Hydrogen Embrittlement in the Austenitic Fe-Cr-Ni Alloys," Stress Corrosion Cracking and Hydrogen Embrittlement of Iron-Base Alloys, National Association of Corrosion Engineers, Houston, Tex., pp. 845-892.

Tokunaga, O., and N. Suzuki, 1984. "Radiation Chemical Reactions in NOx and SO2 Removals from Flue Gas," Radiation, Physics and Chemistry, Vol. 24, No. 1, pp. 145-165.

Travis, B. J., 1984. TRACR3D: A Model of Flow and Transport in Porous/Fractured Media, LA-9667-MS, Los Alamos National Laboratory, Los Alamos, N. Mex.

Travis, B. J., S. W. Hodson, H. E. Nuttall, T. L. Cook, and R. S. Rundberg, 1984. Preliminary Estimates of Water Flow and Radionuclide Transport in Yucca Mountain, LA-UR-84-40 (Rev.), Los Alamos National Laboratory, Los Alamos, N. Mex.

Truman, J. E., 1977. "The Influence of Cloride Content, pH and Temperature of Test Solution on the Occurrence of Stress Corrosion Cracking with Austenitic Stainless Steel," Corrosion Science, Vol. 17, pp. 737-746.

Van Konynenburg, R. A., 1984. Radiation Doses in Granite Around Emplacement Holes in the Spent Fuel Test -- Climax (Final Report), UCRL-53580, Lawrence Livermore National Laboratory, Livermore, Calif.

Van Konynenburg, R. A., 1986. Radiation Chemical Effects in Experiments to Study the Reaction of Glass in an Environment of Gamma-Irradiated Air, Groundwater, and Tuff, UCRL-53719, Lawrence Livermore National Laboratory, Livermore, Calif.

Van Konynenburg, R. A., C. F. Smith, H. W. Culham, and C. H. Otto, Jr., 1984. Behavior of Carbon-14 in Waste Packages for Spent Fuel in a Repository in Tuff, UCRL-90855, Rev. 1, Lawrence Livermore National Laboratory, Livermore, Calif.

Van Konynenburg, R. A., C. F. Smith, H. W. Culham, and H. D. Smith, 1986. "Carbon-14 in Waste Packages for Spent Fuel in a Tuff Repository," Materials Research Society December 1986 Meeting, UCRL-94708, preprint, Boston, Mass.

Vaniman, D. T., D. Bish, D. Broxton, F. Byers, G. Heiken, B. Carlos, E. Semarge, F. Caporuscio, and R. Gooley, 1984. Variations in Authigenic Mineralogy and Sorptive Zeolite Abundance at Yucca Mountain, Nevada, Based on Studies of Drill Cores USW GU-3 and G-3, LA-9707-MS, Los Alamos National Laboratory, Los Alamos, N. Mex.

Verink, E. D., Jr., 1977. "Application of Electrochemical Techniques in the Development of Alloys for Corrosive Service," Electrochemical Techniques for Corrosion, R. Babioan (ed.), National Association of Corrosion Engineers, Houston, Tex., pp. 43-52.

Wald, J. W., 1985. Fabrication and Characterization of MCC Approved Testing Material - ATM-8 Glass, PNL-5577-8, Battelle Pacific Northwest Laboratories, Richland, Wash.

Wallace, R. M., and G. G. Wicks, 1983. "Leaching Chemistry of Defense Borosilicate Glass," Scientific Basis for Nuclear Waste Management VI, Materials Research Society Symposia Proceedings, Boston, Massachusetts, November, 1982, D. G. Brookins (ed.), Vol 15, North-Holland, Elsevier Science Publishing Co., Inc., New York, pp. 23-28.

Wang, J. S. Y., and T. N. Narasimhan, 1985. Hydrologic Mechanisms Governing Fluid Flow in Partially Saturated, Fractured Porous Tuff at Yucca Mountain, SAND84-7202, Sandia National Laboratories, Albuquerque, N. Mex.

Wang, R., 1981. Spent Fuel Special Studies Progress Report: Probable Mechanisms for Oxidation and Dissolution of Single-Crystal UO2 Surfaces, PNL-3566, Battelle Pacific Northwest Laboratories, Richland, Wash.

Wang, R., and Y. B. Katayama, 1982. "Dissolution Mechanisms for UO2 and Spent Fuel," Nuclear and Chemical Waste Management, Vol. 3, pp. 83-90.

Warren, R. G., F. M. Byers, and F. A. Caporuscio, 1984. Petrography and Mineral Chemistry of Units of the Topopah Spring, Calico Hills and Crater Flat Tuffs, and Older Volcanic Units, with Emphasis on Samples from Drill Hole USW G-1, Yucca Mountain, Nevada Test Site, LA-10003-MS, Los Alamos National Laboratory, Los Alamos, N. Mex.

Weeks, E. P., and W. E. Wilson, 1984. Preliminary Evaluation of Hydrologic Properties of Cores of Unsaturated Tuff, Test Well USW H-1, Yucca Mountain, Nevada, USGS-WRI-84-4193, Water-Resources Investigations Report, U.S. Geological Survey, Denver, Colo.

Wegrzyn, J., and A. Klimpel, 1981. "The Effect of Alloying Elements on Sigma Phase Formation in 18-8 Weld Metals," Welding Journal, pp. 146S-154S.

Westerman, R. E., S. G. Pitman, and J. H. Haberman, 1987. Corrosion Testing of Type 304L Stainless Steel in Tuff Groundwater Environments, PNL-5829, Pacific Northwest Laboratories, Richland, Wash.

White, A. F., H. C. Claassen, and L. V. Benson, 1980. The Effect of Dissolution of Volcanic Glass on the Water Chemistry in a Tuffaceous Aquifer, Rainier Mesa, Nevada, USGS-WSP-1535-Q, Water-Supply Paper, U.S. Geological Survey, Washington, D.C.

White, G. D., C. A. Knox, E. R. Gilbert, and A. B. Johnson, Jr., 1984. "Oxidation of UO2 at 150 to 350 deg. C," Proceedings of the U.S. Nuclear Regulatory Commission Workshop on Spent Fuel/Cladding Reaction During Dry Storage, D. W. Reisenweaver (ed.), NUREG/CP-0049, U.S. Nuclear Regulatory Commission, Washington, D.C. pp. F-2 to F-12.

Wilcox, T., 1972. MORSE-L, A Special Version of the MORSE Program Designed to Solve Neutron, Gamma, and Coupled Neutron-Gamma Penetration Problems, UCID-16680, Lawrence Livermore National Laboratory, Livermore, Calif.

Wilcox, T. P., and R. A. Van Konynenburg, 1981. Radiation Dose Calculations for Geologic Media Around Spent Fuel Emplacement Holes in the Climax Granite, Nevada Test Site, UCRL-53159, Lawrence Livermore National Laboratory, Livermore, Calif.

Wilde, B. E., 1974. "On Pitting and Protection Potentials: Their Use and Possible Misuses for Predicting Localized Corrosion Resistance of Stainless Alloys in Halide Media," Localized Corrosion NACE-3, R. W. Staehle, B. F. Brown, J. Kruger and A. Agrawal (eds.), National Association of Corrosion Engineers, Houston, Tex., pp. 342-252.

Williams, W. L., 1957. "Chloride and Caustic Stress Corrosion of Austenitic Stainless Steel in Hot Water and Steam," Corrosion, Vol. 13, National Association of Corrosion Engineers, pp. 539-545.

Wilson, C. N., 1985a. Microstructural Characteristics of PWR Spent Fuel Relative to Its Leaching Behavior, HEDL-SA-3313, Hanford Engineering Development Laboratory, Richland, Wash.

Wilson, C. N., 1985b. Results from NNWSI Series 1 Spent Fuel Leach Test, HEDL-TME-84-30, Hanford Engineering Development Laboratory, Richland, Wash.

Wilson, C. N., 1986. Test Plan for Series 3 NNWSI Spent Fuel Leaching/Dissolution Test, HEDL-7577, Hanford Engineering Development Laboratory, Richland, Wash.

Wilson, C. N., 1987. Results from Cycles 1 and 2 of NNWSI Series 2 Spent-Fuel Dissolution Tests, HEDL-TME-85-22, Hanford Engineering Development Laboratory, Richland, Wash.

Wilson, C. N., and V. M. Oversby, 1985. Radionuclide Release from PWR Fuels in a Reference Tuff Repository Groundwater, UCRL-91464, preprint, Lawrence Livermore National Laboratory, Livermore, Calif.

Wilson, I. L. W., and R. G. Aspden, 1977. "Caustic Stress Corrosion Cracking of Iron-Nickel-Chromium Alloys," Stress Corrosion Cracking and Hydrogen Embrittlement of Iron-Base Alloys, National Association of Corrosion Engineers, Houston, Tex., pp. 1189-1204.

Winograd, I. J., 1981. "Radioactive Waste Disposal in Thick Unsaturated Zones," Science, Vol. 212, No. 4502, pp. 1457-1464.

Wolery, T. J., 1978. "Some Chemical Aspects of Hydrothermal Processes at Mid-Ocean Ridges - A Theoretical Study, I. Basalt-Seawater Reaction and Chemical Cycling Between the Oceanic Crust and the Oceans. II. Calculations of Chemical Equilibrium Between Aqueous Solutions and Minerals," PhD. Dissertation, Northwestern University, Evanston, Ill.

Wolery, T. J., 1979. Calculation of Chemical Equilibrium Between Aqueous Solution and Minerals: The EQ3/6 Software Package, UCRL-52658, Lawrence Livermore Laboratory, Livermore, Calif.

Wolery, T. J., 1980. Chemical Modeling of Geologic Disposal of Nuclear Waste: Progress Report and a Perspective, UCRL-52748, Lawrence Livermore National Laboratory, Livermore, Calif.

Wolery, T. J., 1983. EQ3NR, A Computer Program for Geochemical Aqueous Speciation-Solubility Calculations: User's Guide and Documentation, UCRL-53414, Lawrence Livermore National Laboratory, Livermore, Calif.

Wolery, T. J., 1986. Some Forms of Transition State Theory, Including Non-Equilibrium Steady State Forms, and Their Application in Geochemistry, UCRL-94221, (preprint), Lawrence Livermore National Laboratory, Livermore, Calif.

Wolery, T. J., D. J. Isherwood, K. J. Jackson, J. M. Delany, and I. Puigdomenech, 1984. EQ3/6: Status and Applications, UCRL-91884, Lawrence Livermore National Laboratory, Livermore, Calif.

Wolfsberg, K., and D. T. Vaniman, (Comps.), 1984. Research and Development Related to the Nevada Nuclear Waste Storage Investigations, October 1--December 31, 1983, LA-10032-PR, Los Alamos National Laboratory, Los Alamos, N. Mex.

Woodley, R. E., 1983. The Characteristics of Spent LWR Fuel Relevant to its Storage in Geologic Repositories, HEDL-TME 83-28, Hanford Engineering Development Laboratory, Richland, Wash.

Yow, J. L., Jr., 1985. Field Investigation of Keyblock Stability, UCRL-53632, Lawrence Livermore National Laboratory, Livermore, Calif.

CODES AND REGULATIONS

10 CFR Part 100 and Appendix A (Code of Federal Regulations), 1987. Title 10, "Energy," Part 100 and Appendix A, "Reactor Site Criteria," U.S. Government Printing Office, Washington, D.C.

10 CFR Part 20 (Code of Federal Regulations), 1987. Title 10, "Energy," Part 20, "Standards for Protection Against Radiation," U.S. Government Printing Office, Washington, D.C.

10 CFR Part 60 (Code of Federal Regulations), 1987. Title 10, "Energy," Part 60, "Disposal of High-Level Radioactive Wastes in Geologic Repositories," U.S. Government Printing Office, Washington, D.C.

10 CFR Part 960 (Code of Federal Regulations), 1987. Title 10, "Energy," Part 960, "General Guidelines for the Recommendation of Sites for Nuclear Waste Repositories," U.S. Government Printing Office, Washington, D.C.

10 CFR Part 961 (Code of Federal Regulations), 1987. Title 10, "Energy," Part 961, "Standard Contract for Disposal of Spent Nuclear Fuel and/or High-Level Radioactive Waste," U.S. Government Printing Office, Washington, D.C.

40 CFR Part 191 (Code of Federal Regulations), 1986. Title 40, "Protection of Environment," Part 191, "Environmental Standards for the Management and Disposal of Spent Nuclear Fuel, High-Level and Transuranic Radioactive Wastes," U.S. Government Printing Office, Washington, D.C.